HELLENIC REPUBLIC
UNIVERSITY OF IOANNINA
SCHOOL OF ENGINEERING
DEPARTMENT OF MATERIALS SCIENCE AND ENGINEERING

DEVELOPMENT OF GLASS-CERAMICS FOR DENTAL APPLICATIONS

DIMITRIADIS KONSTANTINOS

PhD THESIS

IOANNINA 2020

ΕΛΛΗΝΙΚΗ ΔΗΜΟΚΡΑΤΙΑ
ΠΑΝΕΠΙΣΤΗΜΙΟ ΙΩΑΝΝΙΝΩΝ
ΠΟΛΥΤΕΧΝΙΚΗ ΣΧΟΛΗ
ΤΜΗΜΑ ΜΗΧΑΝΙΚΩΝ ΕΠΙΣΤΗΜΗΣ ΥΛΙΚΩΝ

ΑΝΑΠΤΥΞΗ ΥΑΛΟΚΕΡΑΜΙΚΩΝ ΥΛΙΚΩΝ ΓΙΑ ΟΔΟΝΤΙΑΤΡΙΚΕΣ ΕΦΑΡΜΟΓΕΣ

ΔΗΜΗΤΡΙΑΔΗΣ ΚΩΝΣΤΑΝΤΙΝΟΣ

ΔΙΔΑΚΤΟΡΙΚΗ ΔΙΑΤΡΙΒΗ

ΙΩΑΝΝΙΝΑ 2020

«Η έγκριση της διδακτορικής διατριβής από το Τμήμα Μηχανικών Επιστήμης Υλικών της Πολυτεχνικής Σχολής του Πανεπιστημίου Ιωαννίνων δεν υποδηλώνει αποδοχή των γνωμών του συγγραφέα (Ν. 5343/32, άρθρο. 202, παράγραφος 2)»

Date of application of Mr. Konstantinos Dimitriadis: 15/01/2016
Date of Appointment of PhD Advisory Committee: 09/02/2016
Members of 3 Member Advisory Committee:

Thesis Advisor

Simeon Agathopoulos, Professor, Department of Materials Science and Engineering, School of Engineering, University of Ioannina

Members

Michael A. Karakassides, Professor, Department of Materials Science and Engineering, School of Engineering, University of Ioannina

Dilshat U. Tulyaganov, Professor, Turin Polytechnic University in Tashkent

Date of Thesis Definition: 09/02/2016

Σχεδιασμός, σύνθεση και χαρακτηρισμός νέων υάλων και υαλοκεραμικών υλικών με βάση το σύστημα R_2O-CaO-MgO-SiO_2-P_2O_5-TR_2O_3 (R:Li, Na, K, TR: B_2O_3, Al_2O_3) για εφαρμογές στην τεχνολογία της οδοντιατρικής

on 19/09/2018 approved by the department's meeting the title and doctoral thesis should be written in English:

Design, synthesis and characterization of novel glasses and glass-ceramics in the system R_2O-*CaO-MgO*-SiO_2-P_2O_5-TR_2O_3 *(R: Li, Na, K, TR:* B_2O_3, Al_2O_3*) for applications in dental technology*

Date of Thesis Modification: 25/09/2019

Development of glass-ceramics for dental applications

DATE OF APPOINTMENT OF THE -MEMBER EXAMINATION COMMITTEE:

1. Simeon Agathopoulos, Professor, Department of Materials Science and Engineering, School of Engineering, University of Ioannina
2. Michael A. Karakassides, Professor, Department of Materials Science and Engineering, School of Engineering, University of Ioannina
3. Dilshat U. Tulyaganov, Professor, Turin Polytechnic University in Tashkent, Uzbekistan
4. Dimitrios Fotiadis, Professor, Department of Materials Science and Engineering, School of Engineering, University of Ioannina
5. Tiverios Vaimakis, Professor, Department of Chemistry, University of Ioannina
6. Athena Tsetsekou, Professor, School of Mining and Metallurgical Engineering, National Technical University of Athens
7. Dionysios Mouzakis, Professor, Helenic Army Academy.

The PhD Thesis is approved with «Excellent» on 23/06/2020

The Chairman of the Department	**The Secretary of the Department**
Alkiviadis Paipetis	**Maria Kontou**

Ημερομηνία αίτησης του κ. Δημητριάδη Κωνσταντίνου: 15/01/2016
Ημερομηνία Ορισμού Τριμελούς Συμβουλευτικής Επιτροπής: 09/02/2016
Μέλη Τριμελούς Συμβουλευτικής Επιτροπής:

Επιβλέπων

Συμεών Αγαθόπουλος, Καθηγητής, Τμήμα Μηχανικών Επιστήμης Υλικών, Πολυτεχνική Σχολή, Πανεπιστήμιο Ιωαννίνων

Μέλη

Μιχαήλ Α. Καρακασίδης, Καθηγητής, Τμήμα Μηχανικών Επιστήμης Υλικών, Πολυτεχνική Σχολή, Πανεπιστήμιο Ιωαννίνων

Dilshat U. Tulyaganov, Καθηγητής, Turin Polytechnic University in Tashkent

Ημερομηνία ορισμού θέματος: 09/02/2016

Σχεδιασμός, σύνθεση και χαρακτηρισμός νέων υάλων και υαλοκεραμικών υλικών με βάση το σύστημα R_2O-CaO-MgO-SiO_2-P_2O_5-TR_2O_3 (R:Li, Na, K, TR: B_2O_3, Al_2O_3) για εφαρμογές στην τεχνολογία της οδοντιατρικής

στις 19/09/2018 εγκρίθηκε από την συνέλευση του τμήματος ο τίτλος και η διδακτορική διατριβή να γραφτούν στην αγγλική γλώσσα:

Design, synthesis and characterization of novel glasses and glass-ceramics in the system R_2O-*CaO-MgO*-SiO_2-P_2O_5-TR_2O_3 *(R: Li, Na, K, TR:* B_2O_3, Al_2O_3*) for applications in dental technology*

Ημερομηνία τροποποίησης θέματος: 25/09/2019
Development of glass-ceramics for dental applications

ΔΙΟΡΙΣΜΟΣ ΕΠΤΑΜΕΛΟΥΣ ΕΞΕΤΑΣΤΙΚΗΣ ΕΠΙΤΡΟΠΗΣ:

1. Συμεών Αγαθόπουλος, Καθηγητής Τμήματος Μηχανικών Επιστήμης Υλικών της Πολυτεχνικής Σχολής Πανεπιστημίου Ιωαννίνων,
2. Μιχαήλ Α. Καρακασίδης, Καθηγητής Τμήματος Μηχανικών Επιστήμης Υλικών της Πολυτεχνικής Σχολής Πανεπιστημίου Ιωαννίνων,
3. Dilshat U. Tulyaganov, Καθηγητής Turin Polytechnic University in Tashkent, Uzbekistan,
4. Δημήτριος Φωτιάδης, Καθηγητής Τμήματος Μηχανικών Επιστήμης Υλικών της Πολυτεχνικής Σχολής Πανεπιστημίου Ιωαννίνων,
5. Τιβέριος Βαϊμάκης, Καθηγητής Τμήματος Χημείας Πανεπιστημίου Ιωαννίνων,
6. Αθηνά Τσετσέκου, Καθηγήτρια Σχολής Μηχανικών Μεταλλείων-Μεταλλουργών Εθνικού Μετσόβιου Πολυτεχνείου,
7. Διονύσιος Μουζάκης, Καθηγητής Στρατιωτικής Σχολής Ευελπίδων

Έγκριση Διδακτορικής Διατριβής με βαθμό «Άριστα» στις 23/06/2020.

Ο Πρόεδρος του Τμήματος	**Η Γραμματέας του Τμήματος**
Αλκιβιάδης Παϊπέτης	**Μαρία Κόντου**

Ιωάννινα, 23/06/2020

Προς
τη Γραμματεία του Τμήματος
Μηχανικών Επιστήμης Υλικών
του Πανεπιστημίου Ιωαννίνων

ΠΡΑΚΤΙΚΟ

της Επταμελούς Εξεταστικής Επιτροπής για την αναγόρευση σε Διδάκτορα του Τμήματος Μηχανικών Επιστήμης Υλικών της Πολυτεχνικής Σχολής του Πανεπιστημίου Ιωαννίνων του **Κωνσταντίνου Δημητριάδη**.

Η Συνέλευση του Τμήματος Μηχανικών Επιστήμης Υλικών της Πολυτεχνικής Σχολής του Πανεπιστημίου Ιωαννίνων στη συνεδρίασή της αριθμ. 350/05-05-2020 ύστερα από την κρίση της Τριμελούς Συμβουλευτικής Επιτροπής ότι η ερευνητική εργασία του υποψήφιου Διδάκτορα **Κωνσταντίνου Δημητριάδη** έχει ολοκληρωθεί και έχει κατατεθεί στο Τμήμα, όρισε σύμφωνα με τις διατάξεις του άρθρου 41 του Ν.4485/2017 (ΦΕΚ 114/04-08-2017), την Εξεταστική Επιτροπή που αποτελείται από τους κ.κ. **Συμεών Αγαθόπουλο**, Καθηγητή του Τμήματος Μηχανικών Επιστήμης Υλικών, της Πολυτεχνικής Σχολής, του Πανεπιστημίου Ιωαννίνων, **Μιχαήλ Καρακασίδη**, Καθηγητή του Τμήματος Μηχανικών Επιστήμης Υλικών, της Πολυτεχνικής Σχολής, του Πανεπιστημίου Ιωαννίνων, **Dilshat Tulyaganov**, Καθηγητή του Turin Polytechnic University, της Τασκένδης, του Ουζμπεκιστάν, **Δημήτριο Φωτιάδη**, Καθηγητή του Τμήματος Μηχανικών Επιστήμης Υλικών, της Πολυτεχνικής Σχολής, του Πανεπιστημίου Ιωαννίνων, **Τιβέριο Βαϊμάκη**, Καθηγητή του Τμήματος Χημείας, της Σχολής Θετικών Επιστημών, του Πανεπιστημίου Ιωαννίνων, **Αθηνά Τσετσέκου**, Καθηγήτρια της Σχολής Μηχανικών Μεταλλείων-Μεταλλουργών, του Εθνικού Μετσόβιου Πολυτεχνείου, και **Διονύσιο Μουζάκη**, Καθηγητή της Στρατιωτικής Σχολής Ευελπίδων, για να αναπτύξει ενώπιον της ο υποψήφιος Διδάκτορας **Κωνσταντίνος Δημητριάδης** τη διατριβή του με θέμα: **Development of glass-ceramics for dental applications.**

Η Επταμελής Εξεταστική Επιτροπή με την παραπάνω σύνθεση της, συνήλθε σήμερα **23 Ιουνίου 2020** ημέρα **Τρίτη** και ώρα **11:00, στην αίθουσα του Τμήματος Μηχανικών Επιστήμης Υλικών του Πανεπιστημίου Ιωαννίνων** για να εξετάσει την διδακτορική διατριβή του υποψήφιου διδάκτορα κ. **Κωνσταντίνου Δημητριάδη**.

Χρέη προέδρου της Εξεταστικής Επιτροπής ανέθεσαν τα μέλη της στον κ. **Συμεών Αγαθόπουλο,** Καθηγητή του Τμήματος Μηχανικών Επιστήμης Υλικών της Πολυτεχνικής Σχολής του Πανεπιστημίου Ιωαννίνων.

Στο σημείο αυτό τίθεται υπόψη της 7μελούς Εξεταστικής Επιτροπής το άρθρου 41 του Ν.4485/2017 (ΦΕΚ 114/04-08-2017), η παρ. 9ε του Εσωτερικού Κανονισμού Διδακτορικών Σπουδών του Τμήματος (ΦΕΚ 832/09.03.2018 τ. Β΄).

Τα μέλη της Επιτροπής έλαβαν εγκαίρως γνώση του κειμένου της διατριβής του υποψήφιου **Κωνσταντίνου Δημητριάδη** και τη μελέτησαν.

Ο υποψήφιος κ. **Κωνσταντίνος Δημητριάδης** ανέπτυξε ενώπιον της Επιτροπής τη διατριβή του με θέμα **Development of glass-ceramics for dental applications** τονίζοντας τα σημεία, στα οποία κατά τη γνώμη του η διατριβή είναι πρωτότυπη και αποτελεί συμβολή στην επιστήμη. Τα μέλη της Εξεταστικής Επιτροπής απηύθυναν ερωτήσεις στον υποψήφιο, μετά την προφορική ανάπτυξη από αυτόν του θέματος. Η ανάπτυξη και οι ερωτήσεις έγιναν σε δημόσια συνεδρίαση.

Στη συνέχεια το ακροατήριο και ο υποψήφιος αποχώρησαν και τα μέλη της Εξεταστικής Επιτροπής συσκέφθηκαν και ψήφισαν, υπέρ της παραδοχής της διατριβής, με ψήφους επτά (7) υπέρ και μηδέν (0) κατά.

Πρότειναν, δε, με ψήφους επτά (7) έναντι μηδενός (0) το βαθμό **Άριστα** εφαρμόζοντας την παρ. 9ε του Εσωτερικού Κανονισμού Διδακτορικών Σπουδών του Τμήματος (ΦΕΚ 832/09.03.2018 τ. Β΄).

Η Εξεταστική Επιτροπή

1. **Συμεών Αγαθόπουλος**
   Καθηγητής, Τμήματος Μηχανικών Επιστήμης Υλικών
   της Πολυτεχνικής Σχολής του Πανεπιστημίου Ιωαννίνων
2. **Μιχαήλ Καρακασίδης**
   Καθηγητής Τμήματος Μηχανικών Επιστήμης Υλικών
   της Πολυτεχνικής Σχολής του Πανεπιστημίου Ιωαννίνων
3. **Dilshat Tulyaganov**
   Καθηγητής του Turin Polytechnic University
   της Τασκένδης του Ουζμπεκιστάν
4. **Δημήτριος Φωτιάδης**
   Καθηγητής Τμήματος Μηχανικών Επιστήμης Υλικών
   της Πολυτεχνικής Σχολής του Πανεπιστημίου Ιωαννίνων
5. **Τιβέριος Βαϊμάκης**
   Καθηγητής Τμήματος Χημείας
   της Σχολής Θετικών Επιστημών του Πανεπιστημίου Ιωαννίνων
6. **Αθηνά Τσετσέκου**
   Καθηγήτρια Σχολής Μηχανικών Μεταλλείων-Μεταλλουργών
   του Εθνικού Μετσόβιου Πολυτεχνείου
7. **Διονύσιος Μουζάκης**
   Καθηγητής Στρατιωτικής Σχολής Ευελπίδων

This PhD Thesis is dedicated to
my parents, Grigoris and Irini,
my lovely Christina
and to those who believed in my success

PREFACE

This PhD thesis was carried out in the Laboratory of Ceramics and Composite Materials (CCL) of the Department Materials Science and Engineering, School of Engineering at the University of Ioannina, Greece. This research was co-financed by Greece and the European Union (European Social Fund-ESF) through the Operational Programme «*Human Resources Development, Education and Lifelong Learning*» in the context of the project «*Strengthening Human Resources Research Potential via Doctorate Research*» (MIS-5000432), implemented by the State Scholarships Foundation (IKY). The thesis aimed at developing novel compositions of glass-ceramic (GC) materials suitable for dental applications, both in the domain of dental implants, and in the domain of fixed prosthetic restorations.

Dental implants are a reliable solution to restore lost teeth. The disadvantages of cpTi and Ti6Al4V dental implants, such as patients' allergic reactions and reduced aesthetic performance in the case of replacing anterior teeth, have been overcome by the introduction of zirconia dental implants. Nonetheless, the problem of the mismatch of the mechanical properties between the human jaw bone and dental implant materials is still in the spotlight. One of the most important mechanical properties is the modulus of elasticity. The mismatch of this property can cause the *stress shielding* phenomenon. According to this phenomenon, after the placement of an implant prosthetic restoration, the dental implant is the one that receives the largest percentage of the load from the occlusal forces rather than the jaw bone. Knowing that the bones are reshaped in response to the loads they receive, reducing this load on the jaw bone results in a decrease in bone density. In this way, the possibility of dental implant failure is increased. Zirconia presents other problems which are related to the nature of this material, such as accelerated aging in the presence of moisture, leading to surface deterioration and propagation of microcracks that can result in spontaneous catastrophic failure.

In the case of dental implants, the expression of bioactivity, beyond the fact that it improves osseointegration by preventing the formation of fibrous tissue around the dental implant (which prevents osteogenesis), would also improve the load distribution between the dental implant and the jaw bone, by means of interfacial bonding, resulting in suppressing *stress shielding* phenomenon. In order to convert non-bioactive surfaces of bioinert Ti and zirconia dental implants into bioactive, various bioactive coatings, such as plasma-sprayed HA (hydroxyapatite) have been developed. Unfortunately, these coatings have not produced the desired results, since "weak points" were present at the bone-coating-implant interfaces.

In the case of fixed prosthetic restorations, the strong interest for better aesthetic results and the questionable biocompatibility of dental alloys motivated researchers in developing all-ceramic systems. The introduction of zirconia as a restorative dental material for all-ceramic systems, while exhibiting the desired aesthetic results, showed the disadvantage of teeth injury, due to the high hardness values of zirconia (12 GPa). The coating of zirconia with porcelain (with a lower hardness), although it provided a solution to the above problem, presented other problems, such as the reduced ceramic-ceramic bond strength due to the different coefficients of thermal expansion of the two materials. Thus, the potential application of GC materials in fixed prosthetic restorations was given priority. These materials meet the aesthetic requirements and a big part of the desirable mechanical properties, as they are quite close to the corresponding properties of enamel. Nevertheless, an important property that limits their application and needs improvement is the fracture toughness.

Given the above, the design, development and production of both bioactive GC materials with mechanical properties close to those of the human jaw bone (which is the environment that a dental implant is placed in) and dentine (which makes up the root of the natural tooth), and bioinert GC materials with mechanical properties close to those of the enamel summarize the aim of the present PhD thesis. More specifically, this thesis reports on the development of novel bioactive GCs in the CaO-MgO-SiO_2 system with Na_2O, K_2O, P_2O_5, CaF_2, and Al_2O_3 additives. The influence of partial substitution of Mg for Ca and of complete substitution of K for Na on bioactivity performance, mechanical properties, and aesthetics was thoroughly investigated. Dense, well-crystallized and bioactive GCs of white color were produced. It was demonstrated that the above substitutions in the produced GCs enable suitable tuning of their mechanical properties in order to approach the mechanical properties of natural jaw bone and dentine, better than the commercial zirconia and titanium implants.

As far as the Al_2O_3 addition is concerned, the small Al_2O_3 addition (1 mol%) to the above bioactive GCs allowed us to approach in a better way the mechanical properties of a human jaw bone and dentine, without jeopardizing the desirable bioactivity, which is reflected by the spontaneous *in vitro* formation of hydroxyapatite layer on the surface of the produced GCs. Thus, these GCs can be qualified as candidate materials for dental implant fabrication. In order to produce bioinert GC materials with mechanical properties close to those of human enamel, a higher Al_2O_3 addition (7-8 mol%) was attempted. Well-sintered, well-crystallized and dense GC bars of white color were produced from glass powder compacts. The produced GCs showed no bioactivity, and their mechanical properties were considerably improved, being a good match with the properties of hard dental tissues (i.e. with enamel those with substitution of Mg for Ca, and with dentine those with substitution of K for Na). These results suggest these GCs be applied in the case of fixed all-ceramics prosthetic restorations (i.e. inlay, onlay, crowns).

Completing my doctoral thesis, I would like to thank the following people.

First of all, I would like to thank my supervisor, Prof. Simeon Agathopoulos, for the assignment of the subject of this thesis, the confidence he showed to me from the first day we met and his support at every stage of the PhD thesis. Moreover, I would like to thank him for his kindness, the valuable advice I have received over the years, and his willingness to guide me steadily and effectively in completing my research.

I am also gratefully indebted to the two co-supervisors. More specifically, I would like to thank warmly, the member of the advisory and examination committee Prof. Dilshat Tulyaganov for his interest, confidence, apt observations and assistance at all stages of this work. I also thank the other member of the advisory and examination committee Prof. Michael Karakasides, who received me with great joy at the Laboratory of Ceramics and Composite Materials (CCL), the confidence he showed me and for the valuable advice I received during my research.

Moreover, I would like to thank the other members of the examination committee, Prof. Tiverios Vaimakis, Prof. Dimitrios Fotiadis, Prof. Athina Tsetsekou, and Prof. Dionysios Mouzakis for the honor they made for joining the examination committee and for the helpful advice I received from everyone. I would particularly like to thank Prof. Vaimakis for the help and the knowledge I gained from him and the confidence he has shown to me by providing, without any time limitations, the Thermal Analysis Laboratory of the Department of Chemistry of the University of Ioannina.

Moreover, I would like to acknowledge the valuable impact of Prof. Triantafillos Papadopoulos who initiated me in the field of Biomaterials and encouraged me to carry out this PhD thesis. A big thank I would like to give to Professor Angela Lekatou, director of the Laboratory of Applied Metallurgy, for the confidence she has shown to me and the hospitality in her laboratory.

Continuing, I should thank the postdoctoral researcher Dr. Konstantinos Vassilopoulos for his willingness, advice and assistance in the glass casting experiments. I would also like to thank the postdoctoral researcher Dr. Dimitrios Moschovas for his willingness, friendly climate and his help in obtaining the SEM images.

From my colleagues, I owe a big thank to my colleagues and friends, Dr. Eleonora Barka and Dr. Anthi Poulia, for their kindness, help and support at all stages of the PhD thesis. I would also like to thank, in particular, my friend and colleague, Dr. Maria Roubi, for her moral support, valuable advice and friendly collaboration in whatever I needed from my first days in the CCL laboratory. A special thank is also expressed to Mr. George Katsimanis for thoroughly reviewing the entire manuscript and improving the language of the text, wherever it was necessary.

Finally, I would like to thank from my heart my family, the people who stood by me in whatever way and supported me, without a second thought. A big thank to my beloved Christina Boukouvala for the trust, tremendous support and encouragement over the years.

Ioannina, June 2020

Konstantinos Dimitriadis

TABLE OF CONTENTS

Chapter page no

PREFACE 13
TABLE OF CONTENTS 17
EXTENDED SUMMARY 21
ΕΚΤΕΝΗΣ ΠΕΡΙΛΗΨΗ 27
LIST OF TABLES 33
LIST OF FIGURES 37

A. Introduction **43**
- **1.** Glass-ceramic (GC) materials 46
  - 1.1 Chemical composition and structural features of glasses and GCs 48
  - 1.2 Sintering and crystallization of GCs 50
- **2.** Glass-ceramics (GCs) in dental applications 55
  - 2.1 The use of GCs in biomedicine 55
  - 2.2 Dental Implants 58
  - 2.3 Dental fixed all-ceramic prosthetic restorations 65

B. State of the art and aim **71**

C. Experimental procedure **85**
- **1.** Glasses: synthesis and thermal analysis 87
- **2.** Glass-ceramics (GCs): preparation, characterization and bioactivity 89

D. Experimental results **95**
- **1.** Development of glass-ceramics (GCs) suitable for dental implant applications 97
  - 1.1 GCs with the initial compositions 1d and 1e 97
  - 1.2 The modified GCs 1d-k, 1d-m, 1e-k and 1e-m 109
- **2.** Development of glass-ceramics (GCs) suitable for dental implant and all-ceramic fixed prosthetic applications 123
  - 2.1 Modified GCs with addition of 1 mol % Al_2O_3 123
  - 2.2 Modified GCs with addition of 7-8 mol % Al_2O_3 139

E. General discussion, conclusions and future work **149**

ANNEXES **161**

REFERENCES 169

CURRICULUM VITAE 181

EXTENDED SUMMARY

AIM

This Ph.D. thesis aims at developing novel compositions in $CaO-MgO-SiO_2$ ternary system, which are suitable for producing glass-ceramic (GC) materials that can potentially be used in dental implant applications. More specifically, based on two well-established parent compositions, novel compositions derived from relatively simple but important (in the light of glass and ceramic technology) modifications and substitutions, in order to produce (a) bioactive GCs with improved mechanical properties (i.e. with values close to those of jaw bone and dentine), being, therefore, suitable for dental implant applications, and (b) bioinert GCs, whose mechanical properties are good match for the properties of tooth enamel, as required in the case of fixed all-ceramic prosthetic restorations.

DESIGN OF NOVEL COMPOSITIONS

The novel compositions were based on the $CaO-MgO-SiO_2$ ternary system, with the additions of Na_2O/K_2O, P_2O_5, CaF_2, and Al_2O_3. The design of the compositions was based on two, already well-established (by our research team) parent compositions, designated as 1d (45.45% SiO_2, 30.30% CaO, 12.99% MgO, 2.60% P_2O_5, 4.33% Na_2O, and 4.33% CaF_2), and 1e (43.10% SiO_2, 32.33% CaO, 12.93% MgO, 3.02% P_2O_5, 4.31% Na_2O, and 4.31 CaF_2; they all refer in mol%), which, in glass state, exhibited bioactivity (i.e. hydroxyapatite (HA) spontaneously forms on the their surface after immersion in simulated body fluid (SBF), at 37 °C, from the early stages of immersion). Moreover, it has been demonstrated that the glass 1d favors jaw bone regeneration, since *in vitro* cell-cultures, *in vivo* animal tests, and clinical trials showed a very good performance, namely low inflammatory infiltration and excellent biocompatibility with the surrounding tissue. The two glasses 1d and 1e differ by about 2 mol% in the content of both SiO_2 and CaO, as well as 1e is richer in P_2O_5 than 1d (3.02 and 2.60%, respectively). Thus, in the context of this Ph.D. thesis, which aims at achieving the two aforementioned goals, i.e. development of novel bioactive GCs for dental implant applications and bioinert GCs for fixed all-ceramic prosthetic applications, modifications/substitutions were made to the above two compositions 1d and 1e, as follows: (a) complete substitution of K_2O for Na_2O (4.31- 4.33 mol%, resulting in the novel compositions 1d-k και 1e-k, where the letter k is after K_2O), (b) partial substitution of MgO for CaO (4.33 mol%, resulting in the novel compositions 1d-m and

1e-m, where the letter m is after MgO), (c) addition of 1 mol% Al_2O_3 to the above compositions (producing the novel compositions 1d/A_1, 1d-k/A_1, 1d-m/A_1, 1e/A_1, 1e-k/A_1, and 1e-m/A_1, where the letter A is after Al_2O_3), and (d) addition of 7-8 mol% Al_2O_3 (producing the novel compositions 1d/A_2, 1d-k/A_2, 1d-m/A_2, 1e/A_2, 1e-k/A_2, and 1e-m/A_2). The first two substitutions (a and b) aimed at producing GCs for dental implant applications, while the addition of 7-8% Al_2O_3 (case d) aimed at developing novel GCs for all-ceramic prostheses. The addition of 1 mol% Al_2O_3 (case c) corresponds to an intermediate regime, aiming at improving the physico-mechanical properties of the resultant GCs by also maintaining bioactivity; therefore, this case obviously aims at producing GCs for dental implant applications.

EXPERIMENTAL PROCEDURE

The glasses were produced by melting of the glass (in a Pt crucible at 1400 °C for 1 h, in air) and subsequent quenching (in cold water). After complete drying, the glass-frit was ground in a high-speed planetary mill and a fine powder was obtained by sieving the milled powder through a sieve of 32 μm (450 mesh). Samples of glasses in bulk form were also produced, by casting the molten glass onto preheated bronze plates and immediately followed by annealing at a temperature close to T_g, which were used in density measurements. Thermal analysis of the parent glasses was performed in order to set-up the optimal crystallization process for producing the GCs. More specifically, dilatometry and DSC (differential scanning calorimetry) measurements for each glass composition were carried out, in order to determine the glass transition temperature (T_g), the crystallization onset temperature (T_c), the sintering window (T_c - T_g), and the crystallization peak temperature (T_p), as well as the liquidus temperature (T_l). Furthermore, DSC thermographs recorded at five different heating rates allowed to calculate the activation energy (E_a) of glass crystallization and the Avrami exponent (n_A), which is an index of crystal growth dimensionality.

The GCs were produced by sintering and controlled crystallization of glass-powder compacts (prepared by uniaxial pressing at 150 - 200 bar and having dimensions according to ISO 6872 “Dentistry - Ceramic Materials”). The heat-treatment schedule set-up was based on the results of the thermal analysis, in order to ensure that successful sintering process is completed before crystallization starts. The crystalline phases developed in the produced GCs were identified by X-ray diffraction analysis, while their microstructure was observed in a scanning electron microscope, equipped with an energy dispersive spectroscopy device for elemental analysis (SEM/EDS). The physical (density, linear shrinkage, and aesthetics), and the mechanical properties (flexural strength, modulus of elasticity, hardness, and fracture toughness) of the produced GC specimens were determined. The bioactivity of the produced GCs was also experimentally determined. More specifically, polished GCs bars as well as fine powders (0.2 g) were immersed in 25 ml SBF (simulated body fluid) solution for 7, 14, and 21 days, at 37 °C. Sampling took place at the aforementioned periods of time. The ability of the GCs to induce HA formation on their surface was evaluated indirectly, by measurements of the pH of the liquid, and directly, by X-ray diffraction analysis of the powders and SEM/EDS analysis of the surface of the GCs bars.

RESULTS

As far as the compositions developed for producing bioactive GCs for dental implants applications are concerned, the experimental results are summarized as follows. Compared to the parent glasses 1d and 1e, the complete substitution of K_2O for Na_2O favors the increase of the temperatures of T_g, T_c, and T_p, as well as the activation energy of crystallization E_a, while, there is a small influence (or a small increase) upon partial substitution of MgO for CaO. Similarly, 1 mol% Al_2O_3 addition also favors a significant increase in these values. The Avrami parameter values showed that some of the produced glasses (1d, 1d-k, 1d-m, 1e, 1e-m, and 1e/A_1) are prone to three-dimensional growth of crystals since $n_A \geq 3$, whereas the other glasses (1d/A_1, 1d-k/A_1, 1d-m/A_1, 1e-k, 1e-k/A_1, and 1e-m/A_1) are prone to two-dimensional crystallization ($n_A \leq 2$). The set-up for the heat-treatment of the parallelepiped bars of the glass powder compacts was chosen by analyzing the results of the thermal analysis of the investigated glasses. More specifically, the glass powder compacts with complete substitution of K_2O for Na_2O were heat-treated at 900 °C, the glass powder compacts with partial substitution of MgO for CaO were heat-treated at 850 °C, while the K-containing glass powder compacts with 1 mol% Al_2O_3 were heat-treated at 900 °C, and the K-free glass powder compacts with 1 mol% Al_2O_3 were heat-treated at 850 °C. The crystallographic analysis of the GCs specimens by X-ray diffraction and the observation of their microstructure in a scanning electron microscope along with elemental analysis conducted by an energy dispersive spectroscopy device showed that diopside, wollastonite, and fluorapatite are crystallized in the K-free specimens, while, in the K-containing GCs, α-PMS was detected instead of wollastonite. The mechanical properties of the produced GCs, with values of 22 - 34 GPa regarding the modulus of elasticity, 5.2 - 6.7 GPa concerning the Vickers microhardness, 1.4 - 2.5 $MPa \cdot m^{0.5}$ regarding the fracture toughness (K_{IC}), and 107 - 177 MPa as regard the flexural strength, were a good match for those of the human jaw bone and dentine. Moreover, the produced GCs displayed bioactivity features, as reflected by their ability to favor spontaneous formation of hydroxyapatite (HA) on their surface after immersion in SBF at 37 °C, even from the first week of immersion.

As far as the compositions with 7-8 mol% Al_2O_3 addition are concerned, aimed at producing bioinert GCs for all-ceramic prosthetic restorations, the experimental results are summarized as follows. The temperatures of T_g, T_c, and T_p were increased, compared to the Al_2O_3-free or 1% Al_2O_3 addition compositions. The 7-8 mol% Al_2O_3 addition favors an increase in the activation energy of crystallization (Ea) of K-containing glasses and a decrease in K-free glasses. The Avrami parameter values of the K-free glasses were $n_A \geq 3$, which suggest that these glasses are prone to three-dimensional growth of crystals, while the K-containing glasses presented $n_A \geq 2$, which means that these two glasses are prone to two-dimensional crystallization. Based on the results of thermal analysis, the temperature of 900 °C was selected for the heat-treatment of the glass powder compacts. Compared to the Al_2O_3-free GCs or the GCs with 1 mol% Al_2O_3 addition, the 7-8 mol% Al_2O_3 addition caused a change in the crystalline phases formed in the resultant GCs, identified by X-ray diffraction and microstructure analyses, which are melilite and diopside in the case of the K-free GCs, and melilite and gehlenite in the case of the K-containing GCs. The mechanical properties of the produced GCs are a good match for the corresponding properties of enamel and dentine, i.e. the flexural strength ranged between 120 and 171 MPa, the modulus of elasticity varied between 28 and 42 GPa, and the Vickers microhardness and the fracture toughness (K_{IC}) values varied from 6.3 to 7.0 GPa and 2.6 to 2.8 $MPa \cdot m^{0.5}$, respectively. Furthermore, the addition of 7-8 mol% Al_2O_3 totally suppressed the bioactivity of the produced GCs, since the SEM/EDS analyses showed no HA formation on the surface of the GC specimens after 7, 14, and 21 days of immersion in SBF.

CONCLUSIONS

This Ph.D. thesis aims at developing novel GCs in the CaO-MgO-SiO_2 ternary system which are suitable for dental applications, either in the domain of dental implants, or in the domain of fixed all-ceramic prosthetic restorations. The influence of the substitution of K_2O for Na_2O, MgO for CaO, and the Al_2O_3 addition (1 and 7-8 mol%) on the properties of the resultant GCs was investigated. The goal was to produce GCs whose mechanical properties are a good match for the mechanical properties of jaw bone as well as of dental hard tissues, enamel and dentine, depending on the particular application that the GCs aim at.

The investigation on developing novel compositions aimed at producing bioactive GCs for dental implant applications resulted in the following conclusions. The complete substitution of K_2O for Na_2O, the partial substitution of MgO for CaO, and the addition of 1 mol% Al_2O_3 led to GCs whose mechanical properties are very close to the corresponding properties of jaw bone and dentine. Thus, these GCs can be qualified as potential candidates for dental implant applications.

On the other hand, the compositions with 7-8 mol% Al_2O_3 addition resulted in bioinert GCs whose mechanical properties were a good match for the properties of enamel and dentine. According to the ISO 6872 “Dentistry-Ceramic Materials”, these features qualify the produced GCs as potential candidates for all-ceramic prosthetic restorations, such as aesthetic ceramic materials, namely as coatings of metal or ceramic substrates for producing single-unit anterior or posterior prostheses, veneers, inlays, or onlays, as well as in the construction of adhesively cemented ceramic substrates for single-unit anterior or posterior prostheses.

ΕΚΤΕΝΗΣ ΠΕΡΙΛΗΨΗ

ΣΚΟΠΟΣ

Η παρούσα διδακτορική διατριβή έχει στόχο το σχεδιασμό καινοτόμων συστάσεων στο τριμερές σύστημα CaO-MgO-SiO_2, και με βάση τις συστάσεις αυτές, να κατασκευαστούν υαλοκεραμικά υλικά που να μπορούν, εν δυνάμει, να χρησιμοποιηθούν ως υλικά κατασκευής οδοντικών εμφυτευμάτων. Πιο συγκεκριμένα, αφού αναπτύχθηκαν οι αρχικές συστάσεις, μελετήθηκαν σχετικά απλές, αλλά σημαντικές, υπό το πρίσμα της εφαρμογής της τεχνολογίας των κόνεων, τροποποιήσεις και υποκαταστάσεις, προκειμένου να κατασκευαστούν αφενός βιοενεργά υαλοκεραμικά υλικά με βελτιωμένες μηχανικές ιδιότητες, δηλαδή με τιμές κοντά στις αντίστοιχες τιμές του οστού της γνάθου και της οδοντίνης, όπως απαιτείται στην περίπτωση των οδοντικών εμφυτευμάτων, αφετέρου μη-βιοενεργά υαλοκεραμικά υλικά, με μηχανικές ιδιότητες οι οποίες απαιτούνται στην περίπτωση ακίνητων ολοκεραμικών προσθετικών αποκαταστάσεων.

ΣΧΕΔΙΑΣΜΟΣ ΝΕΩΝ ΣΥΣΤΑΣΕΩΝ

Στο στάδιο του σχεδιασμού των καινοτόμων συστάσεων των νέων υαλοκεραμικών υλικών με βάση το τριμερές σύστημα CaO-MgO-SiO_2, μελετήθηκαν οι προσθήκες των οξειδίων Na_2O ή K_2O, P_2O_5, CaF_2 και Al_2O_3. Πιο συγκεκριμένα, για την υλοποίηση των δύο παραπάνω στόχων της διδακτορική διατριβής (δηλαδή, κατασκευή υαλοκεραμικών υλικών για βιοενεργά οδοντικά εμφυτεύματα και για βιοαδρανείς ακίνητες ολοκεραμικές προσθετικές αποκαταστάσεις), πραγματοποιήθηκε μια σειρά υποκαταστάσεων/τροποποιήσεων σε δύο αρχικές επιλεγμένες συστάσεις με τις ονομασίες (σύμφωνα με προηγούμενη δημοσιευμένη έρευνα της ερευνητικής μας ομάδας) 1d και 1e, οι οποίες, σε μορφή υάλου, είχαν ήδη χαρακτηριστεί, με έλεγχό τους, τόσο *in vitro*, όσο και *in vivo*, ως βιοενεργές, ενώ σε κλινικές δοκιμές έδειξαν άριστη συμπεριφορά σε οστό γνάθου. Οι δύο αυτές συστάσεις (με περιεκτικότητες (σε mol%) 45.45% SiO_2, 30.30% CaO, 12.99% MgO, 2.60% P_2O_5, 4.33% Na_2O και 4.33% CaF_2 η 1d, και 43.10% SiO_2, 32.33% CaO, 12.93% MgO, 3.02% P_2O_5, 4.31% Na_2O και 4.31 CaF_2 η 1e) διαφέρουν μεταξύ τους κατά περίπου 2 mol% στο περιεχόμενο τόσο του SiO_2 όσο και του CaO, καθώς, επίσης, και η 1e έχει υψηλότερη περιεκτικότητα σε P_2O_5 από την 1d (3.02 και 2.60 mol%, αντίστοιχα). Στα πλαίσια της παρούσας εργασίας, οι τροποποιήσεις που πραγματοποιήθηκαν στις παραπάνω δύο συστάσεις αφορούσαν στην πλήρη υποκατάσταση του Na_2O με K_2O (4.31- 4.33 mol%, στις νέες συστάσεις 1d-k και 1e-k), την μερική υποκατάσταση του CaO με MgO (4.33 mol%, στις νέες συστάσεις 1d-m και 1e-m), και την προσθήκη Al_2O_3 στις παραπάνω συστάσεις σε ποσοστά 1 mol% (παράγοντας τις νέες συστάσεις 1d/A_1, 1d-k/A_1, 1d-m/A_1, 1e/A_1, 1e-k/A_1 και 1e-m/A_1) και 7-8 mol% (παράγοντας τις νέες συστάσεις 1d/A_2, 1d-k/A_2, 1d-m/A_2, 1e/A_2, 1e-k/A_2 και 1e-m/A_2). Οι πρώτες δύο υποκαταστάσεις αφορούσαν στην κατασκευή υαλοκεραμικών υλικών για εφαρμογή σε οδοντικά εμφυτεύματα, ενώ η προσθήκη 7-8% Al_2O_3 στόχευε στην ανάπτυξη συστάσεων για την κατασκευή υλικών για ακίνητες ολοκεραμικές προσθετικές αποκαταστάσεις. Η προσθήκη 1% Al_2O_3 αφορούσε σε μία ενδιάμεση κατάσταση, δηλαδή να επιτευχθεί βελτίωση μηχανικών ιδιοτήτων με ταυτόχρονη επίτευξη βιοενεργότητας, κάτι που προφανώς στοχεύει σε εφαρμογές οδοντικών εμφυτευμάτων.

ΠΕΙΡΑΜΑΤΙΚΗ ΔΙΑΔΙΚΑΣΙΑ

Οι ύαλοι κατασκευάστηκαν με τη μέθοδο της τήξης σε χωνευτήρια πλατίνας στους 1400 ^oC και ελήφθησαν σε μορφή υαλοθραύσματος με υπερταχεία ψύξη του τήγματος με χύτευσή του σε κρύο νερό. Ταυτόχρονα, για διάφορα συγκριτικά πειράματα αναφοράς, παρασκευάστηκαν και δοκίμια υάλου σε συμπαγή μορφή με χύτευση της υάλου σε προθερμασμένη πλάκα από μπρούτζο και αμέσως ανόπτηση σε θερμοκρασίες κοντά στο T_g της υάλου. Αρχικά πραγματοποιήθηκε χαρακτηρισμός της υάλου από την κάθε σύσταση, ο οποίος αφορούσε στη θερμική ανάλυση με μετρήσεις διασταλομετρίας (dilatometry) και διαφορικής θερμιδομετρίας σάρωσης (DSC), με σκοπό τον προσδιορισμό της θερμοκρασίας υαλώδους μετάπτωσης (T_g), της θερμοκρασίας έναρξης της κρυστάλλωσης (T_c), του θερμοκρασιακού παραθύρου της πυροσυσσωμάτωσης (T_c - T_g), και της θερμοκρασίας κρυστάλλωσης (T_p). Από ανάλυση θερμογραφημάτων που ελήφθησαν με διαφορετικούς ρυθμούς θέρμανσης υπολογίστηκαν επίσης η ενέργεια ενεργοποίησης (E_a) της κρυστάλλωσης και η παράμετρος Avrami (n_A).

Τα υαλοκεραμικά υλικά παρήχθησαν με μεθόδους τεχνολογίας κόνεων (κονιομεταλλουργικά) με πυροσυσσωμάτωση και ελεγχόμενη κρυστάλλωση δοκιμίων κόνεων υαλοθραυσμάτων (που παρασκευάστηκαν με συμπίεσή τους σε καλούπι στα 150 - 200 bar και διαστάσεις που ορίζονται στο πρότυπο ISO 6872 “Dentistry - Ceramic Materials”). Με σκοπό να διασφαλιστεί επιτυχής πυροσυσσωμάτωση και μετά κρυστάλλωση, η θερμική κατεργασία σχεδιάστηκε σύμφωνα με τα αποτελέσματα της θερμικής ανάλυσης. Τα παραχθέντα υαλοκεραμικά χαρακτηρίστηκαν πλήρως με κρυσταλλογραφική ανάλυση με περίθλαση ακτίνων X (XRD), με παρατήρηση της μικροδομής τους σε ηλεκτρονικό μικροσκόπιο με στοιχειακό αναλυτή (SEM/EDS) για ταυτοποίηση των κρυστάλλων και με πειραματικό προσδιορισμό των τιμών των φυσικών και των μηχανικών ιδιοτήτων τους, όπως είναι η πυκνότητα, η γραμμική συστολή τους κατά τη θερμική κατεργασία τους, και το χρώμα τους, καθώς η αντοχή σε κάμψη τριών σημείων, το μέτρο ελαστικότητας (E), η σκληρότητα (κατά Vickers, HV), και ο συντελεστής δυσθραυστότητας (K_{IC}), αντίστοιχα. Για τον έλεγχο της βιοενεργότητας, υαλοκεραμικά (σε μορφή πυροσυσσωματωμένων δοκιμίων αλλά και σε μορφή λεπτόκκοκης σκόνης) εμβαπτίστηκαν σε προσομοιωμένο υγρό ανθρώπινου σώματος (SBF) για 7, 14 και 21 ημέρες, στους 37 °C. Στα χρονικά αυτά διαστήματα έγινε δειγματοληψία και στα ληφθέντα δείγματα έγινε έλεγχος σχηματισμού ή μη βιοενεργής επιφάνειας υδροξυαπατίτη, έμμεσα, με προσδιορισμό του pH του διαλύματος, και άμεσα, με περίθλαση ακτίνων X (XRD) και με ηλεκτρονική μικροσκοπία σάρωσης με στοιχειακή ανάλυση (SEM/EDX) στις επιφάνειες των υαλοκεραμικών.

ΑΠΟΤΕΛΕΣΜΑΤΑ

Σε ό,τι αφορά στις συστάσεις που αναπτύχθηκαν για την κατασκευή υαλοκεραμικών υλικών με σκοπό την εφαρμογή τους σε οδοντικά εμφυτεύματα, τα πειραματικά αποτελέσματα συνοψίζονται ως ακολούθως. Οι θερμοκρασίες T_g, T_c και T_p, καθώς και οι τιμές της ενέργειας ενεργοποίησης (E_a) της κρυστάλλωσης, μετά την πλήρη υποκατάσταση του Na_2O από K_2O παρουσίασαν σημαντική αύξηση, ενώ μετά από μερική υποκατάσταση του CaO από MgO οι τιμές των αντίστοιχων θερμοκρασιών και της ενέργειας ενεργοποίησης, είτε παρέμειναν στα ίδια επίπεδα, είτε παρουσίασαν μικρή αύξηση. Μετά από προσθήκη 1 mol% Al_2O_3, οι τιμές των θερμοκρασιών T_g, T_c και T_p, αλλά και οι τιμές της $E_α$ παρουσίασαν σημαντική αύξηση. Όσον αφορά στις τιμές της παραμέτρου n_A, αυτές έδειξαν ότι σε ορισμένες από τις παραχθείσες υάλους (1d, 1d-k, 1d-m, 1e, 1e-m και 1e/A_1) λαμβάνει χώρα τρισδιάστατη ανάπτυξη των κρυστάλλων ($n_A \geq 3$), ενώ σε άλλες (1d/A_1, 1d-k/A_1, 1d-m/A_1, 1e-k, 1e-k/A_1 και 1e-m/A_1) προβλέπεται δισδιάστατη ανάπτυξη ($n_A \leq 2$). Με βάση τα αποτελέσματα της θερμικής ανάλυσης, η επιλογή των θερμοκρασιών θερμικής κατεργασίας των δοκιμίων των υάλων για την κατασκευή των υαλοκεραμικών υλικών ήταν 900 °C για τα δοκίμια με πλήρη υποκατάσταση του Na_2O από K_2O, 850 °C για τα δοκίμια με μερική υποκατάσταση του CaO από MgO, και 900 °C για τα δοκίμια με K και με προσθήκη Al_2O_3 (1 mol%), ή 850 °C για τα αντίστοιχα δοκίμια με 1% αλούμινα αλλά χωρίς K. Η κρυσταλλογραφική ανάλυση των υαλοκεραμικών υλικών που παρήχθησαν με περίθλαση ακτίνων-X και η παρατήρηση της μικροδομής τους σε ηλεκτρονικό μικροσκόπιο σάρωσης με συνδυασμό στοιχειακής ανάλυσης (SEM/EDS) έδειξαν κρυστάλλωση διοψίτη, γουολαστονίτη, και φθοριοαπατίτη (στα δοκίμια που περιείχαν K, αντί για γουολαστονίτη, ανιχνεύτηκε α-PMS). Οι τιμές των μηχανικών ιδιοτήτων των υαλοκεραμικών κυμαίνονταν σε επιθυμητά επίπεδα, σύμφωνα με τους αρχικούς στόχους, δηλαδή, μέσω των υποκαταστάσεων, να προσεγγιστούν οι τιμές των φυσιολογικών ιστών. Πιο συγκεκριμένα, η τιμή της αντοχής σε κάμψη τριών σημείων ήταν μεταξύ 107 - 177 MPa, του μέτρου ελαστικότητας μεταξύ 22 - 34 GPa, η τιμή του συντελεστή δυσθραυστότητας K_{IC} ήταν από 1.40 έως 2.5 MPa·$m^{0.5}$ και η σκληρότητα Vickers ήταν 5.2 - 6.7 GPa. Ο *in vitro* έλεγχος των υαλοκεραμικών υλικών με εμβάπτιση σε προσομοιωμένο υγρό ανθρώπινου σώματος (SBF) στους 37 °C, έδειξε ικανότητα αυθόρμητου σχηματισμού βιοενεργής επιφάνειας από υδροξυαπατίτη στην επιφάνειά τους από την πρώτη εβδομάδα της εμβάπτισης.

Σε ό,τι αφορά στις συστάσεις με προσθήκη 7-8 mol% Al_2O_3 που αναπτύχθηκαν για την κατασκευή υαλοκεραμικών υλικών με σκοπό την εφαρμογή τους σε ακίνητες ολοκεραμικές προσθετικές αποκαταστάσεις, τα πειραματικά αποτελέσματα συνοψίζονται ως ακολούθως. Οι τιμές των θερμοκρασιών T_g, T_c και T_p, αυξήθηκαν με την προθήκη 7-8% Al_2O_3. Σε ότι αφορά τις τιμές της E_a της κρυστάλλωσης, αυτές μετά την πλήρη υποκατάσταση του Na_2O από K_2O παρουσίασαν μικρή αύξηση, ενώ μετά από μερική υποκατάσταση του CaO από MgO οι τιμές της ενέργειας ενεργοποίησης παρουσίασαν μείωση. Οι τιμές της παραμέτρου n_A έδειξαν ότι απουσία K, στις υάλους των συστάσεων αυτών λαμβάνει χώρα τρισδιάστατη ανάπτυξη των κρυστάλλων ($n_A \geq 3$), ενώ στις υάλους με K, δισδιάστατη ανάπτυξη ($n_A \leq 2$). Με βάση τα αποτελέσματα της θερμικής ανάλυσης, επιλέχθηκε η θερμοκρασία των 900 °C για τη θερμική επεξεργασία τους για την κατασκευή των τελικών υαλοκεραμικών υλικών. Η κρυσταλλογραφική ανάλυση των υαλοκεραμικών με περίθλαση ακτίνων X (XRD) και η παρατήρηση της μικροδομής τους σε ηλεκτρονικό μικροσκόπιο σάρωσης σε συνδυασμό με στοιχειακή ανάλυση (SEM/EDS), έδειξαν κρυστάλλωση διοψίτη, μελελίτη και γκελενίτη. Οι τιμές των μηχανικών ιδιοτήτων τους κυμαίνονταν πολύ κοντά στις αντίστοιχες τιμές της φυσικής αδαμαντίνης και οδοντίνης. Συγκεκριμένα, η τιμή της αντοχής σε κάμψη ήταν 120 - 171 MPa, του μέτρου ελαστικότητας μεταξύ 28 και 42 GPa, του συντελεστή δυσθραυστότητας K_{IC} από 2.6 έως 2.8 MPa·$m^{0.5}$ και της σκληρότητας Vickers 6.3 – 7.0 GPa. Έτσι, σύμφωνα με το πρότυπο ISO 6872 “Dentistry-Ceramic Materials”, τα παραχθέντα αυτά υαλοκεραμικά μπορούν να χρησιμοποιηθούν ως ολοκεραμικά υλικά της αισθητικής οδοντιατρικής, και συγκεκριμένα ως υλικά επικάλυψης μετάλλων ή κεραμικών υποστρωμάτων στην περίπτωση μεμονωμένων προσθετικών αποκαταστάσεων προσθίων ή οπίσθιων δοντιών, ως υλικά κατασκευής όψεων, ενθέτων και επενθέτων, αλλά και στην κατασκευή κεραμικών υποστρωμάτων προσθίων ή οπίσθιων δοντιών. Τα παραπάνω υποστηρίζονται από το γεγονός ότι, μετά από *in vitro* έλεγχο των υαλοκεραμικών αυτών με εμβάπτιση σε προσομοιωμένο υγρό ανθρώπινου σώματος (SBF) στους 37 °C, τα δείγματα καταστέλλουν πλήρως το σχηματισμό βιοενεργής επιφάνειας υδροξυαπατίτη, ακόμα και μετά από 1 μήνα εμβάπτισης.

ΣΥΜΠΕΡΑΣΜΑΤΑ

Στα διδακτορική αυτή διατριβή, με στόχο την, εν δυνάμει, επίτευξη εφαρμογής των νέων συστάσεων που αναπτύχθηκαν στις παραπάνω δύο οδοντιατρικές εφαρμογές (οδοντικά εμφυτεύματα και ακίνητες ολοκεραμικές προσθετικές αποκαταστάσεις), ερευνήθηκε η, μέσω διαφόρων υποκαταστάσεων, όσο το δυνατόν καλύτερη προσέγγιση των μηχανικών ιδιοτήτων των παραχθέντων υαλοκεραμικών υλικών (δηλαδή, αντοχή σε κάμψη, μέτρο ελαστικότητας, σκληρότητα και δυσθραυστότητα) στις αντίστοιχες ιδιότητες του οστού της γνάθου αλλά και των σκληρών οδοντικών ιστών, της αδαμαντίνης και της οδοντίνης.

Σε ότι αφορά στα υλικά που παράχθηκαν για εν δυνάμει χρήση τους ως υλικά κατασκευής βιοενεργών οδοντικών εμφυτευμάτων, τα αποτελέσματα έδειξαν ότι από τις συστάσεις των υάλων με πλήρη υποκατάσταση του Na_2O από K_2O, με μερική υποκατάσταση του CaO από MgO, και με προσθήκη 1 mol% Al_2O_3, μπορούν να παραχθούν υαλοκεραμικά υλικά με ιδιότητες που ικανοποιούν τα κριτήρια πρόκρισης για περεταίρω θεώρηση και πειραματικό έλεγχο για τη συγκεκριμένη οδοντιατρική εφαρμογή.

Η αξιολόγηση των υαλοκεραμικών υλικών που κατασκευάστηκαν αναφορικά με την πιθανή χρήση τους ως υλικά κατασκευής ακίνητων ολοκεραμικών (βιοαδρανών) προσθετικών αποκαταστάσεων, έγινε λαμβάνοντας υπόψη τα κατώτερα επιτρεπτά όρια αντοχής σε κάμψη και δυσθραυστότητας που ορίζει το πρότυπο ISO 6872 "Dentistry - Ceramic Materials". Έτσι, τα αποτελέσματα της διατριβής αυτής οδηγούν στο συμπέρασμα ότι τα υαλοκεραμικά υλικά με συστάσεις με προσθήκη Al_2O_3 σε ποσοστό 7-8 mol% ικανοποιούν τα κριτήρια για να προκριθούν για τη συγκεκριμένη οδοντιατρική εφαρμογή, δηλαδή, να προταθούν για να χρησιμοποιηθούν ως υλικά επικάλυψης μετάλλων ή κεραμικών υποστρωμάτων στην περίπτωση μεμονωμένων προσθετικών αποκαταστάσεων προσθίων ή οπίσθιων δοντιών, ως υλικά κατασκευής όψεων, ενθέτων και επενθέτων, ή στην κατασκευή κεραμικών υποστρωμάτων προσθίων ή οπίσθιων δοντιών.

LIST OF TABLES

Table 1. Effect of oxides and a fluoride on glass and GC properties. *49*

Table 2. Values of Avrami parameter (n and m) for various crystallization mechanisms and growth dimensionality of crystals [24, 27]. *54*

Table 3. Various systems of GCs studied by teams of researchers, proposed as potential materials for biomedical applications [4]. *57*

Table 4. Mechanical properties of cortical bone, trabecular bone, and dentine [19, 38, 61, 62]. *61*

Table 5. Mechanical properties of commonly used dental implant materials [44]. *64*

Table 6. **(A)** Mechanical properties of human enamel and dentine [19, 55, 66-68, 81, 84]. **(B)** Classification of ceramics for fixed prostheses by intended clinical use, with the recommended flexural strength and fracture toughness values, according to the **ISO 6872** [85]. *67*

Table 7. Mechanical properties of commercial GCs [19, 68, 87, 88]. *68*

Table 8. Glass compositions (in wt.%) of the previous works, which led to the bioactive glasses 1d and 1e. *78*

Table 9. The investigated (Al_2O_3-free) compositions (in wt.%). *79*

Table 10. Modified alumina containing glass investigated compositions (in wt.%). For comparison purposes, the compositions of the parent Al_2O_3–free glasses from Table 9, are also presented. *81*

Table 11. Mean values (and standard deviation; n = 3) of glass transition temperature (T_g), oncet crystallization temperature (T_c), crystallization temperature (T_p), and liquidus temperature T_l, determined by the thermographs of Fig 20. The sintering window is also (T_c - T_g) is also presented. *98*

Table 12. Mean values (and standard deviation; n = 3) of activation energy (E_a) of crystallization, and Avrami exponent (n_A) of the investigated glasses 1d and 1e. *99*

Table 13. Mean values (and standard deviation, n = 5) of linear shrinkage and density of the parent annealed glasses and investigated GCs 1d and 1e heat-treated at various temperatures for 1 h. *100*

Table 14. Mean values (and standard deviation, n = 10) of the mechanical properties of the investigated GCs 1d and 1e, heat-treated at various temperatures for 1 h. *103*

Table 15. Elemental analysis (in atomic %) of the GC 1d and molar Ca/P ratio for 7, 14 and 21 days soaking in SBF. *106*

Table 16. Elemental analysis (in atomic %) of the GC 1e and molar Ca/P ratio for 7, 14 and 21 days soaking in SBF. *107*

Table 17. Mechanical properties of the produced GCs 1d and 1e, cortical bone, and dentine. *108*

Table 18. Mean values (and standard deviation; n = 3) of glass transition temperature (T_g), oncet crystallization temperature (T_c), crystallization temperature (T_p), liquidus temperature T_l of the modified glasses (determined by the DCS thermographs of Fig. 30). The sintering window (T_c-T_g) is also presented. *110*

Table 19. Mean values (and standard deviation; n = 3) of activation energy (E_a) of crystallization and Avrami exponent (n_A) of the modified glasses. *111*

Table 20. Mean values (and standard deviation, n = 5) of linear shrinkage and density of the investigated GCs. (The SD of density values was < 5%). *112*

Table 21. Mean values (and standard deviation, n = 10) of the mechanical properties of the investigated GCs, heat-treated at 850 °C (for 1d-m and 1e-m) and 900 °C (for 1d-k and 1e-k) temperatures for 1 h. *115*

Table 22. Elemental analysis (in atomic %) of surface of the GC 1d-k and molar Ca/P ratio for 7, 14, and 21 days soaking in SBF. *117*

Table 23. Elemental analysis (in atomic %) of surface of the GC 1d-m and molar Ca/P ratio for 7, 14, and 21 days soaking in SBF. *118*

Table 24. Elemental analysis (in atomic %) of surface of the GC 1e-k and molar Ca/P ratio for 7, 14, and 21 days soaking in SBF. *119*

Table 25. Elemental analysis (in atomic %) of surface of the GC 1e-m and molar Ca/P ratio for 7, 14, and 21 days soaking in SBF. *120*

Table 26. Mechanical properties of dentine and cortical jaw bone. The data were extracted from Table 17. *122*

Table 27. Mean values (and standard deviation; n = 3) of glass transition temperature (T_g), oncet crystallization temperature (T_c), and crystallization temperature (T_p) of the Al_2O_3- containing (1 mol%) glasses (determined by the DCS measurements). The sintering window (T_c-T_g) is also presented. *124*

Table 28. Mean values (and standard deviation; n = 3) of the activation energy (E_a) of crystallization, and Avrami exponent (n_A) of the investigated Al_2O_3-containing (1 mol%) glasses (determined by the DCS measurements). *125*

Table 29. Mean values (and standard deviation, n = 5) of linear shrinkage and density of the Al_2O_3-containing (1 mol%) glasses and GCs heat-treated at 850 °C (1d/A_1, 1d-m/A_1, 1e/A_1, 1e-m/A_1) and 900 °C (1d-k/A_1 and 1e-k/A_1) for 1 h. (The SD of density values was < 5%). *126*

Table 30. Mean values (and standard deviation, n = 10) of the mechanical properties of the Al_2O_3-containing (1 mol%) GCs, heat-treated at 850 °C (K-free GCs) and 900 °C (K-containing GCs) for 1 h. *129*

Table 31. Elemental analysis (in atomic %) of the surface of the GC 1d/A_1 and molar Ca/P ratio for 7, 14, and 21 days soaking in SBF. *131*

Table 32. Elemental analysis (in atomic %) of the surface of the GC 1d-k/A_1 and molar Ca/P ratio for 7, 14, and 21 days soaking in SBF. *132*

Table 33. Elemental analysis (in atomic %) of the surface of the GC 1d-m/A_1 and molar Ca/P ratio for 7, 14, and 21 days soaking in SBF. *133*

Table 34. Elemental analysis (in atomic %) of the surface of the GC 1e/A_1 and molar Ca/P ratio for 7, 14, and 21 days soaking in SBF. *134*

Table 35. Elemental analysis (in atomic %) of the surface of the GC 1e-k/A_1 and molar Ca/P ratio for 7, 14, and 21 days soaking in SBF. *135*

Table 36. Elemental analysis (in atomic %) of the surface of the GC 1e-m/A_1 and molar Ca/P ratio for 7, 14, and 21 days soaking in SBF. *136*

Table 37. Mechanical properties of dentine and cortical jaw bone (it is the same table with the Table 26 but it is repasted here in order to help the reader to immediately compare the mechanical property of the natural tooth tissues with those reported in Figs. 55 and 56). *138*

Table 38. Mean values (and standard deviation; n = 3) of glass transition temperature (T_g), oncet crystallization temperature (T_c), sintering window (T_c-T_g), and crystallization temperature (T_p) of the investigated glasses, which contain 7-8 mol% Al_2O_3. *140*

Table 39. Mean values (and standard deviation; n = 3) of activation energy (E_a), and Avrami exponent (n_A) of the investigated glasses, which contain 7-8 mol% Al_2O_3. *141*

Table 40. Mean values (and standard deviation, n = 5) of linear shrinkage and density of the Al_2O_3-containing (7-8 mol%) glasses and GCs heat-treated at 900 °C for 1 h. (The SD of density was < 5%). *142*

Table 41. Mean values (and standard deviation, n = 10) of the mechanical properties of the Al_2O_3-containg (7-8 mol%) GCs produced after heat-treatment at 900 °C for 1h. *145*

Table 42. Mechanical properties of human dentine and enamel. The data were extracted from Table 17. *147*

LIST OF FIGURES

Figure 1. (a) Temperature-volume diagram, where two ways of solidification are presented. (b) Schematic of DSC trace of a glass, showing glass transition temperature (T_g), crystallization onset temperature (T_c), crystallization peak temperature (T_p), as well as the liquidus temperature (T_l) [3, 5]. *46*

Figure 2. Two-dimensional representation of network structure of (a) vitreous silica, (b) crystalline silica, and (c) vitreous silicate. (BO: bridging oxygen, NBO: non-bridging oxygen, R: stands for a generic network modifier cation) [1]. *48*

Figure 3. The stages of the production of GCs by the glass melting method. *50*

Figure 4. GCs produced from powdered glass. (a) Powdered glass compact, (b) sintering (densification) and crystallization, and (c) the dense crystallized microstructure of GC [4]. *51*

Figure 5. Two-steps heat-treatment process for production of GC materials. *52*

Figure 6. From glass to GC: (a) nuclei formation, (b) crystal growth, (c) GC microstructure [4]. *52*

Figure 7. One-step heat-treatment process for production of GC materials. *52*

Figure 8. Schematic representation of the mechanism of apatite formation on the surface of a bioactive glass [4, 40]. *56*

Figure 9. Number of publications (papers, books, and conference papers) per year extracted from the Scopus database by searching the keywords (a) “bio + glass-ceramic”, and (b) “bioactive + glass-ceramic” in the publication title (blue) and also in the title, abstract and keywords (red) [18]. *57*

Figure 10. (a) Cortical and trabecular bone [49], (b) illustration of a cross-section mandibular cortical and trabecular bone [48], and (c) trabecular bone. *59*

Figure 11. (a) The structure of human tooth; on the left-hand side of the figure, the microstructure of enamel (enamel rods; mag x1000, 10 µm), dentine (dentinal tubule; mag x2000, 50 µm), and cementum (mag x1000, 10 µm) is shown [55]. (b) Tooth incision, showing the extent of dentine in the crown and the root of the tooth (E: enamel, and D: dentine) [59]. *60*

Figure 12. Titanium dental implant [70]. *63*

Figure 13. Zirconia dental implant. The space between the dental implant and bone is getting bigger over implantation time, as a result of chemical degradation of ceramic implant [70]. *64*

Figure 14. (a) Number of scientific publications (papers, books, and conference papers), and (b) number of granted patents related to dental glass-ceramics per year, extracted from the Scopus database by searching the keywords “dental glass-ceramic”, or “teeth glass-ceramic”, or “tooth glass-ceramic” [19]. *69*

Figure 15. Al_2O_3 addition depends on the clinical application. *80*

Figure 16. The processes of (a) decarbonization, and (b) glass melting and production in bulk and frit forms along with the corresponding appearance of the samples. *88*

Figure 17. The heat-treatment process to prepare the GCs along with the appearance of the samples before (glass powder compact) and after the heat-treatment (final GC bar). *89*

Figure 18. Outline of the experimental procedure. *93*

Figure 19. Dilatation curves of bulk annealed glasses (a) 1d, and (b) 1e. The graphical estimation of T_g and T_s is shown (the software of the dilatometry equipment used in this work automatically estimates T_g and T_s through this method). *97*

Figure 20. Thermographs of the investigated glasses (corresponding to the glass (a) 1d and (b) 1e at heating rate of 15 K/min). The insets show the measurement of the full width at the half maximum of the crystallization peak. The graphical estimation of T_g, T_c, T_p and T_l is shown (the software of the equipment used in this work automatically estimates these temperatures through this method). The results are summarized in Table 11 from 3 independent measurements. *98*

Figure 21. The plots of $\ln((T_p^2)/\varphi)$ *vs* $1000/T_p$ for the glasses 1d and 1e. *99*

Figure 22. Well-sintered dense 1d and 1e GC bars of white colour. *100*

Figure 23. X-ray diffractograms of glass-powder compacts (a) 1d and (b) 1e heat-treated at various temperatures for 1 h. The standard patterns of diopside ($CaMgSi_2O_6$), fluorapatite ($Ca_{10}(PO_4)_6F_2$) and wollastonite ($CaSiO_3$) are plotted at the bottom of the diagrams. *101*

Figure 24. Typical microstructure of the produced GCs 1d and 1e, heat-treated at 850 °C, for 1 h, observed after etching of polished surfaces with 2% HF solution. (D: diopside; FA: fluorapatite; W: wollastonite). *102*

Figure 25. Evolution of pH of the solution over immersion time of the GC powders 1d and 1e in SBF (at 37 °C). *104*

Figure 26. X-ray diffractograms of the powders of the investigated GCs 1d and 1e immersed in SBF for 7, 14, and 21 days at 37 °C. *105*

Figure 27. Formation and evolution of HA layer on the 1d GC surface at various immersion periods of time in SBF at 37 °C (7, 14 and 21 days). *106*

Figure 28. Formation and evolution of HA layer on the 1e GC surface at various immersion periods of time in SBF at 37 °C (7, 14 and 21 days). *107*

Figure 29. Dilatation curves of the bulk annealed glasses (a) 1d-k, 1d-m and (b) 1e-k, and 1e-m. *109*

Figure 30. Thermographs of the modified glasses (heating rate of 15 K/min). The results from 3 independent measurments are summarized in Table 18. *110*

Figure 31. Plots of $\ln((T_p^2)/\varphi)$ *vs* $1000/T_p$, of the investigated glasses 1d-k, 1d-m, 1e-k, and 1e-m. *111*

Figure 32. Well-sintered dense 1d-m, 1d-k, 1e-m, and 1e-k GC bars of white colour. *112*

Figure 33. X-ray diffractograms of the modified GCs heat-treated at 850 (1d-m and 1e-m) or 900 °C (1d-k and 1e-k) for 1 h. Diopside ($CaMgSiO_6$, 01-071- *113*

1067); Wollastonite ($CaSiO_3$, 00-042-0550); Fluorapatite ($Ca(PO_4)_3F$, 04-008-0676); alpha-potassium magnesium silicate ($K_2MgSi_3O_8$, 00-019-0973).

Figure 34. Typical microstructures of the produced GCs at 850 °C (1d-m, 1e-m) or 900 °C (1d-k, 1e-k), observed after etching of polished surfaces with 2% HF solution. *114*

Figure 35. Evolution of pH of the solution over immersion time of the GC powders in SBF (at 37 °C). *115*

Figure 36. X-ray diffractograms of the powders of the modified GCs immersed in SBF for 7, 14, and 21 days at 37 °C. *116*

Figure 37. Formation and evolution of HA layer on the 1d-k GC surfaces over immersion time in SBF at 37 °C (7, 14, and 21 days). *117*

Figure 38. Formation and evolution of HA layer on the 1d-m GC surfaces over immersion time in SBF at 37 °C (7, 14, and 21 days). *118*

Figure 39. Formation and evolution of HA layer on the 1e-k GC surfaces over immersion time in SBF at 37 °C (7, 14, and 21 days). *119*

Figure 40. Formation and evolution of HA layer on the 1e-m GC surfaces over immersion time in SBF at 37 °C (7, 14, and 21 days). *120*

Figure 41. Influence of the substitutions of Mg for Ca and of K for Na in the compositions 1d and 1e on the mechanical properties (flexural strength, σ; modulus of elasticity, E; Vickers microhardness, HV; and fracture toughness, K_{IC}) of the produced GCs, 1d-k, 1d-m, 1e-k, and 1e-m. *121*

Figure 42. Dilatation curves of bulk annealed glasses, which contain 1 mol% Al_2O_3. *123*

Figure 43. Thermographs of the Al_2O_3-containing (1 mol%) glasses (a) 1d/A_1, 1d-k/A_1, 1d-m/A_1 and (b) 1e/A_1, 1e-k/A_1, 1e-m/A_1(the heating rate was 15 K/min). *124*

Figure 44. The plots of $\ln((T_p^2)/\varphi)$ *vs* $1000/T_p$ for Al_2O_3-containing (1 mol%) glasses, (a) 1d/A_1, 1d-k/A_1, 1d-m/A_1, and (b) 1e/A_1, 1e-k/A_1, 1e-m/A_1. *125*

Figure 45. Well-sintered dense GC bars of white colour, which contain 1 mol% Al_2O_3. *126*

Figure 46. X-ray diffractograms of the Al_2O_3-containing (1 mol%) GCs heat-treated at 850 (K-free GCs) or 900 °C (K-containing GCs) for 1 h. Diopside ($CaMgSiO_6$, 01-071-1067); wollastonite ($CaSiO_3$, 00-042-0550); fluorapatite ($Ca(PO_4)_3F$, 04-008-0676); alpha-potassium magnesium silicate ($K_2MgSi_3O_8$, 00-019-0973). *127*

Figure 47. Typical microstructures of the Al_2O_3-containing (1 mol%) GCs produced at 850 °C (K-free GCs) or 900 °C (K-containing GCs) observed after etching of polished surfaces with 2% HF solution. D: diopside ($CaMgSiO_6$); W: wollastonite ($CaSiO_3$); F: fluorapatite ($Ca(PO_4)_3F$); α-PMS: alpha-potassium magnesium silicate ($K_2MgSi_3O_8$). *128*

Figure 48. Evolution of pH of the solution over immersion time of the Al_2O_3-containing (1 mol%) GC powders in SBF (at 37 °C). *130*

Figure 49. Formation and evolution of HA layer on the surface of the GC 1d/A_1 over immersion time in SBF at 37 °C (7, 14, and 21 days). *131*

Figure 50. Formation and evolution of HA layer on the surface of the GC 1d-k/A_1 over immersion time in SBF at 37 °C (7, 14, and 21 days). *132*

Figure 51. Formation and evolution of HA layer on the surface of the GC 1d-m/A_1 over immersion time in SBF at 37 °C (7, 14, and 21 days). *133*

Figure 52. Formation and evolution of HA layer on the surface of the GC 1e/A_1 over immersion time in SBF at 37 °C (7, 14, and 21 days). *134*

Figure 53. Formation and evolution of HA layer on the surface of the GC 1e-k/A_1 over immersion time in SBF at 37 °C (7, 14, and 21 days). *135*

Figure 54. Formation and evolution of HA layer on the surface of the GC 1e-m/A_1 over immersion time in SBF at 37 °C (7, 14, and 21 days). *136*

Figure 55. Influence of 1 mol% Al_2O_3 addition on the mechanical properties (flexural strength, σ; modulus of elasticity, E; Vickers microhardness, HV; and fracture toughness, K_{IC}) of the produced GCs 1d/A_1, 1d-k/A_1 and 1d-m/A_1. *137*

Figure 56. Influence of 1 mol% Al_2O_3 addition on the mechanical properties (flexural strength, σ; modulus of elasticity, E; Vickers microhardness, HV; and fracture toughness, K_{IC}) of the produced GCs 1e/A_1, 1e-k/A_1 and 1e-m/A_1. *138*

Figure 57. Dilatation curves of bulk annealed glasses (a) 1d/A_2, 1d-k/A_2, 1d-m/A_2 and (b) 1e/ A_2, 1e-k/A_2, 1e-m/A_2. *139*

Figure 58. Thermographs of the Al_2O_3-containing (7-8 mol%) glasses (a) 1d/A_2, 1d-kA_2, 1d-m/A_2, and (b) 1e/A_2, 1e-k/A_2, 1e-m/A_2. The heating rate was 20 K/min. *140*

Figure 59. The plots of $\ln((T_p^2)/\varphi)$ *vs* $1000/T_p$ of the Al_2O_3-containing (7-8 mol%) glasses (a) 1d/A_1, 1d-kA_1, 1d-m/A_1, and (b) 1e/A_1, 1e-k/A_1, 1e-m/A_1. *141*

Figure 60. Well-sintered dense Al_2O_3-containing (7-8 mol%) GC bars of white colour, after heat-treatment at 900 °C. *142*

Figure 61. X-ray diffractograms of the produced Al_2O_3-containing (7-8 mol%) GCs heat-treated at 900 °C for 1 h. Diopside ($CaMgSiO_6$, 01-086-0932); Melilite $Ca_4Al_2MgSi_3O_{14}$, 04-007-7342); Gehlenite ($Ca_2Al(AlSiO_7)$, 01-079-1725). *143*

Figure 62. Characteristic microstructures of the Al_2O_3-containing (7-8 mol%) GCs produced after heat-treatment of glass-powder compacts at 900 °C for 1h, observed after etching of polished surfaces with 2% HF solution. D: diopside ($CaMgSiO_6$); G: Gehlenite ($Ca_2Al(AlSiO_7)$; M: melilite ($Ca_4Al_2MgSi_3O_{14}$). *144*

Figure 63. Influence of 7-8 mol% Al_2O_3 addition on the mechanical properties (flexural strength, σ; modulus of elasticity, E; Vickers microhardness, HV; and fracture toughness, K_{IC}) of the produced GCs 1d/A_2, 1d-k/A_2, and 1d-m/A_2. *144*

Figure 64. Influence of 7-8 mol% Al_2O_3 addition on the mechanical properties (flexural strength, σ; modulus of elasticity, E; Vickers microhardness, HV; and fracture toughness, K_{IC}) of the produced GCs 1e/A_2, 1e-k/A_2, and 1e-m/A_2. *147*

Figure 65. Phase diagrams of (a) the SiO_2-MgO-CaO and (b) the SiO_2-Al_2O_3-CaO ternary systems [4]. *161*

Figure 66. A typical (as-recorded) plot of F (N) *vs* displacement (mm) of the investigated samples (dimensions: 35x3x4 mm^3, according to ISO 6872) *163* from 3-point bending strength experiments (head speed = 1 mm/min) (this curve is from the sample 1d heat-treated at 850 ^{o}C for 1 h). The inset shows the linear region of the curve.

Figure 67. (a) Vickers pyramid diamond indenter indentation, (b) Palmqvist and median crack geometries, propagated from the corners of Vickers indentation, and (c) a typical (as-recorded) result of Vickers measurements on the investigated samples by applying a load of 500 g (or 4.9 N) for 30 s. (This indentation is from the sample 1d heat-treated at 850 ^{o}C for 1 h). The Palmqvist crack length of 2a and l (i.e. $0.25 < l/a < 2.5$), are marked. *164*

Figure 68. Comparison of the mean values (and standard deviation, n = 3) of T_g, T_c, T_p temperatures, along with the sintering window ($T_c - T_g$) of the all the investigated glasses. Influence of (a) K_2O and MgO substutions for Na_2O and CaO, respectively, in the parent glasses 1d and 1e, (b) 1 mol% Al_2O_3 addition, and (c) 7-8 mol% Al_2O_3 addition in the Al_2O_3-free glasses on the above temperatures. *166*

Figure 69. Mean values (and standard deviation, for n = 10) of the mechanical properties of (a) flexural strength (σ), (b) modulus of elasticity (E), (c) Vickers microhardness (HV), and (d) fracture toughness (K_{IC}) of the produced bioactive GCs. The influence of 1 mol% Al_2O_3 addition on the mechanical properties compared to the properties of the Al_2O_3-free GCs is shown, and these properties are compared to the mechanical properties of natural tissues as well as the properties of the common dental implant biomaterials of Ti-alloys and zirconia. *168*

A. Introduction

***1.** Glass-ceramic (GC) materials*

***2.** Glass-ceramics (GCs) in dental applications*

INTRODUCTION

This Thesis focuses its interest on *glass-ceramic* (GC) materials, which aim at being used in *dental applications*. Hence, the present section of Introduction aims at introducing the reader to the research undertaken, as described in the next sections of the aim of the work, the synthesis and the characterization of the produced materials, and the experimental findings along with their discussion. Accordingly, the introduction section substantially shed light research on two main directions related (a) to the GC materials (section 1), which is divided in the sub-directions of their *composition* (section 1.1), and their *thermal- (heat-) treatment* (section 1.2), and (b) the *biomedical* aspect of GCs (section 2), which, after a general introduction of the reader on the use of GCs in biomedicine (section 2.1), is divided in the sub-directions of the particular distinct applications, specifically the *dental implants* (section 2.2), and the *dental fixed all-ceramic prosthetic restorations* (section 2.3). As far as the later sections are concerned (2.2 and 2.3), the necessary relevant information, related to the physiology of the natural teeth and their environment in the body (such as morphological features along with aspects related to biomedical engineering and biomechanics) are provided. According to the modern aspects for developing biomaterials, this perspective is very important. More specifically, in the beginning (mainly around 60s'), biomaterials merely had to feature no toxicity, biocompatibility, bio-acceptability and bio-tolerance. In 70s and 80s, bioactivity had been the principal goal, where the highest performance (e.g. highest chemical and biological bioactivity, highest mechanical properties) was the main aim for developing novel biomaterials. Nowadays, the best biomaterial is the one that is the best possible match (chemically, mechanically, morphologically, aesthetically in the case of teeth) to the natural tissue that aims to replace. This is mostly well achieved in bone or other grafts (e.g. skin, soft tissues), but there is a rather poor progress in dental materials, where the strongest material is still considered to be the best. Consequently, the aspect of achieving the best possible matching between the produced GC materials and the natural tooth tissues is the main novelty in this Thesis, and hence, special emphasis is given to this aspect in this Instruction section and throughout the entire text.

1. Glass-ceramic (GC) materials

GC materials were discovered by Stookey at Corning Inc., USA, in 1953, and can be considered as a combination of a glass with a ceramic [1-4]. GCs are polycrystalline materials, derived from the controlled crystallization of parent a glass, resulting in a final material containing one or more crystalline phases embedded in residual glass, depending on the parent glass composition and the heat-treatment schedule [1-3, 4].

The discovery of the GCs itself immediately reveals the direct relationship between GCs and the parent glasses, which obviously deals with the chemical composition of the glass, but also the way that they were discovered i.e. through heat-treatment [1, 3, 4]. It is important to note that in the production of GC materials the heat-treatment schedule plays an important role, which obviously needs to be done in a controlled way, so that there is a control over sintering and crystallization processes [3, 4, 5]. This relationship between the parent glass and the produced GC, which is bridged with the heat-treatment procedure, is shown in Fig. 1.

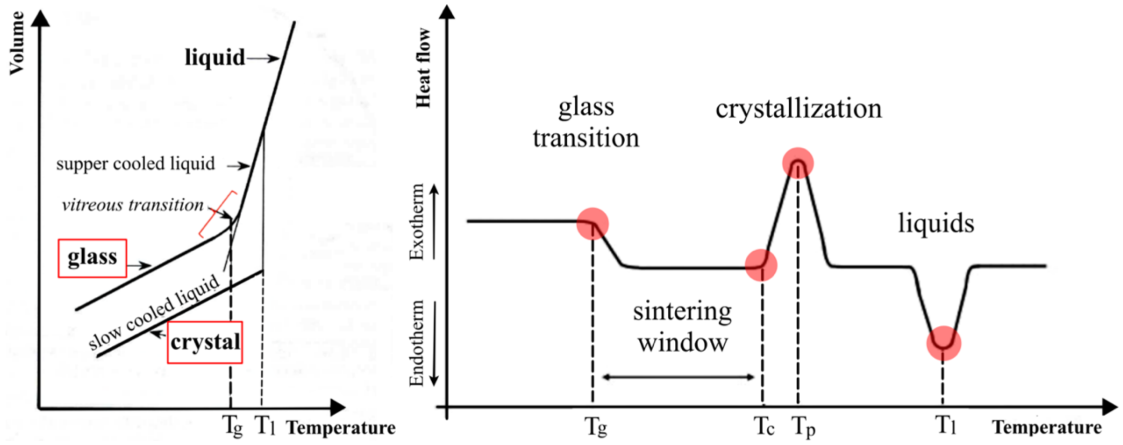

(a) (b)

Figure 1. (a) Temperature-volume diagram, where two ways of solidification are presented. (b) Schematic of DSC trace of a glass powder, showing glass transition temperature (T_g), crystallization onset temperature (T_c), crystallization peak temperature (T_p), as well as the liquidus temperature (T_l) [3, 5].

More specifically, the diagram of Fig. 1(a) shows the volume-temperature diagram where two different ways of solidifying a liquid material are represented. In the case of GC technology and starting from the glass, the classic way to produce a glass is to cool the liquid so quickly that the material is not allowed (when it passes from the liquid to a solid state) to be crystallized. This process is termed as a "**supper-cooled liquid**" process [2, 3, 5]. The temperature range between the equilibrium liquid and the frozen solid is defined as the "*glass transition*" range or *glass transition temperature* (T_g), where some properties of the liquid during its cooling, such as the special volume, the coefficient of thermal expansion, etc., change abruptly [3, 5].

However, if the cooling rate of the same liquid is slow, "**slow-cooled liquid**" process, the material acquires a crystalline structure, which is accompanied by an even greater reduction in the volume of the material, which can be measured by means of dilatometry [2, 3, 5].

As it is mentioned above, GCs are polycrystalline materials, which derive from the controlled crystallization (i.e. controlled heat-treatment) of the parent glasses [1-3]. Therefore, the understanding of the thermal behavior of glasses is very important. Usually, the glasses are manipulated or processed into complex shapes, followed by their heat-treatment for the production of crystalline materials (ceramics or GCs). Except the glass transition temperature (T_g), in which they soften gradually (i.e. their viscosity decreases), it is important to understand the importance of other characteristic temperatures, such as *crystallization onset temperature* (T_c), *crystallization peak temperature* (T_p) as well as the *liquidus temperature* (T_l) [2-5]. In a typical DSC curve of a glass (Fig. 1b), crystallization temperature (T_p) is displayed as an exothermic peak after the glass transition temperature (T_g), whereas the temperature of crystallization onset is T_c [4]. Interestingly the difference between the T_c and T_g temperatures is the termed as sintering window [5]. A wide sintering window means enough time to complete the sintering before the crystallization of the material begins. The fact that the glass transition temperature (T_g) depends, among other things, such as glass compositions, on the cooling rate (the lower the cooling rate, the lower the T_g value of the glass) allows to avoid a narrow sintering window [2, 4, 5]. Finally, upon continuous heating, an endothermic peak is the sign of melting and this temperature is the liquidus temperature (T_l) [2, 5]. Regarding the T_p and T_l temperatures, it is important that the heat-treatment procedure should not extend to temperatures higher than T_p, and never approach the T_l values. T_l is the highest temperature of thermodynamic equilibrium between the solid and the liquid phases of material. Above T_l temperature any crystal is unstable and dissolves in the liquid (i.e. dissolution of the formed crystalline phases occurs) [2, 5].

Thus, the following two sections focus on the two important parameters (production and properties) of GC materials, which are the structural composition and structural characteristics of glasses and GCs (section 1.1), and the heat-treatment procedure (section 1.2), which, in conjuction with the nature of each glass (i.e. its composition), determines the sintering and the crystallization process to produce GCs with the desired characteristics, such the crystalline structure, microstructure, and chemical, biological, mechanical properties and aesthetic characteristics that interest us in the present work.

1.1 Chemical composition and structural features of glasses and GCs

Glasses are amorphous (non-crystalline) materials, which have no crystalline structure, where the atoms appear to have a random distribution. More specifically, unlike crystalline solids, glasses do not show any long-range order or any significant symmetry in their atomic arrangement [1]. Instead, the atoms constituting a glass are organized in a short-range order that depends on the glass composition [1, 2]. On the other hand, GCs, which are formed when amorphous glasses of suitable composition are heat-treated and undergo controlled crystallization, are polycrystalline materials containing one or more crystalline phases embedded in a residual glass matrix [1, 3, 4]. Thus, a GC is a multiphase solid, containing a residual glass phase with finely dispersed crystalline phases [1, 4]. The above regimes are schematically represented in Fig. 2 for the case of silica.

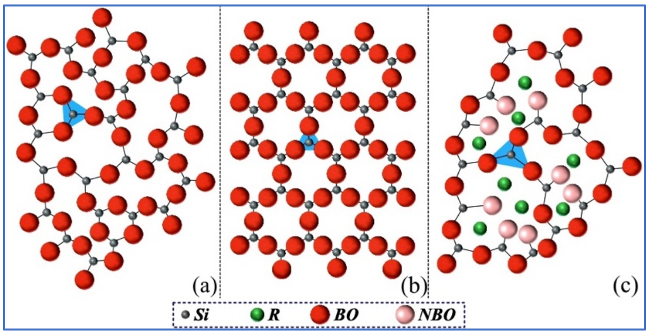

Figure 2. Two-dimensional representation of network structure of (a) vitreous silica, (b) crystalline silica, and (c) vitreous silicate. (BO: bridging oxygen, NBO: non-bridging oxygen, R: stands for a generic network modifier cation) [1].

In 1932, Zachariasen proposed one of the earliest considerations of the glass structure, which is called random network theory [6]. According to Zachariasen, the glass lacks periodicity and symmetry in its structure, compared to crystal [1, 6]. In the course of the analysis of vitreous silica structure, Zachariasen noticed that the glass network is built up of oxygen tetrahedra (or triangles) surrounding silicon atoms and each oxygen atom is linked to two silicon atoms, as shown in Fig. 2a [1]. According to Zachariasen, the components in glasses (i.e. the oxides actually) are categorized according to the types of their structural function, as follows:

1) **Network formers**, such as SiO_2, P_2O_5, are the components that build the glass network by forming oxygen tetrahedra (or oxygen triangles), connected to each other by bridging oxygens, (*BO*, Fig. 2).
2) **Network modifiers**, such as alkali and alkaline earth oxides of Li_2O, K_2O, Na_2O, CaO, MgO, and BaO, are the components that break down the glass network, by non-bridging oxygens (*NBO*, Fig. 2).
3) **Intermediate oxides**, such as Al_2O_3, display the role of either network formers or network modifiers.

The selection of glass composition and the heat-treatment schedule are key factors for GC processing. The components of the glass and their proportions should promote the precipitation of specific crystalline phase (or phases), avoiding long heat-treatments in order to get the desired final properties. The addition of an oxide (network former, modifier, or intermediate oxide) in a glass composition influences the chemical, physical, and mechanical properties of the final material (Table 1). Therefore, in the stage of designing a glass composition, it is important to know the influence of each oxide/fluoride on the final material (glass or GC).

Table 1. Effect of oxides and a fluoride on glass and GC properties.

Category	*Oxide/ Fluoride*	*Effect on properties*
Network formers	SiO_2	• Decrease of the coefficient of thermal expansion [3, 4] • Increase of mechanical strength [4]
	P_2O_5	• Reduce of the tendency to crystallization [7] • Decrease of melting point [8] • Decrease of bioactivity [9] • Decrease of modulus of elasticity [8]
Network modifiers	Na_2O/K_2O	• Fluxing agent [1] • Decrease of glass transition temperature [10] • Decrease of melting temperature [1, 10] • Reduce of production cost [1] • Reduce of viscosity [4] • Increase of the coefficient of thermal expansion [4] • Affect physico-mechanical properties (depending on their ratio) [11]
	CaO	• Stabilize the glass [1] • Increase of melting point [12, 13]
	MgO	• Decrease of glass transition temperature [14] • Suppress crystallization (thus, increase sintering window) [10] • Increase of expansion coefficient [14] • Acting either as a network modifier or as a network former [15, 16] • Affect bioactivity [16]
	CaF_2	• Decrease of glass transition and crystallization temperatures [17] • Facilitate sintering process [1] • No effect on bioactivity [17] • Increase of microhardness [1, 17]
Intermediates oxide	Al_2O_3	• Increase of mechanical properties [1, 16] • Decrease of expansion coefficient [1] • > 1.5 wt.% reduces or zeroing bioactivity [1, 16]

1.2 Sintering and crystallization of GCs

The process for fabricating GCs includes the production of a homogeneous parent glass, either in bulk form or in a glass-frit form (depending on the application), and then, a controlled heat-treatment process, in order to transform the glass into a crystalline GC [1, 4]. A widely used production method of glasses is through melt-quenching process. According to this method, the batch is heated at high temperatures (usually >1300 °C for silicate glasses) and quenched to freeze the disordered atomic structure of the melt and get an amorphous glass [2]. The result of the above method is to produce a glass-frit or a bulk glass (the latter is usually heat-treated at lower temperatures immediately afterwards and this annealing process, aims at relaxing the thermomechanical stresses in the glass structure induced by the rapid cooling) [1-3]. The production of a GC material is completed with the heat-treatment procedure either of glass-powder compacts (which are shaped with the aid of a binder and pressing) or a bulk annealed glass (Fig. 3) [4, 18, 19]. The heat-treatment schedule is based on findings from the thermal analysis experiments.

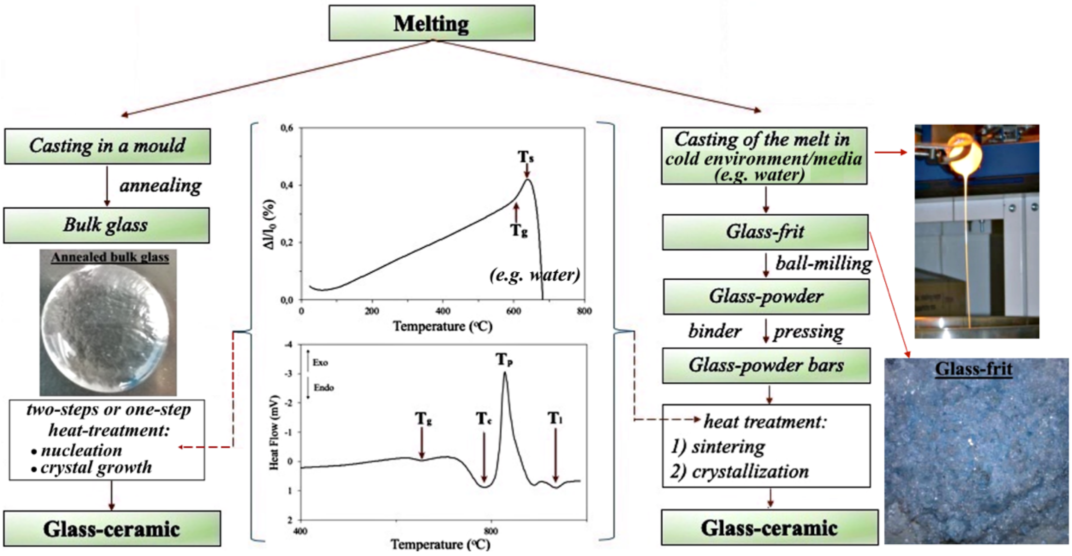
Melting
Casting in a mould
annealing
Bulk glass
Annealed bulk glass
two-steps or one-step heat-treatment:
• nucleation
• crystal growth
Glass-ceramic
0,6
0,4
0,2
0,0
ΔI/I₀ (%)
Tₛ
T_g
(e.g. water)
0
200
400
600
800
Temperature (°C)
Exo
Endo
Heat Flow (mV)
T_g
T_c
T_p
T_l
400
800
Temperature (°C)
Casting of the melt in cold environment/media (e.g. water)
Glass-frit
ball-milling
Glass-powder
binder
pressing
Glass-powder bars
heat treatment:
1) sintering
2) crystallization
Glass-ceramic
Glass-frit

Figure 3. The stages of the production of GCs by the glass melting method.

The recently used GCs manufacturing method involves sintering procedure and crystallization of powdered glass (Fig. 4) which has been proven to be technically and commercially viable. More specifically, this method includes ball-milling of quenched glass-frit into fine glass powder. Then, the powdered glass is formed by conventional *ceramming forming techniques,* which involve the use of binder and then pressing (Fig. 4a). The produced samples of the glass powder compacts are subjected to heat-treatment, whereby sintering and crystallization take place. Ideally, the sintering process must be completed before the crystallization process begins [4].

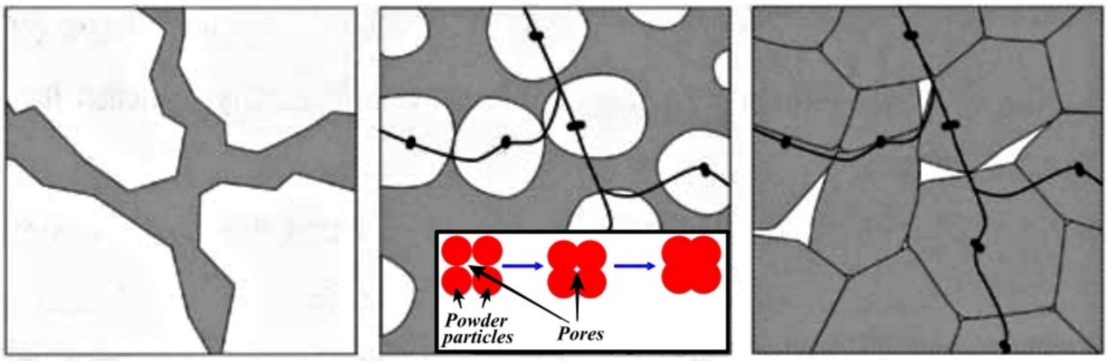

(a) (b) (c)

Figure 4. GCs produced from powdered glass. (a) Powdered glass compact, (b) sintering (densification) and crystallization, and (c) the dense crystallized microstructure of GC [4].

Sintering is the process involving consolidation of powder particles by heating the “green” compact at a high temperature below the melting point (Fig. 4b) [4, 20]. The driving force of sintering is the reduction of the surface energy of the particles and it is caused by decreasing the vapour-solid interfaces [2]. During the diffusion process, taking place in the “green compact”, the pores diminish or even close up (due to neck formation between adjacent grains), resulting in densification of the sample, and therefore in an improvement of the mechanical properties [4, 5]. The decrease of porosity, caused by the sintering process, is determined by the level of the initial porosity of the “green” compact, the sintering temperature, and the heat-treatment time. Sintering is enhanced if a liquid phase takes part in the process (liquid phase sintering). Moreover, applying pressure decreases sintering time and the resultant porosity [3, 21].

Crystallization (Fig. 4c) is accomplished by subjecting suitable glasses to a carefully regulated heat-treatment schedule, which results firstly in the *nucleation* (i.e. the formation of crystallization centers) and then in *growth* of crystal phases within the glass [4, 20]. An effective crystallization should initiate with the production of a large number of small crystals, rather than a small number of large crystals. Good selection of the heating rate, crystallization temperature, and period of time at crystallization temperature results in effective crystallization [20]. It is worthy of note that the heating rate must also be carefully controlled to avoid deformation of the GC during the heat process [4].

The advantages of the above method are that:

1) traditional forming processes can be used, such as slip-casting and pressing,

2) GCs can be applied as “coatings” on metal or other ceramic materials, because of the high flow rates before crystallization, and

3) the surface imperfections in the quenched frit can effectively act as nucleation sites [4].

The process of heat-treatment of annealed bulk glass can take place in two stages (i.e. two-steps heat-treatment, Fig. 5). First, heating at a relatively low temperatures (not far from the glass transition, T_g) induces internal nucleation (at T_N which is selected between T_1 and T_2), (Fig. 6a), which is followed by a second stage at a higher temperature to promote the growth the crystalline phases (at T_C which is selected between T_3 and T_4), (Fig. 6b) [4, 18, 22]. The produced GC (Fig. 6c) material is cooled to room temperature slowly [4, 23].

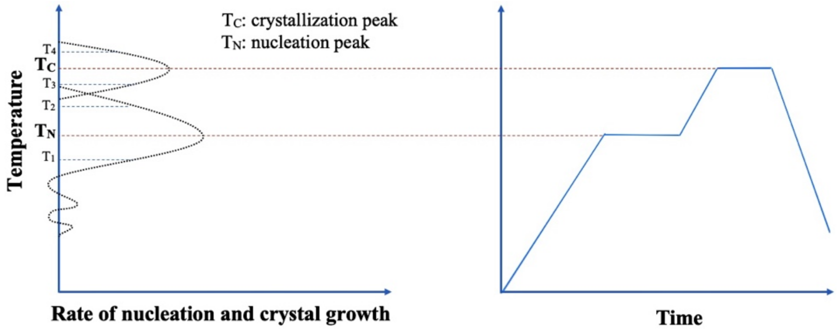
T_C: crystallization peak
T_N: nucleation peak
T_4
T_C
T_3
T_2
T_N
T_1
Temperature
Rate of nucleation and crystal growth
Time

Figure 5. Two-steps heat-treatment process for production of GC materials.

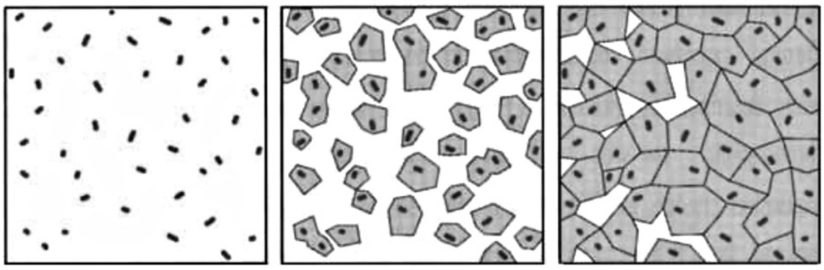
(a) (b) (c)

Figure 6. From glass to GC: (a) nuclei formation, (b) crystal growth, (c) GC microstructure [4].

A single heat-treatment as shown in Fig.7 can also be selected as the desired heat-treatment procedure. More specifically, the nucleation and the crystal growth curves must overlap partially in a certain temperature range ($T_2 \sim T_3$). The single heat-treatment process allows a slow nuclei formation and growth simultaneously [4, 23].

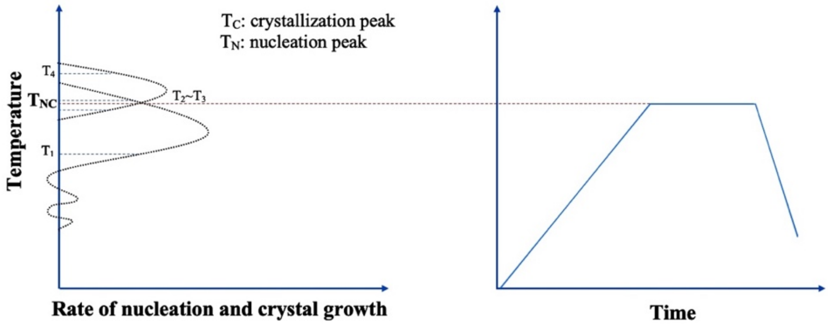
T_C: crystallization peak
T_N: nucleation peak
T_4
T_{NC}
T_2~T_3
T_1
Temperature
Rate of nucleation and crystal growth
Time

Figure 7. One-step heat-treatment process for production of GC materials.

Crystallization kinetics

The controlled transformation of a glass (i.e. a non-crystalline material) into a GC (i.e. a polycrystalline material) is achieved by the selection of appropriate heat-treatment process. The important parameters required for the heat-treatment are obtained from crystallization kinetics studies. The crystallization kinetics of amorphous materials can be investigated by both isothermal and/or non-isothermal methods, using the results from differential thermal analysis (DTA), or differential scanning calorimetry (DSC) [24-28]. The non-isothermal method is more simple and quicker than the isothermal method. The most important issues related to the kinetic of the crystallization of the glasses are the crystallization mechanism and the activation energy (E_α), which can be obtained by the above experimental methods [27, 29].

Isothermal methods

The kinetics of isothermal crystallization is usually analyzed by employing the Kolmogorov–Johnson–Mehl–Avrami transformation kinetics equation, given below [4, 28]:

$$x = 1 - e^{-kt^n} \tag{1}$$

where x is the fraction crystallized at a given temperature in time t, k is the reaction rate constant, and n is the Avrami parameter. The knowledge of the Avrami parameter is very helpful to understand the mechanism of phase transformation at given temperature and to inform about the growth dimensionality of crystals.

To determine the value of Avrami parameter, n, from Eq. 1 (taking natural logarithms), the following mathematical manipulation is performed:

$$1 - x = e^{-kt^n}$$

$$\ln(1 - x) = -kt^n$$

$$-\ln(1 - x) = kt^n$$

$$\ln(-\ln(1 - x)) = n \cdot \ln(k) + n \cdot \ln(t) \tag{2}$$

Thus, the Avrami parameter (n) is the slope of the plot of the logarithm of ln(1 – x) *versus* the the logarithm of t [25].

The reaction rate constant, k, is related to the activation energy for crystallization (or for crystal growth), E_α, through the Arhenius temperature dependence [27]:

$$k = \nu \cdot e^{-Ea/RT} \tag{3}$$

where ν is the frequency factor, R is the ideal gas constant, and T is the (isothermal) absolute temperature (in Kelvin degrees). By taking logarithms, equation (3) may be rewritten as:

$$\ln k = \ln \nu - E_\alpha/RT \tag{4}$$

Non-isothermal methods

Usually, the kinetics of non-isothermal crystallization is studied by DTA/DSC methods, by conductus a series of experiments, carried out at different heating rates φ.

The activation energy, E_α (in kJ/mol), is evaluated by the Kissinger equation [28, 30]:

$$\frac{E\alpha}{RTp} = \ln\frac{Tp^2}{\varphi} + \text{constant} \tag{5}$$

where T_p is the temperature of the crystallization exothermal peak, R is the ideal gas constant (8.314 J/mol·K), and φ is the heating rate. The plot of $\ln((T_p^2)/\varphi)$ *vs* $1000/T_p$ should yield a straight line whose slope can be used to calculate the value of E_α.

The Avrami parameter, n_A (it is also designed often with the letter m), can be estimated by using the Augis-Bennet equation [31]:

$$n_A = \frac{2.5/\Delta T}{RTp^2/E\alpha} \tag{6}$$

where ΔT is the full width at the half maximum of the exothermic crystallization peak, T_p is the temperature of the crystallization exothermal peak, E_a is the activation energy of crystallization, and R is the universal gas constant (8.314 J/mol·K). The Avrami parameter depends on the growth direction and the mechanism of nucleation and crystal growth [24]. The Avrami parameter can be used to indicate the dimensionality of the crystal growth (Table 2). In order to estimate the dimensionality of the crystal growth using non-isothermal methods, the determination of the nucleation rate in glasses is not required. This is because the values of Avrami parameter in non-isothermal methods are the same, whether bulk crystallization is observed with a constant number of nuclei or with an increasing number of nuclei.

Table 2. Values of Avrami parameter (n and m) for various crystallization mechanisms and growth dimensionality of crystals [24, 27].

Crystallization mechanism	n *(isothermal methods)*	n_A (or m) *(non-isothermal methods)*
Bulk crystallization (constant nuclei rate)		
Three-dimensional growth of crystals	3	3
Two-dimensional growth of crystals	2	2
One-dimensional growth of crystals	1	1
Bulk crystallization (increasing nuclei rate)		
Three-dimensional growth of crystals	4	3
Two-dimensional growth of crystals	3	2
One-dimensional growth of crystals	2	1
Surface crystallization	1	1

2. Glass-ceramics (GCs) in dental applications

2.1 The use of GCs in biomedicine

Glasses and GCs attract a great interest in biomedical applications, especially in repairing and replacing natural bone and dental hard tissues, owing to their biocompatibility [1, 3, 32-35]. Also, various glasses and GCs exhibit, apart from biocompatibility, bioactivity that is the ability to develop chemical bond to bones and soft tissues [1, 3, 36]. The first and best-known bioactive glass is 45S5 Bioglass, invented by Larry Hench and his co-workers in Florida, USA, at the end of 1960s [36, 37]. The strong chemical bond between the bioactive glasses/GCs and living bone is due to the formation of a biologically active layer of hydroxyapatite (HA), which is developed on the surface of the glasses/GCs, when they are in biological environment [37]. This surface HA layer is chemically and structurally similar to the mineral apatite phase in bone tissue. Larry Hench proposed a 12-stages model to describe the interfacial reaction between a bioactive glass and the body environment [1, 37, 38, 39]. The first five stages, reported below, are directly ralted to the material itself (Fig. 8), while the subsequent stages (6 - 12) involve cells and proteins.

1st stage: Exchange of alkali and alkaline earth ions from the glass with H^+ ions from body fluids, which leads to an increase of the local pH, causing the rupture of the Si–O–Si bonds.

2nd stage: Network dissolution permits the release of silicon from glass surface towards the fluid in the form of silanol $Si(OH)_4$ groups.

3rd stage: For local pH values lower than 9.5, $Si(OH)_4$ groups undergo condensation forming a polymerized silica gel layer on the surface of the glass.

4th stage: The open structure of silica gel allows the continuity of ion exchange between the glass and the fluid: the Ca^{2+} and P^{5+} ions are diffused from the glass, together with the Ca^{2+} and P^{5+} ions present in the fluid, forming an amorphous calcium phosphate layer over the silica gel.

5th stage: The amorphous calcium phosphate layer incorporates carbonate species and the crystallization of the HCA (carbonated HA) layer begins.

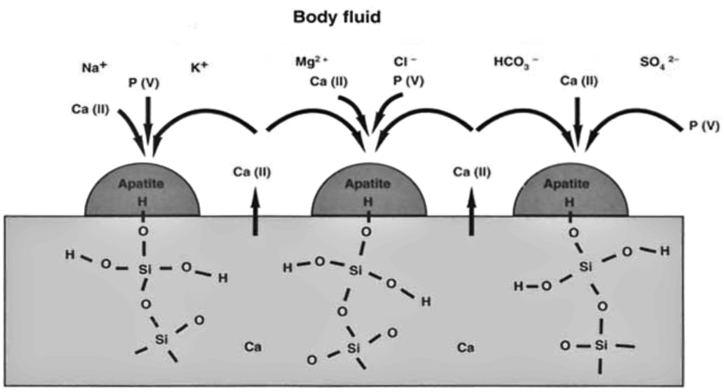

Figure 8. Schematic representation of the mechanism of apatite formation on the surface of a bioactive glass [4, 40].

Bioactive glasses, which are characterized by both osteoconduction (i.e. the bone grows on the surface) and osteoinduction abilities (the process by which osteogenesis is induced, because it implies the recruit, ment of immature cells and the stimulation of these cells to be developed into preosteoblasts), can be used in a variety of medical applications, such as **1.** bone grafting, **2.** scaffolding, **3.** drug delivery, **4.** coatings on metal or other ceramic materials, and **5.** soft tissue engineering [3, 37]. Nevertheless, it was soon realized that bioactive glasses cannot be used in load-bearing applications (orthopedics and dentistry) due to their low mechanical strength [32], as the bioactive glasses have a bending strength of ~70 MPa and K_{IC} of ~0.5 $MPa{\cdot}m^{0.5}$ [18].

Therefore, the scientific interest was shifted to bioactive GC materials, because they can combine the characteristics of the bioactive glass (i.e. high bioactivity) and of the ceramic of the same composition (i.e. high mechanical properties) [1, 3, 4, 40]. Bromer introduced, in 1973, the first bioactive GC material named Ceravital® (Na_2O-K_2O-MgO-CaO-SiO_2-P_2O_5), which has been a milestone for many research groups to develop bioactive GCs with improved mechanical properties, like those aimed to be used as dental materials (dental implants) etc. [4, 18]. Research on bioactive GCs continued, and in the late 1980s, Kokubo et al. developed a bioactive apatite-wollastonite (A-W) GC, commercially known as Cerabone® (MgO-CaO-SiO_2-P_2O_5), which exhibits excellent mechanical properties ($\sigma = 180 \pm 20$ MPa; $K_{IC} = 2.0 \pm 0.1$ $MPa{\cdot}m^{1/2}$; $E = 117$ GPa) [18, 41, 42]. Höland et al. developed in 1985 an apatite-mica bioactive GC in Na_2O–MgO-CaO-Al_2O_3-SiO_2-P_2O_5-F system, known as Bioverit® [43]. Although the bioactive GCs exhibit significantly better mechanical properties compared to bioactive glasses, they demonstrate lower values of fracture toughness than that of human jaw bone ($K_{IC} = 2 - 12$ $MPa{\cdot}m^{0.5}$) [18]. Hence, this property still needs to be significantly improved by developing novel GCs.

Over the years, various systems of GCs have been studied by teams of researchers and have been proposed as potential materials for biomedical applications (Table 3) [4]. According to Montazerian and Zanotto [18], who searched the Scopus database using the keywords "bio + glass-ceramic" firstly only in the publication title and secondly in the title, abstract and keywords, the number of publications increases over the past four decades (Fig. 9a). When the same authors used as keywords "bioactive + glass-ceramic", they observed an increase of the research related to bioactive GCs in the past four decades, as well (Fig. 9b). Comparing the two graphs, these researchers observed that almost 50% of research related to bio-GCs is actually related to bioactive GCs, while the other 50% is connected to bioinert (biocompatible) dental GCs [18].

Table 3. Various systems of GCs studied by teams of researchers, proposed as potential materials for biomedical applications [4].

Glass composition/GC system		Crystalline phase
Alkaline and alkaline earth silicates:	SiO_2-Li_2O	Lithium Disilicate
Aluminosilicates:	SiO_2-Al_2O_3-CaO SiO_2-Al_2O_3- K_2O	Wollastonite Leucite
Fluorosilicates:	SiO_2-Al_2O_3-MgO-CaO-ZrO_2-F	Mica, Zirconia
Silicophosphates:	SiO_2-CaO-Na_2O-P_2O_5 SiO_2-MgO-CaO-P_2O_5-F SiO_2-MgO-Na_2O/ K_2O- CaO- P_2O_5	Apatite Apatite, Wollastonite Mica, Apatite
Phosphates:	P_2O_5- Al_2O_3- CaO	Apatite

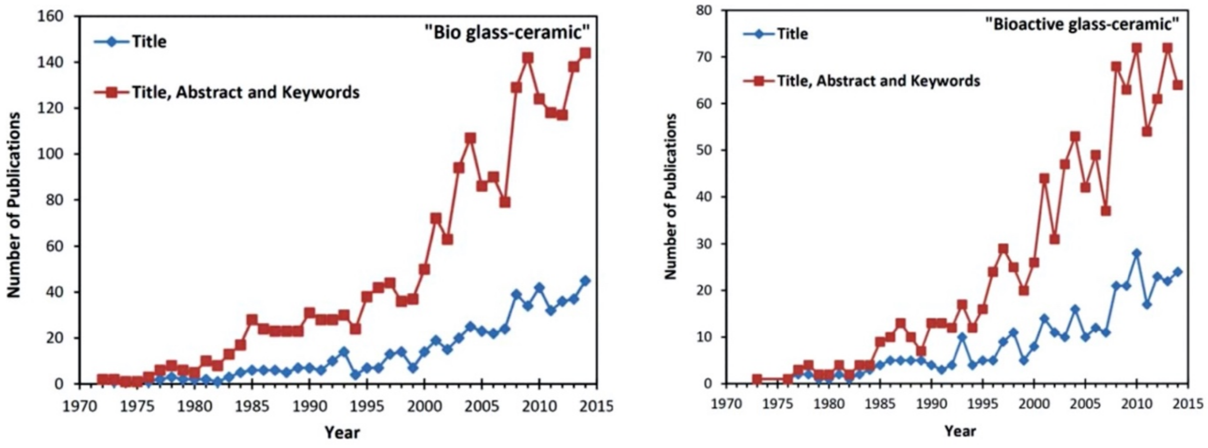

(a) (b)

Figure 9. Number of publications (papers, books, and conference papers) per year extracted from the Scopus database by searching the keywords (a) "bio + glass-ceramic", and (b) "bioactive + glass-ceramic" in the publication title (blue) and also in the title, abstract and keywords (red) [18].

As the bioactive GCs are characterized by both osteoconduction and osteoinduction, they find immediate biomedical application, especially in applications where the materials are subjected to dynamically changing loads, such as in orthopedics and dentistry [38]. More specifically, so far, the bioactive GCs are used to coat dental or orthopedic implants, to repair root canal/dentine and to heal periodontal diseases [19]. The application of GC materials in biomedicine is not limited only in the case of bioactive GCs. On the contrary, bioinert GCs, such as IPS Empress®, IPS e.max Press® etc., find daily application in dental fixed prosthetic restorations. The above dental applications of GCs, as dental implant materials and in dental fixed prosthetic restorations are discussed in more detail in the next sections, 2.2 and 2.3 respectively.

2.2 Dental implants

Biomaterials aim at replacing parts or functions of the human body, which have been damaged or lost, in a safe, reliable, and naturally acceptable manner, and, surely, at low cost, in order to restore the original function of the human body. As it has already been mentioned, this means that an ideal biomaterial must display properties as close as possible to those of the tissues that the biomaterial will replace, and thereby to have a good relation with the tissues that were directly adjacent to the lost tissue, as the Mother Nature has wisely anticipated for all body tissues. This section focuses its interest on dental implants. Accordingly, we shall present (i) where (i.e. anatomically, at which point) a dental implant will be placed and which hard dental tissue a dental implant is called on to replace, (ii) what requirements a dental implant should meet (i.e. which properties must reach specific values, which are similar to the adjacent physiological tissues), and (iii) the materials which are used nowadays, in order to highlight how much they satisfy the above requirements and consequently to emerge the challenges that the future research has to face, as the present work does.

(i) Dental implant placement and the replaced dental hard tissue by a dental implant

Dental implantology has become a reliable treatment for patients with missing teeth [44, 45]. A dental implant is a prosthetic device of alloplastic materials that is surgically placed on the jaw bone to replace one or more missing teeth, and, specifically, is called on to replace the root of the tooth. In this way, dental implants provide retention and support for fixed or removable dental prosthetic restorations [44, 46]. At this point, it is essential to mention some important information (such as structure, mechanical properties) of the human jaw bone, which is the environment that a dental implant is placed in, and the dental hard tissues of dentine and cementum, which makes up the root of the natural tooth.

Jaw bone

Macroscopically the human jaw bone, like most human bones, is divided, based on porosity, into (Fig. 10):

- an external dense **cortical bone**, whose structure and microstructure (bony cylinders, consolidated around a central blood vessels or osteon) provide the principal mechanical strength of the jaw bone, and its thickness and the inside cross-sectional areas are strong indicators of gross bone strength and fracture resistance [47], and
- an internal **trabecular bone** (spongy or cancellous), the structure of which is less in density and has a greater degree of macro-porosity than the cortical bone [48].

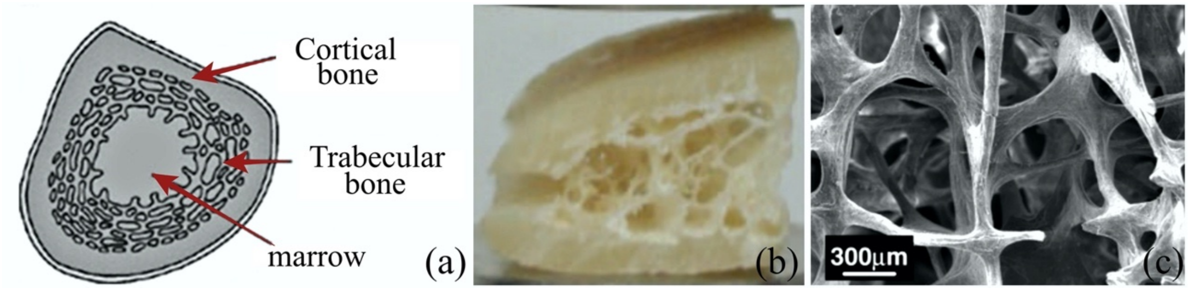

Figure 10. (a) Cortical and trabecular bone [49], (b) illustration of a cross-section of mandibular cortical and trabecular bone [48], and (c) trabecular bone.

Microscopically, the human jaw bone is made up of an extracellular matrix, bone cells, blood vessels, and nerves. In the case of dental implants, cells are inevitably involved in the formation of the strong bond between the jaw bone and an implanted materials. This process was discovered by Brånemark in the 1950s and it is called osseointegration [50, 51]. Osteoblasts, osteocytes, and osteoclasts are the major types of cells, which are related to bone physiology. *Osteoblasts* (mononuclear, highly secretory cells) are the major cellular components of bone, which are derived from multi-potential mesenchymal progenitor cells. The main function of mature osteoblasts is to produce bone's organic matrix. Once the bone's organic matrix production is successfully completed, a small portion of osteoblasts that had been embedded in the organic matrix transforms into osteocytes, while the majority of the osteoblasts undergo programmed cell death [50, 52]. *Osteocytes*, developed from osteoblasts and represent the metabolic centres of the bone, are the most abundant bone cells, 90-95% of all bone cells. Osteocytes contribute to conservation of the extracellular matrix, by responding to local strains resulted from external loads applied on bone. In the case of the human jaw bone, these external loads come mainly from the forces of the repeated chewing cycles. Finally, *osteoclasts* are multinucleated cells, ~50 nuclei, known as "large motile" cells [50]. Osteoclasts are responsible for bone resorption. It is important to note that, in order to sustain skeletal remodeling and to maintain bone mass, there is a continuous balanced interaction between osteoblasts and osteoclasts [53].

Dentine

As mentioned above, a dental implant is called on to replace the root of a tooth. The root is located in the human jaw bone. The dental hard tissue that the root is mainly made up is **dentine** (Fig. 11) [19, 54-56]. More specifically, dentine is a hard tissue that extends both to the crown and the root of the tooth. In the crown region, dentine is covered by enamel, which is the hardest substance in the human body (harder even than bone) and has a primary role in protecting the underlying dentine and pulp cavity from extrinsic traumatic stimuli [55, 57]. In the root region, dentine is covered by cementum, which is the smallest dental hard tissue (10 - 200 μm thickness) and has a similar structure to that of bone tissue, but a lower hardness than dentine (< 0.6 GPa) [55-59]. Cementum does not contribute to the mechanical strength of natural tooth, but its role is limited only to lining the root and maintaining the tooth in the alveolar [55, 59].

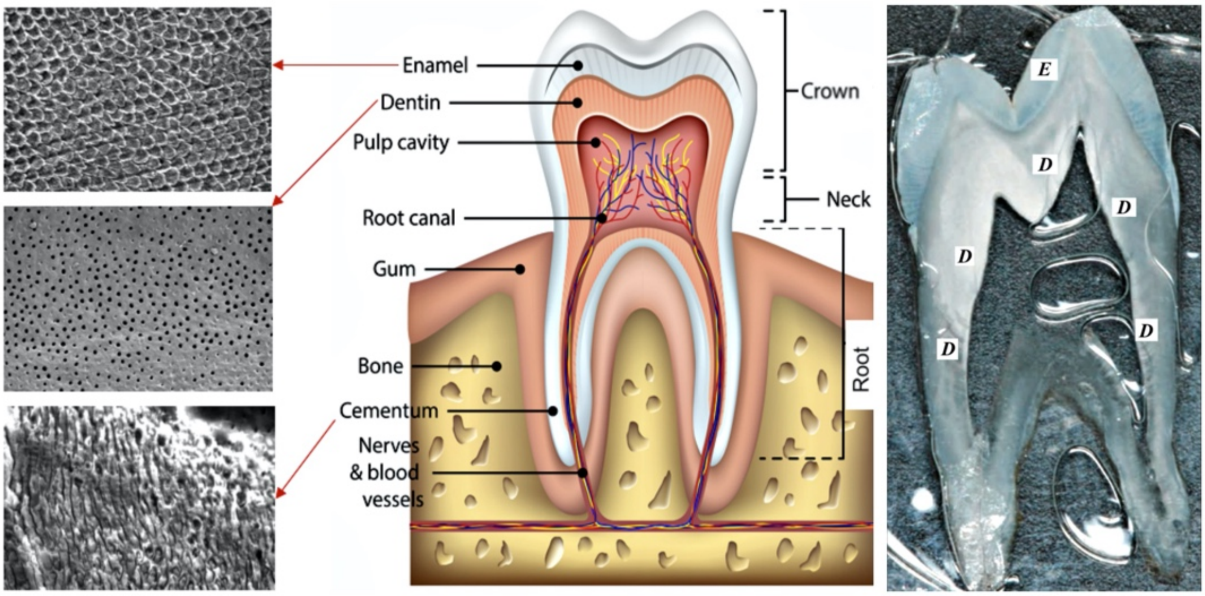

(a) (b)

Figure 11. (a) The structure of human tooth; on the left-hand side of the figure, the microstructure of enamel (enamel rods; mag x1000, 10 μm), dentine (dentinal tubule; mag x2000, 50 μm), and cementum (mag x1000, 10 μm) is shown [55]. (b) Tooth incision, showing the extent of dentine in the crown and the root of the tooth (E: enamel, and D: dentine) [59].

(ii) The importance of the mechanical properties of dental implants

The knowledge of the rules of biomechanics in living jaw tissues crucially important role the longevity of a dental implant in the oral cavity. Thus, the evaluation of the factors that play an important role in the ultimate success of dental implant restorations is necessary. The above factors, among others, concern the knowledge of the mechanical properties of both the human jaw bone and the materials used for the production of a dental implant [60]. More specifically, the mechanical properties of the cortical and trabecular bones (Table 4) are of the utmost importance in cases where the bones come in contact with biomaterials (due to either loss or destruction of a natural hard/soft tissue). Ideally, in most clinical cases and even more in the case of dental implants (which are in an intensely continuous changing dynamic environment), the mechanical properties of the implanted biomaterial should be a good match for the mechanical properties of the jaw bone. Otherwise, a mismatch of the above properties may cause injury to the human tissue or fracture of the restoration.

Table 4. Mechanical properties of cortical bone, trabecular bone, and dentine [19, 38, 61, 62].

	Flexural strength (σ, *MPa*)	*Modulus of elasticity* (E, *GPa*)	*Vickers microhardness* (HV, *GPa*)	*Fracture toughness* (K_{IC}, $MPa \cdot m^{0.5}$)
Cortical jaw bone	50 - 150	7 – 30	0.06 - 0.075	2 - 12
Trabecular jaw bone	10 - 20	0.05 - 0.5	0.04 - 0.06	0.7 - 1.1
Dentine	230 - 305	15 – 30	< 0.6	3

The *modulus of elasticity* (whose values is used to measure the rigidity of a material and is defined as the ratio of stress to strain in an elastic state regime) is an important property for dental implants, since a mismatch of the modulus of elasticity between the material and the jaw bone can favor *stress shielding* effect [63, 64]. According to Wolff [65], the bones are reshaped in response to the loads they receive. Therefore, reducing the bone load results in a decrease in tooth density, because there is no stimulus for a continuous remodeling required to maintain bone mass, and consequently leads to the failure of the dental implant. After the placement of the prosthetic restoration the body of the dental implant is now the one that receives the largest percentage of occlusal forces [44, 60]. Thus, besides bioactivity, a dental implant material must have the ability to distribute the load to the adjacent bone and thereby to maintain its density. This means that if the values of the modulus of elasticity of the dental implant material and the adjacent bone are close to one another, then the stress distribution will approach the natural mode of distribution. Thus, stress shielding is suppressed.

Understanding of the clinical significance of the *hardness* values, which reflect the ability of a material to resist a permanent indentation [55, 58, 66, 67], and the susceptibility to abrasive wear [67] is necessary, in the case of dental implants as well. Therefore, during the selection of the restorative dental material, in order to avoid the abrasion of the cortical jaw bone, it should be ideal the above property to range, as close as possible, between the corresponding values of dentine (Table 4) (the dental hard tissue that makes up the root of the natural tooth, which the tissue that the dental implant is called on to replace) and human jaw bone (which is the environment that will host the dental implant).

Admittedly, the *fracture toughness* values, which are measure of the resistance of a material to crack propagation or, otherwise the ability to resist fracture, play an equally important role in the success of a dental implant. The lower the fracture toughness, the lower the clinical reliability of the restoration, because the fracture toughness value defines the critical stress at which catastrophic failure occurs due to a micro-defect (e.g. in a ceramic restoration) [68].

(iii) Popular dental implant materials in clinical practice and future challenges

Pure titanium (cpTi) and Ti6Al4V alloy have been the first choice as materials for manufacturing dental implants, due to their mechanical, chemical, and biological properties (biocompatibility and resistance to corrosion), as well as the osseointegration properties (Fig. 12) [51, 69]. Osseointegration is not an isolated phenomenon. Instead, it depends on previous *osteoinduction* (the process by which osteogenesis is induced, because it implies the recruitment of immature cells and the stimulation of these cells to develop into preosteoblasts) and *osteoconduction,* which is associated to the formation of HA (i.e. newly formed bone grows on HA surface; an osteoconductive surface permits bone growth on its surface or down into pores, channels, or pipes) [1, 51]. A successful osseointegrated implant comprises of pores for migration of osteoblasts and supporting connective tissue. The interface between the implant and bone must be closely direct with no presence fibrous tissue or collagen [70, 71]. In order to create dental implant surface roughness, acid etching, plasma spraying, sandblasting as well as hydroxyapatite (HA) coating, have been conducted. Also, the roughness of dental implant surfaces, except stimulating differentiation, growth, and attachment of bone cells, has an effect in enhancing of mineralization [70].

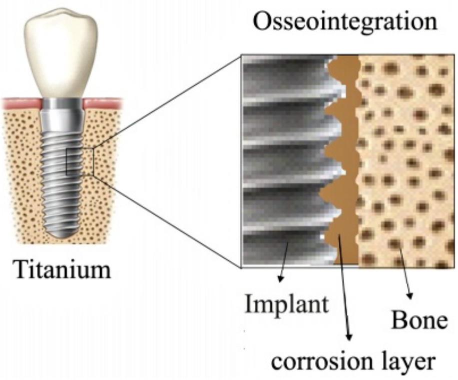

Figure 12. Titanium dental implant [70].

Like any other dental material, Ti has some minor drawbacks. For instance, according to Simonis et al., who conducted a long-term clinical study with Ti dental implants, frequent occurrences of biological (such as peri-implant mucositis and peri-implantitis) and technical complications, were observed [72]. In addition, a disadvantage of Ti dental implants is the reduced aesthetic performance in the gingival area, especially in the case of anterior teeth, because of the dark grayish color of titanium [45, 73]. These disadvantages of Ti dental implants motivated the researchers to develop novel implant materials, such as ceramic materials [74-76].

Thus, in recent years, the material of choice, among other ceramic materials (e.g. ceria-stabilized TZP, Ce-TZP), is yttria-stabilized tetragonal zirconia (Y-TZP). Y-TZP exhibits very good aesthetic performance (tooth-like color), excellent mechanical properties (bending strength 1200 MPa, modulus of elasticity 200 GPa, and fracture toughness of 6-10 $MPa{\cdot}m^{0.5}$) and attractive biological properties [45, 76]. Nonetheless, early clinical findings showed that there is a main drawback for zirconia related to an inherent accelerated ageing, which is reinforced in the presence of moisture, known as “low-temperature degradation (LTD)”. This problem is own to spontaneous phase transformation of the zirconia crystals from the tetragonal phase to the weaker monoclinic phase. The above problem affects the fracture toughness of the dental implant materials, resulting in surface deterioration and microcracks propagation [45, 77]. The process of chemical degradation of the zirconia ceramic implants results in formation of a space between the dental implant and the bone which is getting bigger over implantation time (Fig. 13). It is argued if this phenomenon creates the necessary space for newly formed bone growth between the implant and the bone (i.e. it may favor osseointegration process also known as biointegration) leads to formation of fibrous tissue or collagen. The above mechanism is not completely known, yet [70].

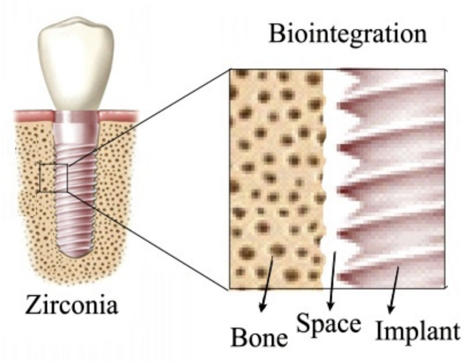

Figure 13. Zirconia dental implant. The space between the dental implant and bone is getting bigger over implantation time, as a result of chemical degradation of ceramic implant [70].

Beyond the mismatch of mechanical properties of the above-mentioned dental implant materials (Ti and zirconia) with those of human jaw bone and dentine, since the mechanical properties of Ti and Y-TZP (Table 5) are higher than those of the human jaw bone and dentine (Table 4), these materials are is also non-bioactive or bioinert. The surface of such bioinert materials can obtain bioactive properties through bioactive coatings, for instance plasma-sprayed HA. Nevertheless, this configuration has the drawback of not displaying a uniform degradation, giving rise to weak points at the bone-coating interface [45, 64, 78, 79].

Table 5. Mechanical properties of commonly used dental implant materials [44, 45, 64, 76].

	Modulus of elasticity (E, GPa)	*Vickers microhardness (HV, GPa)*	*Fracture toughness (K_{IC}, $MPa{\cdot}m^{0.5}$)*
cpTi	105	2.2	-
Ti6Al4V	110	4	-
Zirconia	210	12	6 - 10

Thus, the development of novel bioactive dental implant materials, which can develop a strong chemical bond between the dental implant and the jaw bone, as well as to accelerate implant anchorage by inducing the formation of an HA layer on the implant surface [45, 64, 78], is vitally important in these applications. The HA layer will not only speed up the process of *osteoconduction,* but the formation of such an HA surface layer adjacent to the bone will prevent the formation of fibrous tissue around the dental implant, and it will favor osteointegration, and suppress stress shielding [79, 80].

Bearing the above in mind and being aware of the problems arising from the mismatch of the mechanical properties between the natural tissues (i.e. jaw bone and dentine) and dental implant materials, it is important to develop new materials, such as GC materials, capable of producing dental implants. Research teams around the world, have been involved in the development of GC materials for dental implant applications [19, 45, 64, 80-82]. Although the results of their studies (which will be discussed in more detail in the Discussion chapter) meet the desired chemical and biological properties, the values of the mechanical properties (whenever reported) are higher than the desired ones, namely referring to values which are far beyond those of the human jaw bone.

2.3 Dental fixed all-ceramic prosthetic restorations

Considering that the biomaterials aim at replacing damaged or lost parts or functions of the human body in a safe, reliable, and naturally acceptable manner, at low cost, in order to restore the original function of the human body, the properties of an ideal biomaterial must be a good match for the properties of the tissues that the biomaterial comes to replace, closing therefore the gap between the properties of the foreign material and tissues that are directly adjacent, as the Mother Nature has wisely anticipated for all body tissues. This section reports on all-ceramic dental restorations. Accordingly, here we present (i) where (i.e. anatomically, at which point) the all-ceramic prosthetic restoration is placed and which hard dental tissue it is called on to replace, (ii) which requirements should be met (i.e. what properties values must be reached in order to be similar to those of the physiological tissues), and (iii) the materials which are used nowadays, in order to highlight how much they satisfy the above requirements and to reveal the challenges that the future research has to face, as the present work does.

(i) All-ceramic restorations placement and the replaced dental hard tissue

Metal-ceramic prosthetic restorations are the dominant way of repairing damaged teeth over 40 years. Nonetheles, the strong interest in better aesthetic results and the questionable biocompatibility of dental alloys sparked researchers' interest in developing all-ceramic systems [83]. The all-ceramic prosthetic restorations are called on to restore the damaged crown of the teeth, and in particular to replace the natural enamel and dentine in order to restore the physical function of the oral cavity system. At this point, it is essential to mention some important information (such as structure and mechanical properties) about the enamel and dentine, the dental hard tissues which a prosthetic restoration is called on to replace.

Enamel and Dentine

As mentioned above, an all-ceramic prosthetic restoration is called on to replace the crown of the tooth. The dental hard tissues that mainly makes crown up are enamel and dentine (Fig. 11) [19, 54 - 56]. More specifically, enamel is the hardest substance in the human body (harder even than bone), which surrounds the crown of the tooth and has a primary role in protecting the underlying dentine and the pulp cavity from extrinsic traumatic stimuli. The enamel consists of the enamel prisms (or rods, with a diameter of ~5 μm), which are perpendicular to the dentinal - enamel junction [55]. Dentine is a hard tissue that extends to the crown and the root of the tooth, where it covered by enamel and cementum, respectively [19, 54-57]. The all-ceramic prosthetic restoration is placed and adhesively cemented to the cavity of the natural tooth (inlays, onlays), or to the underlying natural dentine (veneer, crown), which has previously been fitted properly by the dentist [66].

(ii) The importance of mechanical properties in fixed all-ceramic prosthetic restorations

The mechanical properties of natural dental hard tissues enable the oral cavity to perform its basic functions (i.e. grinding of food during mastication). Understanding of the clinical significance of the mechanical properties of natural dental hard tissues is the basis of dental restoration materials research [55]. The modulus of elasticity, also known as Young's modulus, in the case of human teeth, during the repeating chewing cycles, presents the ability of enamel and dentine to resist elastic deformation. Thus, in the case of damage in a part of a tooth or in the whole tooth, the restorative material must exhibit a modulus of elasticity close to the corresponding values of tooth [55, 66, 84]. Regarding the hardness values, which reflects the susceptibility to abrasive wear [67], in the case of prosthetic restorations, which aim at restoring the tooth crown, it is important the selected material to exhibit hardness values close to those of enamel, in order to avoid abrasion of the teeth in the opposite jaw [66]. The hardness values of dentine, in this case, does not play an important role, as only the outer layer of the tooth, enamel, comes in contact with the teeth of the opposite jaw. Finally, the higher the fracture toughness, the higher the clinical reliability of the prosthetic restoration, because the fracture toughness value defines the critical stress at which catastrophic failure occurs, due to a micro-defect (i.e. in a ceramic restoration) [68].

Matching of the properties of restorative materials to the properties of teeth is very important to enhance the longevity of the restoration [66, 84]. According to the ISO 6872 "Dentistry - Ceramic Materials" [85], ceramics are divided into six classes, depending on the values of flexural strength and fracture toughness. Table 6 summarizes the values of flexural strength and fracture toughness (according to the ISO 6872 "Dentistry - Ceramic Materials") of ceramic materials which aim at each category of dental application. The comparison of the flexural strength and fracture toughness values (according to the ISO 6872) with those of dental tissues (enamel and dentine), as shown in Table 6, shows that the ISO 6872 recommended values range between the corresponding values of dentine and enamel. The increase of the values of flexural strength (>300 MPa) and fracture toughness (> 3 MPa·m$^{0.5}$) of ceramics **5** and **6** is reasonable because they refer to extensive restorations (i.e. three or more units' prostheses).

Table 6. (A) Mechanical properties of human enamel and dentine [19, 55, 66-68, 81, 84]. **(B)** Classification of ceramics for fixed prostheses by intended clinical use, with the recommended flexural strength and fracture toughness values, according to the **ISO 6872** [85].

			Flexural strength (σ, MPa)	*Fracture toughness (K_{IC}, MPa·$m^{0.5}$)*	*Modulus of elasticity (E, GPa)*	*Vickers microhardness (HV, GPa)*
A		Dentine	230 - 305	3	15 - 30	< 0.6
		Enamel	60 - 200 (260 - 290) *	1.0 - 1.5	70 - 100	3.0 - 5.5
*Recommended clinical indications, according to **ISO 6872** "Dentistry - Ceramic Materials" [85].*						
B	**1.**	**a.** Aesthetic ceramic for coverage of a metal or a ceramic substructure. **b.** Aesthetic ceramic: single-unit anterior prostheses, veneers, inlays or onlays.	50	0.7	-	-
	2.	**a.** Aesthetic ceramic: adhesively cemented, single unit, anterior or posterior prostheses. **b.** Adhesively cemented, substructure ceramic for single-unit anterior or posterior prostheses.	100	1.0	-	-
	3.	Aesthetic-ceramic: non-adhesively cemented, single-unit, anterior or posterior prostheses.	300	2.0	-	-
	4.	**a.** Substructure ceramic for non-adhesively cemented, single-unit, anterior or posterior prostheses. **b.** Substructure ceramic for three-unit prostheses not involving molar restoration.	300	3.0	-	-
	5.	Substructure ceramic for three-unit prostheses involving molar restoration.	500	3.5	-	-
	6.	Substructure ceramic for prostheses involving four or more units.	800	5.0	-	-

*if supported by dentine

(iii) Popular materials in clinical practice of all-ceramic restorations and future challenges

The first castable mica-based dental GC, known as Dicor® (SiO_2-Al_2O_3-MgO- K_2O-ZrO_2- CeO_2 glass system), was introduced by Malament and Grossman in the mid-1980s [4, 19]. Due to the complicated dental laboratory process and the introduction of a CAD/CAM technology in dentistry (1970), the above GC was modified. The modified machinable GC is known as Dicor® MGC [19]. The applications of Dicor® and Dicor® MGC GCs in restorative dentistry are veneers, inlays, onlays, and crowns. Although these GCs have excellent mechanical properties (Table 7), their extensive clinical application in prosthetic restorations is limited due to the low value of fracture toughness [86].

Table 7. Mechanical properties of commercial GCs [19, 68, 87, 88].

GC	Company	*Flexural strength (σ, MPa)*	*Modulus of elasticity (E, GPa)*	*Vickers microhardness (HV, GPa)*	*Fracture toughness (K_{IC}, MPa·$m^{0.5}$)*
Mica-based GCs	Dicor®	150	70	3.5	1.4 - 1.5
Leucite GCs	IPS Empress®	160	65	6.2	1.3
Lithium disilicate GCs	IPS e.max Press	400	~90	5.8	2.7
	IPS e.max CAD	360	~85	5.8	2.5

Leucite-containing GCs (SiO_2–Al_2O_3–K_2O glass system) were introduced in the early 1990s and were the first heat-pressed GCs [4, 19, 89]. Leucite crystals are precipitated in a glass matrix through controlled surface crystallization. This crystallization mechanism results in GCs with desirable mechanical properties for fixed prosthetic restorations (Table 7) [19]. These mechanical properties are attributed to the ability of leucite crystals to arrest the crack propagation [4]. The CAD/CAM technology can also be used in leucite-based GCs. Leucite IPS Empress® and IPS Empress®CAD GCs are recommended for fabricating dental prosthetic restorations, such as veneer, inlays, onlays, and crowns [4, 87].

Lithium disilicate GCs (SiO_2-Li_2O-K_2O glass system) was introduced in dentistry in 1998 and until now is the most popular restorative dental GC [90]. The glass composition was designed in such a way that the final GC contains at least 65 wt.% fine rod-like entangled lithium disilicate crystals (which crystallizes at 750 - 850 °C). Lithium disilicate GCs have a characteristic microstructure, in which there are embedded/dispersed interlocked lithium disilicate crystals in a glassy matrix. These crystals result in GCs with excellent mechanical and optical properties (Table 7) [19, 91-93]. For this reason, lithium disilicate GCs are suggested for single and multiple framework (for example bridges), either by lost-wax casting (IPS

Empress II), or by heat-pressing (IPS e.max Press), or by CAD/CAM (IPS e.max CAD) technologies [19].

Over the years and especially with the introduction of digital technology in dentistry (CAD/CAM technology), various systems of bioinert GCs (machinable or not) have been studied by teams of researchers and have been proposed as potential materials for dental applications [83]. Montazerian and Zanotto [19] searched the scientific publications in Scopus database using the keywords “dental glass-ceramic”, or “teeth glass-ceramic”, or “tooth glass-ceramic” in the article, or patent title and the title, abstract, and keywords. As shown in Fig.14, there is an increasing research activity, especially after 2005. Bearing the above in mind and being aware of the problems arising from the mismatch of the mechanical properties between the enamel and the dental aesthetic materials, it is important to develop new machinable bioinert GC materials, capable of producing aesthetic dental restorations, showing the highest possible fracture toughness and flexural strength values without being characterized by high hardness values.

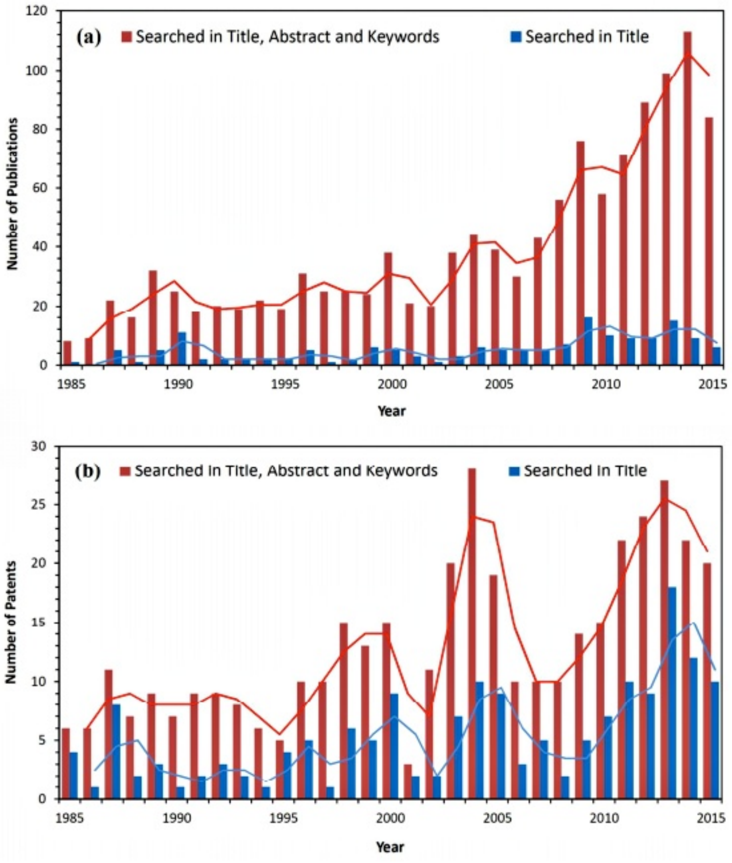

Figure 14. (a) Number of scientific publications (papers, books, and conference papers), and (b) number of granted patents related to dental glass-ceramics per year, extracted from the Scopus database by searching the keywords “dental glass-ceramic”, or “teeth glass-ceramic”, or “tooth glass-ceramic” [19].

B. State of the art and aim

STATE OF THE ART AND AIM

State of the art

The discovery of the bioactive glass 45S5 by Prof. Hench 50 years ago, inaugurated the field of modern bioactive glasses and ceramics [40]. These materials are able to spontaneously transform their surface into a hydroxyapatite (HA) layer, when they are in a biological environment, either natural (i.e. in the body) or artificial (e.g. in simulated body fluid, SBF) [3, 36, 38, 94, 95]. However, the relatively poor mechanical properties of the bioactive glasses limit their application in many areas of biomedical applications. The need to satisfy the requirements related to mechanical properties, along with the chemical ones associated with bioactivity, in conjunction with the intrinsic poor mechanical properties of bioactive glasses, which significantly limit their application in biomedicine [96], triggered the research towards glass-ceramics (GCs) [45, 82, 97-103]. Bioactive GCs, prepared by controlled crystallization of specific glass compositions, attract increasing interest in biomedicine, either in bulk form or as coatings, [4] because they can optimally combine the characteristics of the bioactive glass and the high mechanical strength of the ceramic of the same composition [3, 38]. Bromer introduced the first bioactive GC material (Ceravital®) in 1973, which has been a milestone for many research groups to develop bioactive GCs with improved mechanical properties, so as to be used as dental materials (dental implants) and so on [18].

A fundamental presupposition for a successful hard tissue implantation is a continuation at the interface between the implant and the living part. The HA layer formed onto the surface of bioactive glasses or ceramics serves a dual purpose, where the optimum combination of these two functions is the key to the success of an implantation [103]. First, the chemical resemblance of the newly formed HA on the surface of the bioactive material with the biological HA of the living bone assures the development of a strong chemical bonding with the living tissue at the interface and favors osteointegration. Additionally, this HA layer facilitates the distribution of the stress between the biomaterial and the surrounding bone and thereby reduces stress shielding [80].

Biomechanics within living jaw tissues rules the longevity of dental implants in the oral cavity. The changes in the intensity and the direction of occlusal loads, the mechanical properties of jaw bones, the design of the dental implants, the treatment of the implant surface, the design of prosthetic restorations, and the materials used for the production of a dental implant are factors whose proper evaluation play a decisive role in the ultimate success of dental implant restorations [60]. Unlike natural teeth, the body of dental implant, after the placement of the prosthetic restoration, is now the one that receives the largest percentage of occlusal forces, despite the jaw bone. Taking into account the above and knowing the problems that may arise from the mismatch of the physico-mechanical properties of the implant materials to those of the jaw bone (mainly modulus of elasticity and fracture toughness), the nature of the materials used for the production of a dental implant may be one of the most important factors for the success of dental implant [46].

In dental implant applications, the most popular materials used, such as Ti or zirconia, are non-bioactive or bioinert. The surface of such bioinert materials can display bioactive properties through bioactive coatings, for instance plasma-sprayed HA. Nevertheless, this configuration has the drawback of not displaying a uniform degradation, giving rise to weak points at the bone-coating interface [35, 45, 78, 83]. Thus, the development of novel bioactive materials, which can create a strong chemical bond between the dental implant and the jaw bone, as well as accelerate implant anchorage by inducing an HA layer on the implant surface [82], is vitally important in these applications.

The success of a material intended for use as a dental material is based on its ability to work in balance with the surrounding tissues without causing injury to them. Thus, according to the ISO 6872 standard, a dental material, should exhibit good chemical, mechanical, and optical properties, comparable to those of natural teeth [85]. Hence, in the case of dental implant materials, in the stage of the design of the compositions, it would be useful to take into account the mechanical properties of human jaw bone. A dental implant aims of restoring the root of natural teeth that comes in contact with the jaw bone, which, in contrast to a crown (which protrudes into the oral cavity), is mostly composed of dentine, which is covered by a thin layer of cementum (it is the smallest dental hard tissue, of 10-200 μm thickness). Cementum has a structure similar to that of bone tissue but has a lower hardness than dentine (<0.6 GPa); thus it has no contribution to the mechanical strength of the natural tooth, but its role is limited only to lining the root and maintaining the tooth in the alveolar [19, 55]. So, an ideal dental implant material should exhibit mechanical properties that are close to those of the natural teeth without (far) exceeding those of the jaw bone.

Taking into account the above and knowing the problems arising from the mismatch of the mechanical properties between the natural tissues (i.e. jaw bone and dentine) and dental implant materials, it is important to develop new materials, such as GC materials, capable of being used in the production of dental implants. Research teams, around the world, have been involved in developing GC materials for dental implant applications [19, 45, 64]. Although, their results cover the desired chemical and biological properties, the values of the mechanical properties are often higher than the desired ones, and far beyond those of the human jaw bone and dentine.

In the case of restorative dental bioinert GCs, which are used as "fixed all ceramic prosthetic restorations" in reconstruction of the crown of the teeth, and do not come in contact with the jaw bone, it is important to exhibit mechanical properties that do not lead to an injury of the abutment, adjacent and opposite teeth [18, 19]. In these applications, where bioactivity is not necessary, the most commonly used materials are IPS-Empress-1$^{®}$, IPS-Empress-2$^{®}$, IPS e.max Ceram, Dicor$^{®}$ MGC, zirconia ceramics, and Vita In-Ceram Alumina. Although these materials satisfy the aesthetic requirements, due to their white color, they have been blamed for injury of the opposite natural teeth because of their high mechanical properties and in particular their high values of hardness (> 7 GPa), compared to that of natural enamel (3-5 GPa).

Over the years, various systems of glasses and GCs have been proposed and studied as potential materials for biomedical applications. However, glasses in the CaO-MgO-SiO_2 ternary system, which contain both wollastonite ($CaSiO_3$) and diopside ($CaMgSi_2O_6$), lead to attractive GCs, which display good mechanical, chemical, and biological properties (such as bioactivity) [1, 20, 32-34]. In an earlier study, GCs in the CaO–MgO–SiO_2 system which contained diopside ($CaMgSi_2O_6$), wollastonite ($CaSiO_3$) and fluorapatite ($Ca_5(PO_4)_3F$), were suggested as potential candidate materials for producing bone grafts [104].

The physico-mechanical properties and the *in vitro* and *in vivo* performance of bioactive glasses and GCs can be modified and improved with the addition of oxides (Al_2O_3, B_2O_3, Li_2O, Ti_2O, Fe_2O_3 ZrO_2, etc.). However, this needs to be done carefully, as the addition of oxides can lead to one property being improved but eventually destroying another desired property [1, 4, 16, 104, 105]. For example, the addition of Al_2O_3, which is the most characteristic representative of biocompatible, completely safe non-toxic, non-allergenic and non-carcinogenic ceramic oxide, to bioactive compositions, although it improves the mechanical properties and the chemical durability, can lead to decreasing the ability of the final material to form HA on its surface [1, 16]. In case of glasses, the addition of Al_2O_3 in the amounts higher than 2 - 3 mol% reduced bioactivity by stabilizing the silica structure enough to impede calcium phosphate build-up within the silica layer, so slowing down the rate of hydroxyapatite (HA) formation [16, 105]. According to Rabiee et al. [16], the percentage of Al_2O_3 which may lead to inhibition of bioactivity depends on the composition and the chemical durability of the parent glass. Thus, the addition of Al_2O_3 can be made in many ways: the resultant GC can be used in applications where bioactivity is the main concern (e.g. dental implants) by improving the physico-mechanical properties, as well (without limiting bioactivity), or in applications where improved mechanical properties play a crucial role and bioactivity must be zero (e.g. fixed all ceramic prosthetic restorations).

Aim of the Thesis

Taking into account the above issues, this Ph.D. thesis aims at developing novel GC materials for dental applications. More specifically:

The initial (first) aim of this doctoral thesis is to design novel compositions in the CaO–MgO–SiO_2 system (after modification or not), which lead to bioactive GC materials suitable for *dental implant applications*.

The second aim is further develop the above novel compositions by (relatively) simple but important (in terms of glass and ceramic technology) modifications/substitutions, in order to lead either to bioactive GC materials with improved physico-mechanical properties (with values close to those of jaw bone and dentine) as required in *dental implant applications*, or to bioinert GC materials with physico-mechanical properties, which are required in the case of *fixed all ceramic prosthetic restorations*.

Design of novel compositions

(a) The exciting experience and the novel GCs 1d and 1e

The design of the compositions studied in the present thesis was based on the already existing experience of our research team. More specifically, the essential ingredients in most bioactive glasses are SiO_2, Na_2O, CaO, and P_2O_5 [3, 104]. As far as the crystalline phases are concerned the GCs used in biomedical applications consist of wollastonite ($CaSiO_3$), fluorapatite ($Ca_5(PO_4)_3F$) and the diopside ($CaMgSi_2O_6$) [4]. Fluorapatite based GCs are potential candidates in various medical and dental applications due to the antibacterial effect of F^- ions [106]. Also, fluorapatite and wollastonite are bioactive materials that form a surface layer of hydroxyapatite (HA) upon their exposure to SBF solution, which is a key requirement for an artificial material to be used as a bioactive bone substitute [3, 107]. Diopside plays an important role in achieving a durable GC material. It provides mechanical strength to GCs, needed in dynamically changing environments [4, 35, 108-111]. Accordingly, the combination of the crystalline phases of diopside, fluorapatite, and wollastonite is expected to result in GCs with high mechanical strength and excellent bioactivity. Despite the above very interesting features, literature survey reveals that GCs of diopside–fluorapatite–wollastonite have received less attention and are poorly documented [35].

The early efforts of our research team for producing GC materials for use in biomedical applications (dentistry and orthopedics) began in 2006, where, according to the researchers Tulyaganov et al. [33], the final GCs, in the CaO-MgO-SiO_2 system with B_2O_3, P_2O_5, Na_2O, and CaF_2 additives, displayed satisfactory physico-mechanical properties, such as modulus of elasticity, hardness etc., for applications in dentistry. Agathopoulos et al. [111], who wanted to study these compositions for their ability in HA formation, used **composition 1** (Table 8), which in the course of the experiments, was modified by increasing the percentage of P_2O_5 (from 3.26 to 4.81 and finally 6.32 wt.%). Thus, after full characterization, they concluded that the increase in the amount of P_2O_5 favored the formation of A-type HA, and named this as **composition 1b**. Tulyaganov et al. [104] used the composition 1b, from which they removed B_2O_3 to achieve increased bioactivity in the final material, resulting in the **composition 1d** and the **composition 1e** (Table 8). It is briefly reminded that the compositions 1d and 1e refer to two glasses which differ by about 2 mol% in the content of both SiO_2 and CaO. Furthermore, 1e has a higher amount of P_2O_5 than 1d (3.02 and 2.60 mol%, respectively). The glasses 1d and 1e were considered as promising materials for biomedical applications since they were biocompatible, bioactive and non-toxic. Moreover, the first approach of composition 1d as a candidate for biomedical applications in the form of glass powder was carried out in Tashkent, Uzbekistan, where glass 1d was studied both *in vitro* and *in vivo* and clinically, as well, in a dental application as a bone missing material, in particular after a cystectomy. Glass 1d exhibited both bioactivity and excellent behavior in the jaw bone environment. Bearing in mind the above, the compositions 1d and 1e were qualified and selected as the initial compositions for this doctoral thesis.

However, only the glasses 1d and 1e had been prepared, so far [104]. There was no experience on the corresponding GCs 1d and 1e, at all. Hence, this thesis shed light on the GCs 1d and 1e prepared by heat-treatment of glass powder compacts. The properties of the produced GCs (i.e. sintering behavior, crystallization, mechanical properties, aesthetics, and bioactivity) were evaluated with regard to their suitability for dental applications, reported in the aim of the work.

Table 8. Glass compositions (in wt.%) of the previous works, which led to the bioactive glasses 1d and 1e.

Tulyaganov DU, Agathopoulos S, Ventura JM, Karakassides MA, Fabrichnaya O, Ferreira JMF. *Synthesis of glass-ceramics in the CaO-MgO-SiO_2 system with B_2O_3, P_2O_5, Na_2O and CaF_2 additives*. J. Eur. Ceram. Soc. **2006**;26:1463-1471 [33].

Glass	**SiO_2**	**B_2O_3**	**CaO**	**MgO**	**P_2O_5**	**Na_2O**	**CaF_2**
1	41.39	5.33	30.05	9.25	3.26	4.74	5.98
2	42.23	4.89	31.54	8.50	2.99	4.36	5.49
3	42.95	4.52	32.80	7.86	2.77	4.03	5.07

Agathopoulos S, Tulyaganov DU, Ventura JM, Kannan S, Karakassides MA, Ferreira JMF. *Formation of hydroxyapatite onto glasses of the CaO-MgO-SiO_2 system with B_2O_3, Na_2O, CaF_2 P_2O_5 additives*. Biomaterials **2006**;27:1832-1840 [111].

Glass	**SiO_2**	**B_2O_3**	**CaO**	**MgO**	**P_2O_5**	**Na_2O**	**CaF_2**
1	41.39	5.33	30.05	9.25	3.26	4.74	5.98
1a	40.73	5.24	29.57	9.10	4.81	4.67	5.88
1b	40.08	5.16	29.10	8.96	6.32	4.59	5.79

Tulyaganov DU, Agathopoulos S, Valerio P, Balamurugan A, Saranti A, Karakassides MA., Ferreira JMF. *Synthesis, bioactivity and preliminary biocompability studies of glasses in the system CaO-MgO-SiO_2-Na_2O-P_2O_5-CaF_2*. J Mater Sci: Mater Med **2011**;22:217-227 [104].

Glass	**SiO_2**	**B_2O_3**	**CaO**	**MgO**	**P_2O_5**	**Na_2O**	**CaF_2**
1b	40.08	5.16	29.10	8.96	6.32	4.59	5.79
1d	46.06	-	28.66	8.83	6.22	4.53	5.70
1e	43.48	-	30.44	8.75	7.19	4.49	5.65

(b) Modified compositions

In order to achieve the two aims of the thesis, modifications of the base compositions 1d and 1e were attempted. In general, the modified glass compositions studied in the present work are based on the CaO-MgO-SiO_2 system with the addition of P_2O_5, Na_2O, K_2O, CaF_2, and Al_2O_3. The role of each additive has been described in the Introduction.

To achieve ***the first aim*** of the doctoral thesis, that is, the production of GCs suitable for dental implant applications, one should have in mind the key role of the resistance of these materials to the occlusal forces of the oral cavity, since the dental implant, unlike the natural tooth, after the placement of the prosthetic restoration, is now the one that receives the largest percentage of occlusal forces, despite the jaw bone, and the problems that may arise from the mismatch of the physico-mechanical properties of the materials with those of the jaw bone. Thus, the selected 1d and 1e compositions were heat-treated, for the first time. Full characterization of the final GCs focused on their bioactivity performance and physico-mechanical properties in order to evaluate if can be used for the production of bioactive GCs dental implants. In order to approach the mechanical properties of the GCs 1d and 1e as close as possible to those of dentine and jaw bone, the following two modifications took place, resulting in two new series of compositions:

- In the first series of the new compositions, complete substitution of K_2O for Na_2O was carried out in both 1d and 1e. These new compositions (Table 9) are designated as 1d-k and 1e-k, (where the letter k is after K_2O).
- In the second series of compositions, partial substitution of MgO for CaO took place in 1d and 1e, and these new compositions (Table 9) are designated as 1d-m and 1e-m, (where the letter m is after MgO).

Table 9. The investigated (Al_2O_3-free) compositions (in wt.%).

Composition	SiO_2	CaO	MgO	P_2O_5	Na_2O	K_2O	CaF_2
Parent glass compositions [104]							
1d	46.06	28.66	8.83	6.22	4.53	0	5.70
1e	43.48	30.44	8.75	7.19	4.49	0	5.65
K_2O for Na_2O substitution							
1d-k	45.01	28.00	8.62	6.06	0	6.72	5.57
1e-k	42.49	29.73	8.55	7.06	0	6.66	5.52
MgO for CaO partial substitution							
1d-m	46.61	24.85	11.90	6.27	4.57	0	5.76
1e-m	43.98	26.68	11.80	7.27	4.53	0	5.71

The ***second aim*** of the doctoral thesis was to modify the above compositions (1d, 1d-k, 1d-m, 1e, 1e-k, 1e-m) in such a way that by choosing the proportion of a single proposed oxide, the above GCs can be used in two different domains of dentistry. In other words, with a simple but significant modification, the above compositions should lead either to GCs with improved physico-mechanical properties (with values corresponding to jaw bones and dentine) in parallel with maintenance of bioactivity, as dental implants require, or to bioinert GCs with desired physico-mechanical properties, as required in the case of fixed all-ceramic prosthetic restorations. Essentially, the second aim of the doctoral thesis required **"an oxide regulator"** to be suggested for both physico-mechanical properties and bioactivity. Thus, after reviewing international literature [1, 4, 16, 18, 104, 105], it was suggested the addition of **Al_2O_3** to the above compositions (1d, 1d-k, 1d-m, 1e, 1e-k, 1e-m) as follows:

- The need for a better approach of the physio-mechanical properties of the jaw bone and dentine, without limiting or inhibiting the bioactivity, in the above compositions (1d, 1d-k, 1d-m, 1e-k, 1e-m) was attempted by adding 1 mol% (1.7-1.75 wt.%) Al_2O_3 (Table 10).
- In order to convert the bioactive GC materials (1d, 1d-k, 1d-m, 1e-k, 1e-m) into bioinert and to increase the physico-mechanical properties, so that they reach to the closest possible level the physico-mechanical properties of enamel, 7-8 mol% (12.5 wt.%) Al_2O_3 was added in the above compositions (1d, 1d-k, 1d-m, 1e-k, 1e-m) (Table 10).

The whole concept of this approach, which refers to the aim of Al_2O_3 addition, is schematically represented in Fig. 15.

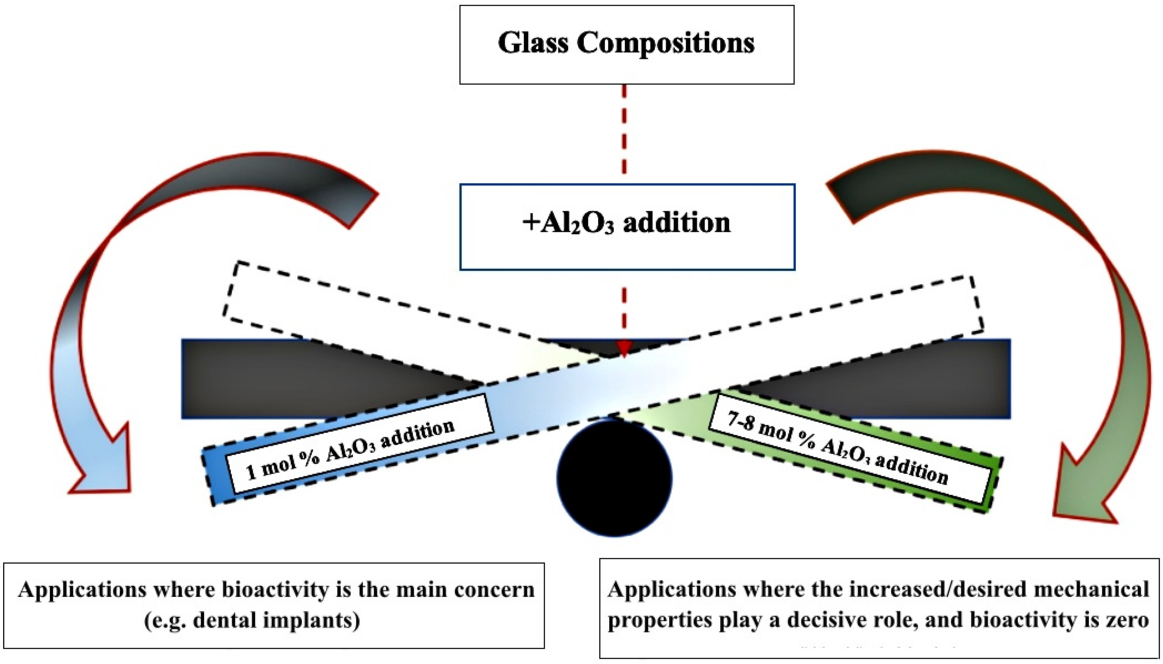
Glass Compositions
+Al₂O₃ addition
1 mol % Al₂O₃ addition
7-8 mol % Al₂O₃ addition
Applications where bioactivity is the main concern (e.g. dental implants)
Applications where the increased/desired mechanical properties play a decisive role, and bioactivity is zero

Figure 15. Al_2O_3 addition depends on the clinical application.

Table 10. Modified alumina containing glass investigated compositions (in wt.%). For comparison purposes, the compositions of the parent Al_2O_3–free glasses from Table 9, are also presented.

Composition	SiO_2	CaO	MgO	P_2O_5	Na_2O	K_2O	CaF_2	Al_2O_3
Parent glass compositions (Al_2O_3–free; Table 9)								
1d	46.06	28.66	8.83	6.22	4.53	0	5.70	0
1d-k	45.01	28.00	8.63	6.07	0	6.72	5.57	0
1d-m	46.62	24.85	11.91	6.27	4.58	0	5.77	0
1e	43.48	30.44	8.75	7.19	4.49	0	5.65	0
1e-k	42.49	29.73	8.55	7.06	0	6.66	5.51	0
1e-m	43.98	26.68	11.81	7.27	4.54	0	5.72	0
Modified alumina (1 mol%) containing glass compositions								
1d/A_1	45.28	28.17	8.68	6.12	4.45	0	5.60	1.70
1d-k/A_1	44.25	27.53	8.48	5.97	0	6.60	5.47	1.70
1d-m/A_1	45.83	24.43	11.70	6.17	4.50	0	5.67	1.70
1e/A_1	42.74	29.92	8.60	7.06	4.40	0	5.55	1.73
1e-k/A_1	41.78	29.25	8.40	6.91	0	6.54	5.42	1.70
1e-m/A_1	43.23	26.22	11.60	7.14	4.45	0	5.61	1.75
Modified alumina (7-8 mol%) containing glass compositions								
1d/A_2	40.30	25.07	7.73	5.45	3.96	0	4.99	12.50
1d-k/A_2	39.38	24.51	7.55	5.32	0	5.87	4.87	12.50
1d-m/A_2	40.78	21.76	10.42	5.50	4.00	0	5.04	12.50
1e/A_2	38.04	26.63	7.65	6.29	3.92	0	4.94	12.50
1e-k/A_2	37.18	26.02	7.48	6.14	0	5.82	4.83	12.50
1e-m/A_2	38.48	23.34	10.32	6.36	3.97	0	5.00	12.50

Structure of the presentation of the dissertation

The experiments carried out, the experimental findings and their discussion are presented in the next chapters and their sections, as follows:

The experiments carried out to accomplish the two aims of this thesis, mentioned above, are delineated in the next chapter of the *Experimental Procedure*, where the preparation of the glasses and the GCs, along with the characterization methods of the resultant materials are described in detail. More specifically, in this chapter, the synthesis and the thermal analysis (by dilatometry and DSC) of the investigated glasses are presented. Thermal analysis was conducted in order to set-up the optimal crystallization process for producing fine GCs, as well as to shed light on the crystallization mechanism. Then, it follows the description of the preparation of the GC specimens (according to the ISO 6872 "Dentistry-Ceramic Materials") and the full characterization of the final GC materials, which includes study of sintering behavior, determination of microstructural and crystallographic features, as well as measurements of the mechanical properties of flexural strength, modulus of elasticity, microhardness, and fracture toughness, along with the *in vitro* evaluation of their bioactivity performance.

Then, the chapter of the *Experimental Results* is following. Based on the aim of the doctoral thesis, it is divided in two main sections, and each section in two sub-sections. More specifically, the first section presents the experimental results related to the *development of GCs suitable for dental implant applications*. In the sub-section **1.1**, the qualification of the parent compositions 1d and 1e, with regard to the production of bioactive GCs which are suitable for fabricating dental implants, is shown. In section **1.2**, the results obtained from the modified compositions (produced by the partial substitution of Mg for Ca and the complete substitution of K for Na in 1d and 1e), are presented. In the second section, the experimental results related to the *development of GCs suitable for dental implant and all-ceramic fixed prosthetic applications*, are presented. The section **2.1** presents the results of the modified, with 1 mol% Al_2O_3 addition, bioactive GCs. In section **2.2**, the results of the modified, with 7-8 mol% Al_2O_3 addition, bioinert GCs, are presented. Considering that the stage of the design of the novel compositions has been adequately described in this chapter, the experimental results in each of the four aforementioned sub-sections (1.1, 1.2, 2.1, and 2.2) are presented according to following general scheme. The first part focuses on the evaluation of the sintering behavior and the crystallization. This includes the results of the thermal analysis of the glasses, which define the set-up of the heat-treatment schedule to produce GCs and shed light on the crystallization mechanism and allows the determination of the activation energy (E_a) of crystallization and the Avrami parameter (n_A), the evaluation of sintering performance, reflected in the values of the density and the linear shrinkage, as well as the appearance of the GC samples, which is also an index for their aesthetics, the crystallographic analysis by X-ray diffraction and the microstructure analysis, by SEM/EDS. Then, the results of the mechanical properties are presented, following by the evaluation of the *in vitro* bioactivity of the produced GCs. At the end, an overall evaluation of the experimental results is provided in the light of the demands of the specific applications that the produced GCs aim at. Thus, in conjunction with bioactivity performance, the mechanical properties of the GCs are compared to those of natural tissues, related to the specific applications (e.g. jaw bone, dentine, or enamel) as well as the properties of other widely used dental materials, such as zirconia or Ti alloys. At the end of each sub-section, a general conclusion is stated with regard to the accomplishment of the specific aim and suggestions for further development of the compositions (e.g. by other substitutions and additions) are proposed.

The last chapter presents a *General Discussion*, the *Conclusions* and proposals for *Future work*. Firstly, a detailed explanation of the results of thermal analysis and their importance in producing GC materials is presented. Then, the focus is shifted to crystalline phases and the microstructure of the produced GC materials. The discussion emphasizes in the importance of each crystalline phase both in the physical-mechanical properties of the final GCs and in their bioactivity performance. More specifically, in the case of dental implants, the importance of bioactivity and the mechanical properties of the materials produced is thoroughly discussed in comparison to the corresponding values of dentine and jaw bone, as well as other commercial dental implant materials, such as titanium alloys and zirconia. In the case of all-ceramic restorations, the discussion focuses on the comparison of the mechanical properties of the produced bioinert GCs with the corresponding values of enamel and commercial GC materials and the evaluation of the mechanical properties of the produced GCs according to the ISO 6872 "Dentistry-Ceramic Materials", so as to be potentially proposed for the dental applications as veneers, inlays, onlays etc. The chapter is completed by summarizing the conclusions of this work and by suggesting specific topics for future research.

C. Experimental Procedure

1. *Glasses: synthesis and thermal analysis*

2. *Glass-ceramics (GCs): preparation, characterization and bioactivity*

EXPERIMENTAL PROCEDURE

The experiments that took place during this PhD thesis, described in more detail below, included synthesis of glasses, thermal analysis (dilatometry, DSC), synthesis of glass-ceramics (GCs), crystalline phases analysis of GCs (XRD), microstructure observation of GCs (SEM/EDX), calculation of physico-mechanical properties of GCs, and *in-vitro* bioactivity tests.

1. Glasses: synthesis and thermal analysis

Synthesis of glasses

Fine powders of SiO_2 (Sigma Aldrich; 99.8%), $CaCO_3$ (Fluka; ≥99.0%), $Mg(NO_3)_2{\cdot}6H_2O$ (Sigma Aldrich; ≥99.0%), $(NH_4)_2HPO_4$ (Merck; ≥99.0%), Na_2CO_3 (Lachner; 99.6%), K_2CO_3 (Sigma Aldrich; 99.99%), CaF_2 (Alfa Aesar; 99%), and Al_2O_3 (Merck; 99.0%) were used as raw materials. For each composition, batches of 100 g were prepared by weighing the raw powders and then by thorough homogenization through ball-milling. Next, each mixture was preheated at 900 ºC for 1 h in air (Controller S5, Nabertherm®, Germany) in an Al_2O_3 crucible, at a heating rate of 1.5 K/min (Fig. 16a). Then for each composition, the obtained oxide powder mixture was melted (Fornos Electricos, Termolab, Portugal) in a Pt crucible (Platinum Crucible, Alfa Aesar, Germany) at 1400 ºC for 1 h, in air (Fig. 16b).

Bulk glasses with no crystalline inclusions (confirmed by X-ray diffraction analysis) were produced by casting the molten glass into preheated bronze moulds, which were then immediately subjected to annealing at 650 ºC (that is close to the glass transition temperature) for 1 h, in air, and then let to slow cooling inside the furnace (Fig. 16b). Glass frit was also produced by rapid pouring of the molten glass into cold water (Fig. 16b). The glass frit was dried, ground in a planetary ball-mill (Pulverisette, Fritisch, Germany; at 400 rpm, for 45 min) resulting in a fine glass powder and then sieved through a sieve of 32 microns. This allowed to exclude relatively course particles and to get fine glass powder with a final particle size < 32 μm.

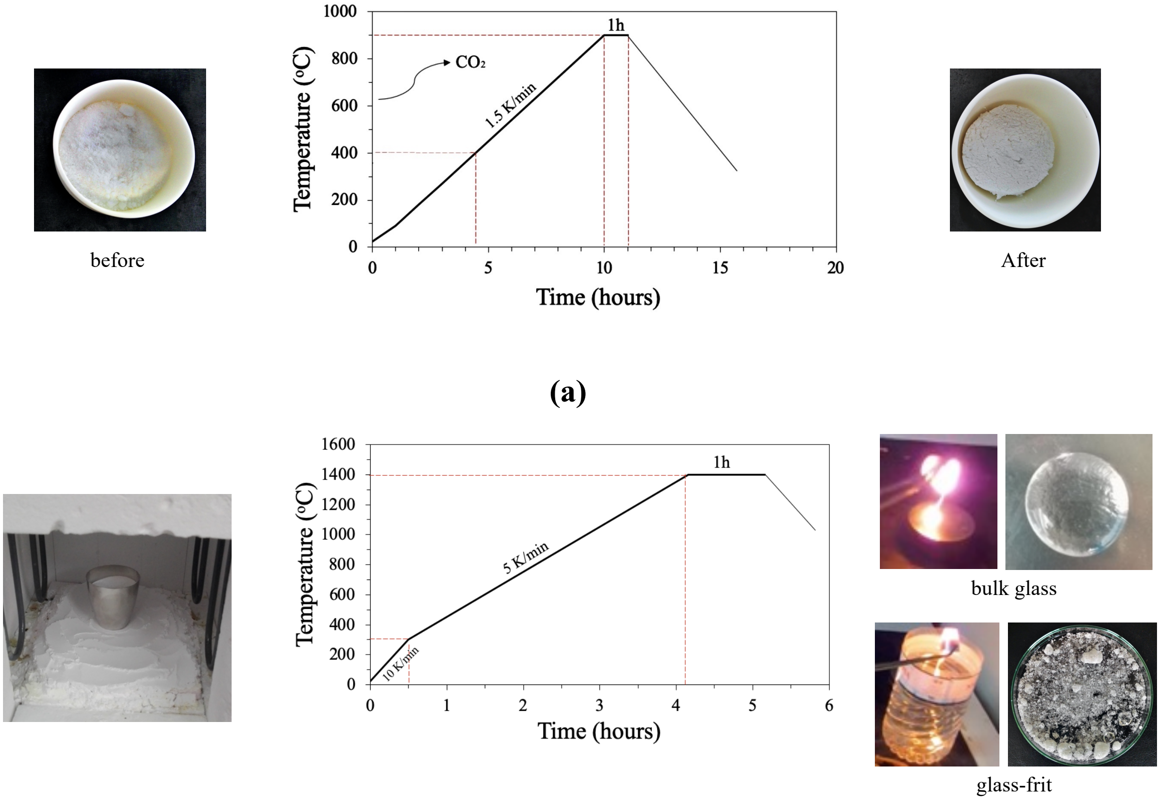

(a)

(b)

Figure 16. The processes of (a) decarbonization, and (b) glass melting and production in bulk and frit forms along with the corresponding appearance of the samples.

Thermal analysis

In order to decide on the crystallization process that had to be followed to produce the GCs, full characterization of the thermal properties of the produced glasses was performed. Dilatometry measurements (by a dilatometer DIL 402 C, Netzsch, Germany) in the temperature range of 20 – 770 °C at a heating rate of 5 K/min, were perfomed in air, so as to determine the glass transition temperature (T_g) and the softening point (T_s) of the glasses. Bulk glass prismatic samples were used in these experiments.

Differential scanning calorimetry (DSC, STA 449 C, Netzsch, Selb Germany), in the temperature range of 25 – 1000 ºC in air, was also conducted, where ~15 mg of glass powder was placed into an Al_2O_3 crucible in the DSC equipment. The recorded thermographs allowed the determination of the glass transition (T_g), the onset crystallization (T_c), and the peak of crystallization (T_p) temperatures (at which crystallization of the glass occurs) for each investigated composition, as well as the calculation of the two important thermodynamic magnitudes, the activation energy (E_a) of glass crystallization and the Avrami exponent (n_A or m), which is an index of the growth dimensionality. In order to determine these two thermodynamic parameters, DSC experiments were performed at five different heating rates (φ) between 5 and 25 (i.e. 5, 10, 15, 20, and 25) K/min. For each heating rate, three independent runs ($n = 3$) were performed. For each glass comostion, the values of the activation energy of crystallizaiton E_α (in kJ/mol) were calculated from the plots of $\ln((Tp^2)/\varphi)$ vs 1000/Tp, according to the equation (5) (as explained in detail in the section 1.2 in the Introduction chapter), and the values of the Avrami paramener n_A were calculated by applying the equation (6), using the results of the thermographs, and more specifically by analyzing the exothermic crystallization peak (as also explained in detail the same section 1.2 in the Introduction chapter). In this study the crystallization kinetics of glasses was investigated by non-isothermal methods (Kissenger and Augis-Bennet methods) using DSC, three-dimensional growth of crystal occurring for $n_A \geq 3$, $n_A \geq 2$ signifies a two-dimensional crystallization and for $n_A \geq 1.0$ it corresponds to one-dimensional growth of crystals [24, 27, 112].

2. Glass-ceramics (GCs): preparation, characterization and bioactivity

Preparation of GCs

Fine powder from each parent glass was granulated by mixing with a 2.5 vol% polyvinyl alcohol (PVA) solution (glass powder / PVA = 97.5/2.5, in wt%). Parallelepiped bars (5 x 4 x 40 mm^3) were prepared by uniaxial pressing (150 - 200 bar). The bars of the glass powder compacts were heat-treated at 450 °C for 2 h in air, for debinding, and then at various temperatures, according to the results from thermal analysis for 1 h, in air (Fig. 17).

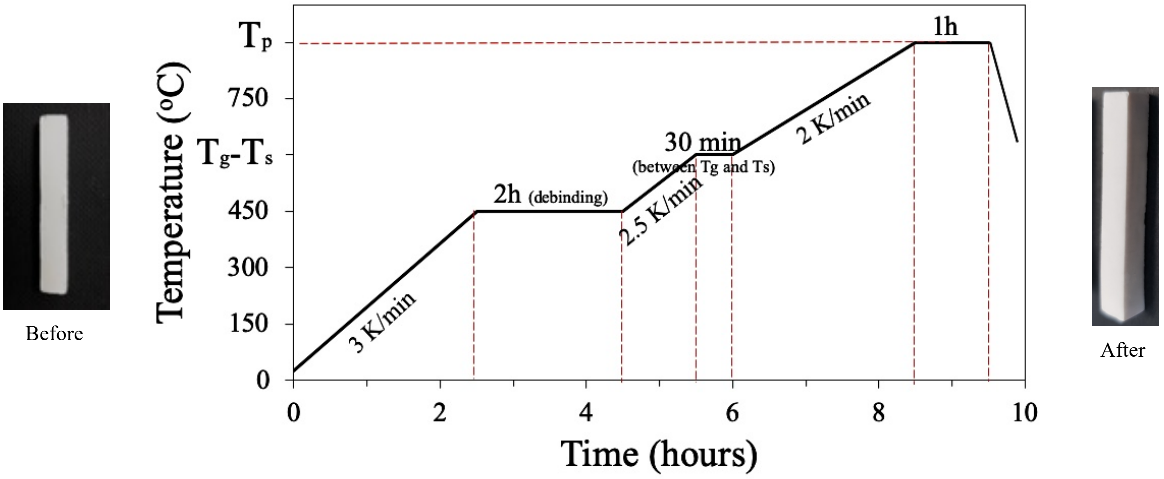

Figure 17. The heat-treatment process to prepare the GCs along with the appearance of the samples before (glass powder compact) and after the heat-treatment (final GC bar).

Crystalline phase analysis of GCs (XRD)

The crystalline phases developed in the produced GCs were identified by X-ray diffraction analysis (XRD, D8 Advance, Bruker AXS, Billerica, Massachusetts, USA; Cu K_α radiation ($\lambda = 1.5406$ Å), produced at 30 kV and 25 mA, was used), in the range of diffraction angles (2θ) between 20 and 60^o with a 2θ step of 0.02 ^{o}/s. The diffractograms were compared to standards complied by the International Center for Diffraction Data (ICDD).

Microstructure of GCs (SEM/EDX)

The microstructure of the GCs was observed in a scanning electron microscope (SEM, 6510 LV, JEOL, Freising, Germany), using an acceleration voltage of 20 kV equipped with an energy dispersive spectroscopy (EDS) device for elemental analysis. The sample preparation was as follows. The GC specimen was embedded in an acrylic resin (Resine Phenolique, Presi, France) and ground using SiC papers (from 200 - 1400 grid) in a polishing machine (RotoPol-25, Struers, Denmark) under continuous water cooling. Then, they were polished with diamond pastes (Diamant Mecaprex Spray, Presi, France), using a diamond paste of 1 μm as a final polishing step i.e. mirror finishing,. The polished surfaces, after being cleaned in an ultrasonic bath with distilled water and dried, were chemically etched by immersion in 2 vol.% HF solution for 30 s. Immediately after this period of time, they were washed with tap water in order to stop the etching process and avoid the formation of fluorides on the GCs surface, and finally cleaned with distilled water. To obtain a conductive surface, the samples were sputtered with a Au-Pd thin film (4-8 nm) in a sputtering machine.

Determination of physical and mechanical properties of GCs

The linear shrinkage during sintering was calculated from the difference of the dimensions between the green and the sintered bars. The Archimedes immersion method (in water) was used to measure the density of the sintered GC specimens (which were fully-dense with no porosity).

In order to determine the mechanical properties of the produced GCs, the bars were rectified by grinding with SiC papers (from 200 - 1400 grid) to obtain the dimensions, accoridng to the ISO 6872 “Dentistry – Ceramic materials” [85]. More specifically, the dimensions of the specimens were: width 4.0 (± 0.2) mm, thickness 3.0 (± 0.2) mm, and length 35.0 (± 0.2) mm (according to this standard, the samples must be at least 2 mm longer than the span between the supporting rods, and the ratio of thickness to length (b/L) must be ≤ 0.1).

The flexural strength (σ) and the modulus of elasticity (E) were calculated according to the ISO 6872 “Dentistry – Ceramic materials” [85] by using the results of three-point bending strength tests (Autograph AGS-H, Shimadzu, Japan), carried out with a head speed of 1.0 mm/min and a span of 25 mm between the supporting rods. The values of σ and E were calculated by using the following equations, respectively:

$$\sigma = \frac{3\mathrm{FL}}{2\mathrm{wh}^2} \tag{7}$$

and

$$\mathrm{E} = \frac{\mathrm{L}^3\mathrm{m}}{4\mathrm{wh}^2} \tag{8}$$

where F is the fracture load, L is the span between the supporting rods (25 mm), w is the specimen width (5 mm), h is the specimen thickness (4 mm), and m is the slope of the straight line in the plot of load *versus* displacement.

Vickers microhardness (HV) measurements were performed on polished surfaces (prepared as reported above for the preparation of the samples for SEM, up to the mirror finishing stage) with the use of a Digital Microhardness Tester (Time Instrument, Indonesia), by applying a load of 500 g (or 4.9 N) for 30 s. From the length (l) of the cracks propagated from the corners of the pyramid indentation, the value of fracture toughness (K_{IC}, in MPa·$m^{0.5}$) was also calculated by using the Lankford equation [114]:

$$\frac{\varphi K_{IC}}{\mathrm{H}\alpha^{\frac{1}{2}}} \left(\frac{\mathrm{H}}{\varphi E}\right)^{\frac{2}{5}} = 0.035 \left(\frac{\mathrm{l}}{\alpha}\right)^{-\frac{1}{2}} \tag{9}$$

where φ is a constraint factor (~3), E is the modulus of elasticity (in GPa), H is the hardness (in GPa), and α is the indent half-diagonal.

The presenting results for the above properties of the GCs are the average (and their standard deviation) from 10 independent measurements made on different GC specimens (i.e. n = 10, for each GC).

Brittleness is a measure of the relative susceptibility of a material to deformation and fracture. It is related with hardness (H), which quantifies the resistance to deformation, and toughness (K_{IC}), which quantifies the resistance to fracture. Accordingly, the ratio of hardness to fracture toughness (H/K_{IC}) has been proposed as a simple index of brittleness (B) [115].

In-vitro bioactivity tests

The *in vitro* bioactivity of the produced GCs was evaluated by their ability for inducing HA formation on their surface, after immersion in SBF (which has an ionic concentration (in mM) of Na^+ 142.0, K^+ 5.0, Ca^{2+} 2.5, Mg^{2+} 1.5, Cl^- 147.8, HCO_3^- 4.2, HPO_4^{2-} 1.0, and SO_4^{2-} 0.5, and buffered at pH = 7.25 by tris-hydroxymethyl-amminomethane and hydrochloric acid) at 37 °C for several periods of time [104, 116] (7, 14, 21, 60, 90, and 120 days). Polished bars and fine powders (0.2 g, which exposed an area of ca. 1 cm^2) of the investigated GCs were immersed (separately) in 25 ml SBF (having passed through a filter of 0.2 μm), sealed in sterilized plastic flasks, and stored at 37 °C. At the aforementioned periods of time, measurements of the pH of the liquid, X-ray diffraction analysis of the powders, and SEM/EDS analysis of the surface of the bars were conducted (the conditions of the XRD and SEM analyses have been reported above).

Figure 18 outlines the above stages of the PhD thesis.

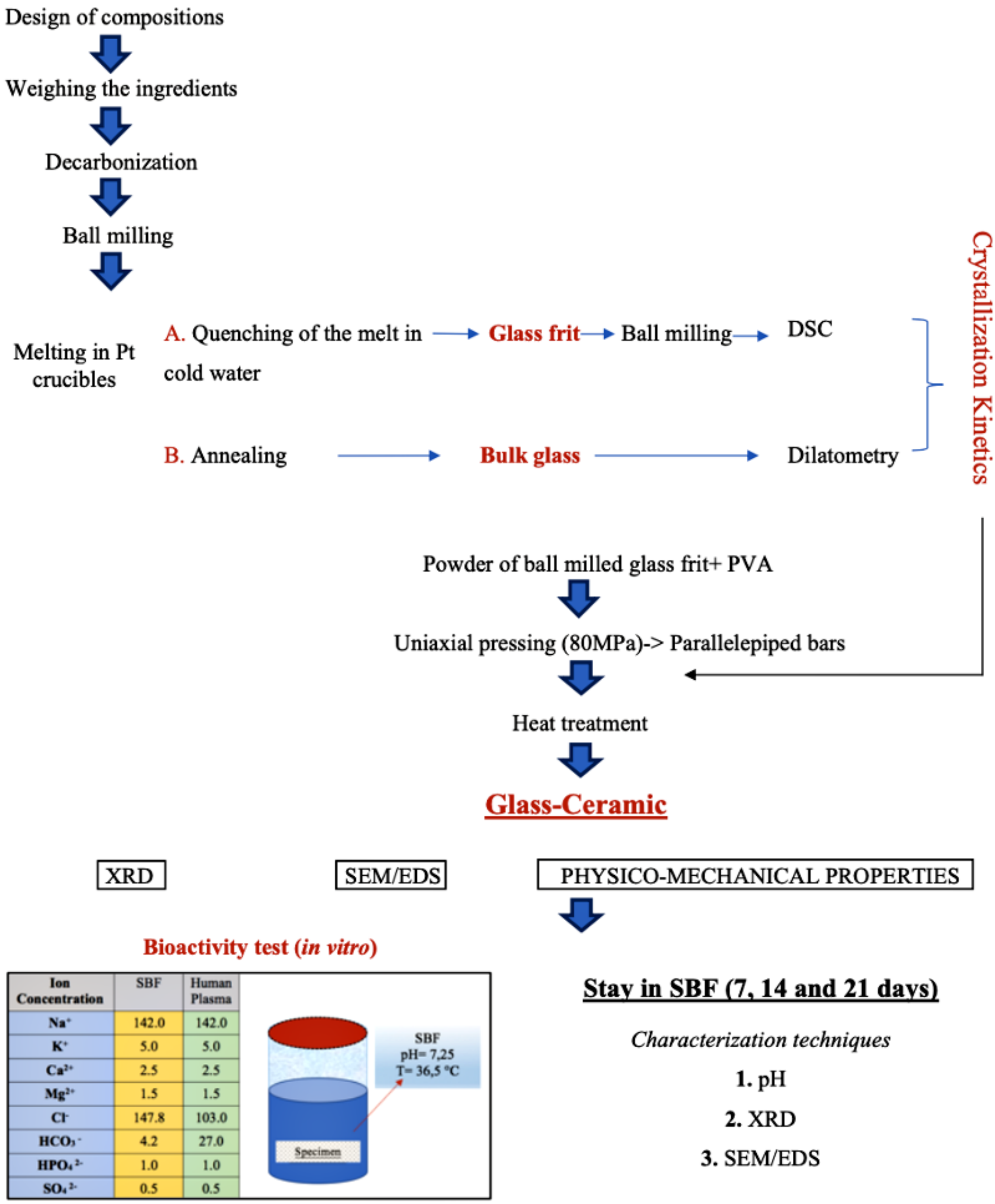
Design of compositions
Weighing the ingredients
Decarbonization
Ball milling
Melting in Pt crucibles
A. Quenching of the melt in cold water
Glass frit
Ball milling
DSC
B. Annealing
Bulk glass
Dilatometry
Crystallization Kinetics
Powder of ball milled glass frit+ PVA
Uniaxial pressing (80MPa)-> Parallelepiped bars
Heat treatment
Glass-Ceramic
XRD
SEM/EDS
PHYSICO-MECHANICAL PROPERTIES
Bioactivity test (in vitro)
SBF
pH= 7,25
T= 36,5 °C
Specimen
Stay in SBF (7, 14 and 21 days)
Characterization techniques
1. pH
2. XRD
3. SEM/EDS

Ion Concentration	SBF	Human Plasma
Na^+	142.0	142.0
K^+	5.0	5.0
Ca^{2+}	2.5	2.5
Mg^{2+}	1.5	1.5
Cl^-	147.8	103.0
HCO_3^-	4.2	27.0
HPO_4^{2-}	1.0	1.0
SO_4^{2-}	0.5	0.5

Figure 18. Outline of the experimental procedure.

D. Experimental results

__1.__ Development of GCs suitable for dental implant applications

__2.__ Development of GCs suitable for dental implant & all-ceramic fixed prosthetic applications

EXPERIMENTAL RESULTS

1. Development of glass-ceramics (GCs) suitable for dental implant applications

This chapter presents and analyzes the results of the experiments performed to achieve the first objective of the doctoral thesis. It is divided in two main sections. The first section (**1.1**) presents the qualification of the compositions 1d and 1e in the production of bioactive GCs suitable for constructing dental implants. More specifically, in conjunction with bioactivity, these GCs exhibited mechanical properties that suggest them make these materials for possible production of dental implants. The second section (**1.2**) presents the results of the modifications made to the parent glasses (1d and 1e), in order the mechanical properties of GCs to be as close as possible to those of dentine and human jaw bone. These modifications include complete substitution of K_2O for Na_2O (1d-k and 1e-k) and partial substitution of MgO for CaO (1d-m and 1e-m) in the parent compositions.

1.1 GCs with the initial compositions 1d and 1e

I. Densification and crystallization

I-1. Results of thermal analysis

The dilatometry curves of the produced glasses, plotted in Fig. 19, show that the T_g of the glasses 1d and 1e were 607 and 613 °C, respectively, while the T_s 639 to 641 °C, respectively.

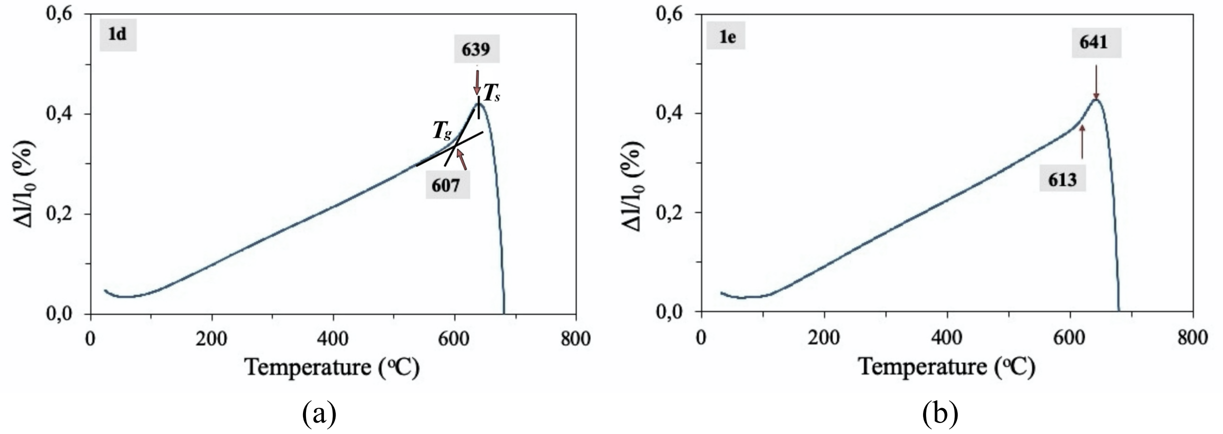

(a) (b)

Figure 19. Dilatation curves of bulk annealed glasses (a) 1d, and (b) 1e. The graphical estimation of T_g and T_s is shown (the software of the dilatometry equipment used in this work automatically estimates T_g and T_s through this method).

The DSC thermographs of the investigated glasses are shown in Fig. 20 (they correspond to heating rate of 15 K/min). The first endothermic peak (marked with the downwards arrow) corresponds to T_g and the second indicates the onset of crystallization T_c, followed by a strong and sharp exothermic peak at T_p, attributed to glass crystallization. The endothermic peak at T_l reveals the liquidus temperature, which resulted from decomposition and dissolution of the crystalline phases produced in the GCs. The values of T_g, T_c, T_p, and T_l are presented in Table 11. DSC was also performed at five different heating rates. The results (not shown) showed that the temperatures of T_g, T_c, T_p, and T_l was increased as the heating rate was increased.

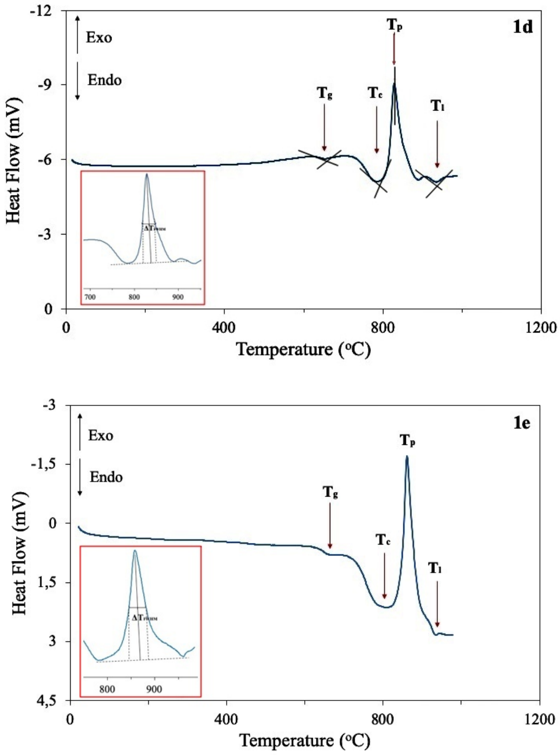

(a)

(b)

Figure 20. Thermographs of the investigated glasses (corresponding to the glass (a) 1d and (b) 1e at heating rate of 15 K/min). The insets show the measurement of the full width at the half maximum of the crystallization peak. The graphical estimation of T_g, T_c, T_p and T_l is shown (the software of the equipment used in this work automatically estimates these temperatures through this method). The results are summarized in Table 11 from 3 independent measurments.

Table 11. Mean values (and standard deviation; n = 3) of glass transition temperature (T_g), oncet crystallization temperature (T_c), crystallization temperature (T_p), and liquidus temperature T_l, determined by the thermographs of Fig 20. The sintering window is also (T_c - T_g) is also presented.

Glass	T_g (°C)	T_c (°C)	T_c - T_g	T_p (°C)	T_l (°C)
1d	649 ± 9	783 ± 2	134	815 ± 13	936 ± 9
1e	653 ± 8	788 ± 8	135	847 ± 16	952 ± 5

I-2. Crystallization mechanism

Besides choosing the heat-treatment processing of the glasses in order to prepare the corresponding GCs, the plots of $\ln((T_p^2)/\varphi)$ *vs* $1000/T_p$ were made, using the results of the DSC analyses. It should be stressed that in the calculations for these plots, temperature was expressed in K. A good linear fitting was obtained for the five tested heating rates in all glasses, as shown in Fig. 21, which corresponds to the 1d and 1e glasses. The calculated activation energy (E_a) of crystallization for each glass is shown in Table 12. The values of E_a, for glasses 1d and 1e were 430 ± 30 and 384 ± 18 kJ/mol, respectively. Furthemore, from the analysis of the exothermic peaks (i.e. from the calculation of the full width at the half maximum at T_p, as shown in the inset of Fig. 20), the Avrami exponent (n_A) for each glass was calculated. The results are listed in Table 12, and suggest that the glasses 1d and 1e are prone to three-dimensional growth of crystals, since $n_A \geq 3$ in all cases.

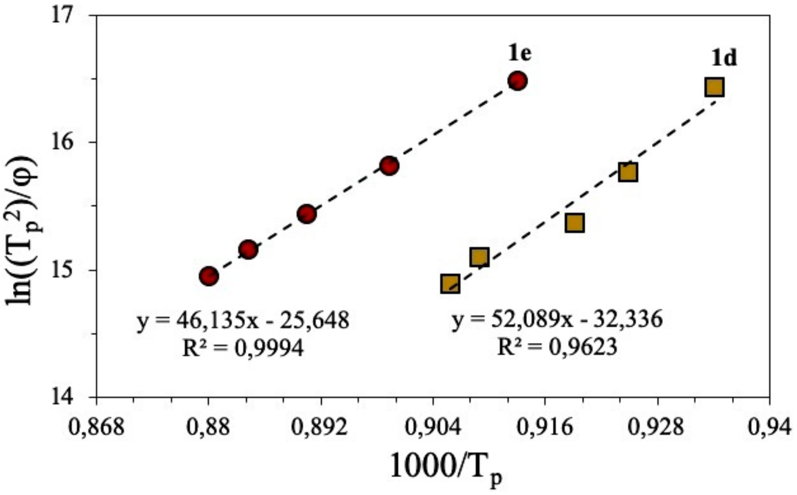

Figure 21. The plots of $\ln((T_p^2)/\varphi)$ *vs* $1000/T_p$ for the glasses 1d and 1e.

Table 12. Mean values (and standard deviation; n = 3) of activation energy (E_a) of crystallization, and Avrami exponent (n_A) of the investigated glasses 1d and 1e.

Glass	E_a (kJ/mol)	n_A
1d	430 ± 30	3.8 ± 0.2
1e	384 ± 18	3.0 ± 0.2

I-3. Sintering and aesthetics

The choice of the heat-treatment temperatures tested for the parallelepiped bars of the glass-powder compacts was based on the three findings of the thermal analysis of the glasses, T_g (i.e. ~ 607 and 613 °C, Fig. 19), T_s (~ 639 and 641, Fig. 19), and T_p (i.e. 825 ± 13 and 847± 16 °C, Table 11). Thus, the heat-treatment of the parallelepiped bars of the glass-powder compacts was carried out at the temperatures of 800, 850, and 900 °C.

Well-sintered dense GC bars of white colour (Fig. 22) were produced from glass powder compacts. Their densities along with the density of the corresponding bulk parent glass (which was always smaller than that of the corresponding GC, suggesting crystallization of the glass) are presented in Table 13. The linear shrinkage of the GCs ranged between 9.6 and 11.6 % (Table 13).

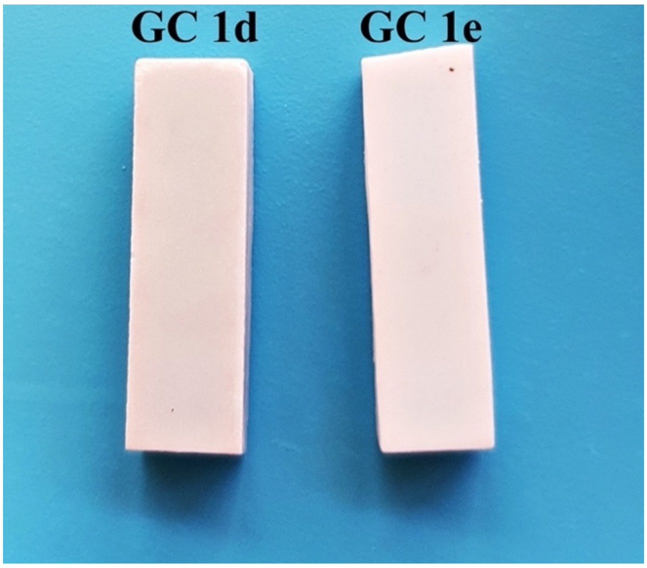

Figure 22. Well-sintered dense 1d and 1e GC bars of white colour.

Table 13. Mean values (and standard deviation, n = 5) of linear shrinkage and density of the parent annealed glasses and investigated GCs 1d and 1e heat-treated at various temperatures for 1 h.

GCs		Heat-treatment temperature (°C)		
	Annealed glass	800	850	900
		Linear shrinkage (%)		
1d	-	11.6 ± 1.14	10.2 ± 1.13	9.6 ± 0.07
1e	-	10.4 ± 0.95	10.2 ± 0.46	9.7 ± 0.32
		Density (ρ, g/cm^3)		
1d	2.57 ± 0.12	3.03 ± 0.33	2.85± 0.31	2.70 ± 0.09
1e	2.53 ± 0.61	3.07 ± 0.51	3.01± 0.15	2.99 ± 0.29

I-4. Crystalline structure

In the GCs 1d and 1e diopside ($CaMgSi_2O_6$), fluorapatite ($Ca_{10}(PO_4)_6F_2$) and wollastonite ($CaSiO_3$) were predominantly crystallized (Fig. 23) (Appendix 1: Phase Diagrams). There is no evidence of formation of other secondary or minor phases, according to the assignment of the peeks in the diffractograms of Fig. 23.

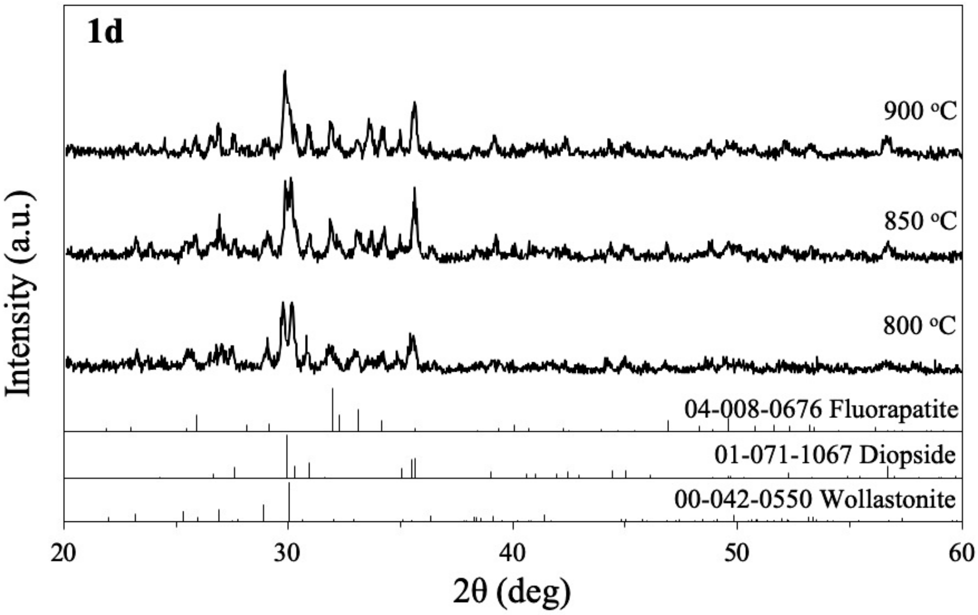

(a)

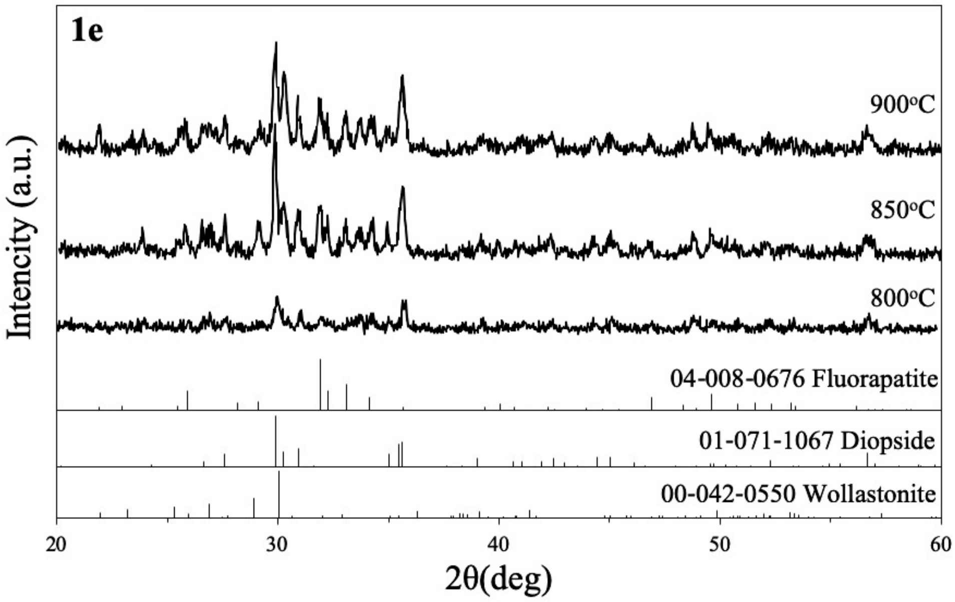

(b)

Figure 23. X-ray diffractograms of glass-powder compacts (a) 1d and (b) 1e heat-treated at various temperatures for 1 h. The standard patterns of diopside ($CaMgSi_2O_6$), fluorapatite ($Ca_{10}(PO_4)_6F_2$) and wollastonite ($CaSiO_3$) are plotted at the bottom of the diagrams.

I-5. Microstructure

Figure 24 shows typical SEM images of the microstructure of the produced GCs, heat-treated at 850 ºC after chemical etching with HF. Three different types of crystals were observed, whose identification was made with the aid of EDS spot analysis in conjunction with the results of the XRD analysis (Fig. 23). More specifically, in the EDS spectra, Mg was registered only in the bigger crystals, where the Mg/Ca/Si/O mol ratio was found as c.a. 1/1/2/6, respectively; thus, these crystals were assigned to diopside (D). Flour was detected in the coralloid-like small crystals marked with FA, assigned, therefore, to fluorapatite. In the crystals marked with the letter W, the Ca/Si mol ratio was 1/1; hence, these crystals were assigned to wollastonite. Consequently, SEM/EDS (Fig. 24) and XRD (Fig. 23) analyses suggest that the microstructure of the produced GCs is composed of a glass matrix with embedded prismatic diopside (D) and smaller acicular wollastonite (W) crystals, along with small crystals of fluorapatite (FA).

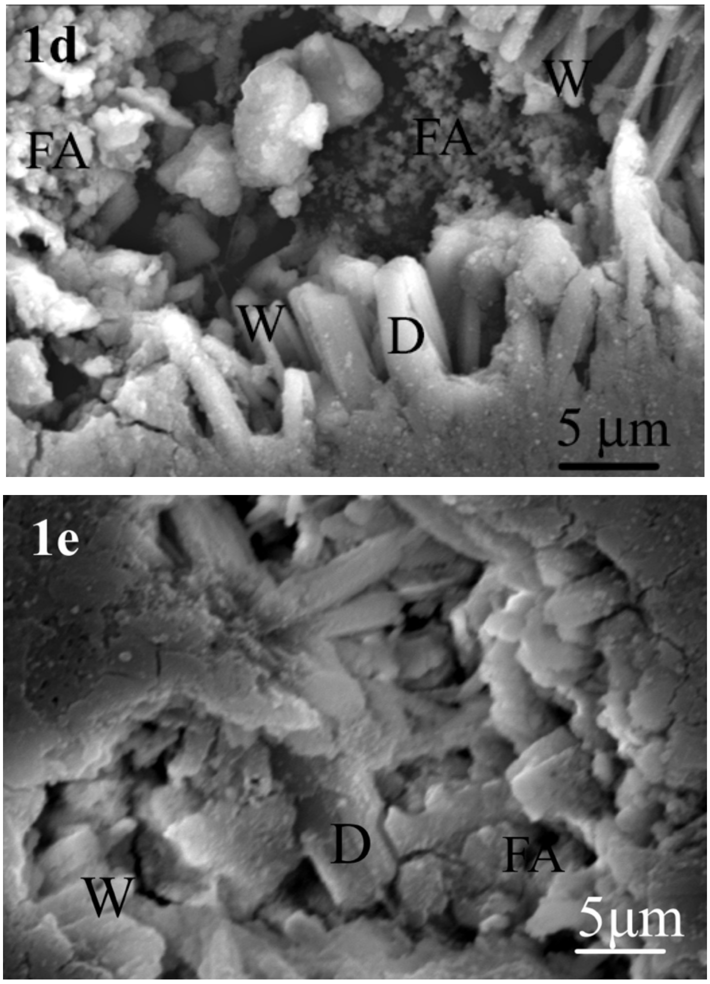

Figure 24. Typical microstructure of the produced GCs 1d and 1e, heat-treated at 850 ºC, for 1 h, observed after etching of polished surfaces with 2% HF solution. (D: diopside; FA: fluorapatite; W: wollastonite).

II. Mechanical properties

The influence of heat-treatment temperature on the mechanical properties of the produced GCs is presented in Table 14 (Appendix 2: (a) Flexural Strength (3-point bending) and (b) Vickers hardness indentation). At 800 °C, crystallization in glass powder compacts 1d and in 1e was seemingly by just initiated (Fig. 23). Owing to the fact that crystallization causes an improvement in mechanical properties, the highest values of mechanical properties, such as flexural strength, modulus of elasticity, hardness, and fracture toughness, were achieved in the GCs heat-treated at temperatures near their corresponding T_p (Table 11).

Finally, the brittleness index values of the produced GCs 1d and 1e ranged between 3.6 - 3.7 and 3.3 - 3.5 $\mu m^{-0.5}$, respectively.

Table 14. Mean values (and standard deviation, n = 10) of the mechanical properties of the investigated GCs 1d and 1e, heat-treated at various temperatures for 1 h.

GCs	Heat-treatment temperature (°C)		
	800	850	900
	Flexural strength (σ, MPa)		
1d	119 ± 10	171 ± 11	141 ± 6
1e	86 ± 19	141 ± 9	122 ± 9
	Modulus of elasticity (E, GPa)		
1d	24 ± 6	27 ± 5	22 ± 4
1e	24 ± 5	30 ± 1	25 ± 1
	Vickers microhardness (HV, GPa)		
1d	6.0 ± 0.4	6.1 ± 0.5	5.2 ± 0.7
1e	5.9 ± 0.5	6.0 ± 0.5	5.8 ± 0.1
	Fracture toughness (K_{IC}, $MPa\cdot m^{0.5}$)		
1d	1.6 ± 0.1	1.7 ± 0.1	1.4 ± 0.1
1e	1.8 ± 0.3	1.9 ± 0.3	1.7 ± 0.2

III. Bioactivity

The excellent mechanical properties of the produced GCs 1d and 1e, motivated to assess their bioactivity by SBF tests. The results of the SBF testing provided a clear evidence of bioactivity. More specifically, the pH of the solution (Fig. 25) was rapidly increased in the first week (from 7.25 to ~9.5), and then there was a slight tendency for a slow increase, suggesting an ion exchange.

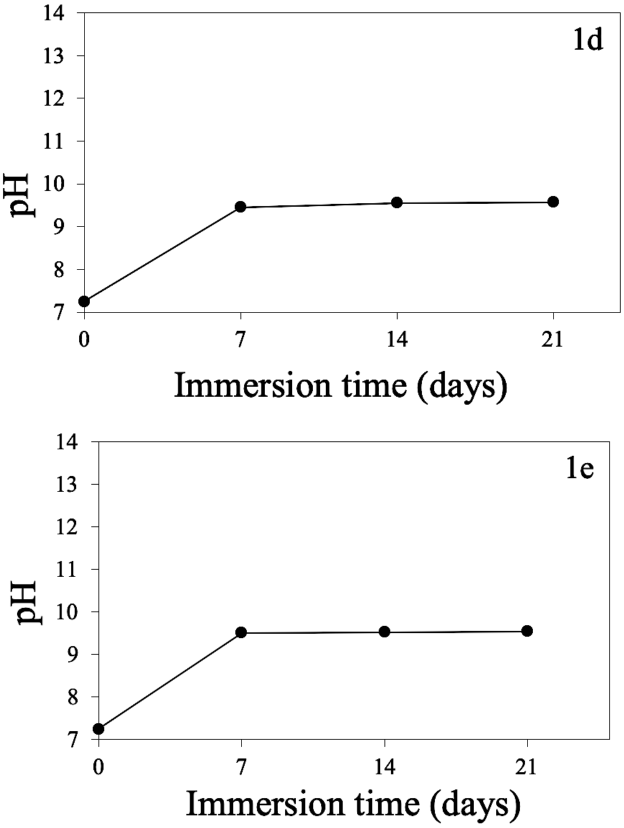

Figure 25. Evolution of pH of the solution over immersion time of the GC powders 1d and 1e in SBF (at 37 °C).

In the X-ray diffractograms of the GCs powders, although there was a background of strong peaks of the crystalline phases of the GCs, there were also peaks (at 2θ 29.2° and 32.02°) which are clearly ascribed to HA (HA card: 01-086-0740), which become stronger over immersion time of the GC powders in SBF. This evolution is presented over the period of time of 7, 14, and 21 days in Fig. 26. Careful observation of the diffractograms in Fig. 26 shows that the intensity of the peaks due to wollastonite (at 2θ 26.92° and 33.7°) becomes weaker over immersion time and, eventually, they totally disappear.

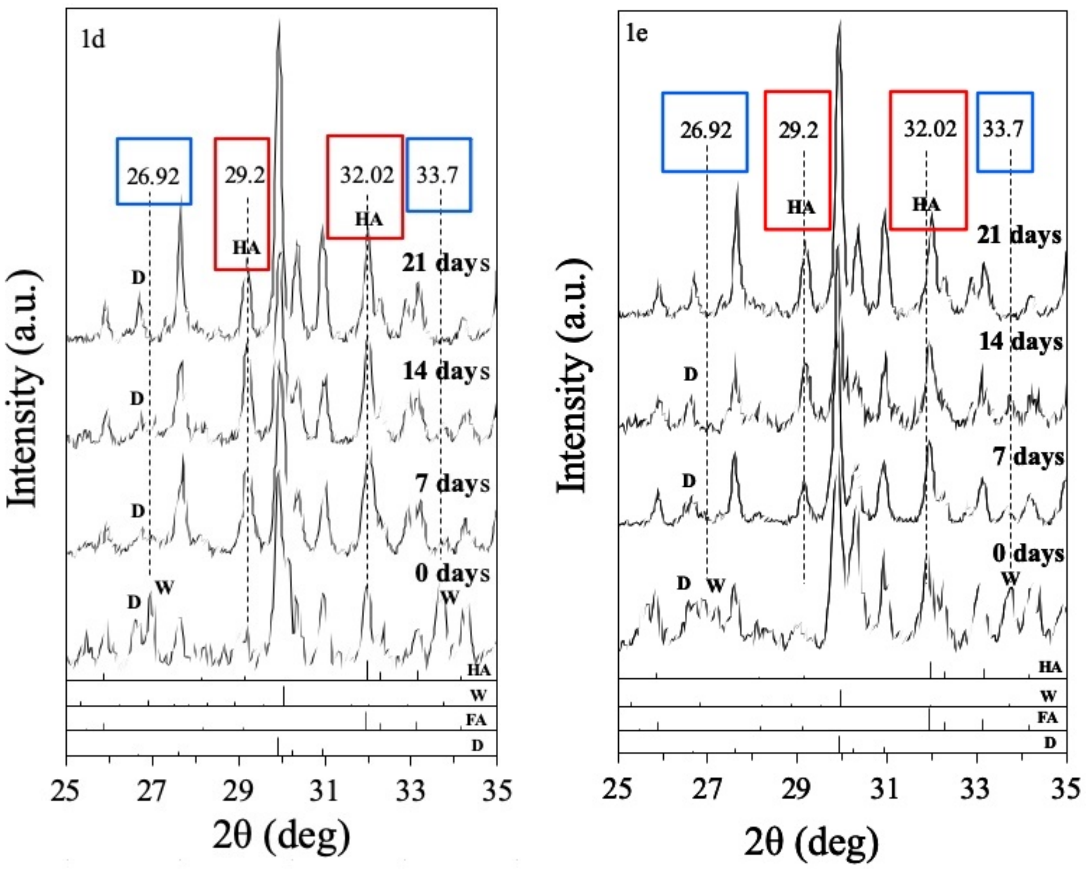

Figure 26. X-ray diffractograms of the powders of the investigated GCs 1d and 1e immersed in SBF for 7, 14, and 21 days at 37 °C.

The formation of HA layer on the surface of the produced GCs was verified by SEM observations (characteristic images for each composition are presented in Figs. 27 and 28) and EDS analyses, which showed that the Ca/P molar ratio (Tables 15 and 16) on the surface of the 1d and 1e samples, after 21 days, was 1.67 and 1.68, respectively. It is noteworthy that the HA layer was already formed after 7 days of immersion in SBF. This layer became denser after 14 and 21 days. More specifically, according to EDS analyses immersion of GCs specimens for 21 days in SBF resulted an increase in the intensity of the peaks attributed to Ca and P and a decline or disappearance of the Si, Na, and Mg peaks (Figs. 27 and 28).

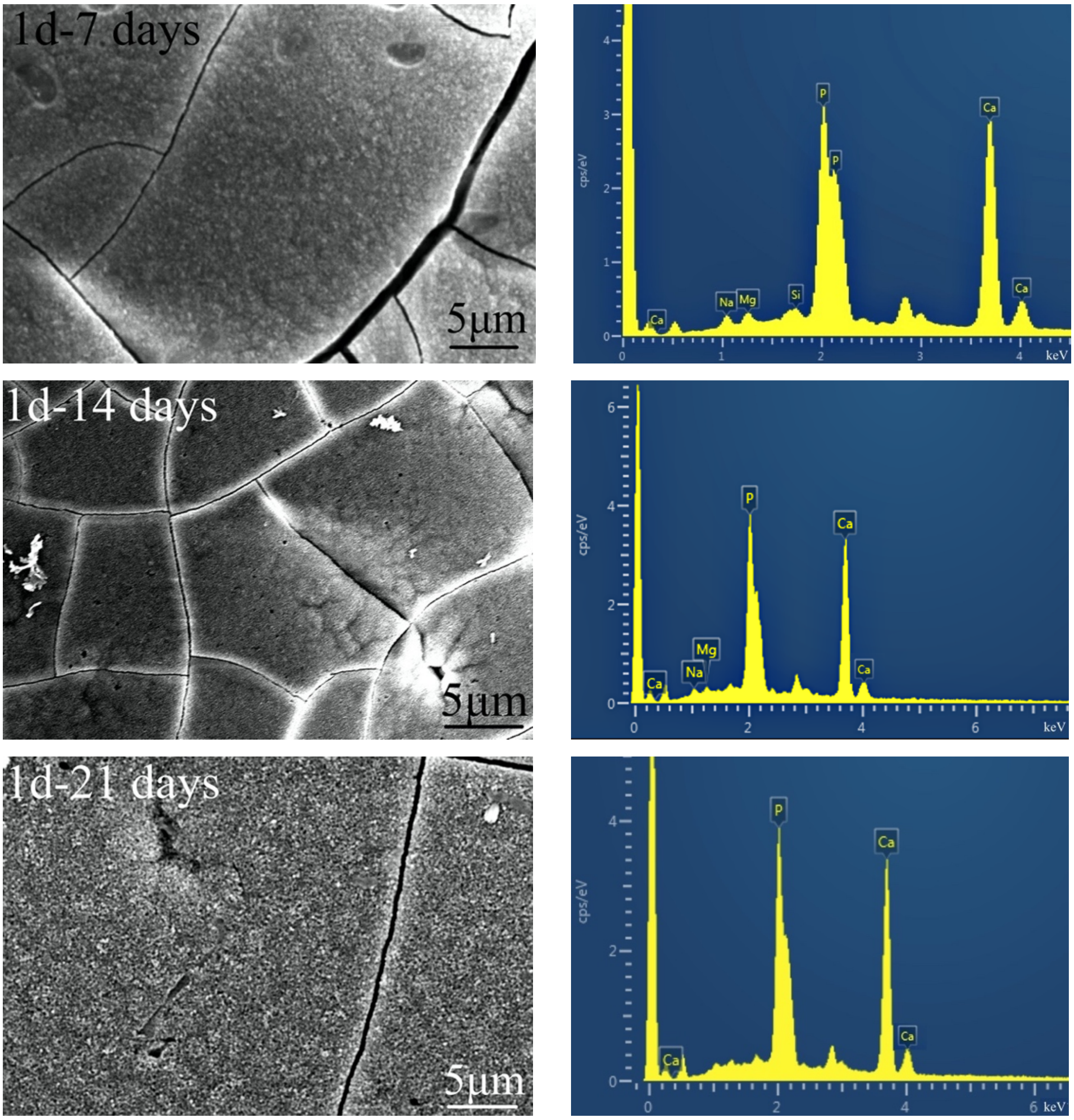

Figure 27. Formation and evolution of HA layer on the 1d GC surface at various immersion periods of time in SBF at 37 °C (7, 14 and 21 days).

Table 15. Elemental analysis (in atomic %) of the GC 1d and molar Ca/P ratio for 7, 14 and 21 days soaking in SBF.

Soaking time in SBF (days)	Si	Na	Mg	Ca	P	Molar Ca/P ratio
7	2.36	2.52	3.72	57.5	33.9	1.69
14	-	1.94	2.57	59.98	35.51	1.68
21	-	-	-	62.51	37.49	1.67

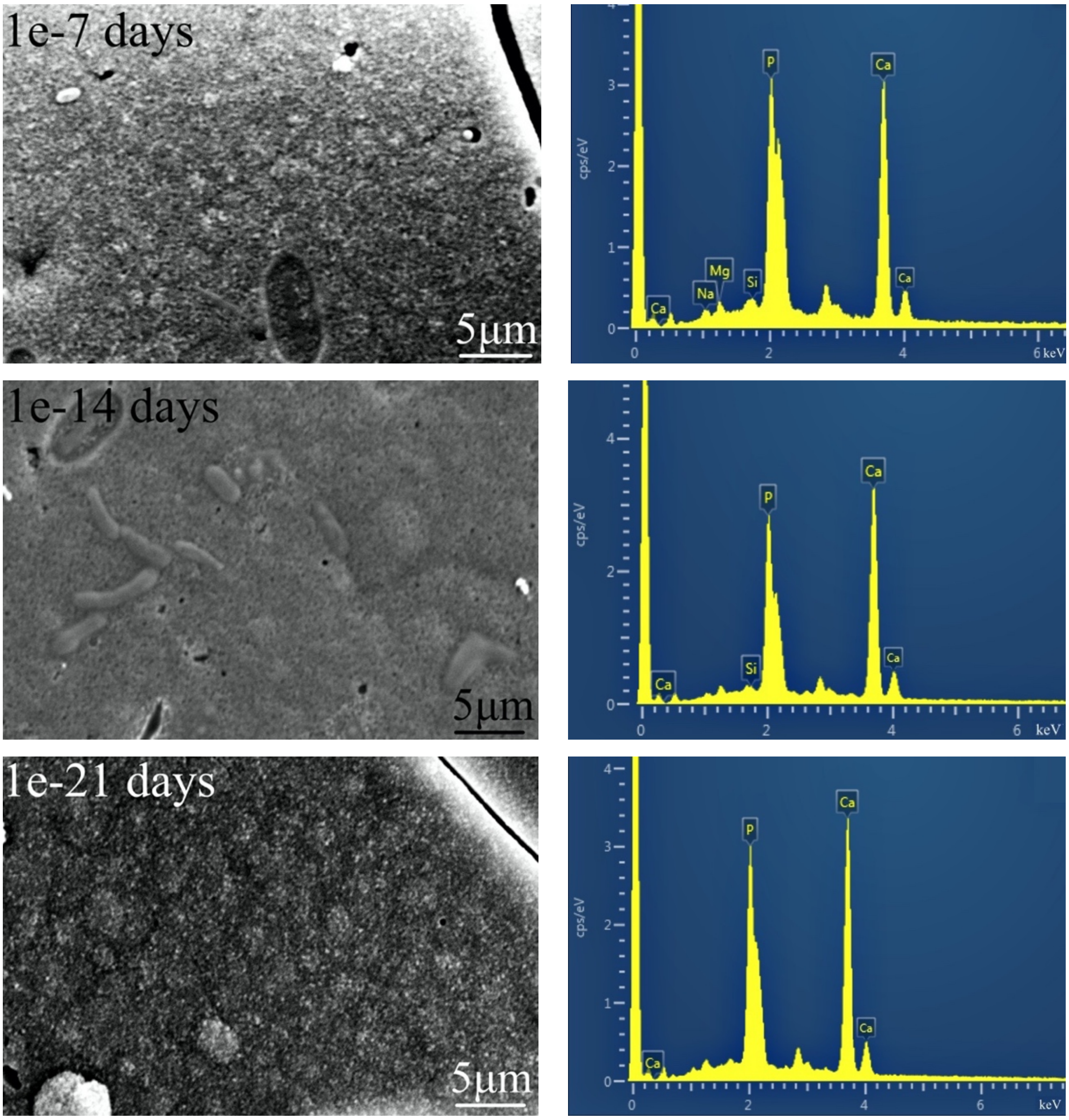

Figure 28. Formation and evolution of HA layer on the 1e GC surface at various immersion periods of time in SBF at 37 °C (7, 14 and 21 days).

Table 16. Elemental analysis (in atomic %) of the GC 1e and molar Ca/P ratio for 7, 14 and 21 days soaking in SBF.

Soaking time in SBF (days)	Si	Na	Mg	Ca	P	Molar Ca/P ratio
7	1.76	2.24	2.43	58.77	34.80	1.69
14	3.08	-	-	60.82	36.1	1.68
21	-	-	-	62.81	37.19	1.68

IV. General evaluation of the initial GCs 1d and 1e

The above experimental results showed that the produced GCs 1d and 1e displayed bioactivity features reflected in their ability to spontaneously form hydroxyapatite (HA) on their surface after immersion in SBF at 37 °C. Besides bioactivity, the phase assemblage led to well-sintered and well-crystallized GCs with a dense microstructure, which affected their mechanical properties. These features, in conjunction with the attractive aesthetics (white color), qualify the produced GCs for further consideration and experimentation as potential dental implant materials. More specifically, heat-treatment of 850 °C resulted in GCs with mechanical properties close enough to those of dentine (which is the biological tissue that a dental implant is called on to replace) and jaw bone (that is biological tissue with which the material of an implant comes into contact) (Table 17).

Table 17. Mechanical properties of the produced GCs 1d and 1e, cortical bone, and dentine.

	Heat-treatment temperature (°C)	*Flexural strength (σ, MPa)*	*Modulus of elasticity (E, GPa)*	*Vickers microhardness (HV, GPa)*	*Fracture toughness (K_{IC}, $MPa{\cdot}m^{0.5}$)*
GC **1d**	800	119 ± 10	24 ± 6	6.0 ± 0.4	1.6 ± 0.1
	850	171 ± 11	27 ± 5	6.1 ± 0.5	1.7 ± 0.1
	900	141 ± 6	22 ± 4	5.2 ± 0.7	1.4 ± 0.1
GC **1e**	800	86 ± 19	24 ± 5	5.9 ± 0.5	1.8 ± 0.3
	850	141 ± 9	30 ± 1	6.0 ± 0.5	1.9 ± 0.3
	900	122 ± 9	25 ± 1	5.8 ± 0.1	1.7 ± 0.2
Cortical jaw bone	-	50 – 150	7 – 30	0.06 – 0.07	2 – 12
Dentine	-	230 – 305	15 – 30	< 0.6	3

Further development:

The mechanical properties of the produced GCs have to be as close as possible to those of dentine and jaw bone. This can be achieved by reducing the modulus of elasticity (at a level not lower than 20 GPa) and hardness, but, at the same time, by maintaining or increasing the values of the fracture toughness. Hence, the following two modifications are proposed in the compositions 1d and 1e. The first modification concerns the complete substitution of K_2O for Na_2O, while the second modification concerns the partial substitution of MgO for CaO.

1.2 The modified GCs 1d-k, 1d-m, 1e-k and 1e-m

As mentioned above, the section **1.2** presents the results of the modifications made in the initial glasses 1d and 1e, in order the mechanical properties of the resultant GCs to be as close as possible to those of the dentine and the human jaw bone. More specifically, the modifications include complete substitution of K_2O for Na_2O (1d-k and 1e-k) and partial substitution of MgO for CaO (1d-m and 1e-m), in the parent compositions (1d and 1e, respectively).

I. Densification and crystallization

I-1. Results of thermal analysis

The dilatometry curves of the produced glasses, plotted in Fig. 29, show that the T_g of the glasses 1d-k and 1d-m were 614 and 630 ºC respectively, while the T_s values were 647 and 663 ºC. In the case of the glasses 1e-k and 1e-m the T_g were 616 and 636 ºC, while the T_s values were 648 and 662 ºC, respectively.

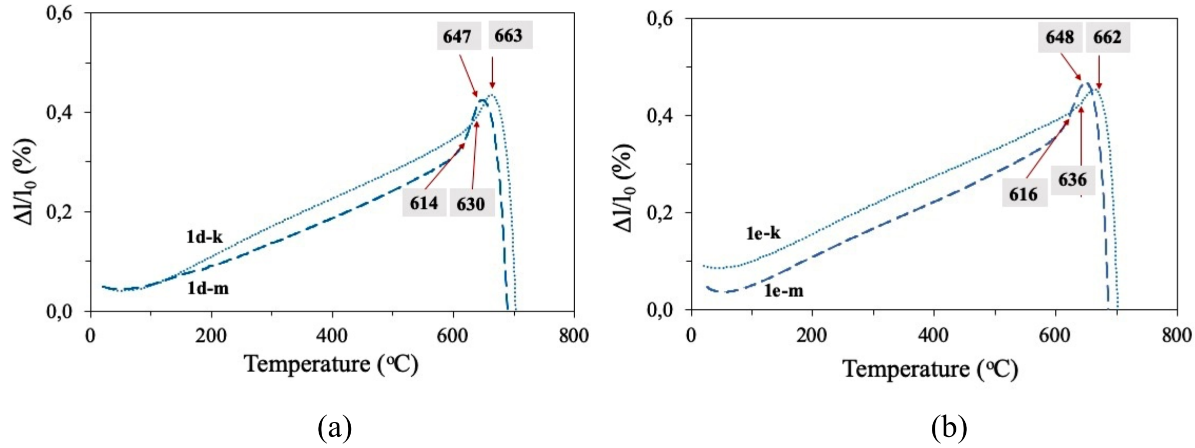

Figure 29. Dilatation curves of the bulk annealed glasses (a) 1d-k, 1d-m and (b) 1e-k, and 1e-m.

The DSC thermographs of the investigated glasses, plotted in Fig. 30, clearly show the endothermic peak of T_g, the onset of crystallization T_c, a unique exothermic crystallization peak (T_p) for each glass, and finally the endothermic peak T_l, revealing the liquidus temperature. The values of T_g, T_c, T_p, and T_l are presented in Table 18. The K-free glasses (1d-m and 1e-m) had a T_g between 650 - 660 ºC and a T_p close to 850 ºC. K substitution (in the glasses 1d-k and 1e-k) caused an increase in both temperatures, i.e. T_g was 670 - 677 and T_p ~900 ºC.

DSC was also performed at five different heating rates. The experimental results (not shown) showed that the temperatures of T_g, T_c, T_p, and T_l were increased as the heating rate was increased.

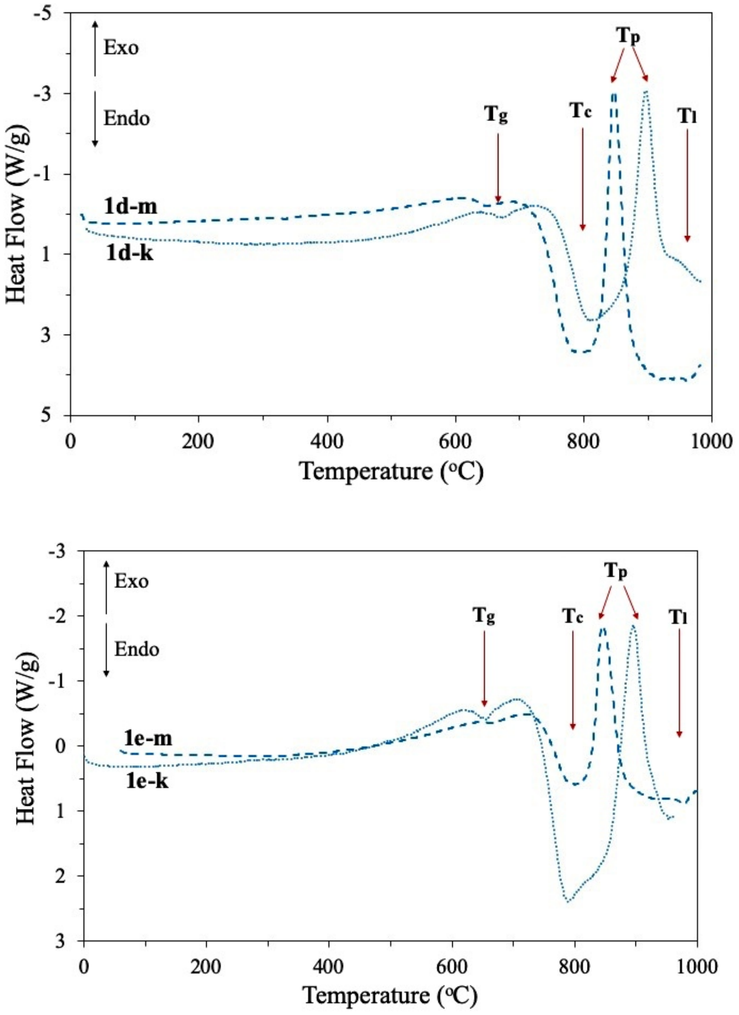

Figure 30. Thermographs of the modified glasses (at heating rate of 15 K/min). The results from 3 independent measurments are summarized in Table 18.

Table 18. Mean values (and standard deviation; n = 3) of glass transition temperature (T_g), oncet crystallization temperature (T_c), crystallization temperature (T_p), liquidus temperature T_l of the modified glasses (determined by the DCS thermographs of Fig. 30). The sintering window (T_c-T_g) is also presented.

Glass	T_g (°C)	T_c (°C)	T_c - T_g	T_p (°C)	T_l (°C)
1d-k	670 ± 8	816 ± 7	146	872 ± 14	> 988
1d-m	652 ± 8	785 ± 3	133	824 ± 14	973 ± 3
1e-k	677 ± 9	820 ± 11	143	907 ± 15	> 992
1e-m	660 ± 7	788 ± 9	128	838 ± 16	960 ± 8

I-2. Crystallization mechanism

The activation energy (E_a) of crystallization for each glass (Table 19) was caluclated using the plots of $\ln((T_p^2)/\varphi)$ *vs* $1000/T_p$ (Fig. 31). The n_A value for each glass (Table 19) was calculated from the analysis of the exthothermic peaks through the calculation of the full width at the half maximum at T_p. The results listed in Table 19 suggest that the modified glasses, are prone to three-dimensional growth of crystals since $n_A \geq 3$, while the glass 1e-k is prone to two-dimensional crystallization ($n_A \geq 2$).

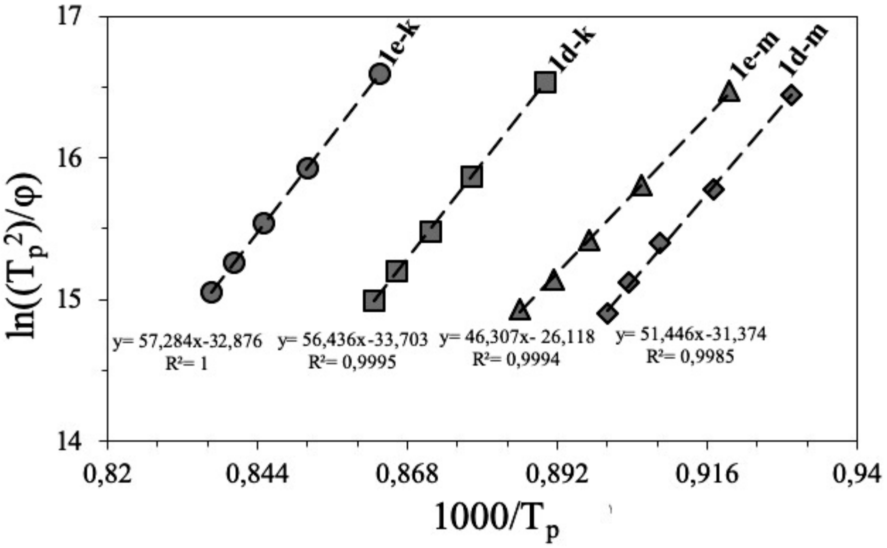

Figure 31. Plots of $\ln((T_p^2)/\varphi)$ *vs* $1000/T_p$, of the investigated glasses 1d-k, 1d-m, 1e-k, and 1e-m.

Table 19. Mean values (and standard deviation; n = 3) of activation energy (E_a) of crystallization and Avrami exponent (n_A) of the modified glasses.

Glass	E_a (kJ/mol)	n_A
1d-k	469 ± 9	3.3 ± 0.4
1d-m	428 ± 15	3.7 ± 0.2
1e-k	476 ± 29	2.6 ± 0.2
1e-m	385 ± 31	3.3 ± 0.1

I-3. Sintering and aesthetics

The choice of the heat-treatment temperatures tested for the parallelepiped bars of the glass-powder compacts was based on the three findings of the thermal analysis of the glasses, T_g (i.e. ~ 614 and 636 °C, Fig. 29), T_s (~ 647 and 663, Fig. 29), and T_p (i.e. 824 – 907 °C Table 18). Hence, after the plateau at 450 °C for 2 h (to complete the de-binding), the K-free glasses were heat-treated at 850 °C and the K-containing glasses at 900 °C.

Indeed, well-sintered GCs were produced at 850 °C in the case of the 1d-m, and 1e-m GCs, and at 900 °C in the case of the 1d-k and 1e-k GCs. The density values of the produced GCs at these temperatures, along with the density of the corresponding parent bulk glass (which was always smaller than that of the corresponding GC, suggesting crystallization of the glass) are presented in Table 20. The linear shrinkage of the GCs ranged between 9.1 and 10.6 % (Table 20). As regards the aesthetics, the produced GCs had a white color, but K substitution favored this effect markedly (Fig. 32).

Table 20. Mean values (and standard deviation, n = 5) of linear shrinkage and density of the investigated GCs. (The SD of density values was < 5%).

Composition	*Density (g/cm^3)*		*Linear shrinkage (%)*
	Glass	GC	GC
1d-k	2.49	2.61	9.4 ± 0.3
1d-m	2.58	2.77	10.6 ± 0.3
1e-k	2.48	2.80	9.1 ± 0.3
1e-m	2.55	2.68	9.3 ± 0.8

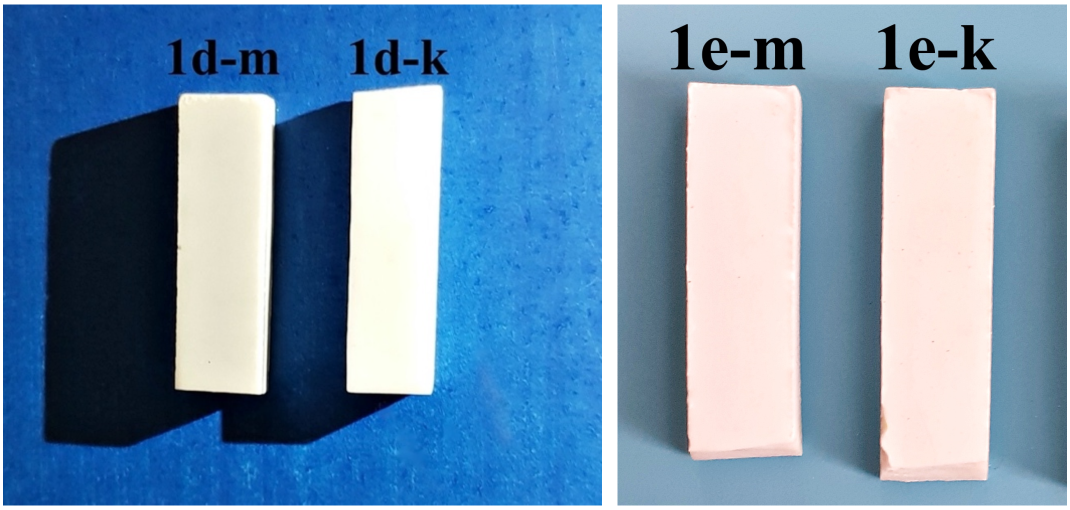

Figure 32. Well-sintered dense 1d-m, 1d-k, 1e-m, and 1e-k GC bars of white colour.

I-4. Crystalline structure

The GCs 1d, 1d-m, 1e, and 1e-m were comprised of diopside ($CaMgSi_2O_6$), wollastonite ($CaSiO_3$), and fluorapatite ($Ca_{10}(PO_4)_6F_2$) (Fig. 33a), while diopside ($CaMgSi_2O_6$), fluorapatite ($Ca_{10}(PO_4)_6F_2$), and alpha-potassium magnesium silicate (α-PMS, $K_2MgSi_3O_8$) were formed in the 1d-k and 1e-k GCs (Fig. 33b) (Appendix 1: Phase Diagrams). There is no evidence of formation of other secondary or minor phases, according to the assignment of the peaks in the diffractograms.

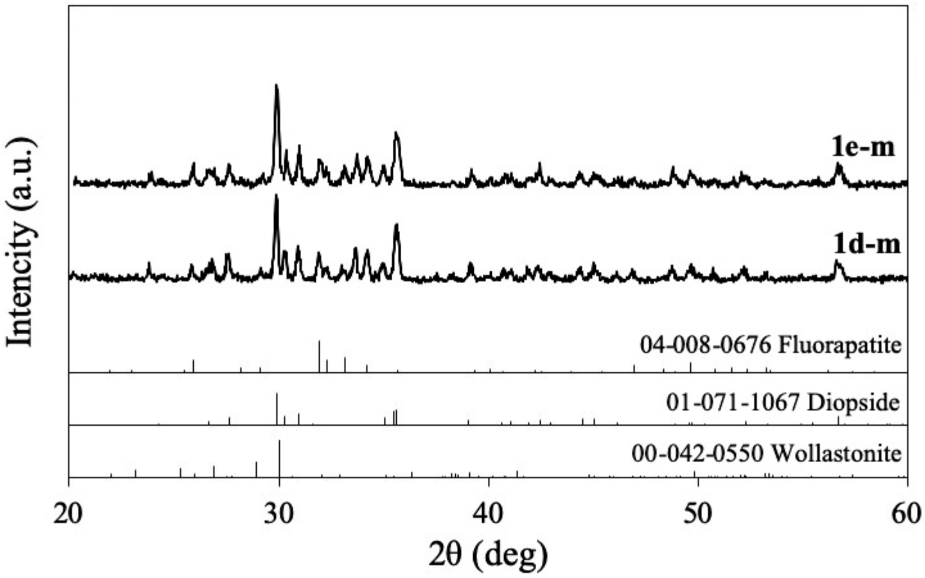

(a)

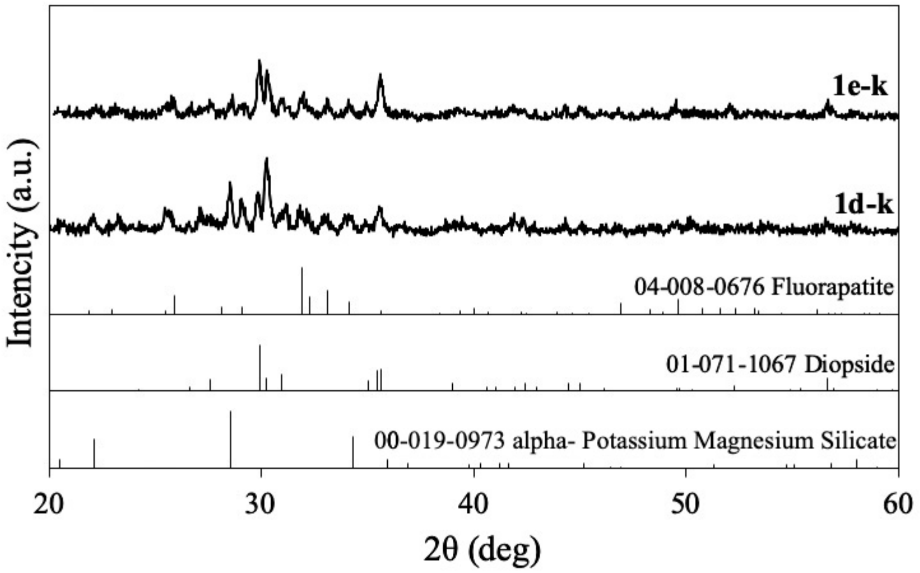

(b)

Figure 33. X-ray diffractograms of the modified GCs heat-treated at 850 (1d-m and 1e-m) or 900 °C (1d-k and 1e-k**)** for 1 h. Diopside ($CaMgSiO_6$, 01-071-1067); Wollastonite ($CaSiO_3$, 00-042-0550); Fluorapatite ($Ca(PO_4)_3F$, 04-008-0676); alpha-potassium magnesium silicate ($K_2MgSi_3O_8$, 00-019-0973).

I-5. Microstructure

The microstructure of the produced GCs (Fig. 34), according to elemental EDS analysis, is composed of well-defined big prismatic crystals assigned to diopside (D, the Mg/Ca/Si/O mol ratio was found as c.a. 1/1/2/6, respectively), and smaller acicular crystals assigned to wollastonite, W (the Ca/Si mol ratio was 1/1), or to α-PMS, in the case of the potassium-substituted GCs (as potassium was recorded), whose thickness was smaller than those of wollastonite, embedded in a glassy phase. Flour was detected in the coralloid-like small crystals marked with FA, assigned, therefore, to fluorapatite. The microstructure observations are consistent with the results of the X-ray diffraction analysis (Fig. 33).

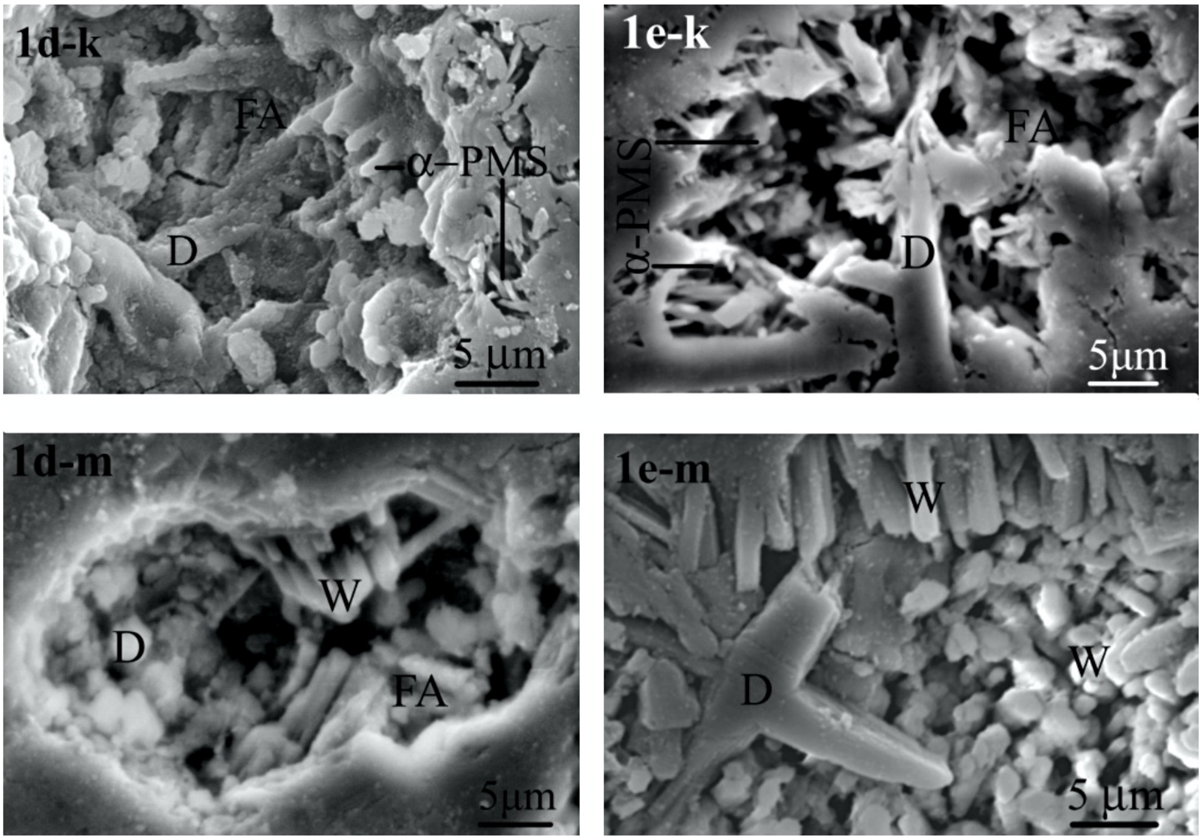

Figure 34. Typical microstructures of the produced GCs at 850 °C (1d-m, 1e-m) or 900 °C (1d-k, 1e-k), observed after etching of polished surfaces with 2% HF solution.

II. Mechanical Properties

The mechanical properties of the produced GCs, which are summarized in the Table 21, are a direct result of both the crystalline assemblage and the microstructure. The flexural strength varied from 107 to 129 and the modulus of elasticity ranged between 23 and 31 GPa. The microhardness and fracture toughness values of the GCs ranged between 5.4 - 5.6 GPa, and 1.7 – 1.9 MPa·m$^{0.5}$, respectively.

Additionally, the brittleness index (BI) values for the GCs 1d-k, 1dm, 1e-k, and 1e-m were 3.0 ± 0.6, 3.3 ± 0.5, 3.0 ± 0.4, and 3.0 ± 0.4, respectively. Because of their excellent mechanical properties, the produced 1d-k, 1dm, 1e-k, and 1e-m GCs were subjected to further studies to assess their bioactivity in SBF.

Table 21. Mean values (and standard deviation, n = 10) of the mechanical properties of the investigated GCs, heat-treated at 850 °C (for 1d-m and 1e-m) and 900 °C (for 1d-k and 1e-k) temperatures for 1 h.

Mechanical properties	*GCs*			
	1d-k	1d-m	1e-k	1e-m
Flexural strength (σ, MPa)	129 ± 5	128 ± 10	117 ± 5	107 ± 16
Modulus of elasticity (E, GPa)	26 ± 1	23 ± 1	26 ± 1	31 ± 2
Vickers microhardness (HV, GPa)	5.6 ± 0.4	5.6 ± 0.4	5.4 ± 0.4	5.6 ± 0.3
Fracture toughness(K_{IC}, MPa·m$^{0.5}$)	1.9 ± 0.5	1.7 ± 0.2	1.8 ± 0.2	1.9 ± 0.2

III. Bioactivity

The results of the SBF testing provided clear evidence of bioactivity of all the modified GCs. The pH of the SBF solution (Fig. 35) was rapidly increased in the first week (from 7.25 to ~ 9.5 and ~ 9.7), and over the immersion time there was a tendency for a slow increase, suggesting an ion exchange.

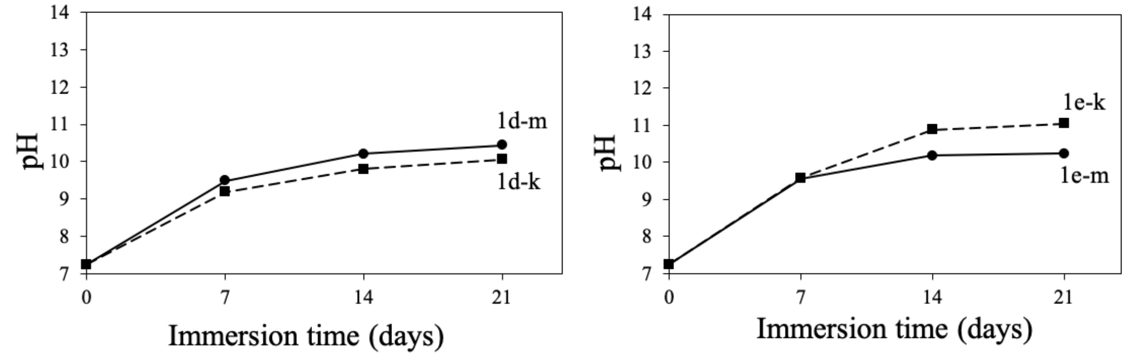

Figure 35. Evolution of pH of the solution over immersion time of the GC powders in SBF (at 37 °C).

The X-ray diffractograms of the GCs powders after immersion in SBF (Fig. 36) confirmed the formation of an HA layer (HA card: 01-086-0740). More specifically, although there was a background of strong peaks of the crystalline phases of the GCs, there were also peaks (at 2θ 29.2° and 32.02°) clearly ascribed to HA. Careful observation of the diffractograms in Fig. 36 shows that the intensity of the peaks due to wollastonite (at 2θ 26.92° and 33.7°) and α-PMS (at 2θ 20.71°, 22.27°, and 28.63°) is reduced and eventually the peaks disappear, whereas the HA peaks become stronger over the period of immersion time in SBF.

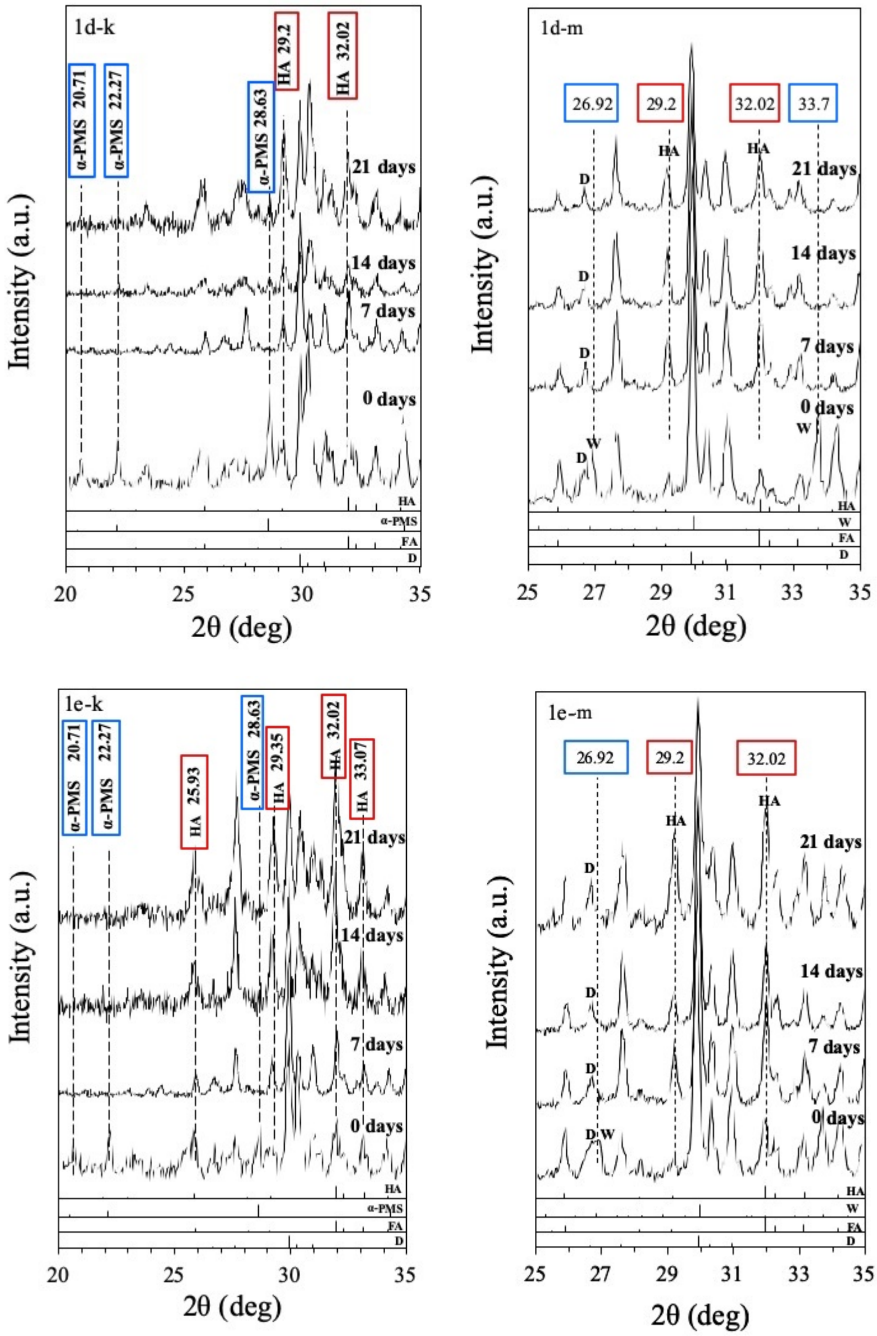

Figure 36. X-ray diffractograms of the powders of the modified GCs immersed in SBF for 7, 14, and 21 days at 37 °C.

The bioactivity performance of these GCs was confirmed by SEM/EDS analysis on their surface. Characteristic images for each GCs are presented in Figs. 37-40. The EDS analyses showed that the Ca/P molar ratio was in the range of 1.67 - 1.69 (Ca/P of stoichiometric HA is 1.67) (Tables 22-25). The HA layer, which was formed after 7 days of immersion in SBF, became denser after 14 and 21 days in SBF. More specifically, according to EDS analyses immersion of GCs specimens for 21 days in SBF resulted in an increase in the intensity of the peaks attributed to Ca and P and in a decline or disappearance of the Si, Na, and Mg peaks.

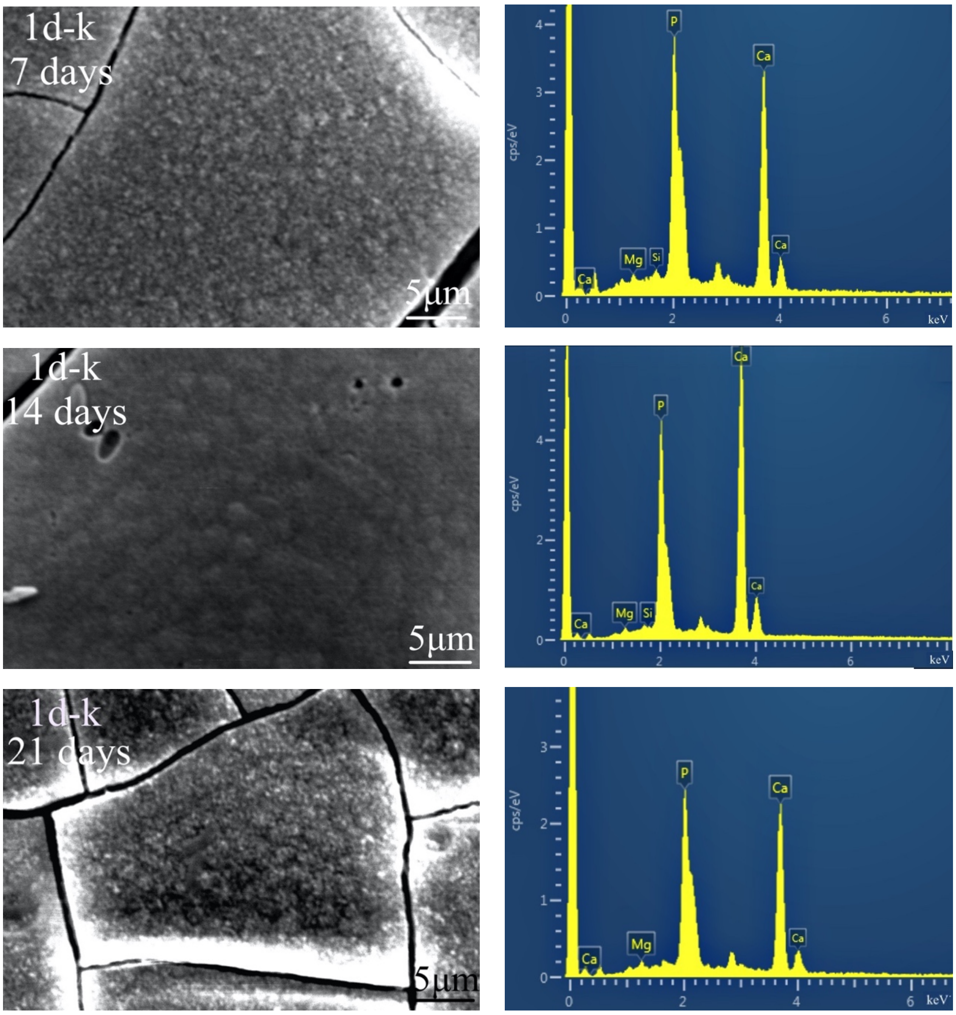

Figure 37. Formation and evolution of HA layer on the 1d-k GC surfaces over immersion time in SBF at 37 °C (7, 14, and 21 days).

Table 22. Elemental analysis (in atomic %) of surface of the GC 1d-k and molar Ca/P ratio for 7, 14, and 21 days soaking in SBF.

Soaking time in SBF (days)	Si	K	Mg	Ca	P	Molar Ca/P ratio
7	9.17	-	13.06	48.92	28.85	1.69
14	4.36	-	5.66	56.56	33.42	1.69
21	-	-	9.09	57.08	33.83	1.68

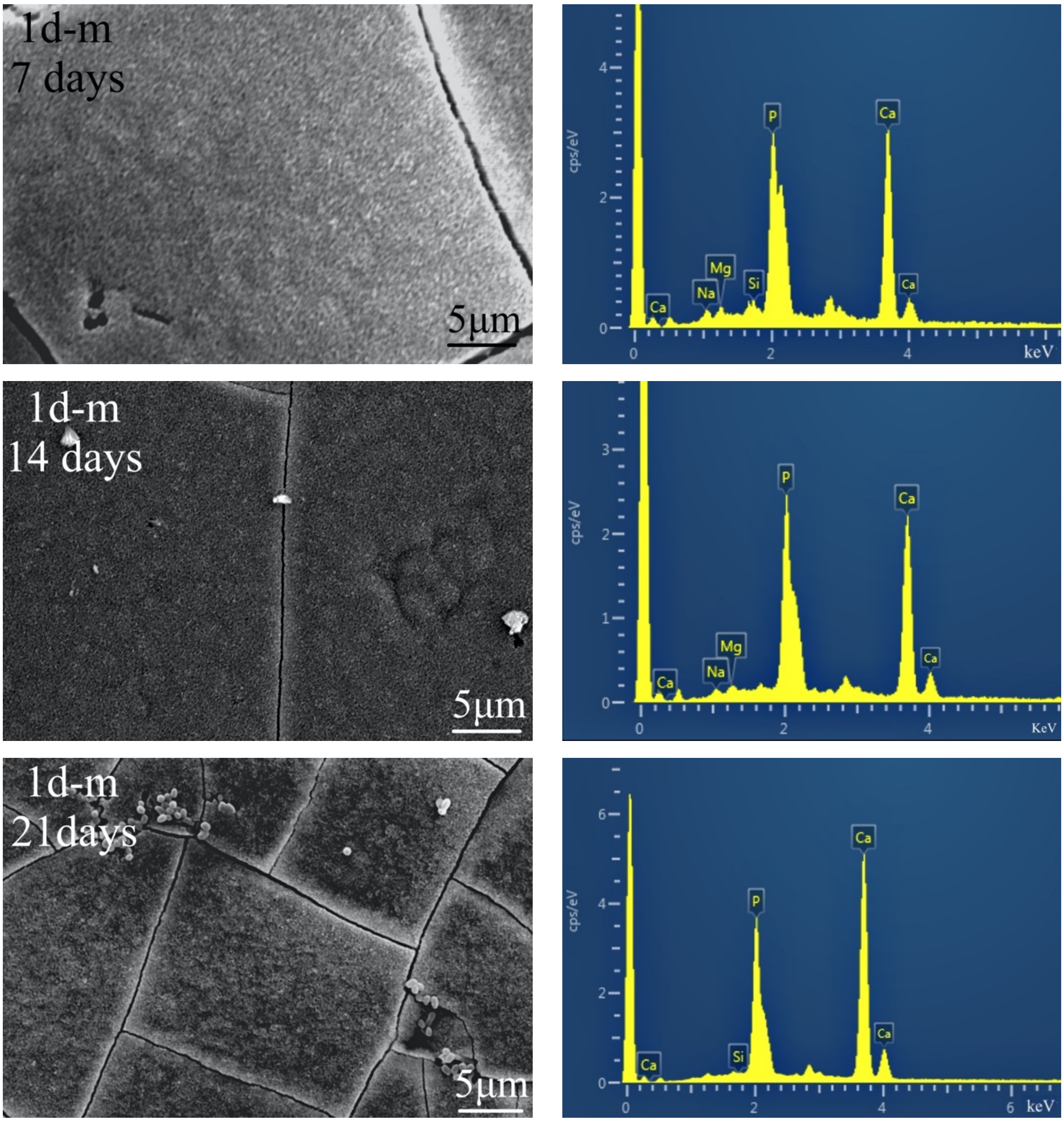

Figure 38. Formation and evolution of HA layer on the 1d-m GC surfaces over immersion time in SBF at 37 ºC (7, 14, and 21 days).

Table 23. Elemental analysis (in atomic %) of surface of the GC 1d-m and molar Ca/P ratio for 7, 14, and 21 days soaking in SBF.

Soaking time in SBF (days)	Si	Na	Mg	Ca	P	Molar Ca/P ratio
7	2.76	4.24	5.30	55.00	32.70	1.68
14	-	2.98	3.68	58.45	34.89	1.69
21	6.09	-	-	59.08	34.83	1.68

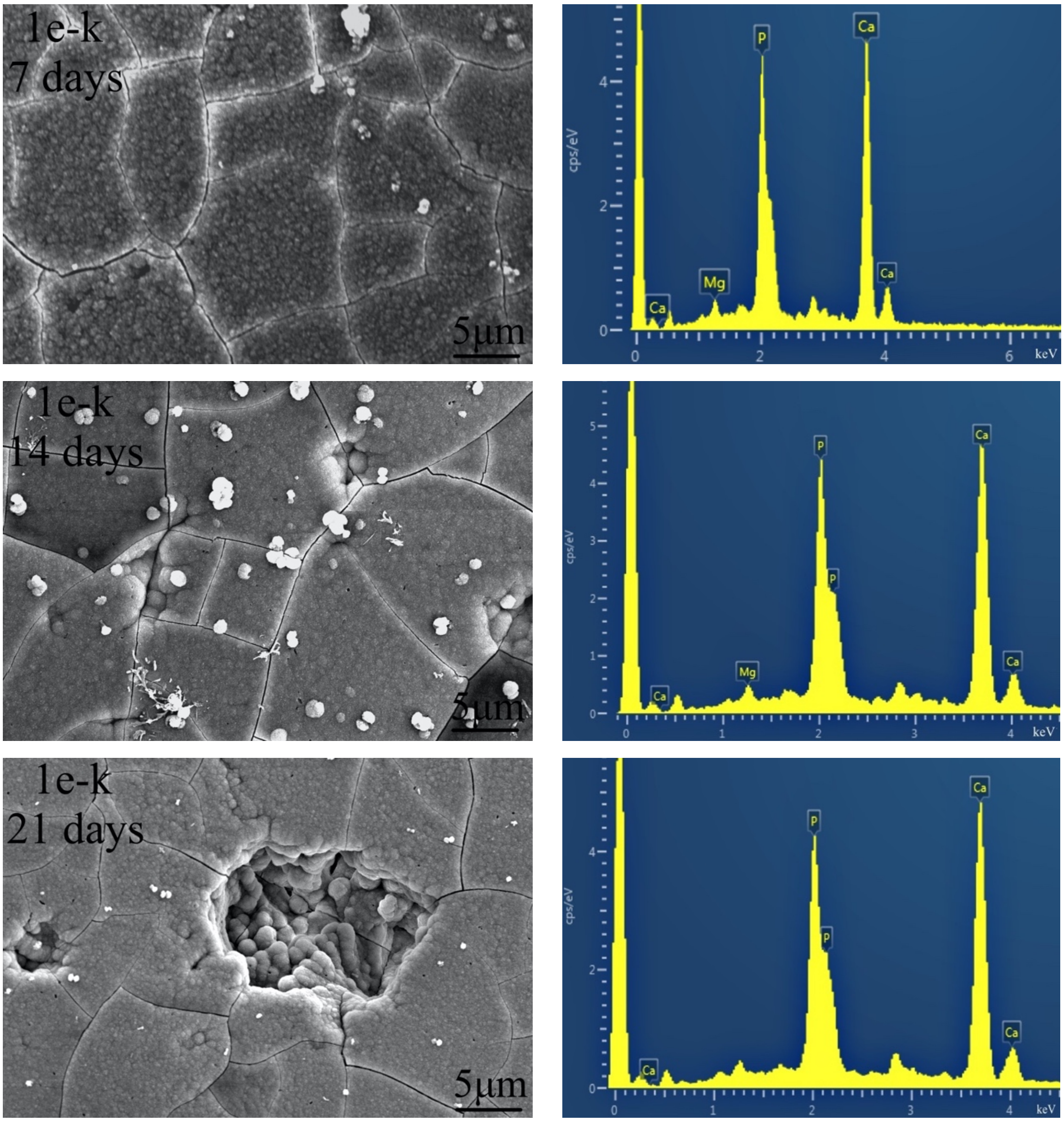
1e-k
7 days
5µm
1e-k
14 days
5µm
1e-k
21 days
5µm
cps/eV
keV
Ca
Mg
P
Ca
Ca

Figure 39. Formation and evolution of HA layer on the 1e-k GC surfaces over immersion time in SBF at 37 ºC (7, 14, and 21 days).

Table 24. Elemental analysis (in atomic %) of surface of the GC 1e-k and molar Ca/P ratio for 7, 14, and 21 days soaking in SBF.

Soaking time in SBF (days)	Si	K	Mg	Ca	P	Molar Ca/P ratio
7	-	-	7.65	57.85	34.50	1.67
14	-	-	6.20	58.90	34.90	1.68
21	5.15	-	-	59.47	35.38	1.68

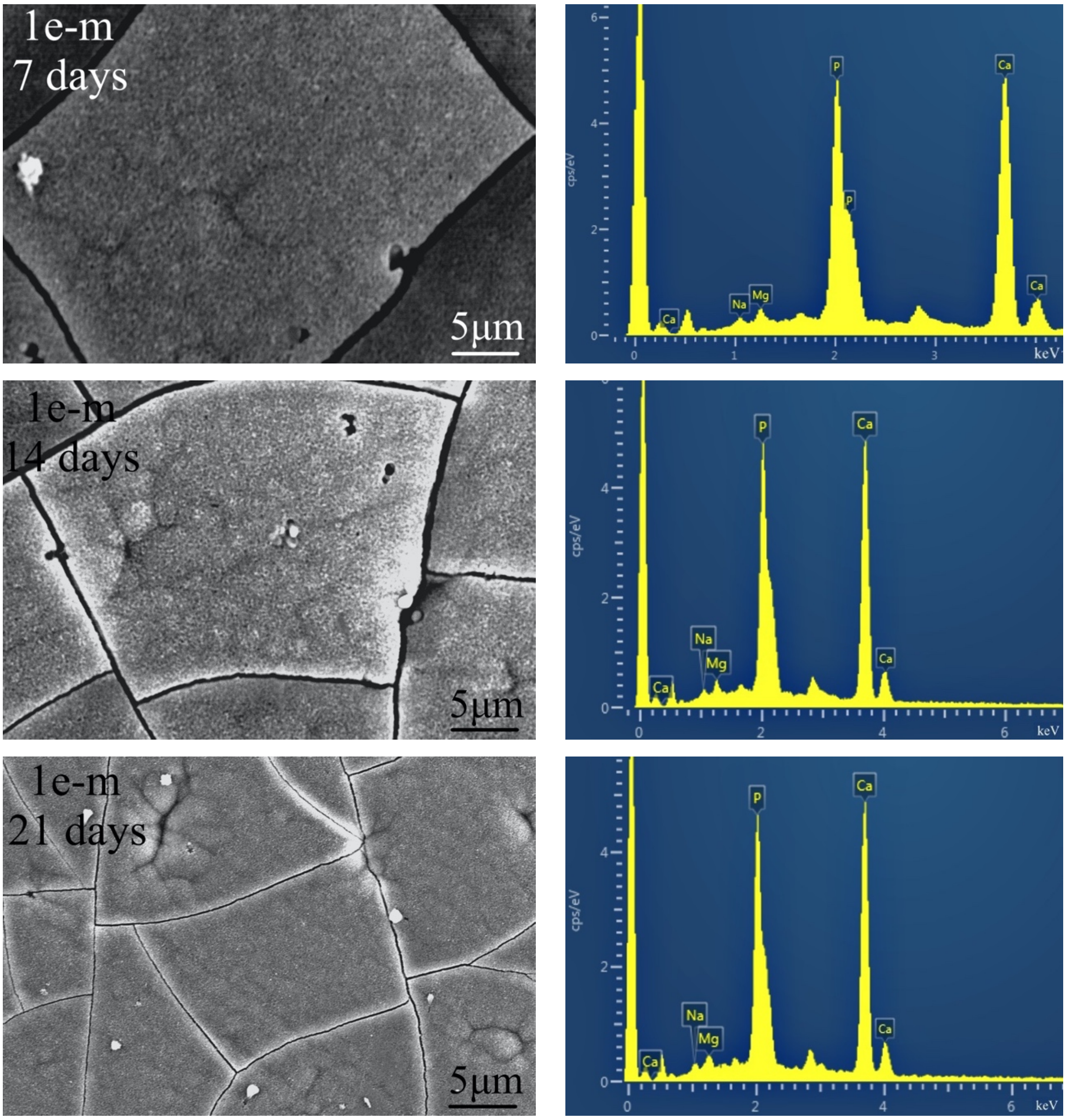

Figure 40. Formation and evolution of HA layer on the 1e-m GC surfaces over immersion time in SBF at 37 ºC (7, 14, and 21 days).

Table 25. Elemental analysis (in atomic %) of surface of the GC 1e-m and molar Ca/P ratio for 7, 14, and 21 days soaking in SBF.

Soaking time in SBF (days)	Si	Na	Mg	Ca	P	Molar Ca/P ratio
7	-	8.80	9.58	51.12	30.50	1.67
14	-	2.30	6.97	57.0	33.73	1.68
21	-	3.32	3.95	58.12	34.61	1.67

IV. General evaluation of the modified GCs 1d-k, 1d-m, 1e-k, and 1e-m

The results showed that the modified GCs 1d-k, 1d-m, 1e-k. and 1e-m displayed the ability to spontaneously form hydroxyapatite (HA) on their surface after immersion in SBF at 37 °C. Besides bioactivity, the results show that both substitutions (i.e. K for Na, and Mg for Ca) in group 1d resulted in lowering the modulus of elasticity from 27 to 26 and 23 GPa and in increasing the fracture toughness, from 1.7 to 1.9 MPa·m$^{0.5}$, respectively. In group 1e, K-substitution led to a reduction of the modulus of elasticity from 30 to 26 GPa, but there is a negligible effect of this substitution on the value of fracture toughness, which remained almost stable (1.9 - 1.8 MPa·m$^{0.5}$). In all cases, the attempted substitutions caused a reduction in the microhardness of the produced GCs (Fig. 41). It is important to note that the proposed modifications resulted in GCs with mechanical properties even more close (than those of the non-modified 1d and 1e GCs) to those of dentine (which is the biological tissue that the dental implant is called on to replace) and jaw bone (that is biological tissue with which the material of the implant comes into contact) (Table 26).

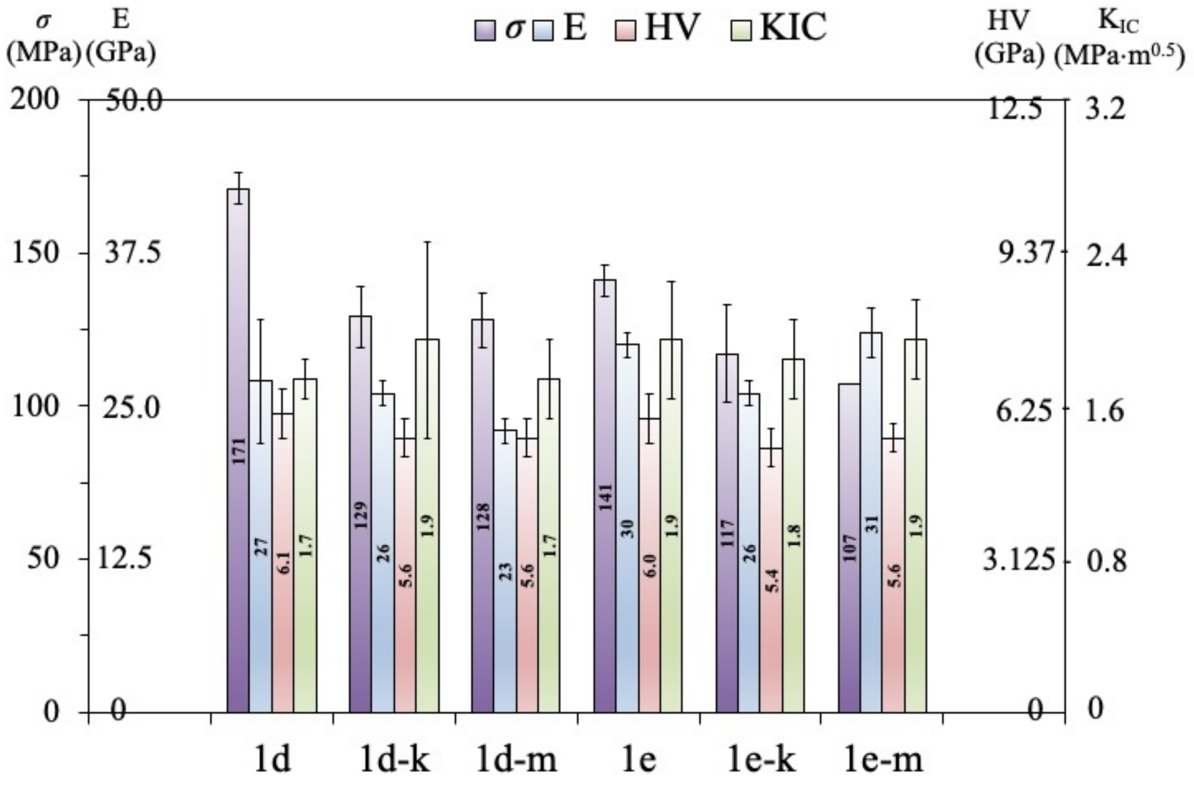

Figure 41. Influence of the substitutions of K for Na and of Mg for Ca in the compositions 1d and 1e on the mechanical properties (flexural strength, σ; modulus of elasticity, E; Vickers microhardness, HV; and fracture toughness, K_{IC}) of the produced GCs, 1d-k, 1d-m, 1e-k, and 1e-m.

Table 26. Mechanical properties of dentine and cortical jaw bone. The data were extracted from Table 17.

	Flexural strength (σ, MPa)	*Modulus of elasticity (E, GPa)*	*Vickers microhardness (HV, GPa)*	*Fracture toughness (K_{IC}, MPa·$m^{0.5}$)*
Cortical jaw bone	50-150	7-30	0.06-0.07	2-12
Dentine	230-305	15-30	< 0.6	3

Accordingly, the above results, namely the values of mechanical properties, the obtained aesthetic characteristics (e.g. white color) as well as the good bioactivity performance for all the investigated compositions, qualify the produced modified GCs as potential candidates for dental implant applications. So, ***the first aim*** of this doctoral thesis, i.e. the production of bioactive GC materials suitable for dental implant applications, was fulfilled.

Further development:

The mechanical properties of the produced GCs (1d, 1d-k, 1d-m, 1e, 1e-k, and 1e-m), especially after the modifications made, are very close to the mechanical properties of the dentine and the human jaw bone. Nevertheless, the only mechanical property that still needs improvement is the fracture toughness (as its values do not exceed 2 MPa·$m^{0.5}$). Thus, it is necessary to propose an oxide, which will increase the fracture toughness value without significantly increasing the other mechanical properties (especially the modulus of elasticity values) and without reducing or zeroing the desired bioactivity of the produced GCs.

On the other hand, all-ceramic fixed restoration is a big challenge for GC materials. The produced GCs satisfy the aesthetic requirements because of their white color (Figs. 22 and 32). As mentioned in the introduction, although the bioinert commercial GCs satisfy the aesthetic requirements due to their white color, they have been blamed for injury of the opposite natural tooth because of their high mechanical properties and in particular their high values of hardness (> 7 GPa), compared to that of natural enamel (3 - 5.5 GPa). Thus, it would also be interesting to modify the above GCs (1d, 1d-k, 1d-m, 1e, 1e-k, and 1e-m) in such a way that the values of their mechanical properties approach those of enamel and at the same time to zero the bioactivity.

Taking into account the above two paragraphs, in the present study, we suggested the addition of **Al_2O_3** to the initial and modified compositions (1d, 1d-k, 1d-m, 1e, 1e-k, 1e-m), the proportion of which, in the parent composition, will vary according to the desired application, as mentioned above.

2. Development of glass-ceramics (GCs) suitable for dental implant & all-ceramic fixed prosthetic applications

This section presents and analyzes the results of the experiments performed to achieve the second aim of the doctoral thesis and is divided into two subsections. The first section (**2.1**) presents the results of the modifications made to the glasses 1d, 1d-k, 1d-m, 1e, 1e-k, and 1e-m, in order the physico-mechanical properties of the obtained GCs to be as close as possible to those of dentine and human jaw bone, without reducing or zeroing the bioactivity. The need of a greater approach of the physico-mechanical properties of the dentine and the jaw bone, without limiting or inhibiting the bioactivity, in the above compositions led to adding 1 mol% Al_2O_3 (see Table 10 in the State of the Art and Aim). The second section (**2.2**) presents the results of the modifications made to these glasses in order the physico-mechanical properties of GCs the produced to be as close as possible to those of the human enamel. So, to convert the bioactive GCs (1d, 1d-k, 1d-m, 1e, 1e-k, and 1e-m) into bioinert and to increase the physico-mechanical properties, so that they reach to the closest possible level the physico-mechanical properties of enamel, 7-8 mol% Al_2O_3 was added in the above compositions (see Table 10 in the State of the Art and Aim).

2.1 Modified GCs with addition of 1 mol% Al_2O_3

I. Densification and crystallization

I-1. Results of Thermal analysis

The dilatometry curves of the prepared glasses (Fig. 42) demonstrate that in the group 1d/A_1, 1d-k/A_1, and 1d-m/A_1 (Fig. 42a), the T_g values ranged between 610 and 621 °C, whilst the T_s varied from 647 to 657 °C. In Fig. 42b, the dilatometry curves demonstrate that in the group 1e/A_1, 1e-k/A_1, and 1e-m/A_1, the T_g values ranged between 616 and 639 °C, while the T_s varied from 655 to 672 °C.

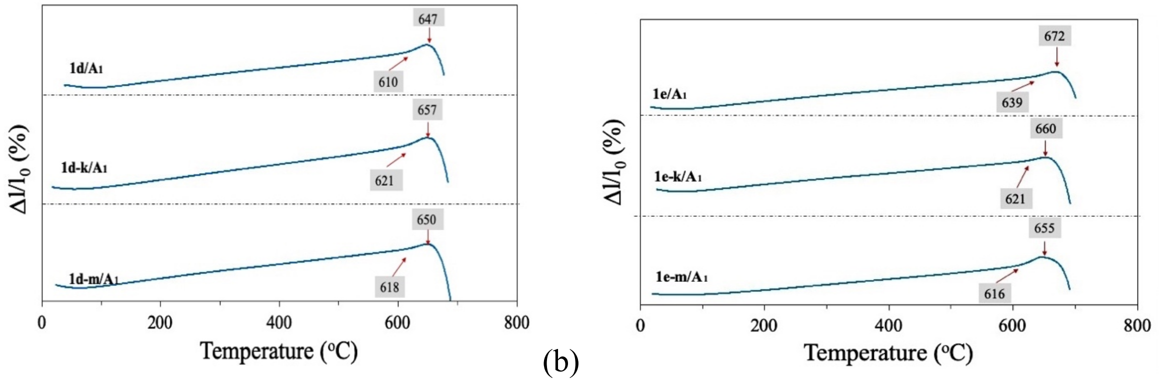

(a) (b)

Figure 42. Dilatation curves of bulk annealed glasses, which contain 1 mol% Al_2O_3.

The DSC thermographs of these glasses are shown in Fig. 43. The endothermic peaks are attributed to T_g, and the T_c attributed to the oncet crystallization, while the unique exothermic peak (T_p) corresponds to crystallization temperature. The values of T_g, T_c, and T_p determined from 3 dependent experiments, are summarized in Table 27. The choice the heat-treatment (i.e. 850 and 900°C) of the glass-powder specimens was based on the results of thermal analysis.

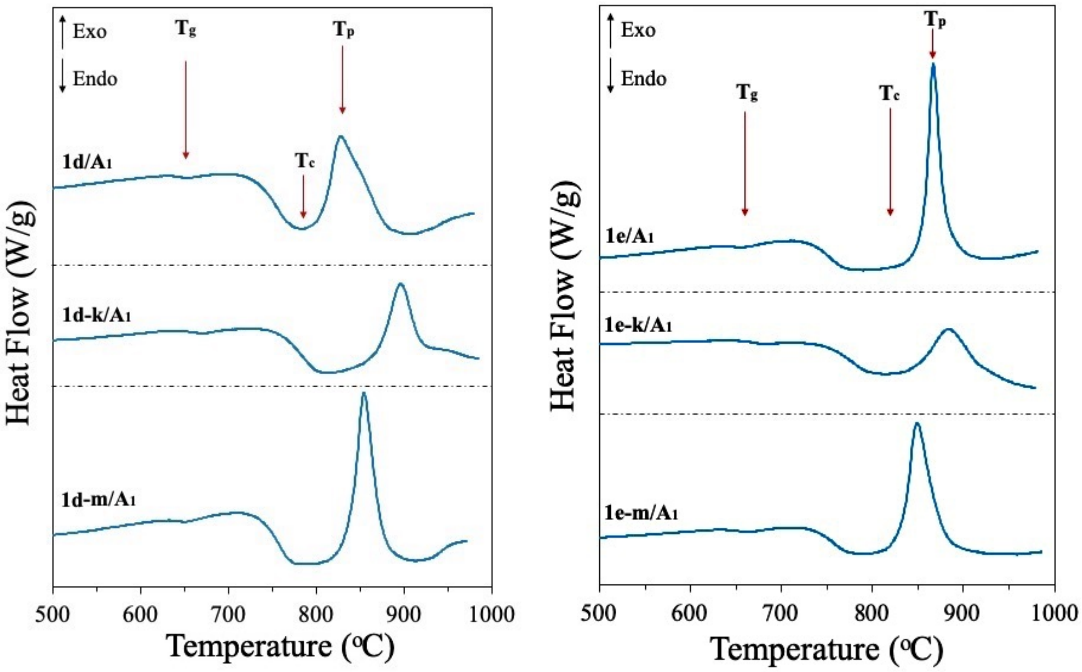

(a) (b)

Figure 43. Thermographs of the Al_2O_3-containing (1 mol%) glasses (a) 1d/A_1, 1d-k/A_1, 1d-m/A_1 and (b) 1e/A_1, 1e-k/A_1, 1e-m/A_1 (at heating rate of 15 K/min).

Table 27. Mean values (and standard deviation; n = 3) of glass transition temperature (T_g), oncet crystallization temperature (T_c), and crystallization temperature (T_p) of the Al_2O_3-containing (1 mol%) glasses (determined by the DCS measurements). The sintering window (T_c-T_g) is also presented.

Glass	T_g (°C)	T_c (°C)	T_c - T_g	T_p (°C)
1d/A_1	650 ± 19	785 ± 3	135	827 ± 14
1d-k/A_1	682 ± 6	815 ± 16	133	885 ± 13
1d-m/A_1	654 ± 8	804 ± 11	150	852 ± 16
1e/A_1	655 ± 8	810 ± 16	155	857 ± 17
1e-k/A_1	678 ± 7	846 ± 23	168	908 ± 13
1e-m/A_1	661 ± 7	809 ± 10	148	840 ± 14

I-2. Crystallization mechanism

The activation energy of crystallization for each Al_2O_3-containing (1 mol%) glass was caluclated from the plots of $\ln((T_p^2)/\varphi)$ *vs* $1000/T_p$ (Fig. 44). The n_A value for each glass was calculated from the analysis of the exthothermic peaks through the calculation of the full width at the half maximum at T_p. The results which are listed in Table 28, suggest that the produced glasses are prone to two-dimensional growth of crystals since $n_A \geq 2$, while the glass $1e/A_1$ is prone to three-dimensional crystallization ($n_A \geq 3$).

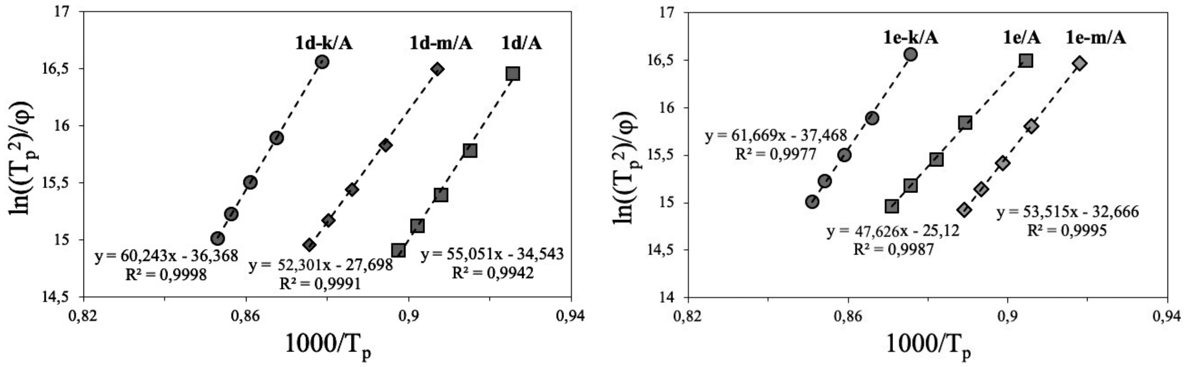

(a) (b)

Figure 44. The plots of $\ln((T_p^2)/\varphi)$ *vs* $1000/T_p$ for Al_2O_3-containing (1 mol%) glasses, (a) $1d/A_1$, $1d\text{-}k/A_1$, $1d\text{-}m/A_1$, and (b) $1e/A_1$, $1e\text{-}k/A_1$, $1e\text{-}m/A_1$.

Table 28. Mean values (and standard deviation; n = 3) of the activation energy (E_a) of crystallization, and Avrami exponent (n_A) of the investigated Al_2O_3-containing (1 mol%) glasses.

Glass	E_a (kJ/mol)	n_A
$1d/A_1$	458 ± 10	2.5 ± 0.4
$1d\text{-}k/A_1$	498 ± 9	2.6 ± 0.4
$1d\text{-}m/A_1$	434 ± 9	2.7 ± 0.3
$1e/A_1$	395 ± 14	3.0 ± 0.2
$1e\text{-}k/A_1$	512 ± 29	2.5 ± 0.4
$1e\text{-}m/A_1$	445 ± 11	2.6 ± 0.2

I-3. Sintering and aesthetics

The choice of the heat-treatment temperatures for the Al_2O_3-containing (1 mol%) specimens (i.e. the parallelepiped bars of the glass-powder compacts) was based on the three findings of the thermal analysis of the glasses, T_g (i.e. 610 and 639 °C, Fig. 42), T_s (647 and 672, Fig. 42), and T_p (i.e. 827 – 908 °C Table 27). Hence, after the plateau at 450 °C for 2 h (to complete the de-binding), the K-free parallelepiped bars of the glass-powder compacts were heat-treated at 850 °C and the K-containing glasses at 900 °C.

The density of bulk glasses varied between 2.59 - 2.72 g/cm^3 and increased after sintering-crystallization to be in the interval 2.71 – 3.04 g/cm^3; the linear shrinkage of produced GCs ranged between 10.0 - 11.0 % (Table 29). As regards the aesthetics, all the GCs had a white color (Fig. 45).

Table 29. Mean values (and standard deviation, n = 5) of linear shrinkage and density of the Al_2O_3-containing (1 mol%) glasses and GCs heat-treated at 850 °C (1d/A_1, 1d-m/A_1, 1e/A_1, 1e-m/A_1) and 900 °C (1d-k/A_1 and 1e-k/A_1) for 1 h. (The SD of density values was < 5%).

Composition	*Linear shrinkage (%)*	*Density (ρ, g/cm^3)*	
		Glass	*GCs*
1d/A_1	10.1 ± 0.3	2.59	2.88
1d-k/A_1	10.0 ± 0.4	2.55	2.71
1d-m/A_1	11.0 ± 0.8	2.61	2.82
1e/A_1	10.3 ± 1.2	2.59	3.04
1e-k/A_1	10.0 ± 0.6	2.60	2.99
1e-m/A_1	10.0 ± 0.9	2.72	3.02

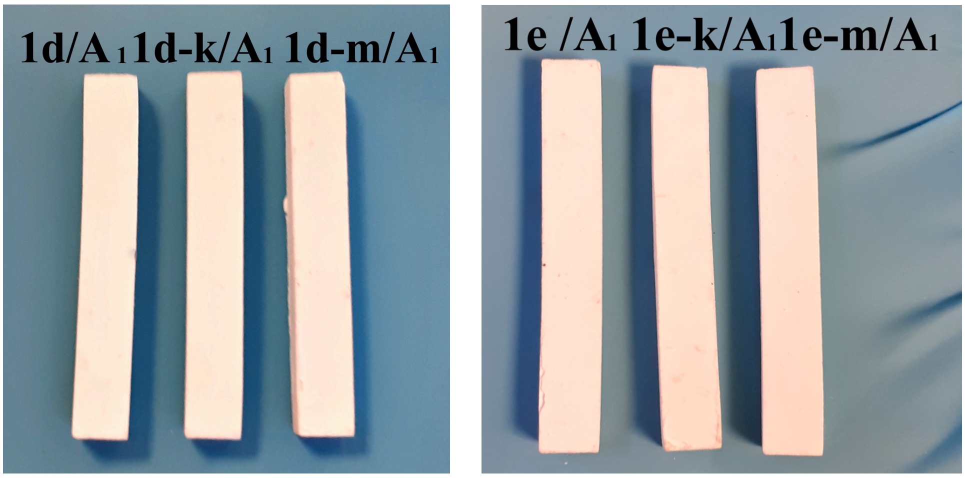

Figure 45. Well-sintered dense GC bars of white colour, which contain 1 mol% Al_2O_3.

I-4. Crystalline structure

Diopside, wollastonite and fluorapatite, phases were recorded in the GCs fired at 850 °C in the case of 1d/A_1, 1d-m/A_1, 1e/A_1, and 1e-m/A_1 GCs, while, diopside, fluorapatite, and alpha-potassium magnesium silicate (α-PMS) were formed in the GCs heated at 900 °C in the case of 1d-k/A_1 and 1e-k/A_1 GCs (Fig. 46) (Appendix 1: Phase Diagrams).

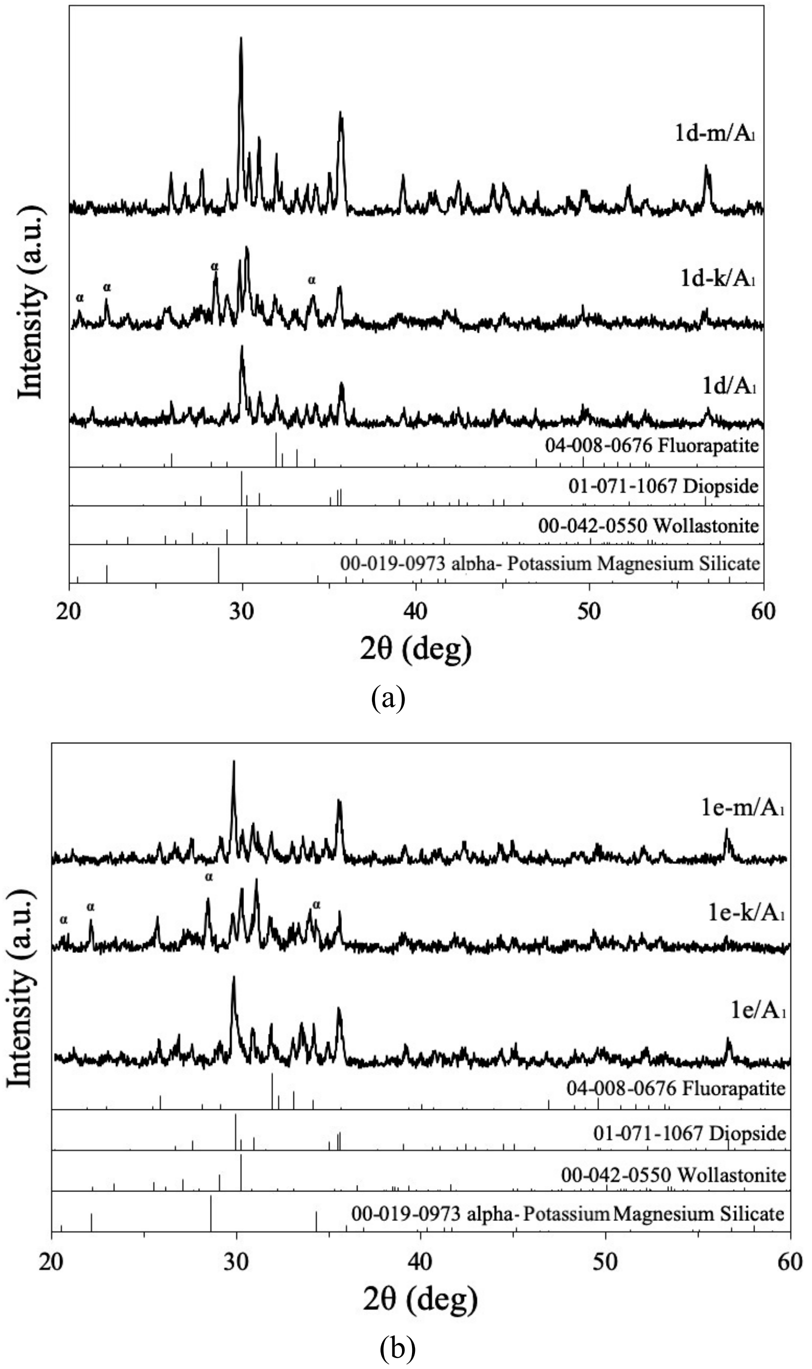

(a)

(b)

Figure 46. X-ray diffractograms of the Al_2O_3-containing (1 mol%) GCs heat-treated at 850 (K-free GCs) or 900 °C (K-containing GCs) for 1 h. Diopside ($CaMgSiO_6$, 01-071-1067); wollastonite ($CaSiO_3$, 00-042-0550); fluorapatite ($Ca(PO_4)_3F$, 04-008-0676); alpha-potassium magnesium silicate ($K_2MgSi_3O_8$, 00-019-0973).

I-5 Microstructure

Figure 47 shows SEM images of the microstructure of the produced Al_2O_3-containing (1 mol%) GCs. According to EDS results and taking into account the results of the XRD analysis, three different types of crystals were observed in each produced GC. The relatively big crystals in all GCs specimens were assigned to diopside (D) as the atomic ratio Mg/Ca/Si/O was found to be 1/1/2/6. Fluorine was detected in the coralloid-like small crystals (FA), assigned, therefore, to fluorapatite. In GC specimens 1d/A_1, 1d-m/A_1, 1e/A_1 and 1e-m/A_1 the crystals where the Ca/Si mol ratio was 1/1, were attributed to wollastonite (W). Finally, in the GC specimens 1d-k/A_1 and 1e-k/A_1, potassium was recorded in some crystals, which were thereby assigned to α-PMS.

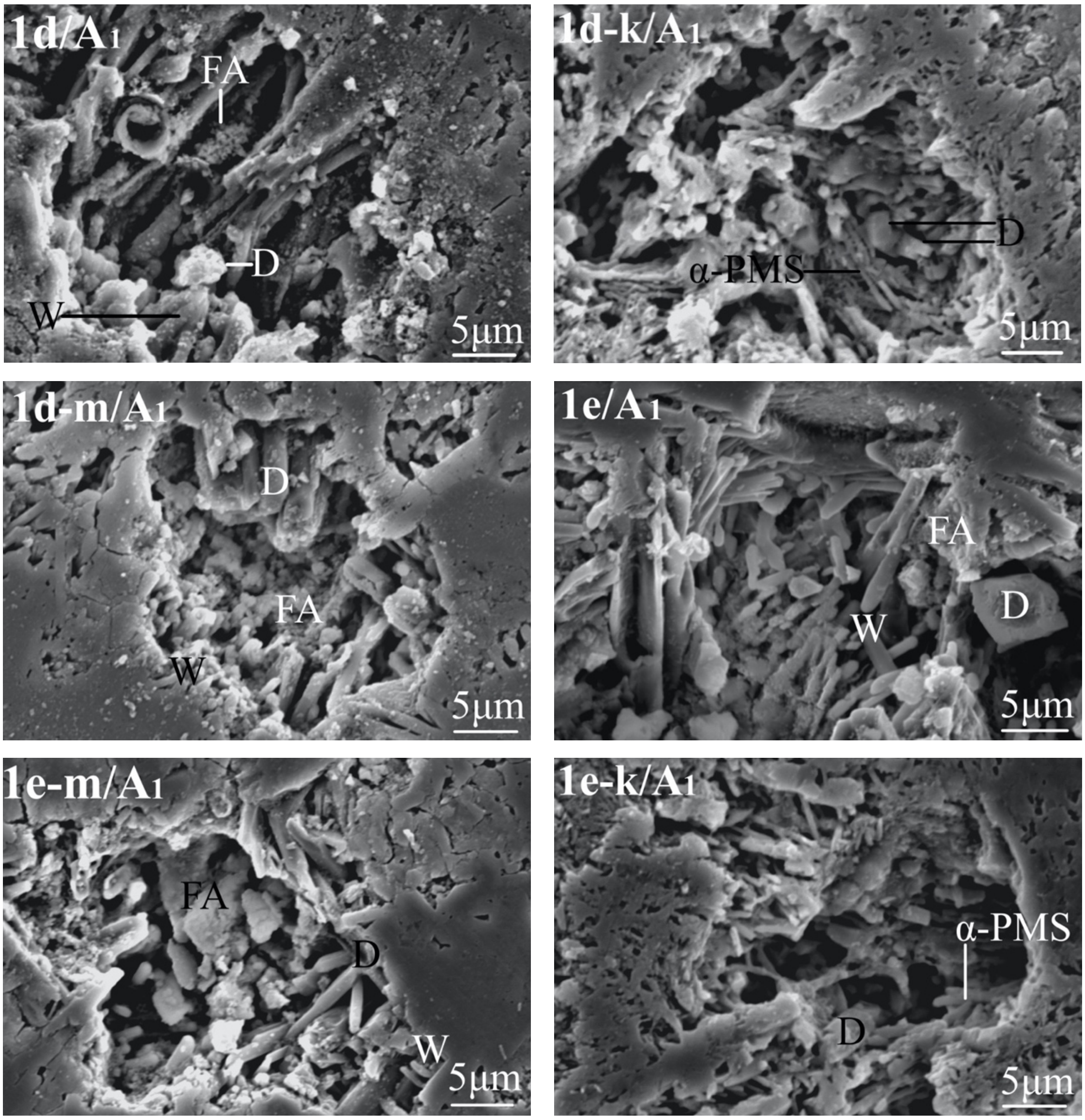

Figure 47. Typical microstructures of the Al_2O_3-containing (1 mol%) GCs, produced at 850 °C (K-free GCs) or 900 °C (K-containing GCs), observed after etching of polished surfaces with 2% HF solution. D: diopside ($CaMgSiO_6$); W: wollastonite ($CaSiO_3$); F: fluorapatite ($Ca(PO_4)_3F$); α-PMS: alpha-potassium magnesium silicate ($K_2MgSi_3O_8$).

II. Mechanical properties

The mechanical properties of the produced Al_2O_3-containing (1 mol%) GCs are summarized in Table 30. The flexural strength values ranged between 124 - 177 MPa. The modulus of elasticity values was 27 - 34 GPa. Furthermore, the hardness and the fracture toughness values were 6.0 - 6.7 GPa and 2.1 - 2.6 MPa·$m^{0.5}$, respectively.

The brittleness index (BI) values for the GCs 1d/A_1, 1d-k/A_1, and 1d-m/A_1 were 3.0 ± 0.1, 2.4 ± 0.1, and 2.8 ± 0.1, respectively, while the same property for the GCs 1e/A_1, 1e-k/A_1, and 1e-m/A_1 were 2.8 ± 0.1, 2.6 ± 0.1, and 2.4 ± 0.1, respectively.

Table 30. Mean values (and standard deviation, n = 10) of the mechanical properties of the Al_2O_3-containing (1 mol%) GCs, heat-treated at 850 ºC (K-free GCs) and 900 ºC (K-containing GCs) for 1 h.

GCs	Mechanical properties			
	Flexural strength (σ, MPa)	*Modulus of elasticity (E, GPa)*	*Vickers microhardness (HV, GPa)*	*Fracture toughness (K_{IC}, MPa·$m^{0.5}$)*
1d/A_1	177 ± 19	28 ± 3	6.5 ± 0.2	2.1 ± 0.2
1d-k/A_1	176 ± 17	28 ± 1	6.1 ± 0.1	2.5 ± 0.7
1d-m/A_1	125 ± 8	27 ± 1	6.4 ± 0.2	2.3 ± 0.3
1e/A_1	150 ± 2	34 ± 4	6.7 ± 0.2	2.4 ± 0.3
1e-k/A_1	124 ± 15	29 ± 5	6.0 ± 0.3	2.3 ± 0.3
1e-m/A_1	120 ± 9	34 ± 2	6.3 ± 0.2	2.6 ± 0.2

III. Bioactivity

The *in vitro* SBF testing showed clear evidence of bioactivity for all the produced GCs containing 1 mol% Al_2O_3. The pH of the SBF solution (Fig. 48) was rapidly increased in the first week (from 7.25 to ~9.5 and ~9.6), and there was a tendency to a slow increase over longer immersion time, suggesting an ion exchange.

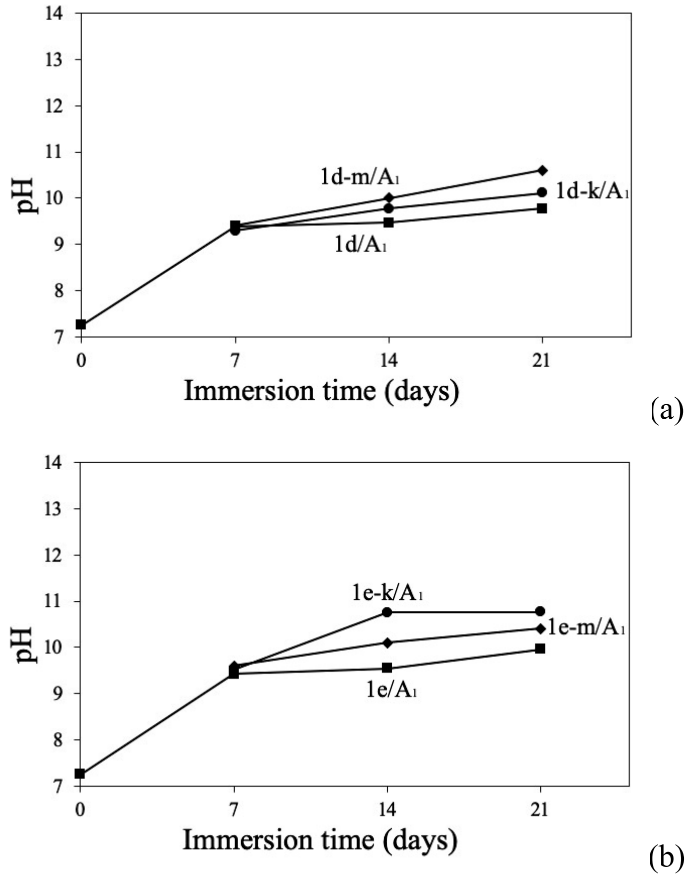

Figure 48. Evolution of pH of the solution over immersion time of the Al_2O_3-containing (1 mol%) GC powders in SBF (at 37 °C).

The SEM images in Figs. 49-54, in combination with EDS analysis, which showed that the Ca/P molar ratio in the HA layer formed on the surface of the GC specimens after immersion in SBF was in the range of 1.67 - 1.69 (Ca/P of stoichiometric HA is 1.67) (Tables 31-36), provide visible evidence about the bioactivity of the Al_2O_3-containing (1 mol%) GCs. More specifically, the HA layer was formed after 7 days of immersion in SBF and this layer became denser, over immersion time resulting in an increase, after 21 days, in the intensity of the peaks attributed to Ca and P and the disappearance of the Si peaks.

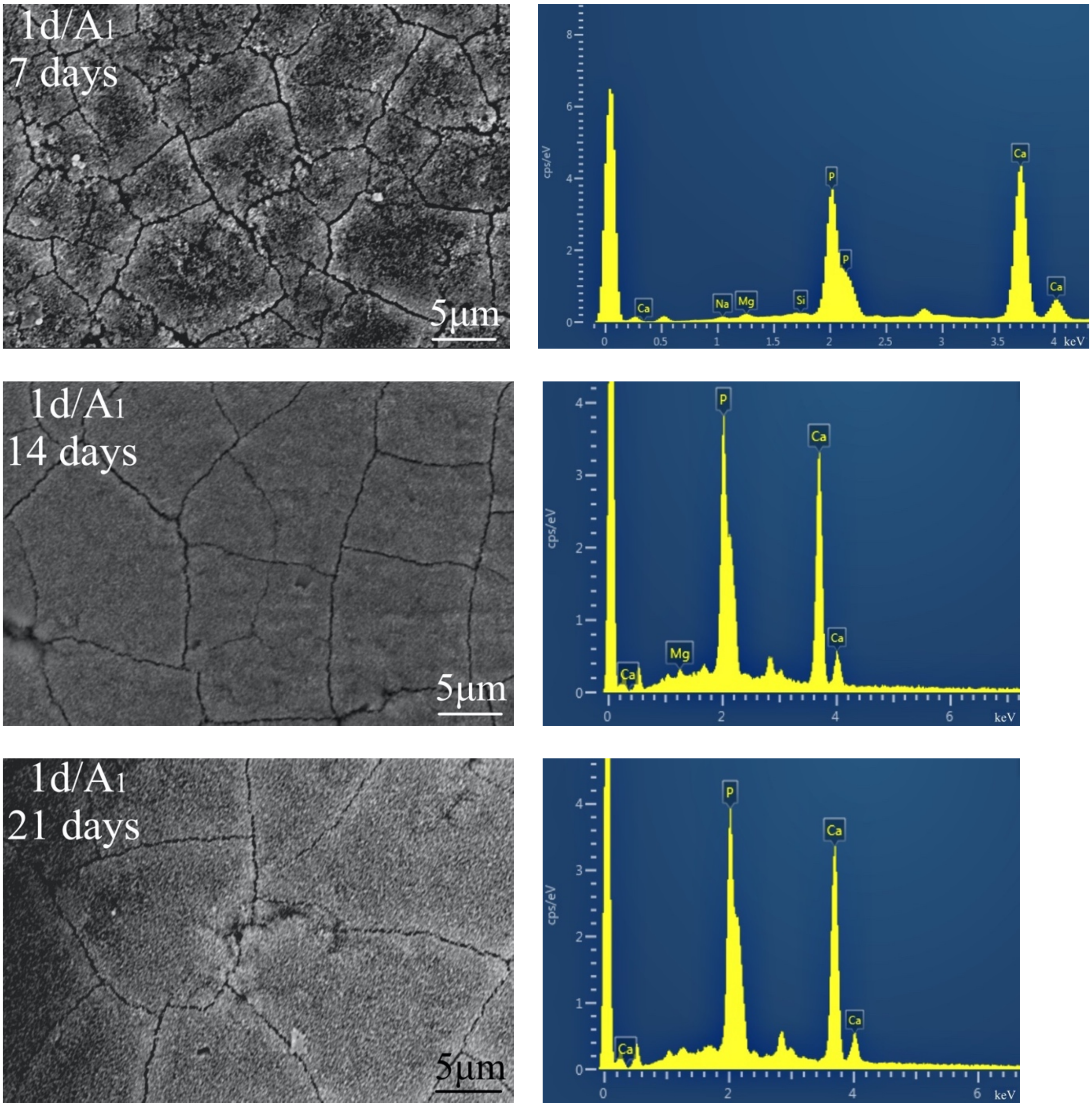

Figure 49. Formation and evolution of HA layer on the surface of the GC 1d/A_1 over immersion time in SBF at 37 °C (7, 14, and 21 days).

Table 31. Elemental analysis (in atomic %) of the surface of the GC 1d/A_1 and molar Ca/P ratio for 7, 14, and 21 days soaking in SBF.

Soaking time in SBF (days)	Si	Na	Mg	Ca	P	Molar Ca/P ratio
7	2.92	4.88	6.64	53.56	32.00	1.67
14	-	-	3.01	60.99	36.00	1.69
21	-	-	-	62.84	37.16	1.69

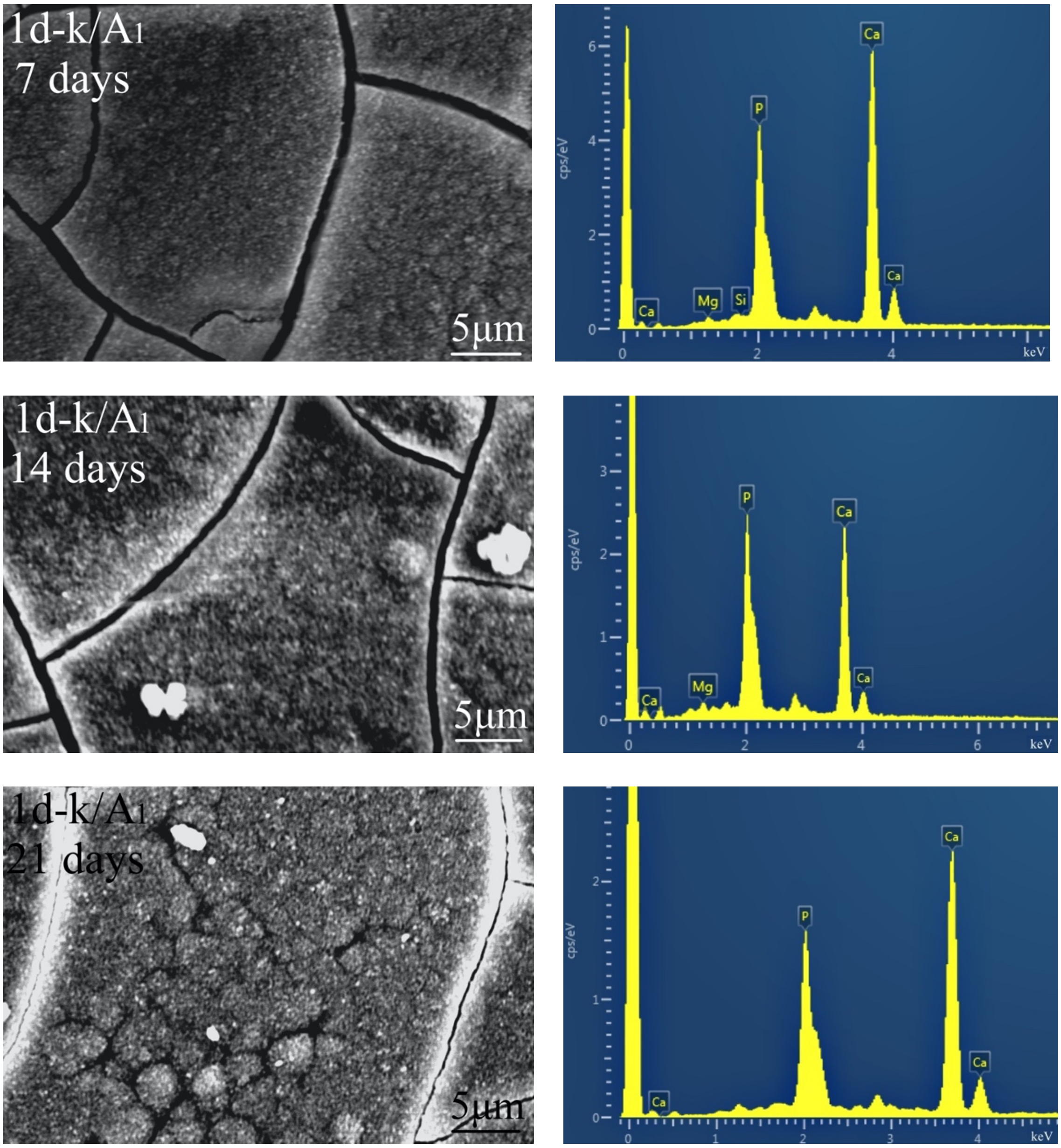

Figure 50. Formation and evolution of HA layer on the surface of the GC 1d-k/A$_1$ over immersion time in SBF at 37 °C (7, 14, and 21 days).

Table 32. Elemental analysis (in atomic %) of the surface of the GC 1d-k/A$_1$ and molar Ca/P ratio for 7, 14, and 21 days soaking in SBF.

Soaking time in SBF (days)	Si	K	Mg	Ca	P	Molar Ca/P ratio
7	3.86	-	4.80	57.33	34.01	1.68
14	-	-	4.75	59.58	35.67	1.67
21	-	-	-	62.75	37.25	1.68

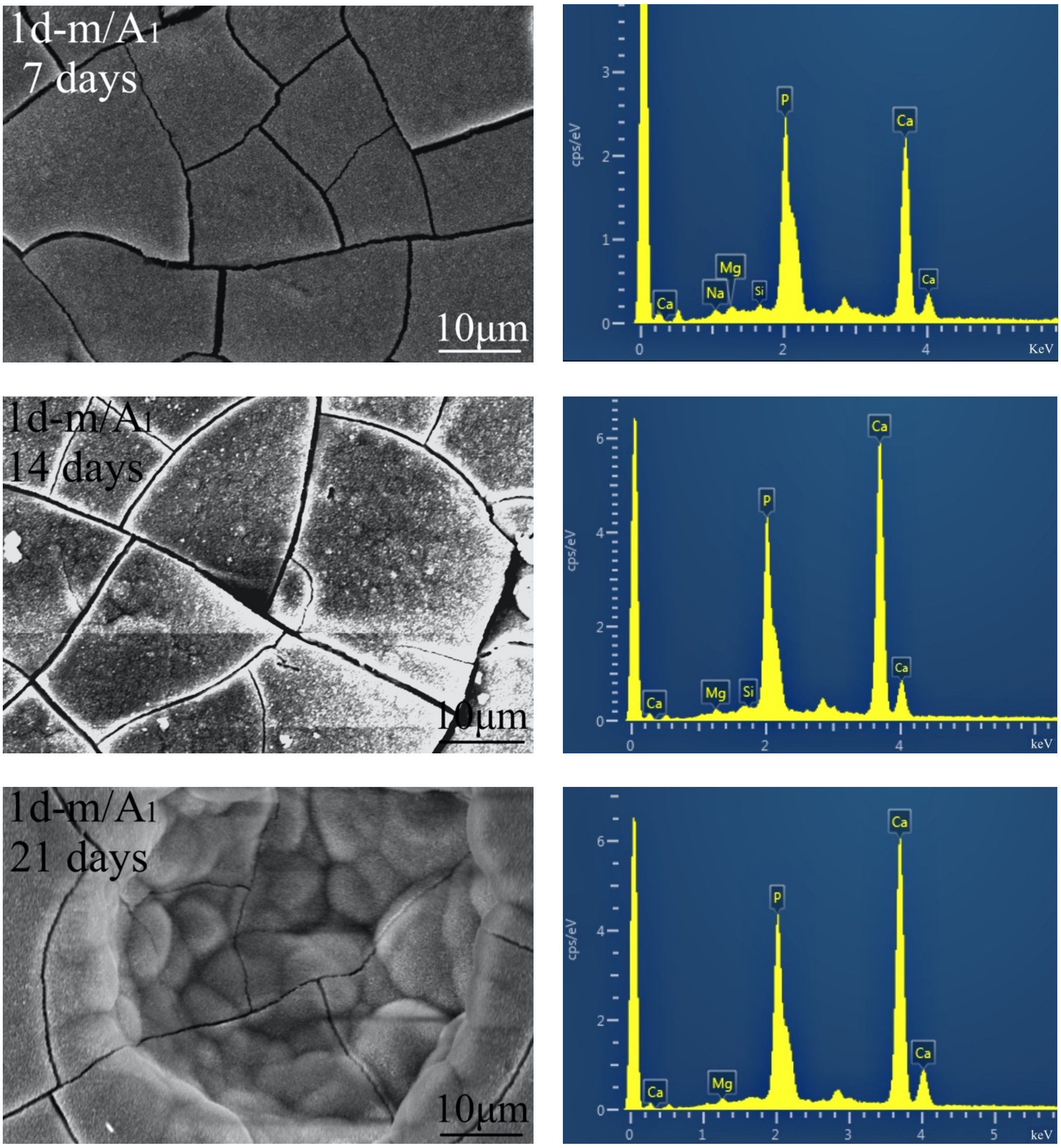

Figure 51. Formation and evolution of HA layer on the surface of the GC 1d-m/A$_1$ over immersion time in SBF at 37 °C (7, 14, and 21 days).

Table 33. Elemental analysis (in atomic %) of the surface of the GC 1d-m/A$_1$ and molar Ca/P ratio for 7, 14, and 21 days soaking in SBF.

Soaking time in SBF (days)	Si	Na	Mg	Ca	P	Molar Ca/P ratio
7	3.76	3.88	4.34	55.22	32.80	1.68
14	7.08	-	9.27	52.58	31.07	1.69
21	-	-	5.77	59.03	35.20	1.67

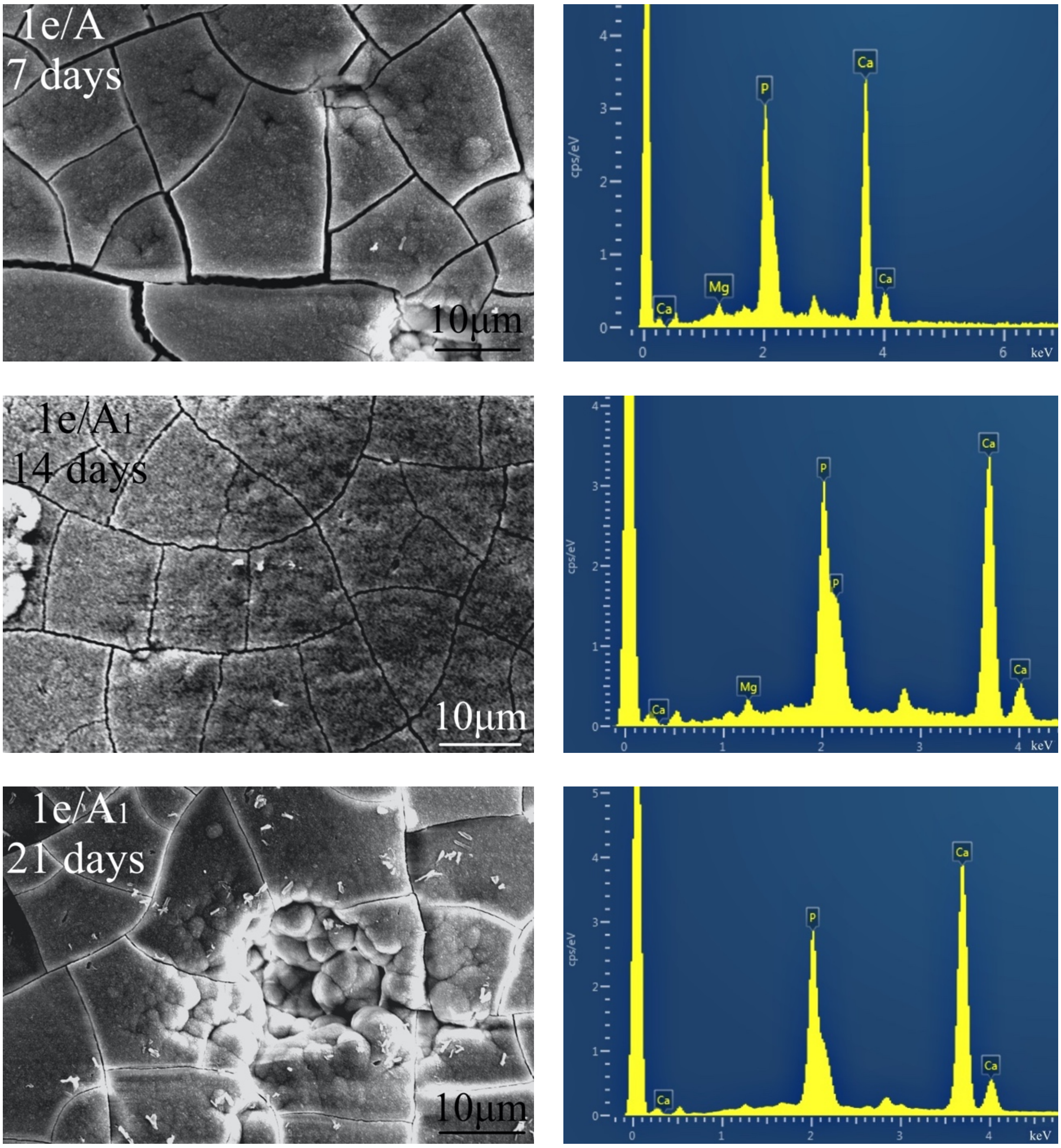

Figure 52. Formation and evolution of HA layer on the surface of the GC 1e/A$_1$ over immersion time in SBF at 37 °C (7, 14, and 21 days).

Table 34. Elemental analysis (in atomic %) of the surface of the GC 1e/A$_1$ and molar Ca/P ratio for 7, 14, and 21 days soaking in SBF.

Soaking time in SBF (days)	Si	Na	Mg	Ca	P	Molar Ca/P ratio
7	-	-	8.43	57.65	33.93	1.69
14	-	-	4.15	59.95	35.90	1.67
21	-	-	-	62.53	37.47	1.67

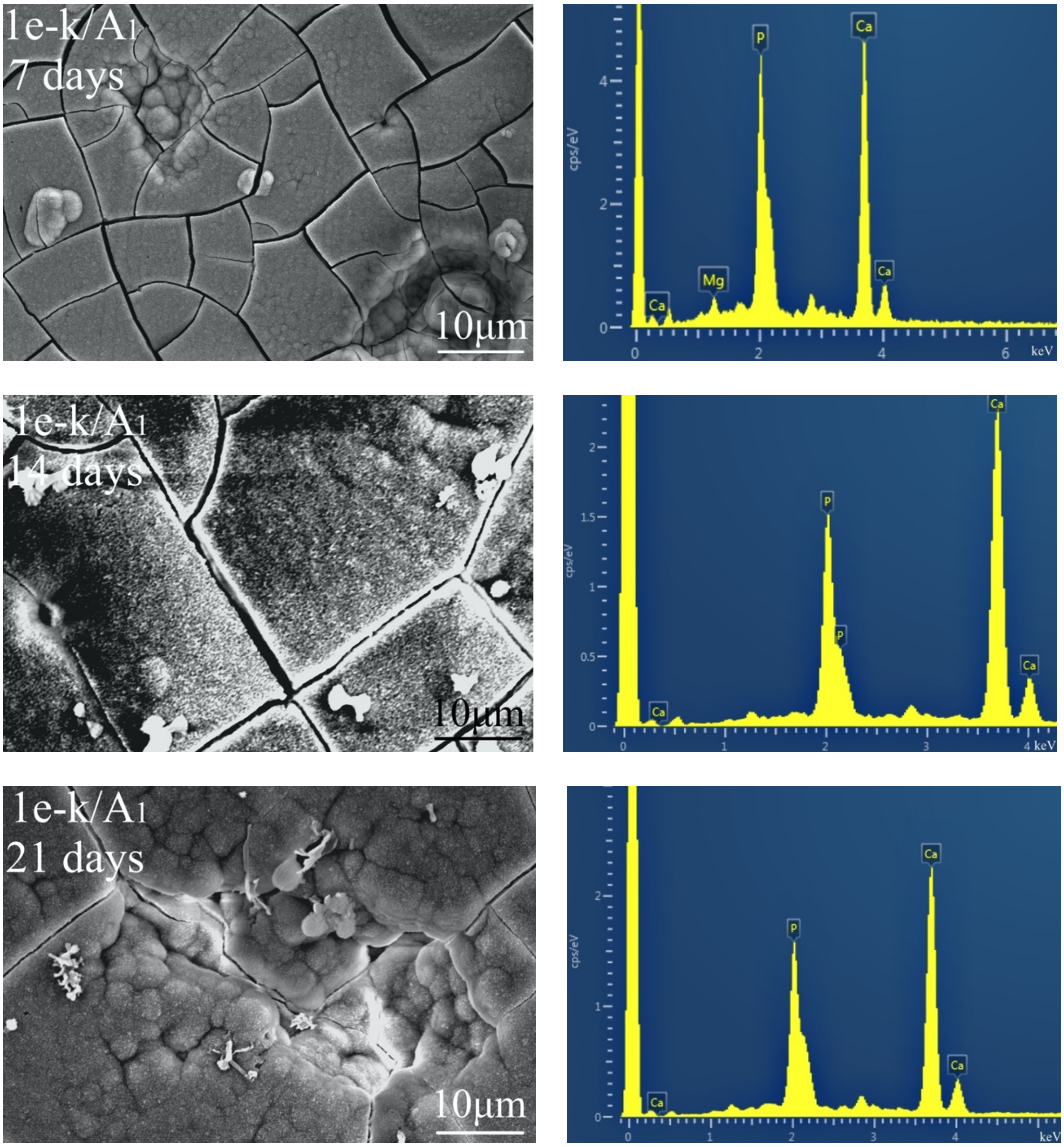

Figure 53. Formation and evolution of HA layer on the surface of the GC 1e-k/A_1 over immersion time in SBF at 37 ºC (7, 14, and 21 days).

Table 35. Elemental analysis (in atomic %) of the surface of the GC 1e-k/A_1 and molar Ca/P ratio for 7, 14, and 21 days soaking in SBF.

Soaking time in SBF (days)	Si	K	Mg	Ca	P	Molar Ca/P ratio
7	-	-	5.54	59.33	35.13	1.68
14	-	-	-	62.50	37.50	1.67
21	-	-	-	62.66	37.34	1.67

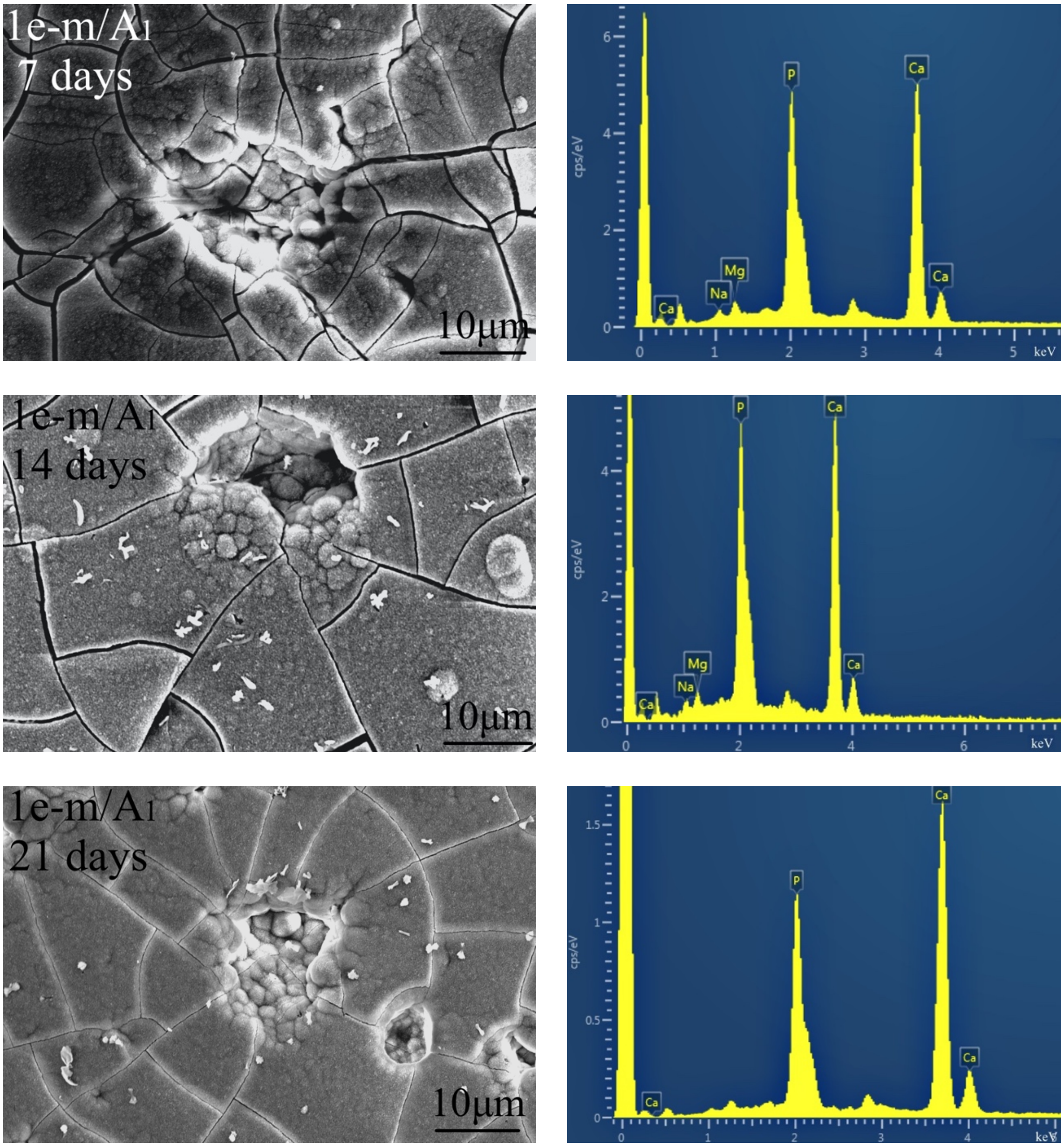

Figure 54. Formation and evolution of HA layer on the surface of the GC 1e-m/A_1 over immersion time in SBF at 37 ºC (7, 14, and 21 days).

Table 36. Elemental analysis (in atomic %) of the surface of the GC 1e-m/A_1 and molar Ca/P ratio for 7, 14, and 21 days soaking in SBF.

Soaking time in SBF (days)	Si	Na	Mg	Ca	P	Molar Ca/P ratio
7	-	6.14	8.56	53.40	31.90	1.67
14	-	5.25	4.92	56.27	33.56	1.67
21	-	-	-	62.58	37.42	1.67

IV. General evaluation of the modified GCs with addition of 1 mol% Al_2O_3

The bioactivity of produced novel GCs remained at a desirable high level, as *in vitro* test showed formation of HA layer on their surface after immersion in SBF at 37 °C. The phase assemblage in the well-sintered GCs resulted in dense microstructure, reflected in their mechanical properties. The 1 mol% addition led to an increase in fracture toughness values, without increasing the values of the other mechanical properties to a level that significantly exceeds the mechanical properties of the human jaw bone and dentine. More specifically, the addition of 1 mol% Al_2O_3 in the produced GCs 1d/A_1, 1d-k/A_1, 1d-m/A_1, and 1e-k/A_1 (Figs. 55 and 56), shifted the fracture toughness value to values greater than 2 MPa·$m^{0.5}$, but the values of modulus of elasticity does not exceed 30 GPa. Only in the case of the GCs 1e/A_1 and 1e-m/A_1 (Fig. 56), the addition of 1 mol% Al_2O_3, shifted the values of the modulus of elasticity to be greater than 30 GPa, but without far exceeding the desired values (they were 34 and 34 GPa, respectively). Finally, it is worth noting that the 1mol% Al_2O_3 addition had a positive effect as far as adaptation of the mechanical properties of produced GCs to those of human jaw bone and dentine (Table 37), revealing these materials as a promising for dental implant applications.

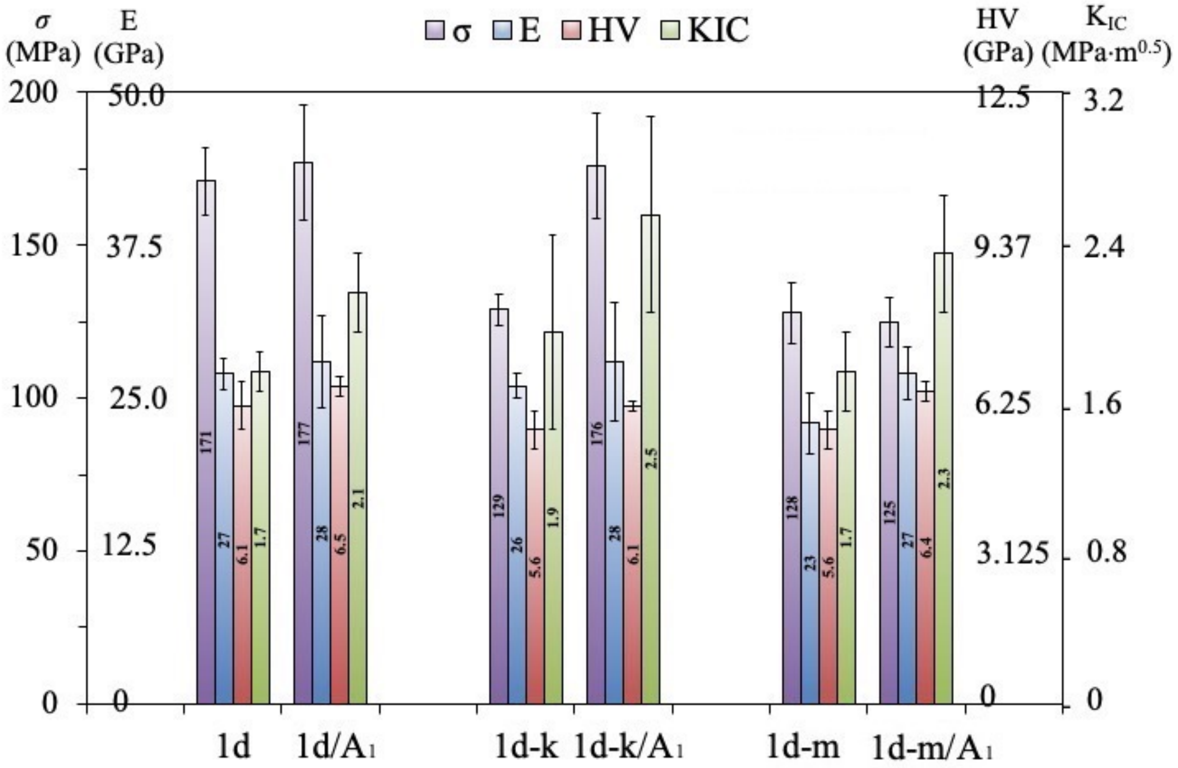

Figure 55. Influence of 1 mol% Al_2O_3 addition on the mechanical properties (flexural strength, σ; modulus of elasticity, E; Vickers microhardness, HV; and fracture toughness, K_{IC}) of the produced GCs 1d/A_1, 1d-k/A_1 and 1d-m/A_1.

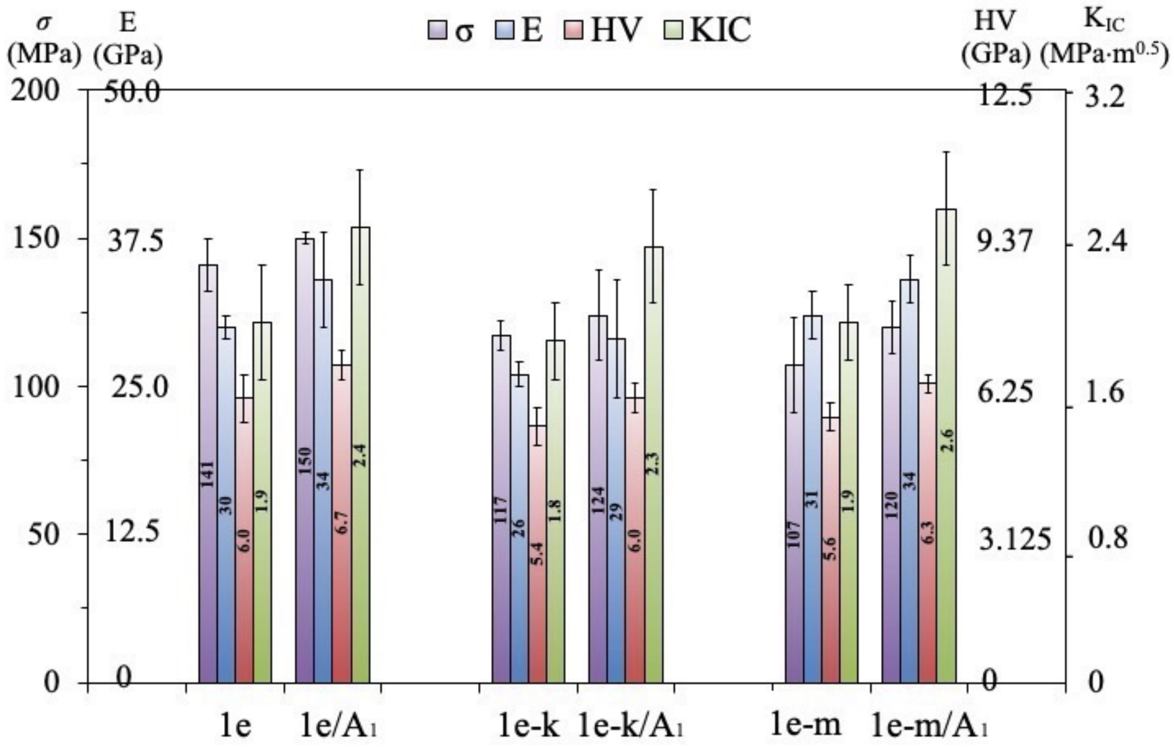

Figure 56. Influence of 1 mol% Al_2O_3 addition on the mechanical properties (flexural strength, σ; modulus of elasticity, E; Vickers microhardness, HV; and fracture toughness, K_{IC}) of the produced GCs 1e/A_1, 1e-k/A_1 and 1e-m/A_1.

Table 37. Mechanical properties of dentine and cortical jaw bone (it is the same table with the Table 26 but it is repasted here in order to help the reader to immediately compare the mechanical property of the natural tissues (cortical jaw bone and dentine) and with those reported in Figs. 55 and 56).

	Flexural strength (σ, MPa)	*Modulus of elasticity (E, GPa)*	*Vickers microhardness (HV, GPa)*	*Fracture toughness ($K_{IC,}$ MPa·m$^{0.5}$)*
Cortical jaw bone	50-150	7-30	0.06-0.07	2-12
Dentine	230-305	15-30	< 0.6	3

2.2 Modified GCs with addition of 7-8 mol% Al_2O_3

As mentioned above, this second section (**2.2**) presents the results of the modifications made to the parent glass compositions in order the physico-mechanical properties of the produced GCs to be as close as possible to those of the human enamel. To convert the bioactive GCs (1d, 1d-k, 1d-m, 1e, 1e-k, 1e-m) into bioinert and to increase the physico-mechanical properties, to reach to the closest possible level the physico-mechanical properties of enamel, 7-8 mol% Al_2O_3 was added in the above compositions.

I. Densification and crystallization

I-1. Results of thermal analysis

The dilatometry curves of the produced 1d/A$_2$, 1d-k/A$_2$, and 1d-m/A$_2$ glasses (Fig. 57), show that the T_g varied from 640 to 669 ^{o}C and the T_s from 670 to 695 ^{o}C, while the above values of the produced 1e/A$_2$, 1e-k/A$_2$, and 1e-m/A$_2$ glasses varied from 639 to 671 ^{o}C and from 670 to 701 ^{o}C, respectively.

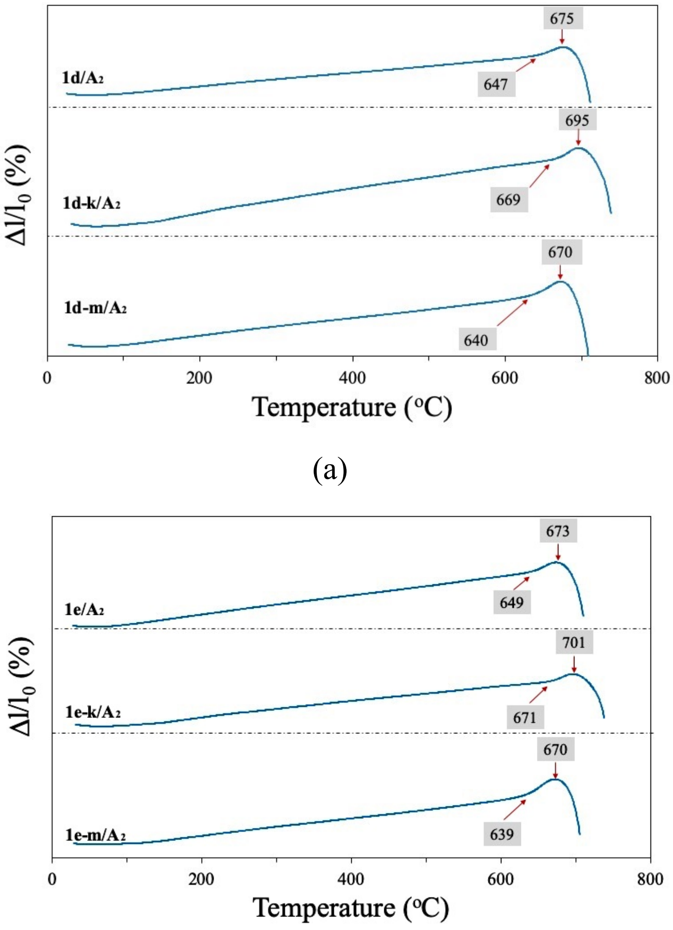

(a)

(b)

Figure 57. Dilatation curves of bulk annealed glasses (a) 1d/A$_2$, 1d-k/A$_2$, 1d-m/A$_2$ and (b) 1e/A$_2$, 1e-k/A$_2$, 1e-m/A$_2$.

The DSC thermographs (Fig. 58) registered an endothermic peak, which attributed to T_g, followed by the oncet of crystallization, T_c, and finally a single exothermic peak, which is considered as the peak of crystallization, T_p. The values of T_g, T_c, and T_p are summarized in Table 38. Therefore according to the resutls of thermal analysis the heat-treatment of the glass-powder-compacts was carried out at 900 °C.

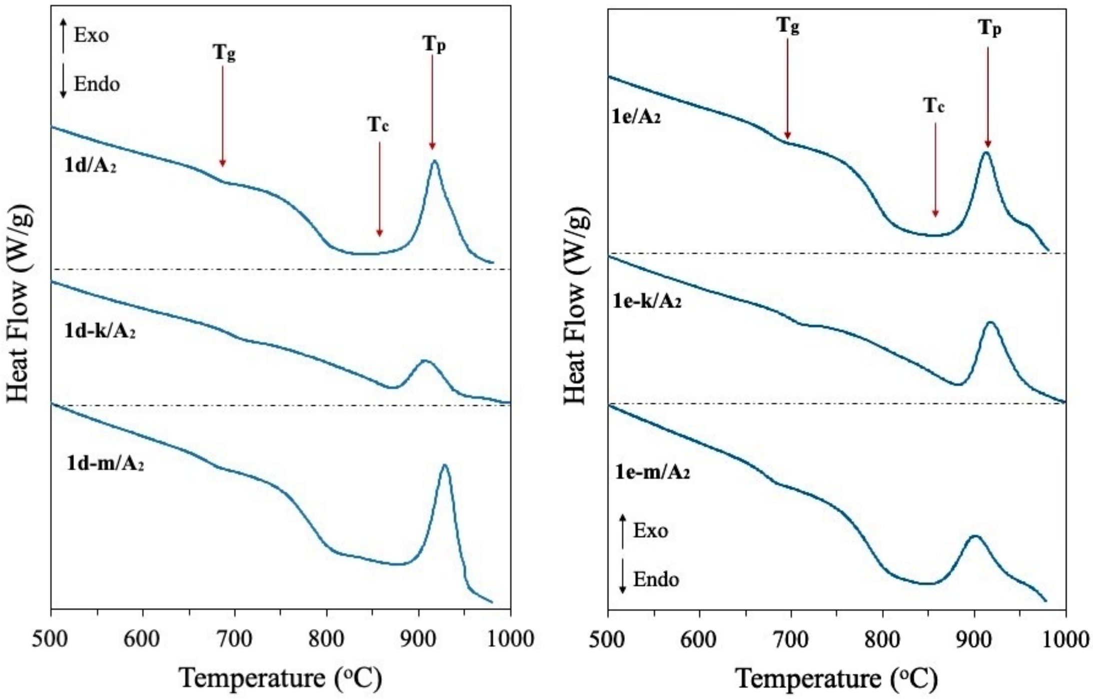

(a) (b)

Figure 58. Thermographs of the Al_2O_3-containing (7-8 mol%) glasses (a) 1d/A_2, 1d-kA_2, 1d-m/A_2, and (b) 1e/A_2, 1e-k/A_2, 1e-m/A_2. The heating rate was 20 K/min.

Table 38. Mean values (and standard deviation; n = 3) of glass transition temperature (T_g), oncet crystallization temperature (T_c), and crystallization temperature (T_p) of the investigated glasses, which contain 7-8 mol% Al_2O_3. The sintering window (T_c-T_g) is also presented.

Glass	T_g (°C)	T_c (°C)	T_c - T_g	T_p (°C)
1d/A_2	683 ± 8	873 ± 2	190	913 ± 19
1d-k/A_2	706 ± 4	874 ± 3	168	902 ± 16
1d-m/A_2	681 ± 8	879 ± 15	198	925 ± 22
1e/A_2	686 ± 4	855 ± 10	169	899 ± 19
1e-k/A_2	711 ± 5	869 ± 4	158	910 ± 22
1e-m/A_2	678 ± 5	849 ± 11	171	889 ± 18

I-2. Crystallization mechanism

Using the plots of $\ln((Tp^2)/\varphi)$ vs 1000/Tp (Fig. 59), the E_a of crystallization of the produced glasses was calculated (Table 39). The analysis of the exothermic peaks of the glasses, allowed the calculation of the n_A values (Table 39). The n_A values of the K-free glasses was $n_A \geq 3$, which means that these glasses are prone to three-dimensional growth of crystals, while, the K-containing glasses present $n_A \geq 2$, which means that these two glasses are prone to two-dimensional crystallization.

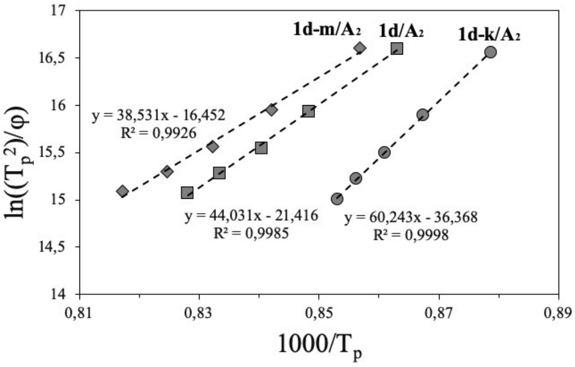

Figure 59. The plots of $\ln((T_p^2)/\varphi)$ *vs* 1000/T_p of the Al_2O_3-containing (7-8 mol%) glasses (a) 1d/A_1, 1d-kA_1, 1d-m/A_1, and (b) 1e/A_1, 1e-k/A_1, 1e-m/A_1.

Table 39. Mean values (and standard deviation; n = 3) of activation energy (E_a), and Avrami exponent (n_A) of the investigated glasses, which contain 7-8 mol% Al_2O_3.

Glass	E_a (kJ/mol)	n_A
1d/A_2	366 ± 8	3.8 ± 0.1
1d-k/A_2	490 ± 10	2.5 ± 0.5
1d-m/A_2	320 ± 1	3.7 ± 0.5
1e/A_2	359 ± 1	3.4 ± 0.8
1e-k/A_2	501 ± 7	2.5 ± 0.4
1e-m/A_2	364 ± 10	3.4 ± 0.2

I-3. Sintering and aesthetics

As mentioned above, the choice of the heat-treatment temperature (900°C) for the parallelepiped bars of the glass-powder compacts was based on the values of T_g (Fig. 57), T_s (Fig. 57), and T_p (Table 38), which were determined experimentally by the thermal analysis of the investigated glasses.

The density of the bulk glasses, varied between 2.56 - 2.93 g/cm^3, increased in the produced GCs; after sintering-crystallization to 2.85 – 3.19 g/cm^3 (Table 40). The linear shrinkage ranged between 10.1 - 11.1 % (Table 40). As regards the aesthetics, all the produced GCs had a white color (Fig. 60).

Table 40. Mean values (and standard deviation, n = 5) of linear shrinkage and density of the Al_2O_3-containing (7-8 mol%) glasses and GCs heat-treated at 900 °C for 1 h. (The SD of density was < 5%).

Composition	*Linear shrinkage (%)*	*Density (ρ, g/cm^3)*	
		Glass	*GCs*
1d/A_2	11.1 ± 0.1	2.58	2.99
1d-k/A_2	10.1 ± 0.1	2.61	2.85
1d-m/A_2	10.9 ± 0.3	2.66	3.02
1e/A_2	11.0 ± 1.1	2.81	3.19
1e-k/A_2	10.6 ± 2.1	2.93	3.11
1e-m/A_2	10.3 ± 4.0	2.56	2.99

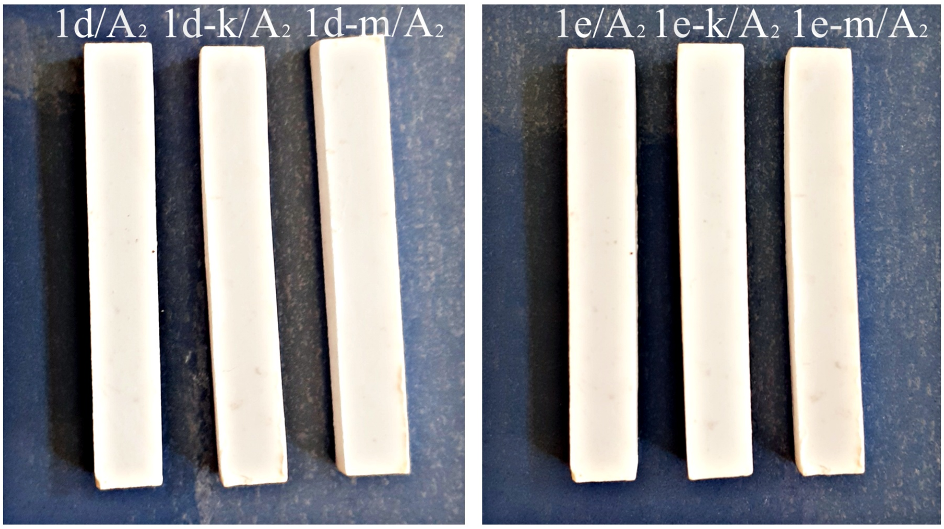

Figure 60. Well-sintered dense Al_2O_3-containing (7-8 mol%) GC bars of white colour, after heat-treatment at 900 °C.

I-4. Crystalline structure

Compared to the Al_2O_3-free GCs, or the GCs with 1 mol% Al_2O_3 addition, the 7-8 mol% Al_2O_3 addition changed the crystalline phases formed in the resultant GCs. More specifically, melilite and diopside were identified in the case of the K-free 1d/A_2, 1d-m/A_2, 1e/A_2, 1e-m/A_2 GCs, whilst melilite and gehlenite were formed in the case of the K-containing 1d-k/A_2 and 1e-k/A_2 GCs (Fig. 61) (Appendix 1: Phase Diagrams).

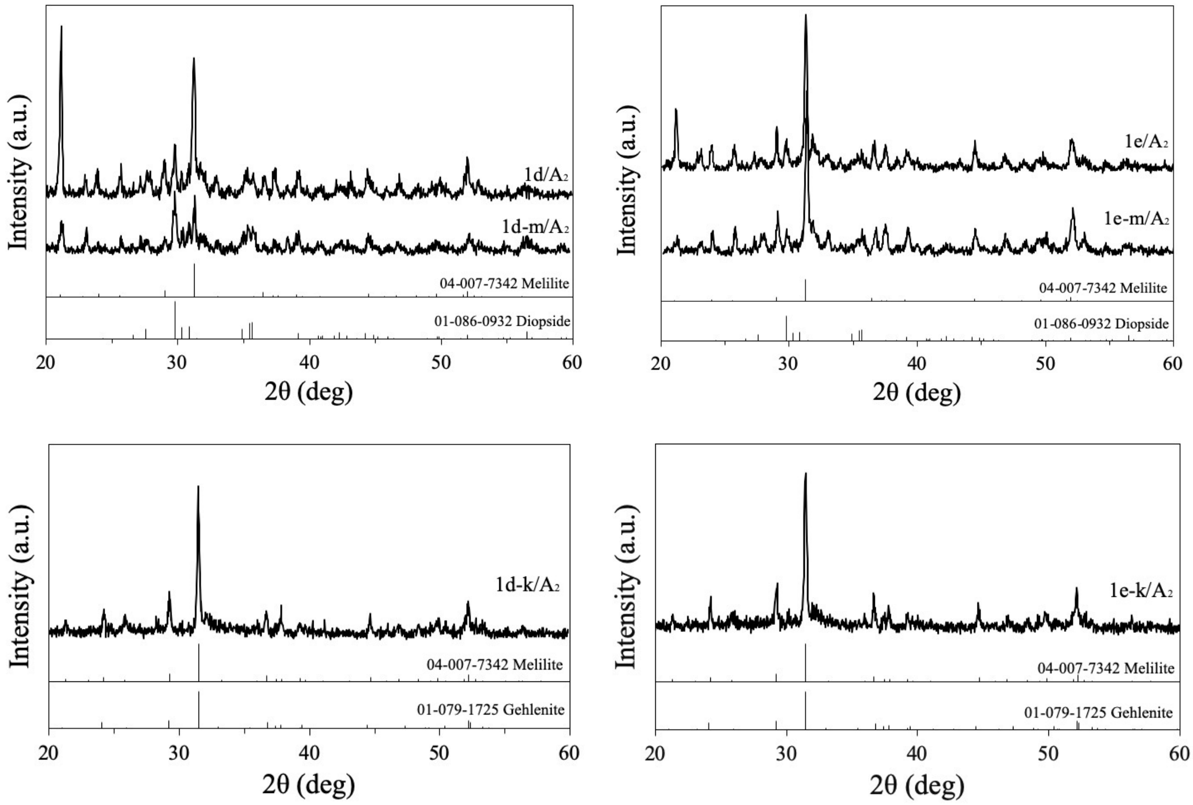

Figure 61. X-ray diffractograms of the produced Al_2O_3-containing (7-8 mol%) GCs heat-treated at 900 °C for 1 h. Diopside ($CaMgSiO_6$, 01-086-0932); Melilite $Ca_4Al_2MgSi_3O_{14}$, 04-007-7342); Gehlenite ($Ca_2Al(AlSiO_7)$, 01-079-1725).

I-5. Microstructure

SEM images of the microstructure of the produced GCs are presented in Fig. 62. According to the elemental analysis by EDS, in conjunction with the XRD results, two types of crystals were observed in each produced GC. More specifically, the big crystals in 1d/A_2, 1d-m/A_2, 1e/A_2, and 1e-m/A_2 GCs were assigned to diopside (D), as the atomic ratio Mg/Ca/Si/O was found to be 1/1/2/6, respectively. In 1d-k/A_2 and 1e-k/A_2 GCs, the big crystals were assigned to gehlenite (G), as their Ca/Al/Si mol ratio was 2/2/1. Finally, the small crystals dispersed among the big crystals of diopside or gehlenite were assigned to melilite (M).

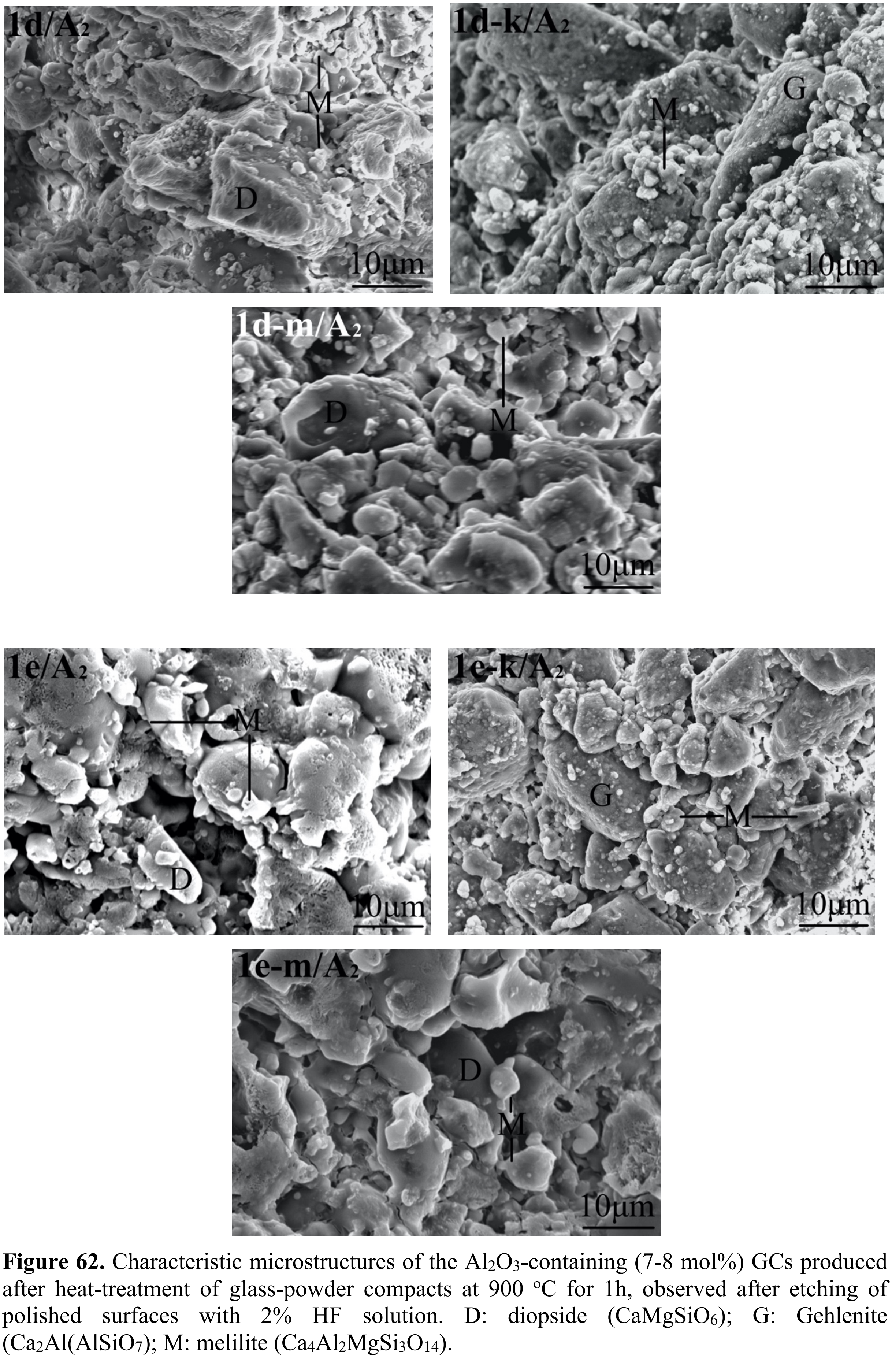
1d/A2
M
D
10µm
1d-k/A2
M
G
10µm
1d-m/A2
D
M
10µm
1e/A2
M
D
10µm
1e-k/A2
G
M
10µm
1e-m/A2
D
M
10µm

Figure 62. Characteristic microstructures of the Al_2O_3-containing (7-8 mol%) GCs produced after heat-treatment of glass-powder compacts at 900 °C for 1h, observed after etching of polished surfaces with 2% HF solution. D: diopside ($CaMgSiO_6$); G: Gehlenite ($Ca_2Al(AlSiO_7)$; M: melilite ($Ca_4Al_2MgSi_3O_{14}$).

II. Mechanical properties

Table 41 summarizes the mechanical properties of the fabricated GCs. The values of the flexural strength ranged between 120 and 171 MPa. The modulus of elasticity of produced GCs varied between 28 and 42 GPa. The hardness and the fracture toughness values varied from 6.3 to 7.0 GPa and 2.6 to 2.8 MPa·m$^{0.5}$, respectively.

Finally, the brittleness index of the produced GCs 1d/A$_2$, 1d-k/A$_2$, 1d-m/A$_2$, 1e/A$_2$, 1e-k/A$_2$, 1e-m/A$_2$ was 2.6 ± 0.7, 2.5 ± 0.6, 2.5 ± 0.2, 2.7 ± 0.1, 2.4 ± 0.2 and 2.5 ± 0.3 μm$^{-0.5}$, respectively.

Table 41. Mean values (and standard deviation, n = 10) of the mechanical properties of the Al$_2$O$_3$-containg (7-8 mol%) GCs produced after heat-treatment at 900 °C for 1h.

GCs	Mechanical properties			
	Flexural strength (σ, MPa)	*Modulus of elasticity (E, GPa)*	*Vickers microhardness (HV, GPa)*	*Fracture toughness (K_{IC}, MPa·m$^{0.5}$)*
1d/A$_2$	171 ± 23	42 ± 4	6.9 ± 0.7	2.7 ± 0.2
1d-k/A$_2$	130 ± 5	28 ± 1	6.4 ± 0.7	2.6 ± 0.5
1d-m/A$_2$	157 ± 22	42 ± 1	7.0 ± 0.4	2.8 ± 0.3
1e/A$_2$	171 ± 3	41 ± 1	7.0 ± 0.3	2.6 ± 0.5
1e-k/A$_2$	120 ± 3	28 ± 2	6.3 ± 0.4	2.6 ± 0.5
1e-m/A$_2$	168 ± 17	39 ± 2	6.8 ± 0.1	2.7 ± 0.4

III. Bioactivity

The addition of 7-8 mol% Al$_2$O$_3$ totally suppressed the bioactivity of the produced GCs 1d, 1d-k, 1d-m, 1e, 1e-k and 1e-m. According to SEM/EDS analyses, no HA formation was observed on the surface of the GC specimens after 7, 14 and 21 days of immersion in SBF.

IV. General evaluation of the modified GCs with addition of 7-8 mol% Al_2O_3

The addition of Al_2O_3, except the fact that it totally eliminated the bioactivity, increased the mechanical properties of the produced GCs. Consequently, the values of the mechanical properties (Figs. 63 and 64), which are very close to the corresponding values of enamel and dentine (Table 42), the obtained aesthetic characteristics (i.e. white color), and the zero bioactivity, qualify the produced GCs as potential candidates for fixed all-ceramic prosthetic restorations. More specifically, according to ISO 6872 "Dentistry-Ceramic Materials", the produced Al_2O_3-containg (7-8 mol%) GCs can be recommended as aesthetic ceramic materials, namely as coatings of a metal or a ceramic substrates for producing single-unit anterior or posterior prostheses, veneers, inlays, or onlays, as well as in the construction of adhesively cemented ceramic substrates for single-unit anterior or posterior prostheses.

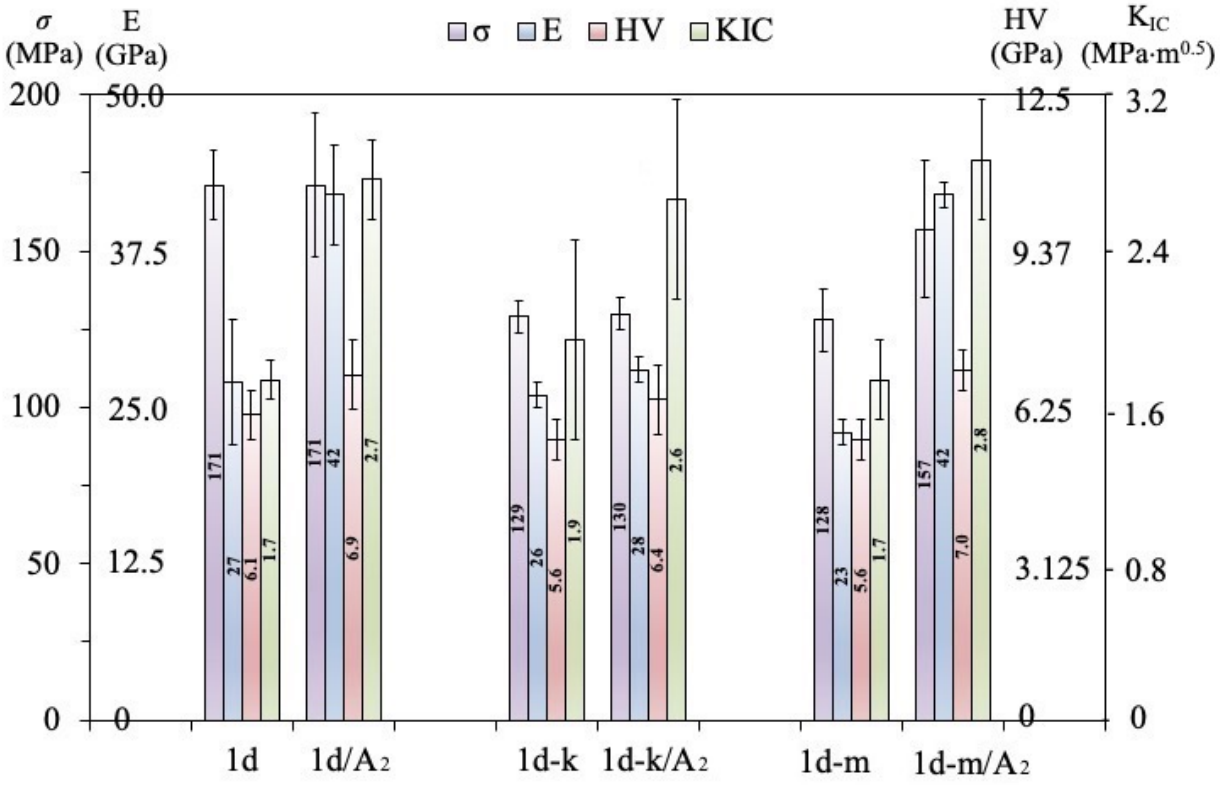

Figure 63. Influence of 7-8 mol% Al_2O_3 addition on the mechanical properties (flexural strength, σ; modulus of elasticity, E; Vickers microhardness, HV; and fracture toughness, K_{IC}) of the produced GCs 1d/A_2, 1d-k/A_2, and 1d-m/A_2.

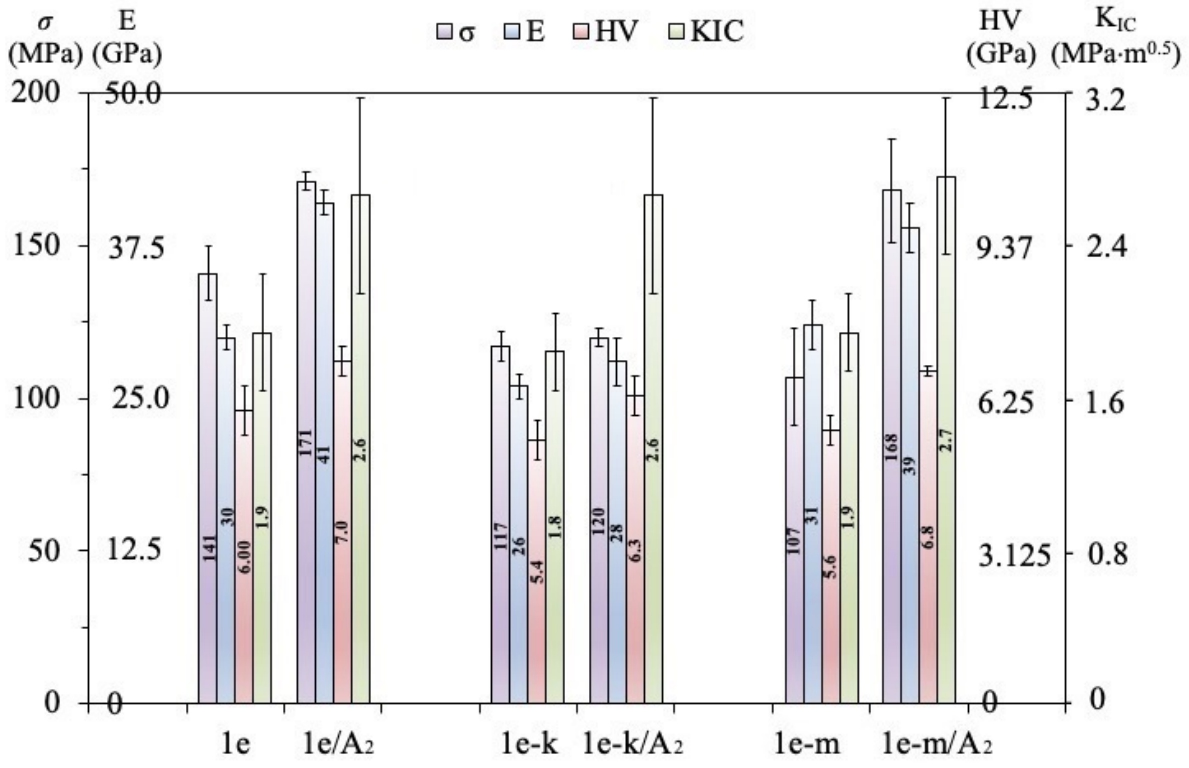

Figure 64. Influence of 7-8 mol% Al_2O_3 addition on the mechanical properties (flexural strength, σ; modulus of elasticity, E; Vickers microhardness, HV; and fracture toughness, K_{IC}) of the produced GCs 1e/A_2, 1e-k/A_2, and 1e-m/A_2.

Table 42. Mechanical properties of human dentine and enamel. The data were extracted from Table 17.

	Flexural strength (σ, MPa)	*Modulus of elasticity (E, GPa)*	*Vickers microhardness (HV, GPa)*	*Fracture toughness ($K_{IC,}$ MPa·$m^{0.5}$*
Dentine	230-305	15-30	< 0.6	3
Enamel	60-200 (260-290) *	70-100	3.0 - 5.5	1.0 - 1.5

*if supported by dentine

Consequently, ***the second aim*** of the doctoral thesis, aiming at modifying the compositions 1d, 1d-k, 1d-m, 1e, 1e-k, and 1e-m by choosing a suitable proportion of a single oxide, was perfectly fulfilled. The addition of Al_2O_3, either 1 mol% or 7-8 mol% resulted in GCs which can be proposed for use in different domains.

GENERAL DISCUSSION, CONCLUSIONS AND FUTURE WORK

General discussion

It is well established that glass-ceramic (GC) materials, in general, demonstrate improved mechanical properties compared to parent glasses [1]. Taking into account the high bioactivity of Bioglass 45S5, many research groups have been involved in the development of GCs based on Na_2O–CaO–SiO_2 system with various additives, such as P_2O_5, MgO, CaF_2, B_2O_3, Al_2O_3 etc., aiming at applications in dentistry and orthopedics [32, 117]. More specifically, GCs are very attractive materials in dental applications because good aesthetics, bioactivity performance, and suitable mechanical properties can potentially be achieved in the same material simultaneously [4, 118]. However, the most important aspect is that the CGs offer almost endless possibilities for these properties to be tuned to the existing demands. This ability of GCs perfectly matches the modern aspects of biomaterials design and biocompatibility, which suggest that the best biomaterial is the one with the nearest approach to the properties of the living tissue. In the case of the dental implants, there are the jaw bone and dentine [4, 18, 19].

There are two decisive factors which allow the tuning of the properties of the resultant GC, (i) the design of the composition of the parent glass, and (ii) the choice of the optimum heat-treatment for glass devitrification [4]. The thermal analysis of the experimental glasses provides all the necessary information required to set up the heat-treatment schedule, as the success of controlled crystallization depends on the heat-treatment including heating-rate, crystallization temperature, and the heating-time at each specific temperature of the schedule of the heat-treatment [4, 24, 27, 112]. In the present work, thermal analysis allowed to select an optimum (for the investigated glass compositions) temperature profile of the heat-treatment process, which resulted in well-consolidated and dense GCs. In CGs technology, the high quality of the produced GCs is clear evidence that sintering ideally preceded crystallization and was completed in the glass-powder compacts before crystallization started [4, 33].

Our research group has progressively developed several novel compositions in the CaO-MgO-SiO_2 ternary system, where P_2O_5, Na_2O, and CaF_2 were incorporated as additives [102, 104, 111]. An earlier study reported on two bioactive glasses in this system, designated as 1d and 1e [104]. These two glasses demonstrated spontaneous formation of HA from the early stages of immersion in SBF (7 days) [104]. Nevertheless, the apatite formation ability of the 1d and the 1e-based GCs had not been documented, yet. It is worth noting that the glass composition 1d favored bone regeneration, since *in vitro* cell-cultures, *in vivo* animal tests, and clinical trials showed a very good performance, mainly low inflammatory infiltration and excellent biocompatibility with the surrounding tissue [97]. Taking into account the above and knowing that there is no experience on the corresponding GCs 1d and 1e at all, these compositions were studied as initial compositions for the purpose of this thesis. The first results showed that the produced GCs 1d and 1e displayed bioactivity features and the heat-treatment schedule led to well-sintered and well-crystallized GCs with dense microstructure, qualifying the produced GCs for further consideration and experimentation as potential dental implant materials, since their mechanical properties were close enough to those of dentine and jaw bone.

Firstly, we attempted substitutions (complete substitution of K_2O for Na_2O and partial substitution of MgO for CaO) in the initial compositions 1d and 1e in order to produce novel GC materials at relatively low temperatures, whose mechanical properties would be a better match with those of the natural tissue (i.e. jaw bone and dentine) and comparable to those of the currently used dental implant materials (e.g. Ti alloys). As far as the influence of cations substitution in the parent 1d and 1e glasses is concerned, the results showed that both T_g and T_p were shifted towards higher temperatures in case of K for Na substitutions, while the sintering window, defined as the temperature interval between T_g and T_c, was expanded (Appendix 3a, Fig. 68a). However, no significant alteration in T_g and T_p was revealed in potassium free (1d-m and 1e-m) compositions compared to their parent glasses 1d and 1e, respectively (Appendix 3a, Fig. 68a). The results of thermal analysis, after the addition of 1 mol% Al_2O_3, demonstrated that T_p values were generally shifted towards higher temperatures. The sintering window of the studied glasses increased after 1 mol% Al_2O_3 addition (Appendix 3a, Fig. 68b). The addition of 7-8 mol% Al_2O_3, according to dilatometry and DSC measurements, led to an increase in T_g, T_c, T_p, and the sintering window (Appendix 3a, Fig. 68c). Concerning the sintering window, taking into account the above, all the modifications did not lead to a narrow sintering window, but on the contrary, they either increased the sintering window or did not cause a significant change. This fact is very important, because in the opposite case, a narrow sintering window would lead to early crystallization just above T_g, as 45S5 Bioglass [119], resulting in GCs with undesirable microstructure.

Regarding the crystallization kinetics of the studied glasses, K_2O for Na_2O substitution in the initial composition (1d and 1e) resulted in reducing of crystallization tendency, as higher E_a values of the modified glasses may suggest that K_2O prevents crystallization [28]. In the case of partial substitution of MgO for CaO the corresponding phenomenon is not observed, as the E_a values are not changed significantly after the modification. Also, the addition of 1 mol% Al_2O_3 led to higher E_a values of the modified glasses, which means that the above addition prevents crystallization. Decidedly, this fact (i.e. that the addition of Al_2O_3 leads to an increase of E_a values) cannot be considered as a general rule, since the addition of 7-8 mol% Al_2O_3 to the same composition did not lead to the same results, since the E_a values either decreased (1d/A_2, 1d-m/A_2, 1e/A_2, 1e-m/A_2) or slightly increased (1d-k/A_2, 1e-k/A_2).

As the crystallization kinetics of glasses was investigated by non-isothermal methods (Kissenger and Augis-Bennet methods) using DSC, in order to determine the dimensionality of the crystal growth, the determination of the nucleation rate in glasses is not required. The n_A values of all the investigated glasses, which were calculated from the analysis of the exothermic peaks, suggested high capability for two-dimensional and three-dimensional crystallization, as the values of n_A were greater than 2 and 3 [24, 27, 112, 113].

Regarding the crystallization mechanism (bulk or surface crystallization), one of the most reliable and widely used methods to study the crystallization mechanism is to observe the microstructure of the bulk glasses specimens, i.e. the direction of the growth of crystals at each crystallized temperature [33]. However, in the recent years there are several research groups [45, 64] which argue that the value of the Avrami parameter in addition to the dimensionality of crystals growth, also refers to the mechanism of glass crystallization (i.e. surface or bulk crystallization). So, according to Saadaldin et al. [45, 64], the produced glasses are prone to bulk crystallization, since $n_A > 2.5$ in all cases.

The white color diopside-fluorapatite-wollastonite GCs 1d and 1e suggest that sintering, which generally starts at temperatures slightly higher than T_g, was completed in the glass powder compacts at about 800 °C, where the highest values of linear shrinkage and density were recorded. Since crystallization typically favors the increase in strength, further heating at 850 °C led to improvement of mechanical properties, such as bending strength, modulus of elasticity, microhardness, and fracture toughness.

The K_2O for Na_2O substitution, compared to the partial substitution of MgO for CaO, resulted in more white GCs specimens, and in a slightly different assemblage of crystalline phases in the resultant GCs (i.e. formation of alpha-potassium magnesium silicate, instead of wollastonite; compared to the other investigated CCs) (Appendix 1: Phase Diagrams). These differences should be attributed to the composition of the parent glass rather than to the higher firing temperature (900 °C).

The addition of 1 mol% Al_2O_3 led to well-sintered, well-crystallized and of white color GCs. It was revealed that 1 mol% Al_2O_3 addition did not cause change in the crystalline phases formed. However, the addition of 7-8 mol% Al_2O_3 resulted in a change of the crystalline phases. More specifically, melilite and diopside phases were identified in the case of the K-free compositions, while melilite and gehlenite were formed in the case of the K-containing compositions (Appendix 1: Phase Diagrams).

SEM observations confirmed formation of dense GCs with small closed porosity, estimated to be less than 1-2 %, assigned to both intergranular residual porosity and the so-called induced or secondary porosity. According to Karamanov [120, 121] the crystallization of diopside as a single phase can lead to appearance of porosity in the final GCs, on account of the significant increase in density from the glass (2.75 g/cm^3) to crystallized diopside (3.27 g/cm^3) [33, 120, 121]. The increase in density from the glass to the crystallized form of wollastonite is small (i.e. 2.87 and 2.92 g/cm^3, respectively). Densification was decreased in the produced 1d and 1e GC specimens after heat-treatment at temperatures $\geq$ 800 °C (i.e. 800, 850 and 900 °C), attributed to the aforementioned difference in density during crystallization, which leads to the appearance of micropores in the intergranular spaces of the crystals (or secondary porosity). However, the experimental results showed that this so-called induced (or secondary) porosity is negligible in the investigated compositions. Hence, it can be proposed that the formation of secondary porosity, created due to the devitrification of the glass that resulted in the formation of large crystals of diopside, provided adequate space for the formation of the smaller crystals of wollastonite or α-PMS, which are crucially important for providing bioactivity in the investigated GCs [107]. Thus, the resultant GCs are densely packed owing to uniform precipitation of crystals through the glass matrix, which is a crucial issue for achieving high mechanical properties. At this point, it should also be stressed that the heating-rate critically affects the rate of the growth of crystals [39]. Accordingly, the slow heating rate of 2-5 K/min should positively influence the development of the final dense microstructure of the GCs. As for the diopside – melilite and gehlenite - melilite GCs, a corresponding phenomenon should also occur, since the formation of secondary porosity, due to the crystallization of diopside or gehlenite (~2.98 g/cm^3), creates sufficient space for the formation of the smaller crystals of melilite (~2.95 g/cm^3).

The SEM images show the microstructure of the produced bioactive GCs consisting of densely stacked crystals of diopside, fluoroapatite, wollastonite or α-PMS randomly dispersed in the glass matrix. It can be concluded that the crystallization of the investigated glasses resulted in bioactive GCs with desirable mechanical properties for dental implant applications. The 7-8 mol% Al_2O_3 addition led to changing the crystalline phases. The microstructure of the produced GCs, that is small melilite crystals stacked between the big prismatic diopside crystals or big gehlenite crystals, contributed to the high mechanical properties of the produced GCs after Al_2O_3 addition.

The investigated GCs (except the 7-8 mol% Al_2O_3 containing GCs) displayed bioactivity features since they are able to spontaneously transform their surface into an HA layer after immersion in SBF at 37 °C. This means that when these GCs are in the body, the formation of an HA surface layer adjacent to the bone will prevent the formation of fibrous tissue around the dental implant, and it will favor osteointegration and suppress stress shielding, as mentioned in the Introduction [80]. More specifically, the recorded increase of pH in the solution of the SBF over immersion time, which creates an ideal chemical environment for HA precipitation (i.e. in a pH range of 9.5 – 12) [122], is characteristic for such silica-containing compositions [111], and it is related to the bioactivity mechanism that involves Ca^+, K^+, and Na^+ ion exchange from the GC for H^+ from the SBF [123]. In the present study, careful observation of the diffractograms of the K-free GCs (1d, 1e, 1d-m, and 1e-m) shows that the intensity of the peaks due to wollastonite (at 2θ 26.92° and 33.7°) becomes weaker over immersion time and, eventually, they totally disappear, whereas the peaks owing to HA (at 2θ 29.2° and 32.02°) become stronger. Similarly, in the K-containing GCs (1d-k and 1e-k), the intensity of the peaks of α-PMS (at 2θ 20.71°, 22.27°, and 28.63°) is reduced and eventually these peaks disappear, whereas the HA peaks become stronger over the period of immersion time in SBF. In literature, the bioacitivity mechanism of wollastonite coating in SBF is described as follows [107]. The calcium ions in wollastonite are exchanged with H^+ ions from the SBF solution, leading to formation of a silanol (Si-OH) surface layer, to an increase of pH value, and eventually to the formation of a negatively charged layer with the functional groups of Si-O. The Ca ions in the SBF solution are attracted to the interface between the material and the solution. Accordingly, the solubility product of apatite ions at the interface is high enough to precipitate apatite on the surface.

Consequently, the experimental results show that the crystallized GCs did not jeopardize or annul the excellent biocompatibility and bioactivity of the parent glasses 1d and 1e, which has been well documented in earlier studies of our research team [97, 104]. In the present study, apart from the residual glassy phase, it might be suggested that wollastonite or α-PMS, in the case of the K-containing GCs, is closely related to the bioactivity performance displayed in the fabricated GCs. Moreover, the GCs which contain alpha-potassium magnesium silicate ($K_2MgSi_3O_8$) phase reached the highest values of pH, which suggests the contribution of this phase to bioactivity of the potassium containing GCs, likely by favoring a faster leaching ability. To our best knowledge, $K_2MgSi_3O_8$ is not a common crystalline phase in GCs, but it was recommended, for instance, as a slow-release fertilizer supplying nutritional components of K, Mg, and Si for crops [124].

Mentioning bioactivity, it is important to note that, in the case of dental implants, Brånemark introduced the term *osseointegration*, which is not an isolated phenomenon, but it depends on previous osteoinduction (the process by which osteogenesis is induced, because it implies the recruitment of immature cells and the stimulation of these cells to develop into preosteoblasts) and osteoconduction, which is associated with the formation of HA (an osteoconductive surface permits bone growth on it, or down into pores, channels, or pipes) [1, 51]. The effect of incorporation of various oxides on bioactivity is well investigated [1, 16, 105]. For example, knowing that the presence of MgO promotes the formation of apatite layer and taking into account several *in vitro* studies which show that Mg increases cell adhesion, proliferation and differentiation of osteoblast cells [1, 125], the presence of Mg in the compositions is this work was essential, as these GCs aim to be implanted in bone areas. The addition of Al_2O_3 to bioactive glasses is mostly attempted to improve the mechanical strength of the produced materials, while considering a drawback of reducing or zeroing bioactivity, alumina is suggested to be used in limited amount. However, there are only a few studies reporting on this phenomenon for GCs materials. According to Fernandes et al. [1], Al_2O_3 can be incorporated into glass compositions without reducing bioactivity by 1.0-1.5 wt.%. The results of this work show that 1.70-1.75 wt.% addition of Al_2O_3 does not impede the bioactivity of the produced GCs. In particular, the SEM and EDX analyses of the produced GCs specimens after immersion in SBF at 37 ^{o}C, have shown ability to form an HA layer on their surface as the Ca/P molar ratio was 1.67 - 1.69, that is a perfect match to stoichiometric HA, (Ca/P of HA = 1.67). The GCs after 7 days immersion in SBF showed the ability to form a calcium phosphate surface layer, which was getting denser with the passing of days. Also, the recorded increase of pH in the solution of the SBF over immersion time, which creates an ideal chemical environment for HA precipitation (i.e. in a pH range of 9.5 – 12) [122], is characteristic for such silica-containing compositions [111], and it is related to the bioactivity mechanism that involves Ca^+, K^+, and Na^+ ion exchange from the GC with H^+ from the SBF [123].

A dental material must have notably good chemical, mechanical, and optical properties comparable to those of the dental hard tissues (i.e. enamel, dentine) and bone, depending on the application [19]. In the case of dental implants, the knowledge of the mechanical properties of cortical bone (flexural strength 50-150 MPa, modulus of elasticity 7-30 GPa, microhardness 0.06-0.075 GPa, fracture toughness 2-12 MPa·$m^{0.5}$), trabecular bone (flexural strength 10-20 MPa, modulus of elasticity 0.05-0.5 GPa, microhardness 0.04-0.06 GPa, fracture toughness 0.7-1.1 MPa·$m^{0.5}$) and dentine (flexural strength 230-305 MPa, modulus of elasticity 15-30 GPa, microhardness < 0.6 GPa, fracture toughness 3 MPa·$m^{0.5}$) will help in designing of the new biomaterials [19, 38, 61, 62]. To make the above mentioned more understandable and because bioactive GCs are still not used as dental implant materials in daily dental clinical practice, it is important to compare the produced GC materials with those of titanium and zirconia (which are used in dental clinical practice).

Starting from the fracture toughness value and knowing that after the placement of a prosthetic restoration, the occlusal forces are mostly received by the body of the dental implant, unlike the natural teeth, where jaw bone plays this role it would be ideal for this property to range from 2 to 12 MPa·$m^{0.5}$ [19]. With the first substitution in initial compositions 1d and 1e, the experimental results showed that the substitutions of K and Mg affected the mechanical properties of the resultant GCs, which suggests that the fracture toughness can be increased. The fracture toughness of the produced GCs, after the substitutions of K and Mg (1.7 - 1.9 MPa·$m^{0.5}$) was clearly lower than that of zirconia implants (6 - 10 MPa·$m^{0.5}$) [45], which are used in the daily clinical dental practice, but very close to that of compact bone (2 - 12 MPa·$m^{0.5}$) [18, 19]. However, the addition of 1 mol % Al_2O_3 led to increasing the fracture toughness values (2.1 - 2.6 MPa·$m^{0.5}$), which are very close to that of compact bone and dentine (3 MPa·$m^{0.5}$).

The modulus of elasticity is an important property for dental implants, since a mismatch between them and the jaw bone can favor *stress shielding* effect [63, 64]. More specifically, according to Wolff [65], the bones are reshaped in response to the loads they receive. Therefore, reducing the bone load results in a decrease in its density because there is no stimulus for a continuous remodeling required to maintain its bone mass and consequently it leads to the failure of the dental implant. Thus, besides bioactivity, a dental implant material must have the ability to distribute the load to the adjacent bone and thereby to maintain its density. This means that if the values of the modulus of elasticity of the dental implant material and the adjacent bone are close to one another, then the stress distribution will approach the natural mode of distribution. For instance, the modulus of elasticity of titanium and zirconia (110 and 220 GPa, respectively) [45, 64], which are popular dental implant materials, is markedly higher than that of the jaw bone (7 - 30 GPa) and dentine (15-30 GPa) [19, 64]. Aiming at increasing the fracture toughness value while maintaining (as far as possible) the modulus of elasticity value, it was initially proposed a complete substitution of K_2O for Na_2O and a partial substitution of MgO for CaO. The experimental results showed that these first substitutions affected the mechanical properties of the resultant GCs, which suggest that the modulus of elasticity can be reduced while the fracture toughness can be increased. The produced GCs have a considerably smaller modulus of elasticity, for instance 26 and 23 GPa for the series 1d, that almost fits the maximum aforementioned value of the jaw bone, therefore an efficient suppression of stress shielding can be anticipated. Earlier studies, which targeted the development of dental implant materials, suggested adding Al_2O_3 to the GCs compositions [45, 64]; however, the mechanical properties of the resultant GCs were far from those of the jaw bone (e.g. E > 70 GPa). In this work, by adding Al_2O_3, neither did we deviate from the values of the mechanical properties of the jaw bone and dentine nor eliminate the bioactivity of the produced GCs. More specifically, with the addition of 1 mol% Al_2O_3, we were able to approach the value range of fracture toughness of the jaw bone and dentine, without increasing the modulus of elasticity above 30 GPa, except 1e/A_1 and 1e-k/A_1 GCs, where the values were 34 GPa.

Concerning microhardness, the initial substitutions resulted in its slight reduction. Nevertheless, these values (5.4 - 5.6 GPa) are higher than those of the spongy bone (0.5 - 1 GPa) [126, 127], with which the dental implant comes into contact, but they are still lower than that of zirconia implants and rather close to that of titanium implants (12 and 4 GPa, respectively) [127-129]. The addition of 1 mol% Al_2O resulted in an unavoidable slight increase of the values of microhardness (up to 6.5 GPa).

The influence of the substitutions on mechanical properties of the produced bioactive GCs and comparison to the properties of natural tissues as well as common dental implant materials, is schematically represented in Appendix 3b, Fig. 69.

Many research teams around the world, have been involved in the development of GC materials for dental implant applications [45, 64, 80-82]. According to their experimental results, the produced GCs are promising materials for dental implant applications; however, they have some disadvantages, for instance, although they achieve the desired values of fracture toughness (from 2 to 3 $MPa \cdot m^{0.5}$ [81] or ~3-6 $MPa \cdot m^{0.5}$ [45, 64, 80], which are very close to that of compact bone and dentine), the values of modulus of elasticity, 55-100 GPa [45, 64, 80, 81], are higher than those of dentine and compact jaw bone. Although, Chen et al. [82]

developed GCs with Young's modulus (29.75 GPa) similar to that of the cortical bone, good bioactivity as well as biocompatibility *in vitro*, their experimental results did not include fracture toughness values. Some of the above research groups [81] suggest interesting ideas, such as the production of a bilayered prototype implant for total tooth replacement. According to Baino et al. [81], this approach represents a novel, attractive option to replace and regenerate dental structures, which deserve further investigation and future in-depth analysis.

In the case of restorative dental GC materials, it is important to exhibit mechanical properties that do not lead to injury of the abutment, adjacent and opposite teeth [66]. Thus, it is a big challenge to develop GC materials with mechanical properties close to those of the natural tooth. The addition of Al_2O_3 in any composition that leads to bioactive materials can both increase the mechanical properties of the material and reduce or eliminate its bioactivity. More specifically, the 7-8 mol% Al_2O_3 addition had the effect of adjusting the mechanical properties of the produced GCs close to those of human enamel and dentine, suggesting these materials as promising ones for dental fixed all-ceramic prostheses.

In the case of bioinert produced GCs, starting from the values of flexural strength (120 - 171 MPa), they are close to the values of both dentine and enamel. The modulus of elasticity of the investigated GCs, 28 - 42 GPa (with the highest values of 1d/A 42 GPa and 1d-m/A 42 GPa), are higher than those of dentine but also slightly lower than those of natural enamel. The hardness values of the developed GCs (6.3 - 7.0 GPa) are close to those of enamel (3 - 5.5), reducing, therefore, the risk of injury to the natural opposite teeth, a phenomenon for which dental zirconia has been implicated (due to high hardness value of zirconia, 12 GPa) [66, 130]. It is important to note that the produced GCs have fracture toughness values ranging from 2.6 - 2.8 $MPa \cdot m^{0.5}$ which are very close to those of the natural tooth (i.e. enamel 1.0-1.5 and dentine 3 $MPa \cdot m^{0.5}$). Finally, the produced bioinert GCs had a brittleness index (2.4 - 2.6 $\mu m^{-0.5}$) very close to the minimum value of the brittleness index of glasses and ceramic materials [115].

According to the ISO 6872 standard "Dentistry-Ceramic Materials" [85], the classification of ceramics for fixed prostheses by intended clinical use depends on flexural strength and fracture toughness values. So, according to ISO 6872, a material with minimum flexural strength of 50 MPa and a fracture toughness of 0.7 $MPa \cdot m^{0.5}$ are recommended for **a**. aesthetic ceramics for coverage of a metal or a ceramic substructure, or **b**. aesthetic-ceramics: single-unit anterior prostheses, veneers, inlays, or onlays, while, ceramic materials with minimum flexural strength of 100 MPa and fracture toughness of 1 $MPa \cdot m^{0.5}$ are recommended for **a**. aesthetic-ceramics: adhesively cemented, single-unit, anterior or posterior prostheses, **b.**

adhesively cemented, substructure ceramics for single-unit anterior or posterior prostheses. The produced bioinert GCs cover the above requirements, as the values of flexural strength and fracture toughness are ranged between 120 - 171 MPa and 2.6 - 2.8 MPa·m$^{0.5}$, respectively. Also, it is important to notice that the produced GCs have higher values of fracture toughness compared to mica-based GCs (Dicor®; 1.4-1.5 MPa·m$^{0.5}$), and leucite GCs (IPS Empress®; 1.3 MPa·m$^{0.5}$) [19, 87].

Certainly, the above idea of Baino et al. [81] is very promising, especially nowadays, as the rapid development of digital technology, that is the introduction of the Computer Aided Design (CAD) technology in dentistry, has introduced new technologies for the fabrication of dental prosthetic restorations, one of which is CAD/CAM technology [39, 45]. The results of the present work showed that all the produced GCs had a brittleness index (parameter to estimate its machinability; 2.3-3.6 μm$^{-0.5}$) very close or more than 3 μm$^{-0.5}$, which is within the range that shows a good brittleness index for GC materials, as the brittleness index of glasses and ceramics generally vary within the range of 3-9 μm$^{-0.5}$ [115, 131, 132].

The above proposal requires the combination of bioactive (in order to fabricate the root of the tooth) and bioinert (in order to fabricate the crown of the tooth) GC materials in the CAD/CAM plate, which will then undergo mechanical cutting. However, the weak point in the above proposal is related to the interface between bioactive and bio-inert GC materials. The solution to the above problem can be provided by SLM (or SLS) technique, sintering of the materials layer takes place layer by layer, in a single mass. More specifically, although, laser-based Additive Manufacturing (AM) processes have been investigated extensively for use with different materials (polymers, metals), fabrication of 3D glass objects using Selective Laser Melting (SLM) technology is not well developed even though it has many applications [133]. The SLM technique features high productivity, almost unlimited shaping ability, and improved internal and marginal fit of prosthetic restorations. Moreover, the final products have minimal porosity and improved mechanical properties. However, the equipment required for SLM is still rather expensive, and the cost is transferred to the final product and eventually to the client/patient or to the national health-care budget [134-136]. So, according to Fateri et al. [133], who, with the help of SLM technique, achieved to fabricate the first GC tooth (the size of which was similar to the average human tooth size), the SLM technique is a very promising technique in construction of dental restorations.

Finally, it should be mentioned that the production of the investigated materials also satisfies the requirements for environmental protection and cost effectiveness, which are both strongly related to the reduction of the temperature of the heat-treatments. Indeed, the melting temperature of the glasses (1400 °C) and the sintering temperature of the glass powder compacts (800 - 900 °C) are lower compared to the temperatures needed for treating commercial GC materials in the $CaO-MgO-SiO_2$ ternary system [4, 136], or other materials in similar systems reported in literature [137-140].

Conclusions

The results of the present work showed that, in all cases, sintered-crystallized and dense materials were produced, attributed to the fact that sintering was completed before crystallization started. Partial substitution of Mg for Ca and complete substitution of K for Na were attempted in two glasses, namely 1d and 1e, whose bioactivity is well documented in literature. In case of K for Na substitution, the glass transition (T_g) and the crystallization temperature (T_p) of the glasses shifted to higher temperatures, while there were no significant alterations in T_g and T_p in the glasses with Mg for Ca substitution. GC materials comprising an assemblage of diopside, wollastonite and fluorapatite or diopside, fluorapatite and alpha-potassium magnesium silicate crystalline phases were synthesized through sintering-crystallization of fine glass-powder compacts in the temperature interval of 800 - 900 °C. The produced GCs displayed bioactivity features reflected in their ability to spontaneously form hydroxyapatite (HA) on their surface after immersion in SBF at 37 °C, even from the first week of immersion, attributed to the phases of wollastonite or α-PMS, depending on the substitution. Besides bioactivity, the phase assemblage led to well-sintered and well-crystallized GCs with a dense microstructure, which affected their mechanical properties. More specifically, reduced modulus of elasticity, higher fracture toughness, and smaller microhardness were achieved, suggesting that the above substitutions offer the ability to suitably tune the mechanical properties of these bioactive GCs in order to approach those of natural bones.

Also, it was revealed that 1 mol% Al_2O_3 addition did not cause any change in the crystalline phases formed. The results showed that 1 mol% Al_2O_3 addition increased the crystallization temperatures (T_p) and decreased the n_A values. It is important to emphasize that addition of 1 mol% Al_2O_3 had no adverse effect on bioactivity. The phase assemblage led to well-sintered GCs with a dense microstructure, which affected their mechanical properties. More specifically, the microstructure of the produced GCs, namely small wollastonite (or α-PMS crystals) stacked between the big prismatic diopside crystals, contributed to high K_{IC} (for example from 1.9 to 2.5 $MPa \cdot m^{0.5}$, in the case of 1d-k GCs). The Al_2O_3 addition allowed adapting the mechanical properties of produced GCs to those of human jaw bone and dentine, suggesting these materials as promising materials for dental implant applications.

On the other hand, the 7-8 mol% Al_2O_3 addition led to a change of the crystalline phases, formed. More specifically, after Al_2O_3 addition, diopside - melilite and gehlenite - melilite GCs were produced. The Al_2O_3 addition increased the T_g, T_c, T_p, and the sintering window of the silicate glasses. The crystalline phases assemblage led to a white color and well-sintered GCs with a dense microstructure, which affected their mechanical properties. The addition of 7-8 mol% Al_2O_3, apart from the fact that it eliminated bioactivity, increased the mechanical properties of the produced GCs, enabling their application in fixed all-ceramics prosthetic restorations.

Future work

The experimental results of this thesis and the recommended dental potential applications of the investigated GCs allow the following suggestions for future research in this field:

1. *In vitro* testing with osteoblast cultures and *in vivo* implantation in experimental animals.
2. Complete or partial substitution of Li_2O for MgO, in order to increase the mechanical properties (i.e. flexural strength > 300 MPa) of bioinert GCs, so as to be used in extensive fixed prosthetic restorations.
3. Application of Selective Laser Melting with the investigated glasses (and GCs) in order to fabricate dental prosthetic restorations, such as dental implants and dental fixed prostheses. It is very important to study the effect of the laser both on sintering-crystallization behavior and on the microstructure of the final GC materials.
4. Construction of porous GCs with consolidation techniques (e.g. based on the gelling property of starch), as candidate materials in dental maxillofacial prosthetics.

ANNEXES

Appendix 1

Phase diagrams of the SiO_2-MgO-CaO and the SiO_2-Al_2O_3-CaO ternary systems

The phase diagrams of the SiO_2-MgO-CaO and the SiO_2-Al_2O_3-CaO ternary systems, presented in Fig. 65 [4], indicate the location of the crystalline phases of diopside ($CaMgSi_2O_6$), wollastonite ($CaSiO_3$), gehlenite ($Ca_2Al(AlSiO_7)$), and melilite ($Ca_4Al_2MgSi_3O_{14}$), detected in the microstructure of the produced GCs (glass-ceramics) in the present study.

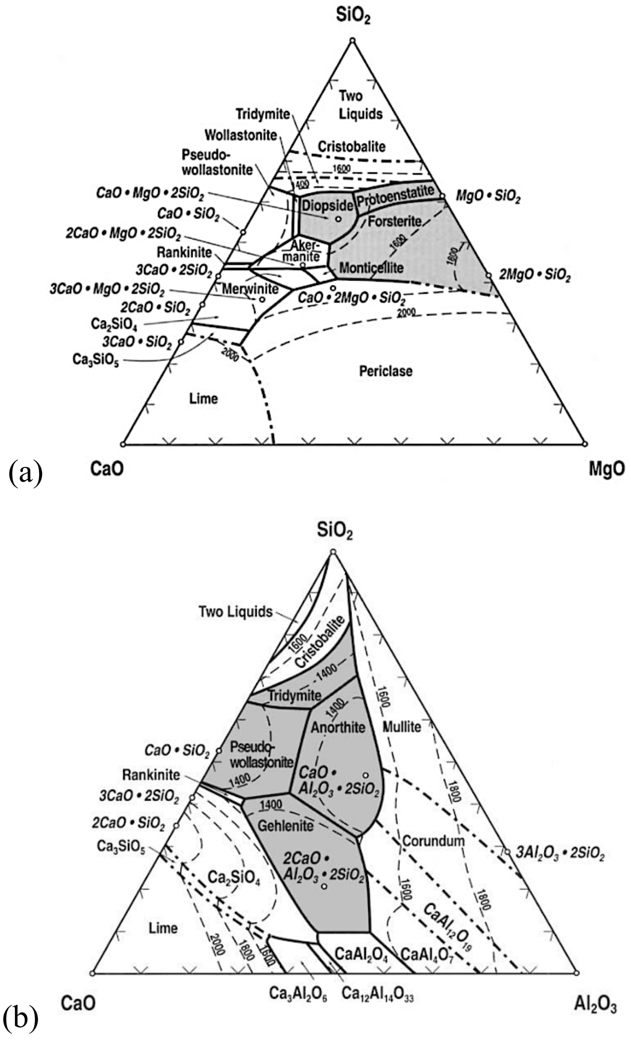
SiO2
Two Liquids
Tridymite
Wollastonite
Cristobalite
Pseudo-wollastonite
1600
1400
CaO • MgO • 2SiO2
Diopside
Protoenstatite
MgO • SiO2
CaO • SiO2
Forsterite
2CaO • MgO • 2SiO2
Rankinite
Aker-manite
1600
1800
3CaO • 2SiO2
Monticellite
2MgO • SiO2
3CaO • MgO • 2SiO2
Merwinite
2CaO • SiO2
CaO • 2MgO • SiO2
Ca2SiO4
2000
3CaO • SiO2
Ca3SiO5
2000
Periclase
Lime
(a)
CaO
MgO
SiO2
Two Liquids
1600
Cristobalite
1400
Tridymite
1400
1600
Anorthite
Mullite
CaO • SiO2
Pseudo-wollastonite
Rankinite
1400
CaO • Al2O3 • 2SiO2
1800
3CaO • 2SiO2
1400
2CaO • SiO2
Gehlenite
Corundum
3Al2O3 • 2SiO2
Ca3SiO5
2CaO • Al2O3 • 2SiO2
Ca2SiO4
1600
CaAl12O19
1800
Lime
2000
1800
1600
CaAl2O4
CaAl4O7
Ca3Al2O6
Ca12Al14O33
(b)
CaO
Al2O3

Figure 65. Phase diagrams of (a) the SiO_2-MgO-CaO and (b) the SiO_2-Al_2O_3-CaO ternary systems [4].

Diopside is a monoclinic pyroxene mineral with composition of $CaMgSi_2O_6$. Diopside exhibits relatively high refractory properties, melting point >1390 °C, and density of 3.25 – 3.55 g/cm^3. It has Mohs hardness of 6, Vickers hardness of 7.7 GPa (at a load of 0.98 N). There are many papers reporting on the influence of the composition of the parent glass on the crystallization of diopside in the resultant GC. According to Xiao et al., the decrease of CaO/MgO ratio favors the increase of the content of diopside in the resultant GC [142]. Yang et al. found that the increase in CaO/SiO_2 ratio favors the formation of diopside crystals [143]. As far as the addition of alumna in small amounts is concerned, as attempted in the GCs produced in the present study, it has been postulated that Al^{3+} ions can diffuse into the diopside network, replacing the Mg^{2+} and the Si^{4+} ions, resulting in $Ca(Mg,Al)(Si_2,Al)O_6$ [4].

Melilite belongs to the family of sorosilicates that consist of calcium silicates of aluminum and magnesium. *Gehlenite* ($Ca_2(Al_2SiO_7)$) is the aluminous end-member, and *akermanite* ($Ca_2(MgSi_2O_7)$) is the magnesian end-member. Melilite usually occurs in igneous and metamorphic rocks and meteorites, but also in the slag of blast furnaces. These features unequivocally evidence their high stability. Melilite and gehlenite display relatively high refractory properties, melting point >1450 °C and density of 2.90 – 3.0 and 2.90 – 3.07 g/cm^3, respectively [147, 148].

Wollastonite is a naturally occurring calcium metasilicate, composed of calcium oxide and silicon oxide ($CaSiO_3$). Wollastonite is a white mineral that occurs in a needle-like particle shape with an aspect ratio from 3 to 20. In terms of physical properties, it has a high melting point (>1550 °C), high brightness, high pH (9.9), an acicular crystal microstructure, density of 2.9 g/cm^3, and it exhibits low moisture absorption, low water solubility, and relatively high hardness (4.5 on Mohs' scale). The crystal structure (i.e. acicular crystal) and physical properties of wollastonite are stable up to ca. 1120 °C. This suggests wollastonite as a substitute for asbestos in thermal insulation applications [144-146]. In the K-containing GCs, *alpha-potassium magnesium silicate* ($K_2MgSi_3O_8$) was formed, instead of wollastonite, found in the K-free GCs. Compared to wollastonite, it is not a common crystalline phase in GCs. Actually, it is recommended as a slow-release fertilizer supplying nutritional components of K, Mg, and Si for crops [124].

Fluorapatite, also formed in the produced GCs (but not shown in the above phase diagrams), is a phosphate mineral with the formula of $Ca_5(PO_4)_3F$. Fluorapatite is a hard crystalline solid. Although samples can have various colors (green, brown, blue, yellow, violet, or colorless), the pure mineral is colorless, as expected for a material lacking transition metals. Along with hydroxyapatite, it can be a component of tooth enamel. In the industrial use, both minerals are mined in the form of phosphates. Fluorapatite has a critical pH of 4.5 (thus it makes tooth structure more resistant to caries attack), density of 3.10 - 3.25 g/cm^3, and a Mohs hardness of 5 [149, 150].

Appendix 2

Original results from mechanical properties measurements

(a) Flexural Strength (3-point bending)

A typical plot of force (F, in N) *versus* head displacement (in mm) of the prismatic samples (with dimensions of 35 x 3 x 4 mm^3, according to ISO 6872), recorded from 3-point bending strength experiments (with a head speed of 1 mm/min), is shown in Fig. 66.

The inset shows the linear region of the curve. The first part of the curve (which is not linear) is owing to the fixing of the bar on the jig, until the full pressure aligns the sample and the jig. Then, the curve is absolutely linear (with $R^2 = 0.9999$).

This curve was recorded from the sample 1d, heat-treated at 850 °C for 1 h. However, similar curves were recorded from all the investigated samples.

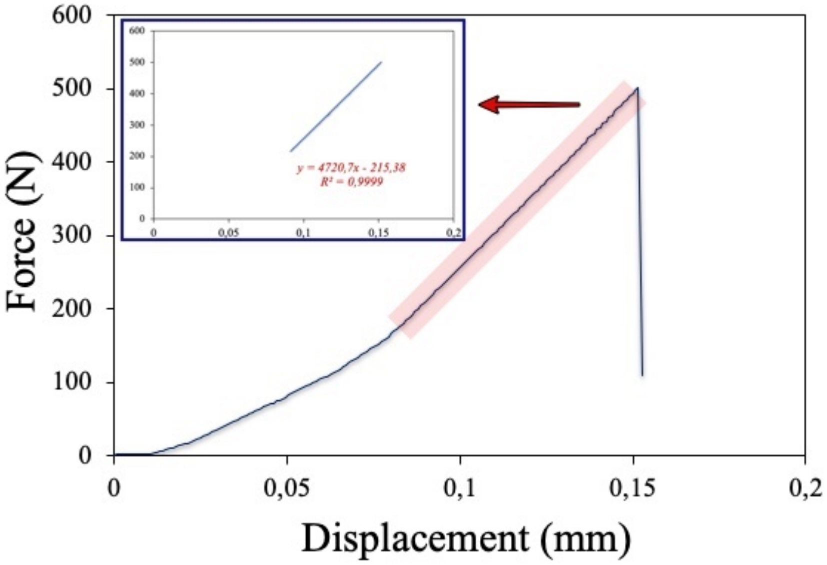

Figure 66. A typical (as-recorded) plot of F (N) *vs* displacement (mm) of the investigated samples (dimensions: 35x3x4 mm^3, according to ISO 6872) from 3-point bending strength experiments (head speed = 1 mm/min) (this curve is from the sample 1d heat-treated at 850 °C for 1 h). The inset shows the linear region of the curve.

(b) Vickers hardness indentation

The Vickers measurements are outlined in Fig. 67. More specifically, it is seen (a) the Vickers pyramid diamond indenter during the indentation process and the profile and the top-view of the indentation, (b) the Palmqvist and median crack geometries propagated from the corners of the Vickers indentation, and (c) a typical (as-recorded) Vickers indentation and the measurement of the Palmqvist crack length of 2a and l (where i.e. 0.25 < l/a < 2.5) observed on the polished surface of the sample 1d, heat-treated at 850 °C for 1 h, by applying a load of 500 g (or 4.9 N) for 30 s. The measurements from the other investigated samples were obtained similarly.

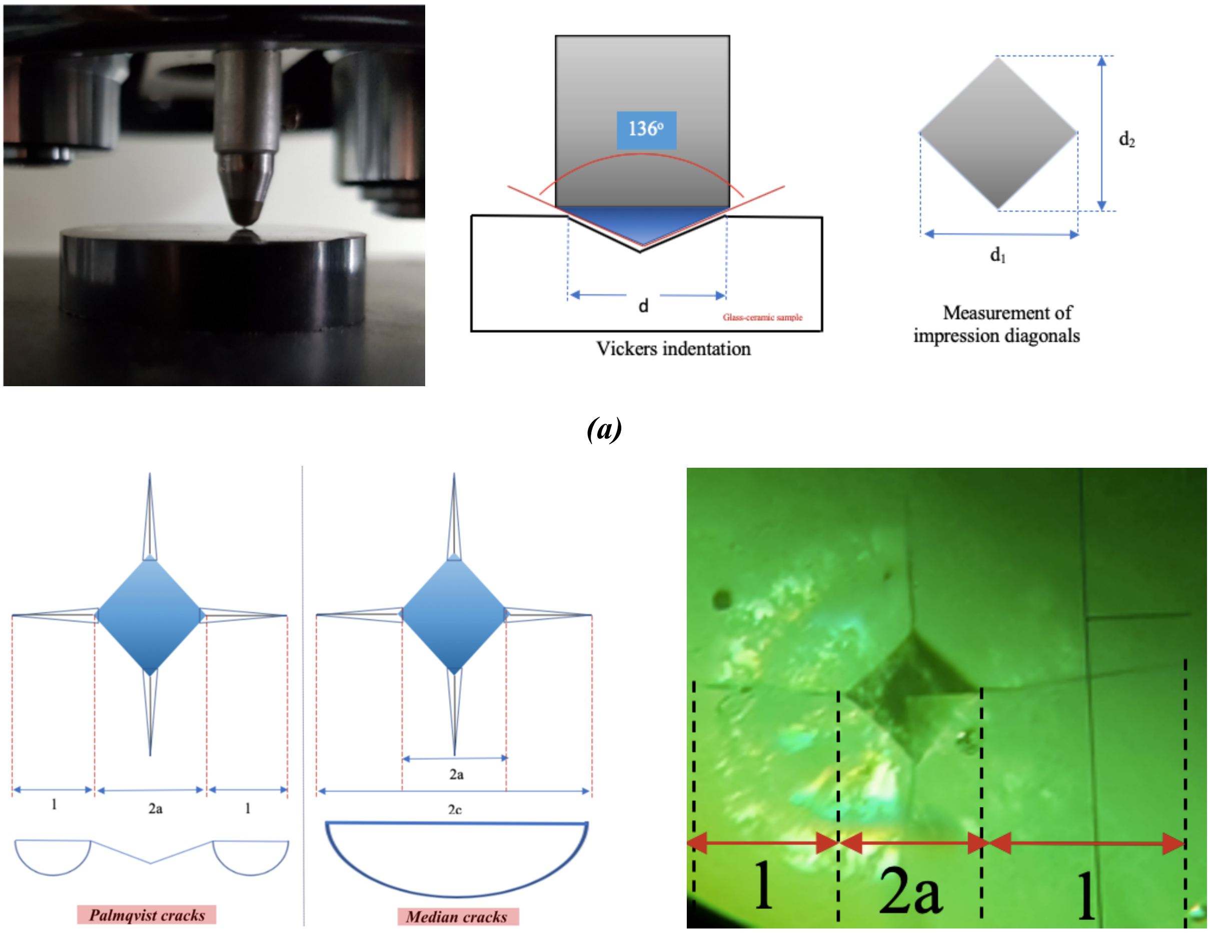
136°
d
Glass-ceramic sample
Vickers indentation
d_2
d_1
Measurement of impression diagonals
l
2a
l
Palmqvist cracks
2a
2c
Median cracks
l
2a
l

(a)

(b) *(c)*

Figure 67. (a) Vickers pyramid diamond indenter indentation, (b) Palmqvist and median crack geometries, propagated from the corners of Vickers indentation, and (c) a typical (as-recorded) result of Vickers measurements on the investigated samples by applying a load of 500 g (or 4.9 N) for 30 s. (This indentation is from the sample 1d heat-treated at 850 °C for 1 h). The Palmqvist crack length of 2a and l (i.e. 0.25 < l/a < 2.5), are marked.

Appendix 3

Concise illustration of the influence of substitutions in an alternative way plotted in diagrams (based on the values reported in Tables in the main text).

(a) Influence of substitutions on T_g, T_c, T_p temperatures and sintering window

In order to reveal immediately the influence of the substitutions attempted in the present study on the temperatures of T_g, T_c, and T_p, determined by the thermographs, along with the sintering window, defined as the difference $T_c - T_g$, these values are plotted in Fig. 68.

More specifically, the complete substitution of K_2O for Na_2O favors the increase of the temperatures of T_g, T_c, and T_p, while, there is a small influence (or a small increase) upon partial substitution of MgO for CaO (Fig. 68a). The addition of 1 mol% Al_2O_3 (Fig. 68b) resulted in an increase of the above temperatures (the highest values were recorded in the potassium-containing compositions), compared to the Al_2O_3-free glasses. The T_g, T_c, and T_p temperatures in the glasses which contained 7-8 mol% Al_2O_3 (Fig. 68c) are higher than those of the Al_2O_3-free glasses. In the same plot, a remarkable widening of the sintering window (T_c - T_g) is observed when a large amount (7-8 mol%) of Al_2O_3 was added, which is very noticeable in the case of glasses 1d (and the corresponding 1d/A), and 1d-m (and the corresponding 1d-m/A).

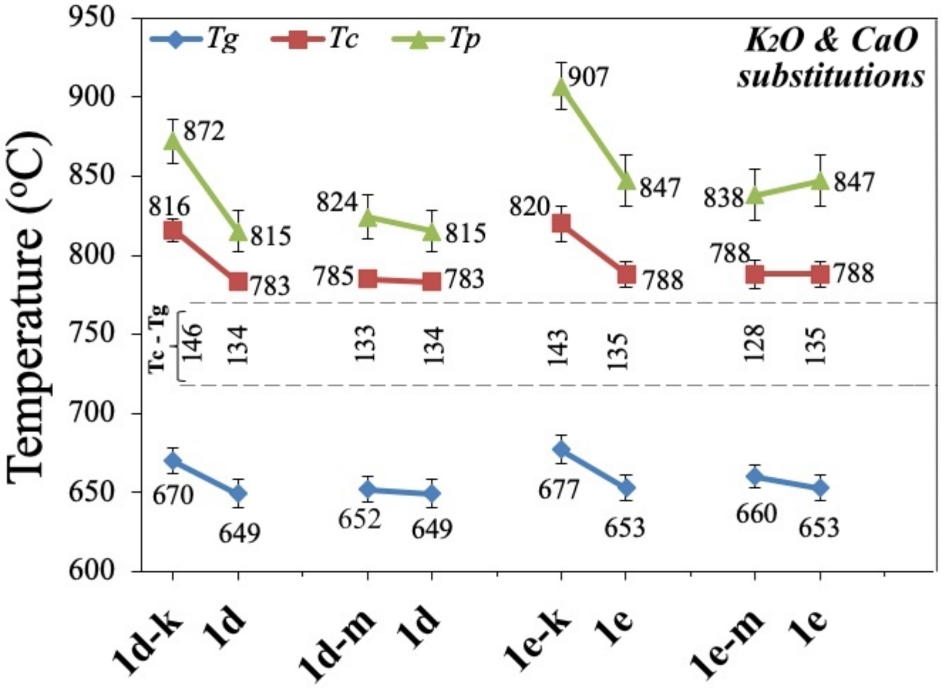

(a)

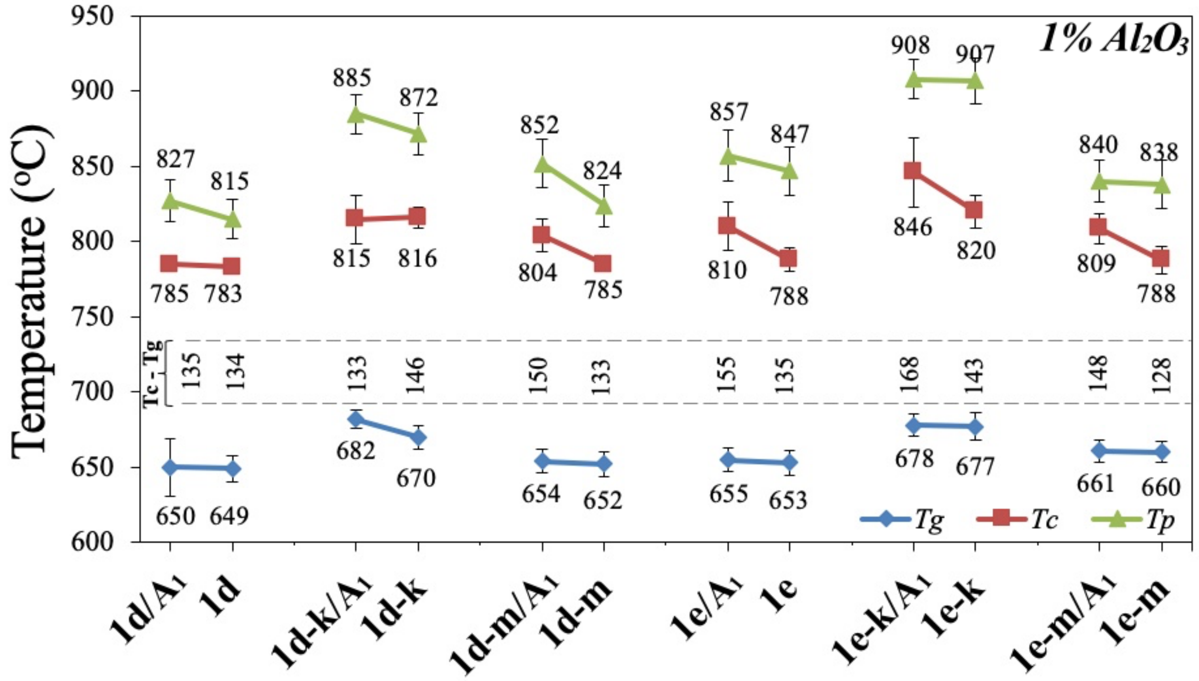

(b)

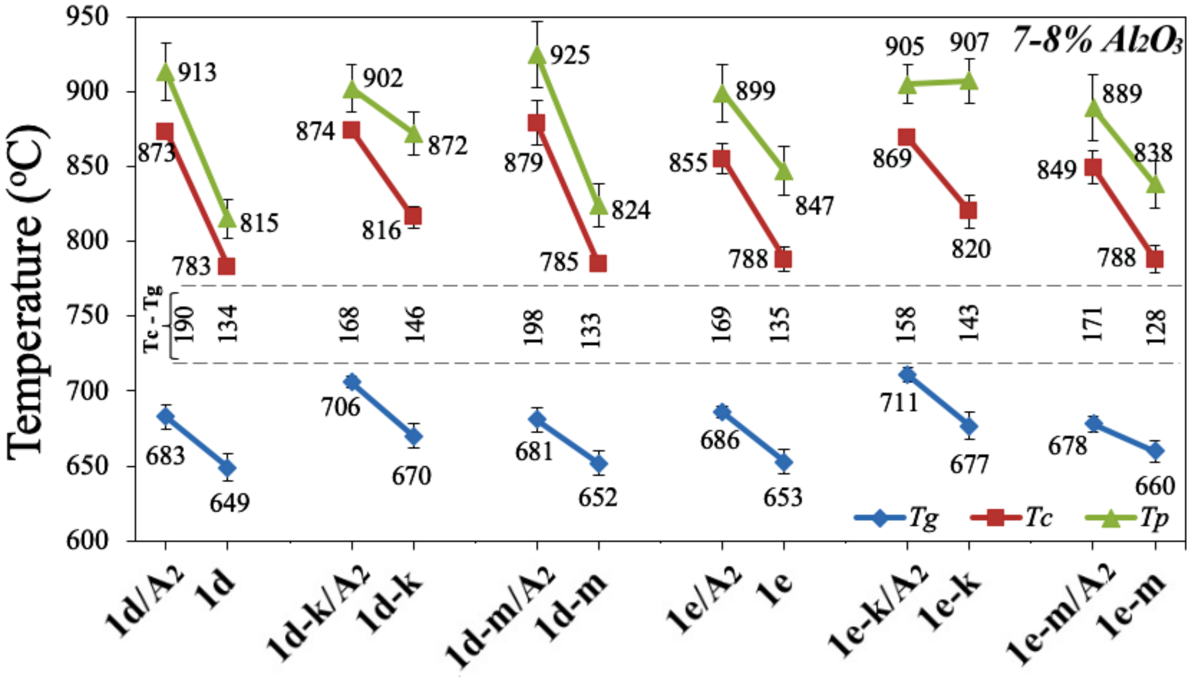

(c)

Figure 68. Comparison of the mean values (and standard deviation, n = 3) of T_g, T_c, T_p temperatures, along with the sintering window ($T_c – T_g$) of the all the investigated glasses. Influence of (a) K_2O and MgO substutions for Na_2O and CaO, respectively, in the parent glasses 1d and 1e, (b) 1 mol% Al_2O_3 addition, and (c) 7-8 mol% Al_2O_3 addition in the Al_2O_3-free glasses on the above temperatures.

(b) Influence of substitutions on mechanical properties of the produced bioactive glass-ceramics and comparison to the properties of natural tissues as well as common dental implant materials

The good matching of the mechanical properties of the produced bioactive glass-ceramics to the properties of the natural tissues is shown concisely in the plots of Fig. 69. The same plots also reveal the superior properties of the produced GCs, compared to the dental materials commonly used in dental practice, i.e. Ti-alloys and zirconia, showing the big gap between their properties and the properties of the natural tissues. The produced GC materials effectively closed this gap, since the complete substitution of K_2O for Na_2O, the partial substitution of MgO for CaO, and the addition of 1 mol% Al_2O_3 led to GCs whose mechanical properties are very close to the corresponding properties of natural tissues. More specifically, the mechanical properties of the produced GCs, with values of 22 - 34 GPa regarding the modulus of elasticity, 5.2 - 6.7 GPa concerning the Vickers microhardness, 1.4 - 2.6 MPa·m$^{0.5}$ regarding the fracture toughness (K_{IC}), and 107 - 177 MPa as regard the flexural strength, are a good match for those of the human jaw bone and dentine. Thus, these GCs can be qualified as potential candidates for dental implant applications.

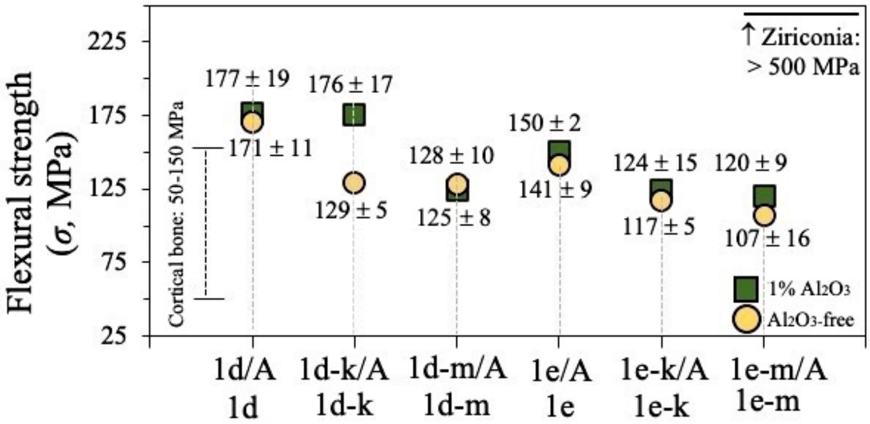

(a)

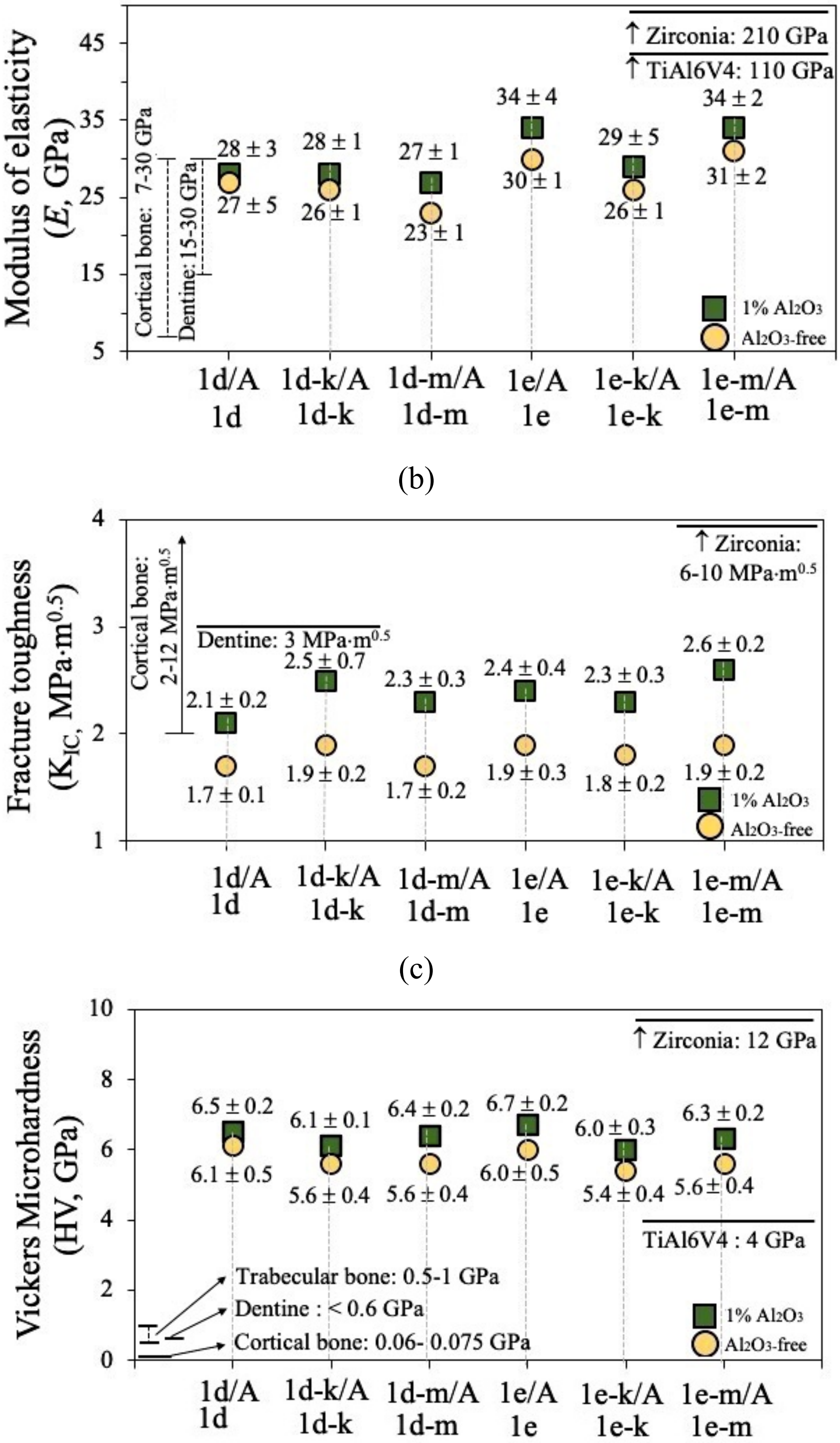

(b)

(c)

(d)

Figure 69. Mean values (and standard deviation, for n = 10) of the mechanical properties of (a) flexural strength (σ), (b) modulus of elasticity (E), (c) Vickers microhardness (HV), and (d) fracture toughness (K_{IC}) of the produced bioactive GCs. The influence of 1 mol% Al_2O_3 addition on the mechanical properties compared to the properties of the Al_2O_3-free GCs is shown, and these properties are compared to the mechanical properties of natural tissues as well as the properties of the common dental implant biomaterials of Ti-alloys and zirconia.

REFERENCES

1. Fernandes HR, Gaddam A, Rebelo A, Brazete D, Stan GE, Ferreira JMF. Bioactive glasses and glass-ceramics for healthcare applications in bone regeneration and tissue engineering. Materials (Basel). 2018;11(12):E2530.
2. Shelby J. Introduction to glass science and technology. Cambridge: The Royal Society of Chemistry; 2005.
3. Jones JR, Clare AG. Bio-glasses: an introduction. New York: John Wiley & Sons; 2012.
4. Höland W, Beall G. Glass-ceramic technology. Ohio: The American Ceramic Society; 2002.
5. Zheng Q, Zhang Y, Montazerian M, Gulbiten O, Mauro JC, Zanotto ED, Yue Y. Understanding glass through differential scanning calorimetry. Chem Rev. 2019;119: 7848−7939.
6. Zachariasen WH. The atomic arrangement in glass. J Am Chem Soc. 1932;54:3841–3851.
7. Cannillo V, Sola A. Potassium-based composition for a bioactive glass. Ceram Int. 2009;35:3389-3393.
8. Marikani A, Maheswaran A, Premanathan M, Amalraj L. Synthesis and characterization of calcium phosphate based bioactive quaternary P_2O_5-CaO-Na_2O-K_2O glasses. J Non-Cryst Solids. 2008;354:3929–3934.
9. Salman SM, Salama SN, Abo-Mosallam HA. The role of strontium and potassium on crystallization and bioactivity of Na_2O-CaO-P_2O_5-SiO_2 glasses. Ceram Int. 2012;38:55-63.
10. Greene K, Pomeroy MJ, Hampshire S, Hill R. Effect of composition on the properties of glasses in the K_2O-BaO-MgO-SiO_2-Al_2O_3-B_2O_3-MgF_2 system. J Non-Cryst Solids. 2003;325(1-3):193-205.
11. Eilaghi M, Montazerian M, Yekta BE. Effect of partial substitution of K_2O for Na_2O on sintering, crystallization and mechanical properties of SiO_2-CaO-K_2O-Na_2O-CaF_2 glass-ceramics. Journal Transactions of the Indian Ceramic Society. 2016;75(1):1-6.
12. Sun T, Xiao H, Cheng Y, Liu H. Effects of MO (M=Ba, Mg, Ca) on the crystallization of B_2O_3-Al_2O_3-SiO_2 glass-ceramics. Ceram Int. 2009;35:1051-1055.
13. Borhan AI, Gromada M, Nedelcu GG, Leontie L. Influence of (CoO, CaO, B_2O_3) additives on thermal and dielectric properties of BaO-Al_2O_3-SiO_2 glass–ceramic sealant for OTM applications. Ceram Int. 2016;42(8):10459-10468.

14. Watts SJ, Hill RG, O'Donnell MD, Law RV. Influence of magnesia on the structure and properties of bioactive glasses. J Non-Cryst Solids. 2010;356:517–524.

15. Karakassides MA, Saranti A, Koutselas I. Preparation and structural study of binary phosphate glasses with high calcium and/or magnesium content. J Non-Cryst Solids. 2004;347:69–79.

16. Rabiee SM, Nazparvara N, Aziziana M, Vashaeeb D, Tayebic L. Effect of ion substitution on properties of bioactive glasses: a review. Ceram Int. 2015;41:7241-7251.

17. Brauer DS, Karpukhina N, O'Donnell MD, Law RV, Hill RG. Fluoride containing bioactive glasses: effect of glass design and structure on degradation, pH and apatite formation in simulated body fluid. Acta Biomater. 2010;6:3275-3282.

18. Montazerian M, Zanotto ED. History and trends of bioactive glass-ceramics. J Biomed Mater Res Part A. 2016;104:1231-1249.

19. Montazerian M, Zanotto ED. Bioactive and inert dental glass-ceramics. Biomed Mater Res A. 2017;105(2):619-639.

20. Tulyaganov DU, Tomalino MU. Porcelain - from Tableware to Dental Restoration. Torino: CLUT; 2017.

21. Callister DW, Rethwisch DG. Materials Science and Engineering: an introduction. New Jersye: Wiley; 2018.

22. Montazerian M, Singh SP, Zanotto ED. An analysis of glass-ceramic research and commercialization. Am Ceram Soc Bull. 2015;94:30–35.

23. Strnad Z. Glass-Ceramic Materials. Amsterdam: Elsevier Science Publishers; 1986.

24. Mastai Y. Advances in Crystallization Processes, in: Çelikbilek M, Ali Erçin Ersundu A.E, Aydın S (Eds.): Crystallization Kinetics of Amorphous Materials. Rijeka: InTechOpen; 2012.

25. Araújo EB, Idalgo E. Non-isothermal studies on crystallization kinetics of tellurite $20Li_2O$-$80TeO_2$ glass. Journal of Thermal Analysis and Calorimetry. 2009;95:37- 42.

26. Araujo EB, Idalgo E, Moraes APA, Souza Filho AG, Mendes Filho J. Crystallization kinetics and thermal properties of $20Li_2O$–$80TeO_2$ glass. Materials Research Bulletin. 2009;44:1596-1600.

27. Erol M, Küçükbayrak S, Ersoy-Meriçboyu A. The application of differential thermal analysis to the study of isothermal and non-isothermal crystallization kinetics of coal fly ash based glasses. J Non-Cryst Solids. 2009;355(9):569–576.

28. Karamanov A, Avramov I, Arrizza L, Pascova R, Gutzow I. Variation of Avrami parameter during non-isothermal surface crystallization of glass powders with different sizes. J Non-Cryst Solids. 2012;358:1486–1490.

29. Koga N. Crystal nucleation and growth in lithium diborate glass by thermal analysis. J Am Ceram Soc. 2000;83(7):1753–1760.

30. Kissinger H. Variation of peak temperature with heating rate in differential thermal analysis. Journal of Research of the National Bureau of Standards. 1956;57(4):217-321.

31. Augis J, Bennett J. Calculation of the Avrami parameters for heterogeneous solid state reactions using a modification of the Kissinger method. Journal of Thermal Analysis and Calorimetry. 1978;13(2):283-292.

32. Antoniac I. Bioceramics and Biocomposites: from research to clinical practice, in: Agathopoulos S, Tulyaganov DU. Bioglasses and Glass-ceramics in the Na_2O–CaO–MgO–SiO_2–P_2O_5–CaF_2 system. New York: Wiley; 2019.

33. Tulyaganov DU, Agathopoulos S, Ventura JM, Karakassides MA, Fabrichnaya O, Ferreira JMF. Synthesis of glass-ceramics in the CaO-MgO-SiO_2 system with B_2O_3, P_2O_5, Na_2O and CaF_2 additives. J Eur Ceram Soc. 2006;26:1463-1471.

34. Agathopoulos S, Tulyaganov DU, Ventura JMG, Kannan S, Saranti A, Karakassides MA, Ferreira JMF. Structural analysis and devitrification of glasses based on the CaO- MgO-SiO_2 system with B_2O_3, Na_2O, CaF_2 and P_2O_5 additives. J Non-Cryst Solids. 2006;352:322-328.

35. Kansal I, Tulyaganov DU, Goel A, Pascual MJ, Ferreira JMF. Structural analysis and thermal behavior of diopside-fluorapatite-wollastonite-based glasses and glass-ceramics. Acta Biomater. 2010;6:4380-4388.

36. Baino F, Marshall M, Kirk N, Vitale-Brovarone. Design, selection and characterization of novel glasses and glass-ceramics for use in prosthetic applications. Ceram Int. 2006;42:1482-1491.

37. Hench LL. The story of Bioglass. J Mater Sci: Mater Med. 2006;17:967-978.

38. Gerhardt LC, Boccaccini AR. Bioactive glass and glass-ceramic scaffolds for bone tissue engineering. Materials. 2010;3:3867-3910.

39. van-Noort R, El-Meliegy E. Glasses and glass ceramics for medical applications. New Yourk: Springer; 2012.

40. Hench LL. Bioceramics: from concept to clinic. J Am Ceram Soc. 1991;74:1487-1510.

41. Kokubo T. Bioactive glass-ceramics: properties and applications. Biomaterials. 1991;12:155-163.

42. Kokubo T, Ito S, Shigematsu M, Sakka S, Yamamuro T. Mechanical properties of a new type of apatite-containing glass-ceramic for prosthetic application. Journal of Material Science. 1985;20:2001-2004.

43. Höland W, Vogel W, Naumann K, Gummel J. Interface reactions between machinable bioactive glass-ceramics and bone. J Biomed Mater Res. 1985;19:303–312.

44. Li J, Jansen JA, Walboomers XF, van den Beucken JJ. Mechanical aspects of dental implants and osseointegration: a narrative review. J Mech Behav Biomed Mater. 2020;103:103574.

45. Saadaldin SA, Dixonb SJ, Costad DO, Rizkallaa AS. Synthesis of bioactive and machinable miserite glass-ceramics for dental implant applications. Dent Mater. 2013;29:645–655.

46. Mish CE. Dental implant prosthetics. St. Louis: CV Mosby; 2005.

47. Augat P, Schorlemmer S. The role of cortical bone and its microstructure in bone strength. Age Ageing. 2006;35:27-31.

48. Lakatos E, Magyar L, Bojtár I. Material properties of the mandibular trabecular bone. J Med Eng. 2014;2014:470539.

49. Pal S. Design of artificial human joints & organs. New Yourk: Springer; 2014.

50. Fanghänel J, Gedrange T, Proff P. Bone quality, quantity and metabolism in terms of dental implantation. Biomed Tech (Berl). 2008;53(5):215-219.

51. Albrektsson T, Johansson C. Osteoinduction, osteoconduction and osseointegration. Eur/ Spine J. 2001;10:S96- S101.

52. Tripuwabhrut P, Mustafa M, Gjerde CG, Brudvik P, Mustafa K. Effect of compressive force on human osteoblast-like cells and bone remodeling: an in vitro study. Arch Oral Biol. 2013;58(7):826-836.

53. Vaananen HK, Zhao H, Mulari M, Halleen JM. The cell biology of osteoclast function. J Cell Sci. 2000;113(3):377-381.

54. Dorozhkin S, Epple M. Biological and medical significance of calcium phosphates. Angew Chem Int Ed Engl. 2002;41:3130-3146.

55. Zhang YR, Du W, Zhou XD, Yu HY. Review of research on the mechanical properties of the human tooth. Int J Oral Sci. 2014;6(2):61-69.

56. Lucas PW, van Casteren A. The wear and tear of teeth. Med Princ Pract. 2015;24(1):3-13.

57. Park S, Wang DH, Zhang D, Romberg E, Arola D. Mechanical properties of human enamel as a function of age and location in the tooth. J Mater Sci Mater Med. 2008;19(6):2317-2324.

58. Kinney JH, Marshall SJ, Marshall GW. The mechanical properties of human dentin: a critical review and re-evaluation of dental literature. Crit Rev Oral Biol Med. 2003;14(1)13-29.

59. Rahiotis C, Vougiouklakis G. Dental caries, in: Rahiotis C, Vougiouklakis G. Dental hard tissue. Athens: Hellenic Academic Libraries Link; 2015.

60. Natali AN. Dental biomechanics. London: CRC Press; 2003.

61. Rezwan K, Chen QZ, Blaker JJ, Boccaccini AR. Biodegradable and bioactive porous polymer/inorganic composite scaffolds for bone tissue engineering. Biomaterials. 2006;27:3413-3431.

62. Kaura G, Kumarb V, Bainoc F, Maurod JC, Pickrelle G, Evansf I, Bretcanuf O. Mechanical properties of bioactive glasses, ceramics, glass-ceramics and composites: state-of-the-art review and future challenges. Materials Science & Engineering C. 2019;104:109895.

63. Koleganova V, Bernier S, Dixon J, Rizkalla A. Bioactive glass/polymer composite materials with mechanical properties matching those of cortical bone. J Biomed Mater Res A. 2006;77:572-579.

64. Saadaldin SA, Rizkallaa AS. Synthesis and characterization of wollastonite glass–ceramics for dental implant applications. Dent Mater. 2014;30:364–371.

65. Hall SJ. Basic biomechanics. New York: McGraw-Hill Education; 2015.

66. Sakaguchi R, Ferracane R: Graig's restorative dental materials. Philadelphia: Elsevier; 2006.

67. Mahoneya EK, Rohanizadeha R, Ismailc FSM, Kilpatrickd NM, Swaine MV. Mechanical properties and microstructure of hypomineralised enamel of permanent teeth. Biomaterials. 2004;25:25:5091–5100.

68. Fischer H, Marx R. Fracture toughness of dental ceramics: comparison of bending and indentation method. Dent Mater. 2002;18:12-19.

69. Anusavice KJ, Phillips RW, Shen C, Rawls HR. Phillips' science of dental materials. St. Louis; 2013.

70. Yazdani J, Ahmadian E, Sharifi S, Shahi S, Maleki Dizaj S. A short view on nanohydroxyapatite as coating of dental implants. Biomed Pharmacother. 2018;105:553-557.

71. Grandin HM, Berner S, Dard M. A review of titanium zirconium (TiZr) alloys for use in endosseous dental implants. Materials. 2012;5:1348–1360.

72. Simonis P, Dufour T, Tenenbaum H. Long-term implant survival and success: a 10–16-year follow-up of non-submerged dental implants. Clinical Oral Implants Research. 2010;21(7):772–777.

73. Ozkut Z, Kazazoglu E. Zirconia dental implants: a literature review. Journal of Oral Implantology. 2011;37(3):367-376.

74. Guess PC, Att W, Strub JR. Zirconia in fixed implant prosthodontics. Clin Implant Dent Relat Res. 2012;14(5):633-645.

75. Kohal RJ, Klaus G. A zirconia implant-crown system: a case report. Int J Periodontics Restorative Dent. 2004;24:147–153.

76. Andreiotelli M, Wenz HJ, Kohal RJ. Are ceramic implants a viable alternative to titanium implants? a systematic literature review. Clinical Oral Implants Research. 2009;20(S4):32-47.

77. Al-Amleh B, Lyons K, Swain M. Clinical trials in zirconia: a systematic review. J Oral Rehabil. 2010;37(8):641-652.

78. Palmquist A, Omar OM, Esposito M, Lausmaa J, Thomsen P. Titanium oral implants: surface characteristics, interface biology and clinical outcome. J R Soc Interface. 2010;7:S515–527.

79. Dimitriadis D, Moschovas D, Tulyaganov DU, Agathopoulos S. Development of novel bioactive glass-ceramics in the Na_2O/K_2O-CaO-MgO-SiO_2-P_2O_5-CaF_2 system. J Non-Crys Solids. 2020;533:119936.

80. Saadaldin S, Dixon J, Rizkalla A. Bioactivity and biocompatibility of a novel wollastonite glass-ceramic biomaterial. J Biomater Tissue Eng. 2014;4:939-946.

81. Baino F, Verné E. Production and characterization of glass-ceramic materials for potential use in dental applications: thermal and mechanical properties, microstructure, and in vitro bioactivity. Appl Sci. 2017;7:1-16.

82. Chen X, Liao X, Huang Z, You P, Chen C, Kang Y, Yin G. Synthesis and characterization of novel multiphase bioactive glass-ceramics in the CaO-MgO-SiO_2 system. J Biomed Mater Res B Appl Biomater. 2010;93(1):194-202.

83. McLean JW. Evolution of dental ceramics in the twentieth century. J Prosthet Dent. 2001;85:61-66.

84. Mahoneya E, Holtb A, Swainb M, Kilpatrickc N. The hardness and modulus of elasticity of primary molar teeth: an ultra-micro-indentation study. Journal of Dentistry. 2000;28:589–594.

85. ISO 6872, Dentistry – Ceramic Materials, third ed., International Organization for Standardization, Geneva, 2008.

86. Rizkalla AS, Jones DW. Mechanical properties of commercial high strength ceramic core materials. Dent Mater. 2004;20(2):207-212.

87. Höland W, Schweiger M, Frank M, Rheinberger V. A Comparison of the microstructure and properties of the IPS Empress® 2 and the IPS Empress® glass-ceramics. J Biomed Mater Res. 2000;53(4):297-303.

88. Albakry M, Guazzato M, Swain MV. Biaxial flexural strength, elastic moduli, and x-ray diffraction characterization of three pressable all-ceramic materials. J Prosthet Dent. 2003;89:374-380.

89. Narasimha Raghavan R. Ceramics in Dentistry, in: Lakshmanan A. Sintering of Ceramics. Rijeka: InTechOpen; 2012.

90. Shen JZ. Advanced Ceramics for Dentistry, in Saint-Jean SJ. Dental glasses and glass-ceramics. Netherland: Elsevier; 2014.

91. Zhang Y, Kelly JR. Dental ceramics for restoration and metal veneering. Dent Clin North Am. 2017;61(4):797-819.

92. Zhang P, Li X, Yang J, Xu S. Effect of heat treatment on the microstructure and properties of lithium disilicate glass-ceramics. J Non-Crys Solids. 2014;402:102-105.

93. Özdemir H, Özdoğan A. The effect of heat treatments applied to superstructure oorcelain on the mechanical properties and microstructure of lithium disilicate glass ceramics. Dent Mater J. 2018;37(1):24-32.

94. Hench LL, Splinter RJ, Allen WC, Greenlee TK. Bonding mechanisms at the interface of ceramic prosthetic material. J Biomed Mater Res. 1971;2:117-141.

95. Kokubo T, Kushitani H, Sakka S, Kitsugi T, Yamamuro T. Solutions able to reproduce bioactive glass-ceramic A-W. J Biomed Mater Res. 1990;24(6):721-734.

96. Thompson ID, Hench LL. Mechanical properties of bioactive glasses, glass-ceramics and composites. Proc Inst Mech Eng H. 1998;212(2):127-136.

97. Tulyaganov DU, Makhkamov ME, Urazbaev A, Goel A, Ferreira JMF. Synthesis, processing and characterization of a bioactive glass composition for bone regeneration. Ceram Int. 2013;39:2519:–2526.

98. Daguano JKMB, Milesi MTB, Rodas ACD, Weber AF, Sarkis JES, Hortellani MA, Zanotto ED. In vitro biocompatibility of new bioactive lithia-silica glass-ceramics. Mater Sci Eng C Mater Biol Appl. 2019;94(1):117-125.

99. Islam MT, Felfel RM, Abou Neel EA, Grant DM, Ahmed I, Hossain KMZ. Bioactive calcium phosphate-based glasses and ceramics and their biomedical applications: a review. J Tissue Eng. 2017;21(8):1-16.

100. Jmal N, Bouaziz J. Synthesis, characterization and bioactivity of a calcium-phosphate glass-ceramics obtained by the sol-gel processing method. Mater Sci Eng C Mater Biol Appl. 2017;71(1):279-288.

101. Bibby JK, Bubb NL, Wood DJ, Mummery PM. Fluorapatite-mullite glass sputter coated Ti6Al4V for biomedical applications. J Mater Sci Mater Med. 2005;16(5):379-385.

102. Agathopoulos S, Tulyaganov DU, Valerio P, Ferreira JMF. A new model formulation of the SiO_2–Al_2O_3–B_2O_3–MgO–CaO–Na_2O–F glass-ceramics. Biomaterials. 2005;26(15): 2255-2264.

103. Chen QZ, Thompson ID, Boccaccini AR. 45S5 Bioglass-derived glass-ceramic scaffolds for bone tissue engineering. Biomaterials. 2006;27:2414-2425.

104. Tulyaganov DU, Agathopoulos S, Valerio P, Balamurugan A, Saranti A, Karakassides MA, Ferreira JMF. Synthesis, bioactivity and preliminary biocompability studies of glasses in the system CaO-MgO-SiO_2-Na_2O-P_2O_5-CaF_2. J Mater Sci Mater Med. 2011;22(2):217-227.

105. Rabiee SM, Ravarian R, Mehmanchi M, Khoshakhlagh P, Azizian M. Effect of alumina on microstructure and compressive strength of a porous silicated hydroxyapatite. J Appl Biomater Funct Mater. 2013;12(2):102–106.

106. Hill RG, Stamboulis A, Law RV, Clifford A, Towler MR, Crowley C. The influence of strontium substitution in fluorapatite glasses and glass–ceramics. J Non-Cryst Solids. 2004;336(3):223–229.

107. Liu X, Ding C, Chu PK. Mechanism of apatite formation on wollastonite coasting in simulated body fluids. Biomaterials. 2004;25(10):1755-1761.

108. Kansal I, Goel A, Tulyaganov DU, Pascual MJ, Lee HY, Kim HW, Ferreira JMF. Diopside ($CaOMgO_2SiO_2$) – fluorapatite ($9CaO_3P_2O_5CaF_2$) glass-ceramics: potential materials for bone tissue engineering. J Mater Chem. 2011;21(40):16247-16256.

109. Toya T, Kameshima Y, Yasumori A, Okada K. Preparation and properties of glass–ceramics from wastes (Kira) of silica sand and kaolin clay refining. J Eur Ceram Soc. 2004;24(8):2367–2372.

110. Nonami T, Tsutsumi S. Study of diopside ceramics for biomaterials. J Mater Sci: Mater Med. 1999;10(8):475–479.

111. Agathopoulos S, Tulyaganov DU, Ventura JM, Kannan S, Karakassides MA, Ferreira JMF. Formation of hydroxyapatite onto glasses of the CaO-MgO-SiO_2 system with B_2O_3, Na_2O, CaF_2, P_2O_5 additives. Biomaterials. 2006;27:1832-1840.

112. Matusita K, Sakka S. Kinetic study on non-isothermal crystallization of glass by thermal analysis. Bulletin of the Institute for Chemical Research. 1981;59(3):159-171.

113. Mullin JW. Crystallization. London: Elsevire; 2001.

114. Sakar-Deliormanlil A, Guden M. Microhardness and fracture toughness of dental materials by indentation method. J Biomed Mater Res B Appl Biomater. 2006;76(2):257-264.

115. Boccaccini AR. Machinability and brittleness of glass-ceramics. Journal of Materials Processing Technology. 1997;65:302-304.

116. Kamitakahara M, Ohtsuki C. Apatite formation on CaO, SiO_2-based glass-ceramics in a simulated body fluid. Phosphorus Research Bulletin. 2006;20:101-110.

117. Schmitz SI, Widholz B, Essers C, Becker M, Tulyaganov DU, Moghaddam A, de Juan G I, Westhauser F. Superior biocompatibility and comparable osteoinductive properties: Sodium-reduced fluoride-containing bioactive glass belonging to the CaO–MgO–SiO_2 system as a promising alternative to 45S5 bioactive glass. Bioactive Materials. 2020;5:55–65.

118. Denry I, Holloway JA. Ceramics for dental applications: a review. Materials. 2010;3:351-368.

119. Bretcanu O, Chatzistavrou X, Paraskevopoulos K, Conradt R, Thompson I, Boccaccini AR. Sintering and crystallization of 45S5 Bioglass powder. J Eur Ceram Soc. 2009;29(16):3299–3306.

120. Karamanov A, Arriza L, Matekovits I, Pelino M. Properties of sintered glass–ceramics in the diopisde–albite system. Ceram Int. 2004;30:2119–2135.

121. Karamanov A, Pelino, M. Evaluation of degree of crystallization in glass–ceramics by density measurements. J Eur Ceram Soc. 1999;19:649–654.

122. Dorozkin SV. Calcium orthophospathe based bioceramics and biocomposites. New York: Willey; 2012.

123. Cortes DA, Medina A, Escobedo S, Lopez MA. Biomimetic apatite formation on a CoCrMo alloy by using wollastonite, bioactive glass or hydroxyapatite. J Mater Sci. 2005;40:3509-3515.

124. Xi M, Hongwen M, Yang J. Sintering preparation and release properties of $K_2MgS_3O_8$ slow-release fertilizer using biotite acid-leaching residues as silicon source. Industrial & Engineering Chemistry Research. 2016;55:10926-10931.

125. Prabhu M, Kavitha K, Manivasakan P, Rajendran V, Kulandaivelu P. Synthesis, characterization and biological response of magnesium-substituted nanobioactive glass particles for biomedical applications. Ceram Int. 2013;39:1683-1694.

126. Agathopoulos S, Nikolopoulos P, Salomoni A, Tucci A, Stamenkovic I. Preparation and properties of binary oxide bioceramics. J Mater Sci-Mater. 1996;M7:629-636.

127. Seong WJ, Kim UK, Swift JQ, Heo YC, Hodges JC, Ko CC. Elastic properties and apparent density of human edentulous maxilla and mandible. Int J Oral Maxillofac Surg. 2009;38:1088-1093.

128. Bankoglu Gungor M, Aydin C, Yilmaz H, Gul EB. An overview of zirconia dental application implants: basic properties and clinical application of three cases. J Oral Implantol. 2014;40:485-494.

129. Niinomi M. Mechanical properties of biomedical titanium alloys. Mater Sci Eng A. 1998;243:231-236.

130. Aboushelib MN, Kleverlann CJ, Feilzer AJ. Microtensile bond strength of different components of core veneered all-ceramic restorations. Part II: Zirconia vennering ceramics. Dent Mater. 2006;22:857-863.

131. Lawn BR, Marshall DB. Hardness, toughness, and brittleness: an indentation analysis. Journal of American Ceramic Society. 1979;62:347-350.

132. Tsitrou EA, Northeast SE. van Noort R. Brittleness index of machinable dental materials and its relation to the marginal chipping factor. J Dent. 2007;35:897-902.

133. Fateri M, Gebhardt A, Thuemmler S, Thurn L. Experimental investigation on selective laser melting of glass. Physics Procedia. 2014;56:357-364.

134. Dimitriadis K, Spiropoulos K, Papadopoulos T. Metal-ceramic bond strength between a feldspathic porcelain and a Co-Cr alloy fabricated with direct metal laser sintering technique. J Adv Prosthodont. 2018;10:25-31.

135. Dimitriadis K, Papadopoulos T, Agathopoulos S. Effect of bonding agent on metal-ceramic bond strength between Co-Cr, fabricated with selective laser melting and dental feldspathic porcelain. J Prosthodont. 2019;28(9):1029-1036.

136. Akova T, Ucar Y, Tukay A, Balkaya MC, Brantley WA. Comparison of the bond strength of laser-sintered and cast base metal dental alloys to porcelain. Dent Mater. 2008;24:1400-1404.

137. Kokubo T, Shigematsu M, Nagashima Y, Tashiro M, Nakamura T, Yamamuro T, Higashi S. Apatite - and wollastonite-containg glass-ceramics for prosthetic application. Bull Inst Chem Res Kyoto Univ. 1982;60:260–268.

138. Torres FJ, Alarcon J. Mechanizm of crystallization of pyroxene-based glass-ceramics glazes. J Non-Cryst Solids. 2004;34:45-51.

139. Abdel-Hameed SAM, El-kheshen AA. Thermal and chemical properties of diopside-wollastonite glass-ceramics in the SiO_2-CaO-MgO system from raw materials. Ceram Int. 2003;29:265-269.

140. Karamanov A, Pelino M. Induced crystallization porosity and properties of sintered diopside and wollastonite glassceramics. J Eur Ceram Soc. 2008;28:555–562.

141. Kang J, Wang J, Cheng J, Yuan J, Hou Y, Qian S. Crystallization behavior and properties of CaO-MgO-Al_2O_3-SiO_2 glass-ceramics synthesized from granite wastes. J Non-Cryst Solids. 2017;457:111-115.

142. Xiao H, Cheng Y, Yu L, Liu H. A study on the preparation of CMAS glass–ceramics by in situ crystallization. Materials Science and Engineering: A. 2006;431:191-195.

143. Yang Z, Lin Q, Lu S, He Y, Liao G, Ke Y. Effect of CaO/SiO_2 ratio on the preparation and crystallization of glass-ceramics from copper slag. Ceram Int. 2014;5(40):7297-7305

144. Maier C, Calafut T. Polypropylene. New York: William Andrew; 1998.

145. Tolinski M. Additives for Polyolefins. New York: William Andrew; 2015.

146. Gilbert M. Brydson's Plastics Materials, in: Rothon R, DeArmitt C. Fillers (Including Fiber Reinforcements). Oxfords: Butterworth-Heinemann; 2017.

147. Reddy AA, Tulyagnov DU, Kapoor S, Goel A, Pascual MJ, Kharton VV, Ferreira JMF. Study of melilite based glasses and glass–ceramics nucleated by Bi_2O_3 for functional application. RSC Advances. 2012;29:10955–10967.

148. Reddy AA, Tulyaganov DU, Goel A, Kapoor S, Pascual MJ, Ferreira JMF. Sintering and devitrification of glass-powder compacts in the akermanite-gehlenite system. Journal of Materials Science. 2013;48(11):4128-4136.

149. Hench L. Bioactive glasses and glass-ceramics. In: Shackelford J, ed. Bioceramics. Baudrain: Trans Tech Publications; 1999.

150. Daculsi G, Passutu N, Martin S, Deudon C, Legeros RZ, Raher S. Macroporous calcium-phosphate ceramic for long-bone surgery in humans and dogs-clinical and histological study. Journal of Biomedical Materials Research. 1990;24:379-396.

CURRICULUM VITAE

DIMITRIADIS KONSTANTINOS

- *Dipl. in Dental Technology (Technological Educational Institution of Athens, Greece, 2011 now Univ. West Attica, Athens)*
- *MSc in Dentistry (Univ. Athens, Greece, 2015)*
- *PhD in Materials Science and Engineering (Univ. Ioannina, Greece, 2020)*

Born : 16 July 1988, Vladikavkaz, North Osetia, Russia

Citizenship : Greek

Current Address : Department of Materials Science and Engineering
University of Ioannina
GR- 451 10 Ioannina, Greece

Education, Research and Professional Experience:

1995-2007 : Basic studies, Vladikavkaz, Russia/Athens, Greece

2007-2011 : BSc in Dept. of Dental Technology, Technological Educational Institution of Athens, Greece

2013-2015 : MSc in "Dental Technology Materials", Dental School, National and Kapodistrian University of Athens (EKPA), Greece

2016-2020 : PhD Candidate in Materials Science and Engineering Department, Lab. of Ceramics and Composite Materials (CCL), University of Ioannina

2017-2018 : Laboratory Collaborator in Dept. of Dental Technology Technological Educational Institution of Athens (TEI-Athens), Greece

2018-2020 : Laboratory Collaborator in Dept. of Biomedical Science, Sector of Dental Technology, University of West Attica (Uni.W.A), Athens, Greece

Military service:

18/01/2016-18/10/2016: Hellenic Forces in Cyprus (EL.DY.K), Nicosia, Cyprus

Fellowships:

2018-2020 : Scholarship of the State Scholarships Foundation of Greece ("IKY") (2018-2020). Operational Programme «Human Resources Development, Education and Lifelong Learning» (ESPA 2014-2020) in the context of the project "Strengthening Human Resources Research Potential via Doctorate Research» (MIS-5000432).

Research Interests:

His research is in the area of ceramics, glasses, glass-ceramics and composites for dental applications, functional and structural applications. Also, the fixed metal-ceramic and all-ceramic prosthetic restorations, the CAD / CAM and DMLS (SLM) technologies as well as the implant prosthetic applications. Specifically:

1. Dental Bioceramics (development and synthesis of glasses, glass-ceramics and ceramics, preparation methods, thermal properties, mechanical properties, surface characterization, and biocompatibility),
2. Interfaces of ceramics with biological liquids or liquid metals at high temperatures, and ceramic-metal composites.

Assistance of Conference Organization

- 6th Hellenic Conference on Metallic Materials, Ioannina, 7-9 December 2016 (volunteer).

Member of Scientific Societies:

1. Hellenic Ceramic Society (which is associated member of the European Ceramic Society).
2. Hellenic Society of Biomechanics (which is associated member of the International Society of Biomechanics).
3. Hellenic Society of Biomaterials (which is associated member of the European Society of Biomaterials).

Teaching:

***A**. Assistance in Dental School, EKPA, Athens, Greece (2013-2015):*

1. Laboratory of "Dental Biomaterials" (semester B – 2 semesters)

***B.** Assistance in Dental Technology Department, TEI-Athens, Athens, Greece (2014-2015):*

1. Laboratory of "Removable Prosthodontics I" (semester B – 1 semesters)
2. Laboratory of "Dental ceramics II" (semester F– 1 semesters)

***C.** Assistance in Materials Science and Engineering Department, University of Ioannina, Greece (2016-2020):*

1. Laboratory of "Chemistry" (semester A – 1 semesters)
2. Laboratory of "Physical-chemistry" (semester C – 3 semesters)
3. Laboratory "Materials II: Ceramics and Composites" (semester F – 3 semesters)
4. Diploma Theses of 5 students (1 undegraduare and 4 post-graduate (Masters) students)

***D.** Dental Technology Department, TEI-Athens, Athens, Greece (2017-2018):*

1. Laboratory of "Fixed Prosthodontics I" (semester E).
2. Laboratory of "Fixed Prosthodontics II" (semester F)
3. Laboratory of "Removable Prosthodontics II" (semester B)

***E.** Biomedical Science Department, Sector of Dental Technology, Uni.W.A, Athens, Greece (2018-2020):*

1. Laboratory of "Fixed Prosthodontics I" (semester E)
2. Laboratory of "Fixed Prosthodontics II" (semester F)
3. Laboratory of "Fixed Prosthodontics III" (semester G)
4. Laboratory of "Dental ceramics II" (semester G)
5. Diploma Theses of 2 students.

Publications in International Refereed Journals:

1. Metal-ceramic bond strength between a feldspathic porcelain and a Co-Cr alloy fabricated with Direct Metal Laser Sintering technique.
   K. Dimitriadis, K. Spiropoulos, T. Papadopoulos
   J.Adv.Prosthodont. 2018;10:25-31. https://doi.org/10.1111/jopr.13058.

2. Effect of bonding agent on metal-ceramic bond strength between Co-Cr, fabricated with selective laser melting (SLM) technique and dental feldspathic porcelain.
   K. Dimitriadis, T. Papadopoulos, S. Agathopoulos
   J.Prosthodont. 2019;28:1029-1036. https://doi.org/10.4047/jap.2018.10.1.25.

3. Development of novel bioactive glass-ceramics in the Na_2O/K_2O-CaO-MgO-SiO_2-P_2O_5-CaF_2 system.
   K. Dimitriadis, D. Moschovas, D.U. Tulyaganov, S. Agathopoulos
   J.Non-Cryst.Solids 2020;533:119936. https://doi.org/10.1016/j.jnoncrysol.2020.119936.

4. Synthesis of glass-ceramics in the Na_2O/K_2O-CaO-MgO-SiO_2-P_2O_5-CaF_2 system as candidate materials for dental applications.
   K. Dimitriadis, K.C. Vasilopoulos, T.C. Vaimakis, M.A. Karakassides, D.U. Tulyaganov, S. Agathopoulos
   Int.J.Appl.Ceram.Technol. (in press). https://doi.org/10.1111/ijac.13509.

5. Development of novel alumina-containing bioactive glass-ceramics in the CaO-MgO-SiO_2 system as possible candidates for dental implant applications.
   K. Dimitriadis, D.U. Tulyaganov, S. Agathopoulos
   Journal of the European Ceramic Society (submitted - under review).

Other Referred Publications - Reports – Theses:

1. Occlusal relationship for implant supported prosthetic restorations (in Greek).
   K. Dimitriadis.
   Diploma Thesis, Department of Dental Technology, TEI-Athens, 2011
2. Comparative study of the metal-ceramic bond strength of Co-Cr alloys fabricated by Casting and Direct Metal Laser Sintering techniques (in Greek).
   K. Dimitriadis.
   MSc Thesis, Dental School, EKPA, 2015

3 Development of glass-ceramics for dental applications.

PhD Thesis, Department of Materials Science and Engineering, Univ. of Ioannina, 2020.

Refereed Publications in Conference Proceedings and Lectures:

1. The Selective Laser Sintering Technique in the production of dental bioconstructions.
   K. Dimitriadis, K. Spiropoulos, T. Papadopoulos.
   10th National Conference of the Greek Association for Biomaterials, Athens, 7-9 November 2014.

2. Application of the Selective Laser Sintering (SLS) technique in the construction of the dental bioconstructions.

K. Dimitriadis, K. Spiropoulos, T. Papadopoulos.
International Conference on BIO-Medical Instrumentation and related Engineering and Physical Sciences, Athens, 18-20 June 2015.

3. Comparative study of the metal-ceramic bond strength of Co-Cr alloys fabricated by different techniques.
   K. Dimitriadis, K. Spiropoulos, T. Papadopoulos.
   10th National Conference of the Greek Association for Biomaterials, Athens, 26-27 November 2015.

4. Glasses and Glass-ceramics in biomedicine.
   S. Agathopoulos, **K. Dimitriadis**, M.A. Karakasides, D.U. Tulyaganov.
   7th National Conference of the Greek Association for Biomechanics, Athens, 24-26 June 2016.

5. Comparative study of the metal-ceramic bond strength of Co-Cr alloys fabricated by casting and direct metal laser sintering technique.
   K. Dimitriadis, K. Spiropoulos, T. Papadopoulos.
   2nd Dental Technology Training Conference, Athens, 20-21 May 2017.

6. Glasses in the $Na_2O(K_2O)$-CaO-MgO-SiO_2-P_2O_5-CaF_2 system and their devitrification behavior.
   K. Dimitriadis, M. Karakassides, D. Tulyaganov, S. Agathopoulos.
   Euromat 2017, European Congress & Exhibition of Advanced Materials and Process, Thessaloniki, 01-02 September 2017.

7. Interface characterization of dental metal-ceramic fixed prosthetic restorations after bonding agent application.
   K. Dimitriadis, N. Sargioti, T. Papadopoulos, S. Agathopoulos.
   8th National (Greek) Conference of the Greek Association for Biomechanics, Thessaloniki, 01-02 September 2018.

8. Effect of mechanical and chemical surface treatment of Co-Cr metal substrates on metal-ceramic bond strength in fixed dental prosthetic restorations.
   K. Dimitriadis, N. Sargioti, T. Papadopoulos, S. Agathopoulos.
   11th National (Greek) Conference of the Greek Association for Biomaterials, Athens, 23-25 November 2018.

9. Design, synthesis and characterization of new glass-ceramics based on the Na_2O-CaO-MgO-SiO_2-P_2O_5-CaF_2 system for dental implant applications.
   K. Dimitriadis, D. Tulyaganov, K.C. Vasilopoulous, M. A. Karakassides. S. Agathopoulos.
   11th National (Greek) Conference of the Greek Association for Biomaterials, Athens, 23-25 November 2018.

10. From the laboratory to clinics: design of novel synthesis of bioceramics – the case of glass-ceramics in the system Na_2O-CaO-MgO-SiO_2-P_2O_5-CaF_2.
    S. Agathopoulos, **K. Dimitriadis**, D. U. Tulyaganov.

11th National (Greek) Conference of the Greek Association for Biomaterials, Athens, 23-25 November 2018.

11. The active involvement of the Dental Technologist in the research and development of new dental materials.
    K. Dimitriadis, S. Agathopoulos.
    Conference "Dental Technology in Higher Education: Evolution and Prospects", Athens, 22 June 2019.

12. Evaluation of the Selective Laser Melting (SLM) for the production of Co-Cr alloys for dental metal-ceramic prosthetic restorations.
    K. Dimitriadis, S. Tsouli, M. Roumpi, A. Poulia, A. Lekatou, S. Agathopoulos.
    7th Hellenic Conference on Metallic Materials, Athens, 11-13 December 2019.

Conference and Course Attendance:

1. 8th Training Day of Dental Technologist, Athens, 10-11 May 2014,
2. 9th National Conference of the Greek Association for Biomaterials, Athens, 7-8 November 2014,
3. Conference "New materials for biomedical applications", Athens, 6 April 2015,
4. International Conference on BIO-Medical Instrumentation and related Engineering and Physical Sciences, Athens, 18-20 June 2015,
5. 10th National Conference of the Greek Association for Biomaterials, Athens, 26-27 November 2015,
6. 7th National Conference of the Greek Association for Biomechanics, Athens, 24-26 June 2016,
7. 6th Hellenic Conference on Metallic Materials, Ioannina, 7-9 December 2016.
8. Training School "Non-living materials meet living Biology" of the European Ceramic Society, 9-12 May 2017, Patras, Greece
9. 2nd Dental Technology Training Conference, Athens, 20-21 May 2017.
10. Dental Prosthetics for Dental Technologist Conference, Athens, January 2018.
11. 8th National (Greek) Conference of the Greek Association for Biomechanics, Thessaloniki, 01-02 September 2018.
12. 11th National (Greek) Conference of the Greek Association for Biomaterials, Athens, 23-25 November 2018.
13. Conference "Dental Technology in Higher Education: Evolution and Prospects", Athens, 22 June 2019.
14. 7th Hellenic Conference on Metallic Materials, Athens, 11-13 December 2019.